Stony Brook University

Murine gammaherpesvirus ORF75A tegument protein promotes virus replication and is required for the efficient establishment of latency *in vivo*

A Dissertation Presented

by

Nana Kwaku Minkah

to

The Graduate School

in Partial Fulfillment of the

Requirements

for the Degree of

Doctor of Philosophy

in

Molecular Genetics and Microbiology

Stony Brook University

December 2015

Stony Brook University

The Graduate School

Nana Kwaku Minkah

We, the dissertation committee for the above candidate for the
Doctor of Philosophy degree, hereby recommend
acceptance of this dissertation.

Laurie T. Krug Ph.D. (Advisor), Assistant Professor
Department of Molecular Genetics and Microbiology

Carol Carter Ph.D. (Chair), Professor
Department of Molecular Genetics and Microbiology

Patrick Hearing Ph.D., Professor
Department of Molecular Genetics and Microbiology

Wei-Xing Zong, Ph.D., Professor
Department of Molecular Genetics and Microbiology

Jarrod B. French Ph.D., Assistant Professor
Department of Chemistry

This dissertation is accepted by the Graduate School

Charles Taber
Dean of the Graduate School

Abstract of the Dissertation

Murine gammaherpesvirus ORF75A tegument protein promotes virus replication and is required for the efficient establishment of latency *in vivo.*

by

Nana Kwaku Minkah

Doctor of Philosophy

in

Molecular Genetics and Microbiology

Stony Brook University

2015

Herpesviruses establish a chronic infection in the host that is characterized by intervals of lytic replication, quiescent latency, and reactivation from latency. Understanding the viral determinants of productive replication is critical for the development of novel therapeutic interventions against chronic infection with oncogenic gammaherpesviruses. Herpesviruses package proteins and RNA of host and virus origin into the viral tegument, a proteinaceous layer located between the nucleocapsid and envelope. Tegument proteins may function immediately upon deposition with the virion and throughout virus replication. Each gammaherpesvirus encodes one or more tegument proteins with homology to the cellular purine metabolism enzyme, formyl-glycineamide-phosphoribosyl-amidotransferases (FGARAT). These viral FGARATs (vFGARATs) do not retain enzymatic activity, but share a common strategy of inactivating components of ND10-nuclear bodies to counteract host intrinsic defenses. Murine gammaherpesvirus 68 (MHV68) encodes three vFGARATs: ORF75A, ORF75B, and ORF75C. ORF75C is essential for replication, but functions for ORF75A and ORF75B have not been identified. To investigate the functions of ORF75A and ORF75B, we generated a series of mutant viruses lacking ORF75A or ORF75B. MHV68Δ75B had no phenotype in culture or in mice, and was not pursued further. In contrast, MHV68Δ75A exhibited replication defects in fibroblasts and, to a greater extent, in primary macrophages. The replication defect in macrophages was accompanied by an increase in viral gene expression across all kinetic classes and a decrease in cell viability. Furthermore, the levels of newly delivered ORF75C tegument protein were increased in the absence of ORF75A. We next examined the contribution of ORF75A to MHV68 pathogenesis in mice. After intranasal infection, MHV68Δ75A exhibited a

transient one-log reduction in acute replication in the lungs that preceded a severe defect in the establishment of latency in the spleen. Intraperitoneal inoculation partially rescued the ORF75A latency defect with no added impact on reactivation from latency. These studies identify a novel role for a gammaherpesvirus vFGARAT tegument protein in replication and pathogenesis in the host. We propose a model whereby ORF75A influences the levels of tegument proteins in the virion that impact early infection events, leading to a loss of pathogenesis *in vivo*.

Table of Contents

List of Figures

List of tables

List of Abbreviations

aa - Amino acid

AIDS - acquired immunodeficiency syndrome

ATRX - alpha thalassemia/mental retardation syndrome X-linked protein

BAC - Bacterial artificial chromosome

BMDM - Bone marrow derived macrophage

CHX - Cyclohexamide

CPE - Cytopathic effect

Daxx - Death-associated protein 6

EBV - Epstein-Barr virus

FBS - Fetal bovine serum

FGAM/FGARAT - formyl-glycineamide-phosphoribosyl-amidotransferase

HHV-6A - Human herpesvirus 6A

HHV-6B - Human herpesvirus 6B

HHV-7 - Human herpesvirus 7

HSV-1 - Herpes simplex virus strain 1

HSV-2 - Herpes simplex virus strain 2

Hpi - hours-post infection

HVS - Herpesvirus Saimiri

IFN – Interferon

IKK2 - Inhibitor of nuclear factor kappa-B subunit 2

IN - Intranasal

IP - Intraperitoneal

KS - Kaposi's sarcoma

KSHV - Kaposi's sarcoma associated herpesvirus

LDH - Lactate dehydrogenase

MAVS - Mitochondrial antiviral signaling protein

MCD - Multicentric Castleman's disease

MEF - Mouse embryonic fibroblast

MHV68 - Murine gammaherpesvirus 68

MOI - Multiplicity of infection

PAA - Phosphonoacetic acid

PEC - Peritoneal exudate cell

PEL - Primary effusion lymphoma

PFU - Plaque forming unit

PML- Promyelocytic leukemia nuclear body

PTLD - Post-transplant lymphoproliferative disease

ND10 - Nuclear domain 10

NF-κB - Nuclear factor kappa B

RIG-I - Retinoic acid induced gene I

Sp100 - Sp100 nuclear antigen

VZV - Varicella zoster virus

γHV - gammaherpesvirus

Acknowledgements

This dissertation would not have been possible without the support of a myriad of people. I thank my thesis advisor, Dr. Laurie Krug, for her mentorship, her enthusiasm for this work and for providing the perfect environment necessary for it's completion. I am indebted to my undergraduate mentees, Robert Stockton, Jammie Law and Kevin Chavez as well as my fellow MGM classmates, Eve Klajbor, Rebecca Bridges, and Nick Van Skike, for direct contributions to this work. I thank members of the Krug laboratory for valuable discussions and helpful suggestions along the way. I am especially grateful to Dr. Orlando Scharer and his graduate student, Upasana Roy for help with setting up the UNGase assay and general advice concerning base excision repair. I also thank the members of my thesis committee for their advice and suggestions these past years.

Above all, the dissertation would not have been possible without my wonderful family. I thank my parents and sisters for their endless love and unwavering faith in me. I thank my wife for her love, patience and support throughout this process.

Chapter 1: Introduction

1.1 *Herpesviridae*

The *Herpesviridae* is a family of large, enveloped DNA viruses that establish life-long infections in their hosts. Herpesviruses infect both vertebrates and invertebrates and over one hundred herpesviruses have been identified. A herpes virion comprises a linear, double-stranded DNA molecule of 100 to 250 kilobase pairs enclosed in an icosahedral capsid, an outer lipid envelope containing the viral glycoproteins necessary for attachment and entry into target cells, and an ordered proteinaceous matrix located between the nucleocapsid and the lipid envelope termed the tegument (**Fig. 1.1**). All herpesviruses exhibit a dynamic life cycle. Upon initial infection of a host, a herpesvirus will often undergo a period of lytic, productive replication followed by the establishment of a quiescent latent infection, typically in a distinct cell-type. Periodic reactivation from latency into lytic replication seeds new latency reservoirs and is critical for dissemination to naïve hosts.

In general, herpesviruses exhibit strict host tropism, with most herpesviruses co-evolving with their cognate hosts over time (1). As such, herpesvirus infections are typically not associated with severe disease, although in very young or immunocompromised individuals, life-threatening infections can occur. In livestock, the economic consequences of herpesvirus infection can be quite significant with herpes-related mass mortality events in fish (2), oysters (3),(4) and cattle (5) recorded over the last decade. Herpesvirus infection is ubiquitous in humans with over 90% of all adults infected with at least one herpesvirus. Nine human herpesviruses have been discovered and these are further divided into three sub-families: Alphaherpesvirinae, Betaherpesvirinae and Gammaherpesvirinae. This classification is based on genome architecture, the site of latency within the infected host and the length of their productive lytic replication cycle.

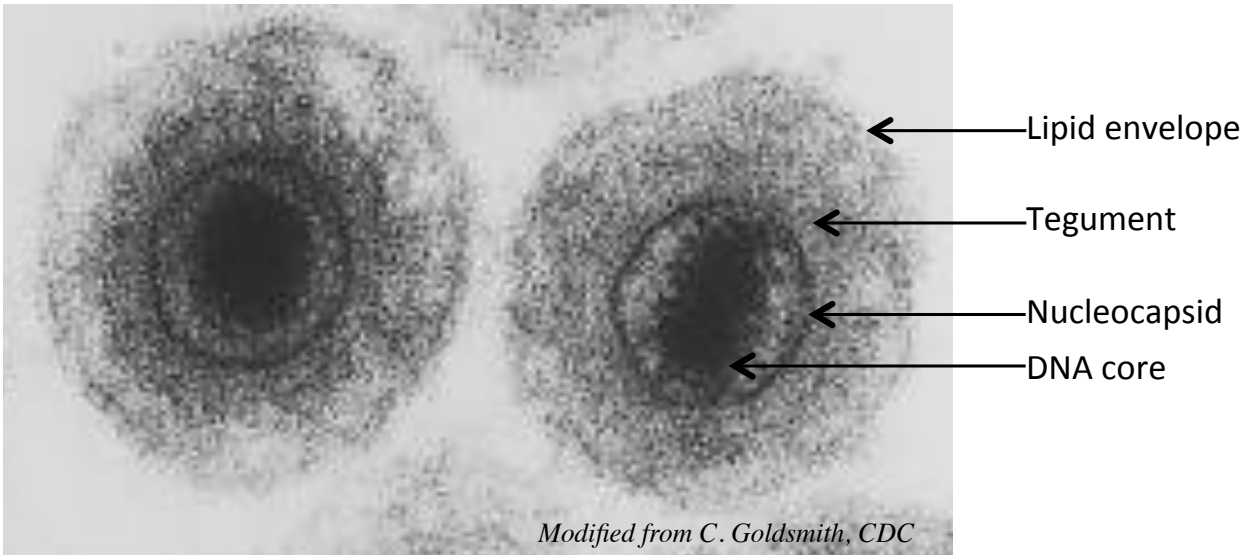

Figure 1.1. Structural features of a herpesvirus virion.
Electron micrograph of a herpesvirus virion. The electron dense core is the herpesvirus double stranded genome. This is surrounded by the viral nucleocapsid. The lipid envelope contains the glycoproteins necessary for cell entry. The tegument lies between the nucleocapsid and the lipid envelope.

Alphaherpesvirinae

Alphaherpesviruses have a broad host range, are neurotropic and have rapid replication rates in cultured cells and in the animal (6). Human simplex virus serotypes 1 and 2 (HSV-1 and HSV-2) and varicella zoster virus (VZV) are the human alphaherpesviruses. Alphaherpesvirus infection typically begins with infection and replication in mucosal epithelial cells followed by dissemination to the nervous system. Alphaherpesviruses enter the nerve termini of the peripheral nervous system (PNS) and utilize retrograde transport towards the cell body of these non-dividing cells to establish latency that can be maintained for days to decades. Anterograde transport back towards the periphery is critical for reactivation (6). In rare cases, alphaherpesvirus infection results in a fatal infection of the central nervous system (7). HSV-1 and HSV-2 are primarily associated with oral-facial, ocular or genital mucosal infections (8, 9). Primary VZV infection causes chicken pox while reactivating VZV results in zoster/shingles. No vaccines exist for HSV, although treatment with multiple antivirals limits virus shedding at mucosal tissues in the periphery (10), (11). An effective live attenuated vaccine exists for VZV, and mass vaccination programs have reduced VZV associated disease. However in immunocompromised individuals, administration of this vaccine can result in VZV associated disease (12).

Betaherpesvirinae

Human cytomegalovirus (HCMV) and the Roseoloviruses (Human herpesvirus 6A, Human herpesvirus 6B and Human herpesvirus 7) are all members of the human betaherpesvirus subfamily. These viruses have slow replication cycles and HCMV, the most studied member of this subfamily infects and establishes latency in multiple cell types including monocytes, lymphocytes, hematopoietic progenitor cells and epithelial cells (13-15). HCMV infection causes severe disease in immunocompromised individuals and is associated with graft loss after organ transplants, retinitis and blindness in AIDS patients and birth defects in neonates (16, 17). There is no vaccine to prevent HCMV infection and current HCMV antivirals exhibit low bioavailability and significant toxicity (18). Although the Roseoloviruses are ubiquitous in the

human population, they remain grossly understudied. HHV 6B and HHV 7 cause *roseola infantum* and febrile illnesses and are associated with early childhood diseases. No antivirals exist for these viruses and very little is known about the molecular mechanisms underlining viral latency (19), (20).

Gammaherpesvirinae

The work presented in this dissertation is focused on the replication of a member of the gammaherpesvirus subfamily. Gammaherpesviruses are subdivided into two groups: the lymphocryptoviruses, of which the human Epstein-Barr virus (EBV/HHV4) is the prototypical member and the rhadinoviruses typified by Kaposi's sarcoma associated herpesvirus (KSHV/HHV8). Gammaherpesviruses infect multiple cell types including epithelial and endothelial cells but establish long-term latency in lymphocytes, specifically B cells for EBV and KSHV. These viruses are also associated with the development of numerous lymphomas and lymphoproliferative diseases (21-24).

The initial discovery of EBV was by electron microscopy analysis of virus particles isolated from suspension cultures of Burkitt's lymphoma in 1964 (25). Henle and colleagues then linked EBV infection to the development of infectious mononucleosis (26). Approximately 90% of adults over the age of 40 have antibodies to EBV. A little under half of these adults presented with infectious mononucleosis at primary infection. EBV is thought to infect via the oral (mainly tonsilar) compartment after which the virus replicates in the epithelial cells and lymphocytes of the oralpharynx. EBV infection before the age of 10 usually results in asymptomatic or mild acute infection. On the other hand, primary infection in adolescents and young adults can present as infectious mononucleosis. There is no vaccine for EBV and most adults suffering from primary EBV infection are treated with palliative measures including rest, fluid administration and over the counter pain relievers to treat fevers and aches. Of concern is the impact of EBV infection on cancers and lymphoproliferative diseases. EBV DNA has been identified in nasopharyngeal carcinomas, non-Hodgkin's lymphomas, oral hairy leukoplakia, and T cell lymphomas (27). During normal EBV pathogenesis in the host the virus utilizes several viral

factors to activate the B cell growth program, to drive immune evasion and to inactivate tumor suppressors. All of these likely contribute to EBV-driven oncogenesis (28). Another concern of EBV infection is the development of lymproliferative complications that arise after organ transplants. Immunosuppression of patients undergoing organ transplants can result in the reactivation of latent EBV into the lytic program and the development of post-transplant lymphoproliferative disorder (PTLD) (29). This disease can be fatal and is characterized by uncontrolled B cell proliferation, plasmacytic hyperplasia in younger patients and the development of lymphomas (30). Effective treatment for PTLD involves the reduction of immunosuppression which compromises graft tolerance, or adoptive immunotherapy with primed CD8+ cytotoxic T cells to control lytic EBV replication (31, 32). Additionally chemotherapy might also be utilized to control the EBV-driven lymphomas. Overall, these strategies are costly and in the case of chemotherapy against the lymphoma, are not very well tolerated by patients. Numerous antivirals have been shown to possess *in vitro* efficacy against EBV replication although *in vivo* efficacy remains to be determined.

KSHV also has etiological associations with cancers and lymphoproliferative diseases, including Kaposi's sarcoma (KS), multicentric castleman's disease (MCD) (33) and primary effusion lymphoma (PEL). Prior to the AIDS epidemic, KS was a rare disease restricted mainly to elderly men of Mediterranean and Middle-eastern lineage (34). In the early days of the AIDS epidemic, KS was recognized as one of the leading causes of death in HIV infected patients (35). KSHV was first isolated in 1994 from Kaposi's sarcoma (KS) lesions in HIV+ patients suffering from acquired immunodeficiency syndrome (AIDS) (35) and is now unequivocally recognized as the pathogen responsible for KS. The incidence of KS-associated death in HIV infection has significantly fallen with the advent of Highly active antiretroviral therapy (HAART) against HIV. However KS remains the most common oral malignancy in HIV-infected individuals leading to the majority of all HIV associated-oral cancers.

Although the latent KSHV program contributes to KSHV-induced disease, multiple lines of evidence indicate that lytic KSHV replication is an important contributor to tumorigenesis. Treatment of patients with antivirals that target lytic KSHV production and not latency reduces

KS lesions as well as KS development in HIV-infected patients (36). Moreover, lytic KSHV replication from reactivating latent KSHV is critical for sustaining the pool of latent genomes, as well as seeding the new target cells critical for KSHV-induced tumorigenesis.

Many of the molecular aspects of lytic replication remain woefully understudied in EBV and KSHV infections. EBV and KSHV exhibit strict host tropism, precluding studies of productive replication in laboratory animals. Additionally, most of the existing tissue culture systems for the human gammaherpesviruses recapitulate latency. Recent tissue culture models for lytic EBV replication in stratified epithelial cells (37) and KSHV (38) will likely be useful in understanding the contribution of viral factors to lytic replication in stromal cells. However, since the severity and prevalence of gammaherpesvirus malignancies are increased in immunocompromised hosts, it is likely that the examination of productive events in the absence of complete host immunity will be unable to provide a comprehensive picture of pathogenesis. To that end, major advances in the identification of viral and host factors critical for the understanding of lytic replication, host immune regulation and virion assembly and egress have utilized animal models of gammaherpesvirus replication. Our laboratory utilizes a rodent gammaherpesvirus (discussed in section 1.2) to examine the contribution of viral and host factors to gammaherpesvirus pathogenesis.

1.2 MHV68 infection of mice as a model of gammaherpesvirus pathogenesis

To identify and understand virus and host determinants, our laboratory uses the murine gammaherpesvirus pathogen system. MHV68 was first isolated from bank voles and yellow-necked mice in the former Soviet state of Czechoslovakia (39). Recent serologic and PCR analysis has also identified MHV68 as a natural pathogen of wood mice (*Apodemus sylvaticus*) in England (40, 41) implying that MHV68 likely has a large host range in Europe. Serological analysis has also confirmed that this virus is present in other rodent species, deer and wild boars as well (42). The unique region of the MHV68 genome is approximately 120 kb and encodes 79 open reading frames (ORFs) (43). MHV68 was classified as a gammaherpesvirus based on the organization of the genome and the identification of significant sequence homology to the sequences of the human gammaherpesviruses (43). MHV68 has been further characterized as a rhadinovirus in the gammaherpesvirus subfamily based on greater sequence similarity to herpesvirus saimiri and KSHV. The MHV68 genome retains blocks of conserved genes interspersed with MHV68-specific genes (labeled M1-M12). MHV68 is colinear with KSHV and replicates to high titer *in vitro* with a 12-18 hr single round of lytic replication (44). In addition, genetic systems based on homologous recombination in a bacterial artificial chromosome allow rapid genetic engineering of recombinant MHV68 (45).

A typical round of lytic MHV68 is depicted in Figure 1.2. Receptor engagement by the MHV68 glycoproteins with cell surface receptors results in the entry of MHV68 into target cells either by cell fusion or receptor-mediated endocytosis (46, 47) (**step 1 Fig. 1.2**). Next, the viral capsid is released into the cytoplasm and traffics along the microtubule network to reach the nuclear pore (**step 2 Fig 1.2**). Some tegument proteins stay attached to the viral capsid while others are released into the cytoplasm to modulate the host intracellular environment (47). The viral capsid docks at nuclear pores and the genome is then injected into the nucleus. The linear genome circularizes and initiates an ordered cascade of viral gene expression and DNA replication. Viral genes are subdivided into three classes of successively expressed transcripts (immediate early, early and late genes) (**Step 3 Fig 1.2).** Newly synthesized viral DNA is packaged into progeny nucleocapsids. Capsids bud through the inner nuclear membrane leading to the formation of enveloped viral capsid in the perinuclear space where some inner tegument proteins are acquired (48). Egress from the perinuclear space leads to de-envelopment in the cytoplasm where outer tegument proteins are acquired. Re-envelopment of the capsid and glycosylation of the glycoproteins in the trans-Golgi completes the maturation of progeny virions. Final egress via exocytosis results in the release of the mature virus into the extracellular space (49, 50).

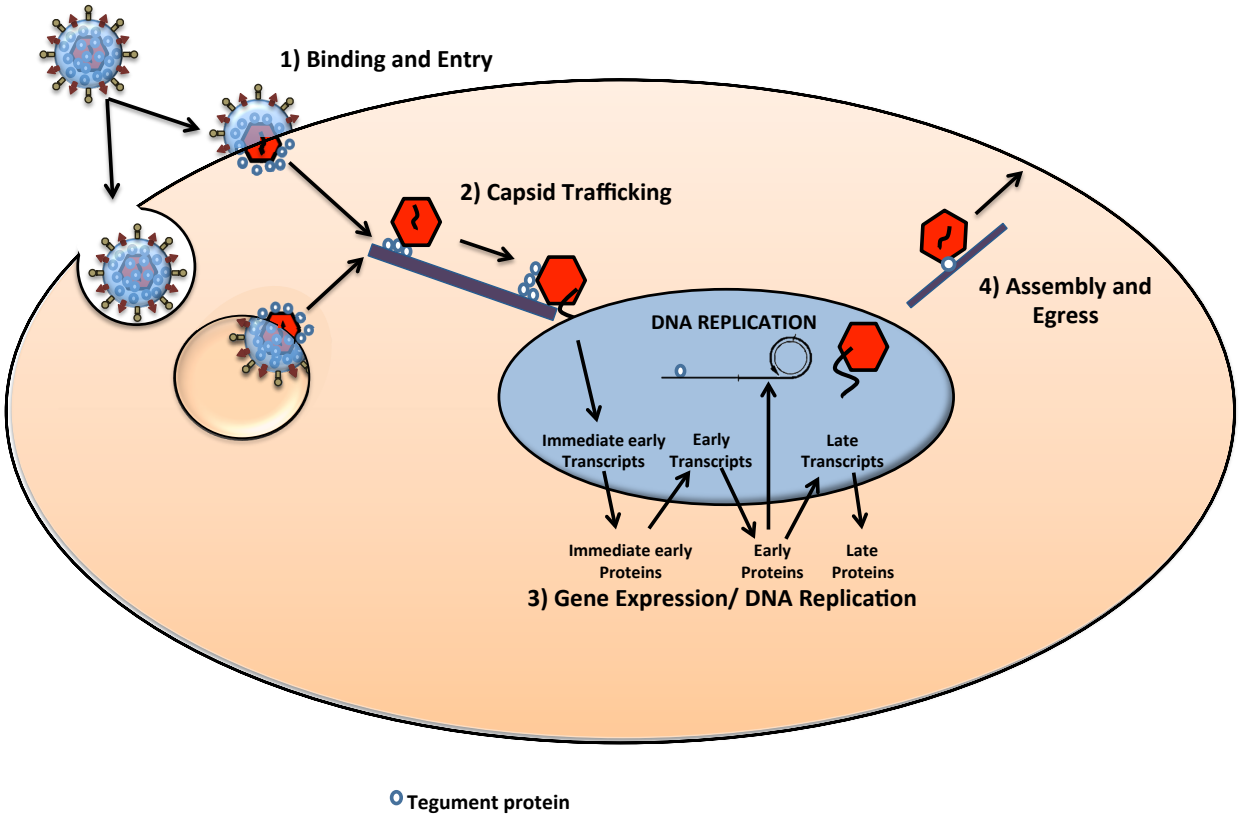

Figure 1.2 The MHV68 lytic replication cycle.
The lytic MHV68 cycle begins with attachment and entry into the cell (1), followed by the trafficking of the viral capsid to nucleus (2). The capsid docks at the nuclear pore, and deposits the viral genome into the nucleus. In the nucleus, the linear genome is circularized and begins the ordered cascade of gene expression and DNA replication (3). Finally, progeny capsids are made and undergo a series of envelopment and de-envelopment steps to acquire tegument components and glycoproteins prior to egress from the infected cell (4).

The MHV68 system has tissue culture systems permissive for lytic replication and to model latency (51) and tumorigenesis (52). This model system is vital for the examination of the biological relevance of cell culture phenotypes and the identification of roles for viral and host factors that do not manifest in culture. Two main routes of infection have been adopted in the MHV68 system. Intranasal infection enables the examination of acute viral replication in the lungs of infected mice prior to establishment of latency in the spleen. This route of infection requires virus replication in stromal cells of the lung mucosa such as epithelial, endothelial and fibroblast cells (**Fig 1.3**) (44, 53). An inflammatory infiltrate composed of dendritic cells, macrophages and B cells are then recruited to the lung and mediate the dissemination of the virus to lymphoid cells in the spleen (54-56). Within two weeks, actively replicating virus is cleared from the mouse lung, and disseminates to the spleen where there is a slight amount of acute replication in the mouse spleen with the initial establishment of latency in B cells, macrophages and to a lesser extent in dendritic cells (53, 57-59) (**Fig 1.3 green curve)**. The peak of latency is 16-18 dpi and long-term latency is maintained in immunoglobulin switched memory B cell (60). The second route of infection is intraperitoneal inoculation that bypasses the respiratory tract, allowing direct latency establishment independent of replication in the lung prior to dissemination.

Infection of mice recapitulates many aspects of the gammaherpesvirus infection of humans. The expansion of the Vβ4 CD8+ T cell population, polyclonal B cell activation and splenomegaly (61, 62) parallels the infectious mononucleosis observed with EBV infection. MHV68 infection leads to pneumonitis marked by an inflammation of alveoli walls in the lung after intranasal infection and also leads to vasculitis (57, 58, 63). The infection of immunocompromised mice is associated with lymphoproliferative disease from infection of immunocompromised mice (64, 65)

The MHV68 system affords a robust examination of virus and host factors that influence all aspects of the gammaherpesvirus life cycle including productive replication, immune evasion, dissemination, latency and tumorigenesis in a natural rodent host.

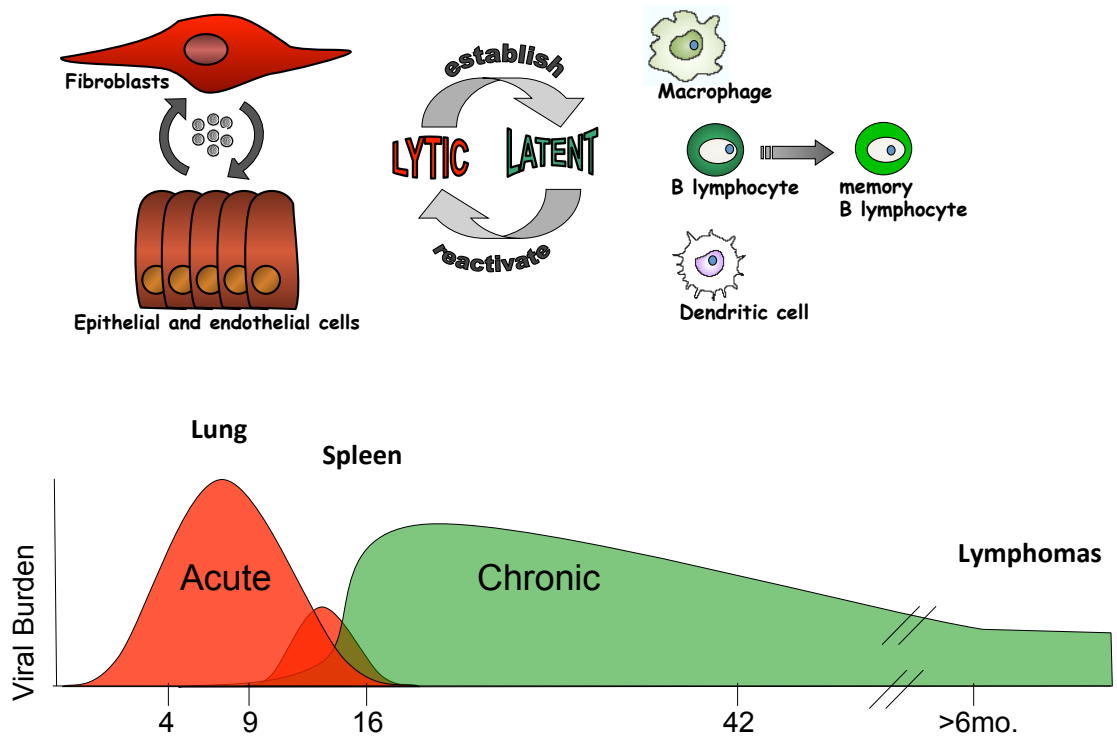

Figure 1.3 Course of an MHV68 infection in mice.
The course of an MHV68 infection in the mouse includes bouts of lytic replication in the stromal cells of the lung (intranasal infection) or the spleen (intraperitoneal infection). Latency is established in the lymphoid and myeloid cells of the spleen and maintained for the lifetime of the host in memory B cells. Peak latency is measured 16-18 dpi. Maintenance of latency is scored at 42 dpi. Lymphomas arise at late stages in immunocompromised animals.

1.3 The tegument as a critical component of a herpesvirus infection.

Characteristics of the Gammaherpesviruses tegument

As previously described, all herpesvirus virions contain a unique structure between the viral nucleocapsid which houses the herpesvirus genome and the viral envelope containing the glycoproteins necessary for attachment and entry into target cells (**Fig 1.1**). The herpesvirus tegument was initially assumed to be an amorphous structure containing viral and host proteins and nucleic acids. However recent high-resolution structures for HSV-1, HCMV, and MHV68 (66, 67), HCMV (68) and MHV68 (69) indicate that the tegument is more ordered, with two independent layers. The inner tegument proteins interact with capsid proteins while outer tegument proteins associate with the cytoplasmic tails of the transmembrane glycoproteins. In addition to the ordered arrangement of viral proteins within the tegument, accumulating evidence has identified the presence of both coding and non-coding viral nucleic acids in the tegument. Viral mRNAs are packaged into HSV-1 (70), (71), HCMV (72-74) and KSHV tegument (75). Moreover, in alpha and gammaherpesvirus tegument, non-coding viral RNAs are also packaged into the virion (76, 77). In the betaherpesviruses, RNA packaging correlates with RNA abundance in the cell and likely correlates with RNA species available at the site of assembly since most of the viral mRNAs are from the late kinetic class species. (72, 74). Packaging seems to be more selective in the alpha and gammaherpesviruses (76). In multiple cases, the packaged RNAs do not correspond to the most abundant transcripts in the cell (71, 75). This implies that, similar to the tegument proteins, viral RNAs are not incorporated through a stochastic, arbitrary event. Interestingly, some HSV-1 tegument proteins retain RNA binding ability and one of these tegument proteins can mediate cell-to-cell transfer of RNA (70). The role of the tegumented RNA species in herpesvirus biology remains an area of active research. Identifying the functions of tegument proteins in the different herpesvirus families will likely unveil additional roles for tegument proteins in the packaging and regulation of viral RNA species.

The viral proteins of the herpesvirus tegument have been well characterized for the alpha and beta herpesviruses with tegument proteins possessing annotated function in entry, gene expression, immune evasion, assembly and egress (78),(79). In the gammaherpesviruses, the tegument is woefully understudied, and most of the knowledge gleaned so far has focused on tegument proteins of KSHV and MHV68. Eleven proteins have been characterized in the tegument of KSHV virions: ORF11, ORF21, ORF50, ORF52, ORF63, ORF64, ORF75 (80), ORF19 and ORF32 (81). In MHV68, two proteomic studies have identified 13 tegument proteins (82, 83). Bortz and colleagues (82) identified ORF45, ORF52, and ORF75C in the MHV68 tegument. In addition to the proteins identified by Bortz and colleagues the Gillet laboratory (83) identified 10 other proteins in the MHV68 virion including ORF11, ORF21, ORF23, ORF33, ORF36, ORF38, ORF55, ORF63, ORF64, and ORF75B have been identified. Additionally, MHV68 ORF49 (84) and ORF75A (85) have also been characterized as tegument proteins. The roles of the tegument proteins characterized in either KSHV or MHV68 are briefly discussed below.

ORF11

ORF11 is unique to gammaherpesviruses. The MHV68 ORF11 gene encodes a 388 amino acid protein and was identified in a screen for viral factors responsible for the impairment of IFN signaling (86). An MHV68 mutant with a transposon insertion in ORF11 was unable to decrease the activation of an IFNβ-dependent luciferase reporter. A stop-disrupted ORF11 mutant exhibited a slight replication defect in MEFs and resulted in a significant release of IFNβ into the supernatant after infection of primary macrophages (86). Lastly, overexpression of ORF11 reduced IRF-3, TBK1 and sendai virus-induced IFNβ production. During MHV68 infection, ORF11 bound to TBK1 and reduced TBK1 interaction with IRF3 to limit TBK- dependent, IRF3 activation of IFN signaling. KSHV ORF11 has not been characterized.

ORF45

ORF45 encodes a 407 amino acid protein specifically conserved in the gammaherpesviruses. KSHV viruses lacking ORF45 exhibit a defect in lytic virus production (87) without defects in DNA replication or viral gene expression. Subsequent studies identified a role for ORF45 in recruitment of the microtubule associated motor protein, KIF3A, to the virus capsid to mediate newly formed capsid along the microtubule network towards the cell periphery (88). Additionally, KSHV ORF45 was also identified to antagonize IFN signaling by inhibiting the phosphorylation and nuclear translocation of IRF-7 (87). MHV68 ORF45 encodes a 207 amino acid protein, is expressed with early kinetics similar to KSHV ORF45. An MHV68 ORF45-null virus is defective for virus replication with dramatically reduced viral gene transcription and DNA replication (89). Although the function of the MHV68 ORF45 protein has not been found, the MHV68 ORF45-null virus defects are partially rescued with expression of KSHV ORF45 in trans (89). This indicates that MHV68 ORF45 and KSHV ORF45 share some functions.

ORF33

MHV68 ORF33 is a 334 amino acid protein. ORF33-null MHV68 viruses do not exhibit defects in viral gene expression, viral DNA replication or capsid assembly but rather in the release of newly formed capsids from the nucleus into the cytoplasm (90). Moreover a recent study has found that MHV68 ORF33 colocalized with capsid proteins, ORF25 and ORF26, in the nucleus and likely drives the recruitment of early tegument proteins that form the inner tegument (48). A role for the KSHV ORF33 protein in KSHV replication has not been examined. However, KSHV ORF33 is found in complex with KSHV ORF64, a tegument protein that interacts with the ORF25 capsid protein (91). It remains to be determined if the MHV68 ORF33 interaction with the ORF25 and ORF26 capsid proteins is through ORF64 as well.

ORF49

ORF49 has not been described as a component of the KSHV virion. In MHV68, a single study identified ORF49 as a tegument protein made late during replication (84). MHV68 ORF49

complexes with MHV68 ORF64 in the virion, and overexpression of the MHV68 ORF49 protein enhances the activity of an RTA promoter by displacing the negative regulator PARP-1 from the RTA promoter. An ORF49 null virus was impaired for replication in culture and latency establishment in the mouse (84)

ORF52

MHV68 ORF52 is a small 21-kDa protein and shares 28% amino acid identity with KSHV ORF52. Loss of MHV68 ORF52 impairs secondary envelopment of MHV68 virions resulting in the absence of enveloped virions in the trans-golgi membrane of infected cells (50) Additionally virions isolated from ORF52-null infected cells lack the ORF45 tegument protein (50) implying that MHV68 might be required to recruit MHV68 ORF45 into the tegument of virions. The KSHV ORF52 tegument protein has not been characterized in KSHV infection, although KSHV ORF52 was found to interact with KSHV ORF45 in a yeast-two hybrid analysis to examine interactions between KSHV virion components (91)

ORF63

KSHV ORF63 shares sequence homology with NLRP1, an upstream activator of the inflammasome, a multi-molecular complex that drives the secretion of host inflammatory cytokines. NLRP1 is a member of the nucleotide binding and oligomerization, leucine-rich (NLR) family of proteins. NLRs belong to a larger family of pattern recognition receptors responsible for recognizing generic molecular patterns on incoming pathogens. Sensing of the molecular patterns by NLRP1 promotes the formation of the multimeric inflammasome complex, which in turn results in the production of the cytokines, Il-18 and Il-1β to recruit neutrophils and inflammatory monocytes to the site of infection (92). Knockdown of KSHV ORF63 in the latent KSHV cell line, BCBL-1 impaired KSHV lytic replication after the induction of reactivation (93). Expression of KSHV ORF63 impairs the oligomerization or NLRP1 and its association with other components of the inflammasome. A role for the MHV68 ORF63 in the antagonism

of the inflammasome has not been documented, although ORF63 is essential for MHV68 replication (94).

ORF64

The KSHV ORF64 proteins encode a viral deubiquitinase protein (DUB) (95). ORF64 homologs in EBV (96) and MHV68 (97) also retain DUB activity. Knockdown of ORF64 in latent B cells impairs KSHV reactivation from latency (95). Additionally KSHV ORF64 has also been shown to important in inhibiting the RIG-I-dependent activation of IFN signaling (98). A recent role for the MHV68 ORF64 in limiting IFN signaling by the cytosolic DNA sensor STING was recently described (99). In this study, DUB-deficient MHV68 ORF64 viruses induce type I IFN signaling through the activation of a cytosolic DNA sensor. Additionally, this mutant virus is impaired for latency establishment in WT but not STING-deficient mice indicating that MHV68 utilizes the DUB activity of ORF64 to limit IFN signaling induced by the STING pathway (99). Thus both KSHV ORF64 and MHV68 ORF64 play roles in limiting IFN signaling induced by the host upon infection.

Overall, only a subset of the predicted tegument proteins in gammaherpesvirus virions has been characterized so far. Of note, in most cases these proteins play structural roles in lytic gammaherpesvirus replication and are usually important in modulating early events critical for kick starting replication. The MHV68 system has been critical to the identification and characterization of tegument dependent functions in gammaherpesvirus replication.

1.4 The gammaherpesvirus vFGARAT family of tegument proteins

All gammaherpesviruses encode one to three large tegument proteins (145-160 kDa) with an approximate 140 amino acid stretch of homology to a cellular enzyme critical for *de novo* purine biosynthesis (100, 101)(**Fig 1.4)**. This enzyme, formyl-glycineamide-phosphoribosyl-amidotransferase (FGARAT/FGAMs) catalyzes the fourth step in the *de novo* purine biosynthetic pathway (100, 101). The viral homologs (herein termed vFGARATs) have not preserved the known active sites of the host enzyme and, as such, are not predicted to retain enzymatic FGARAT activity. In support of this, transfections of MHV68 vFGARATs do not rescue growth of Chinese hamster ovary (CHO) cells lacking host FGARAT in purine-depleted media. We modeled one of the MHV68 vFGARATs, ORF75C, onto the crystal structure of the PurL FGARAT of *Salmonella* Typhimurium (102) and observed that the vFGARATs have retained sequences corresponding to the auxiliary nucleotide-binding pocket of PurL (Nick van Skike and Dr. Jarrod French, data not shown). Additionally, an alignment of the host FGARAT with various viral FGARATs identified several regions of highly conserved residues that form this putative NTP binding pocket and may constitute an important structural feature necessary for function (**Fig 1.4 boxed regions**). The vFGARAT genes have undergone duplications and divergence in the course of gammaherpesvirus evolution(100, 103). Six gammaherpesviruses, including herpesvirus saimiri, have two vFGARATs. MHV68 and wood mouse herpesvirus have three (ORF75A, ORF75B and ORF75C) (43, 104, 105). In MHV68, the pairwise amino acid identity of each ORF75 to the other is about 25%. This is the same as the amino acid identity between each MHV68 ORF75 and the human vFGARATs (85, 106). EBV BNRF1 and KSHV ORF75 exhibit a slightly higher amino acid identity to each other ~ 29% (data not shown). The conservation of the FGARAT domains indicates selective pressure for shared essential functions during chronic infection. So far three functions have been described for vFGRARTs: ND10 antagonism, NF-κB activation and nuclear cytoplasmic trafficking. Each function will be described below.

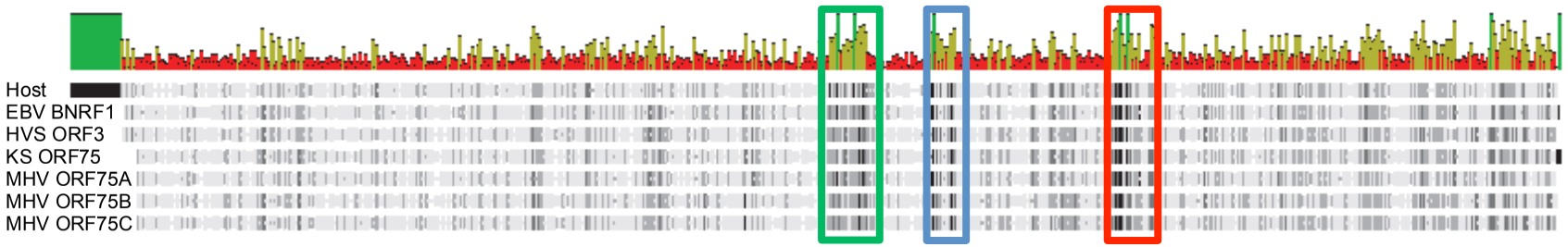
Host
EBV BNRF1
HVS ORF3
KS ORF75
MHV ORF75A
MHV ORF75B
MHV ORF75C

Figure 1.4 Comparison of the host FGARAT to the characterized vFGARATs.
Alignment of human FGARAT protein with the vFGARAT amino acid sequences from EBV BNRF1, HVS Saimiri, KSHV ORF75 and MHV68 ORF75A, ORF75B and ORF75C showing regions of high conservation (highlighted with colored boxes).

ND10 antagonism is a conserved feature of gammaherpevirus vFGARATs.

Nuclear Domain (ND) 10, collectively refers to an antiviral subnuclear complex made up of three permanent components, PML, Daxx and Sp100 (107-110). PML is the nucleating protein and is required for maintaining the integrity of the ND10 complex (111). Interestingly, most proteins recruited to PML nuclear bodies share the capability to be postranslationally modified by SUMO (112); covalent and non-covalent SUMO interactions form the basis of ND10 complex formation. Only sumoylated PML is capable of promoting ND10 formation and PML degradation leads to the disruption of the complex, limiting the antiviral properties of the ND10. Recent findings indicate individual ND10 components have antiviral functions in the absence of a competent ND10 signaling complex. As such, multiple herpesviruses encode multiple ND10 antagonists or encode antagonists that target multiple components of the ND10 complex. HCMV antagonizes PML and Sp100 with the immediate early protein, IE1 (113) and degrades hDaxx with the tegument protein pp71 (114). EBV utilizes EBNA1 to drives the phosphorylation, polyubiquitination and subsequent degradation of PML (115), BZLF1 to disperse PML (116). KSHV also encodes multiple ND10 antagonists. The vIRF3 degrades PML and displaces Sp100 from ND10 bodies (117). Lastly k-RTA retains SUMO-targeting Ubiquitin ligase (STUBL) function to degrade SUMO-modified PML (118).

ND10 antagonism is a conserved function of the vFGARAT family of gammaherpesvirus tegument proteins. The specific functions of these proteins in ND10 antagonism are discussed herein. EBV BNRF1 displaces hDaxx from its cognate partner ATRX, limiting the formation of the repressive hDaxx/ATRX/H3.3 chromatin on viral genomes (119, 120). Of note, BNRF1 dissociation of ATRX from hDaxx is dependent on binding to hDaxx via a Daxx interaction domain of BNRF1. Additionally, deletion of BNRF1 sequences with conservation to host FGARATs did not impair Daxx binding but inhibited dissociation of Daxx from ATRX (120), indicating a role for the conserved FGARAT motifs in BNRF1 function. KSHV ORF75 relocalizes PML, depletes ATRX, and disperses Sp100 (121). Silencing of ATRX, but not Daxx complements reactivation of BNRF1-knock down indicating that ATRX, not Daxx, is the important component targeted by BNRF1 (120). Herpesvirus Saimiri (HVS) encodes two

vFGARATs: ORF3 and ORF75. HVS ORF3 drives the degradation of Sp100 to enhance viral replication. Depletion of Sp100 rescues the replication defect of HVS ORF3-null virus. HVS ORF75 exhibits a slight replication defect and does not degrade Sp100 (122). No function has been described for HVS ORF75, but loss of ORF75 results in an increase in the kinetics of viral gene expression, a phenotype observed in this dissertation with ORF75A-null viruses (122). Interestingly a HVS ORF3/ORF75 double mutant is completely dead for virus replication implying that HVS ORF75 shares function with HVS ORF3 (121). MHV68 encodes three vFGARATs: ORF75A, ORF75B and ORF75C. MHV68 ORF75C is expressed in both the nucleus and cytoplasm of infected cells (85). ORF75C encodes an E3-ligase domain and during MHV68 infection, tegument delivered ORF75C degrades PML within the first two hours of a fibroblast infection (106,123).

Modulation of NF-κB signaling

Thus far two vFGARATs, KSHV ORF75 and MHV68 ORF75C, have been identified to modulate NF-κB signaling. KSHV ORF75 was identified in a screen for viral factors that promote NF-κB signaling (124). However the mechanism of NF-κB activation has not been determined. In contrast, a recent study by He and colleagues (125) identified ORF75C as the MHV68 viral factor critical for activating the upstream NF-κB signaling molecule, IKK2. The authors had previously shown that MHV68 hijacks the retinoic acid-induced gene I/mitochondrial antiviral signaling protein (RIG-I/MAVS) innate immune signaling pathway to activate NF-κB signaling (126, 127). In normal innate immune signaling, the cytosolic sensor RIG-I senses viral RNA, oligomerizes, complexes with its adaptor MAVS and activates upstream NF-κB signaling and the interferon pathway promote the establishment of a potent antiviral state early in viral infection (128),(129). In this study, the authors found MHV68 ORF75C recruits host FGARAT/PFAS to deamidate RIG-I, thereby promoting RIG-I oligomerization and activation. Activated RIG-I, in turn, complexes with MAVS and results in the activation of the upstream NF-κB signaling kinase, IKK2. Activated IKK2 then phosphorylates the MHV68 lytic transactivator, RTA to promote lytic gene expression (125).

MHV68 RTA degrades the p65 NF-κB subunit, thereby limiting the transcription of NF-κB dependent antiviral genes early in infection (126).

Cytoplasm-nucleus trafficking.

After entry of a herpesvirus virion into a cell, inner tegument proteins remain bound to the alpha and beta herpesvirus nucleocapsids and mediate trafficking of the virus capsid towards the nucleus where it docks at the nuclear pore. There, the viral genome is injected into the host cell nucleus, and commences the transcription of immediate early genes (6, 130). The virion component that promotes nuclear trafficking of incoming gammaherpesviruses virions has not been identified. Interestingly, capsids from MHV68 viruses lacking ORF75C accumulate in the cytoplasm and not at nuclear pores (85). Likewise, BNRF1-null EBV viruses fail to reach the B cell nucleus after entry, once again implying a defect in trafficking with loss of the EBV vFGARAT, BNRF1 (131)

1.5 MHV68 ORF75A and ORF75B vFGARAT tegument proteins and rationale for this study.

As outlined in section 1.4, the vFGARATs are routinely duplicated in gammaherpesvirus genomes, yet the selective pressure behind these duplication events is not understood (1). The MHV68 genome encodes three vFGARATs: ORF75A, ORF75B and ORF75C. ORF75C is a tegument protein that is expressed *de novo* with late kinetics (82, 132). Transfected ORF75C is mainly nuclear (85, 106), while both nuclear and cytoplasmic ORF75C species are detected upon MHV68 infection (85). Lastly, ORF75C is essential for MHV68 replication and has documented roles in PML degradation (85, 106), NF-κB signaling (125) and cytoplasmic trafficking of incoming virions (85).

The roles for ORF75A and ORF75B have not been defined in MHV68 replication. Similar to ORF75C, transfected ORF75A or ORF75B is predominantly nuclear (85, 106) while cytoplasmic ORF75A and ORF75B are also detected upon MHV68 infection (85). Neither ORF75A nor ORF75B degrades PML or activates NF-κB (106, 125). ORF75B is found in the MHV68 tegument (83) and microarray analysis of the MHV68 transcriptome indicated that ORF75B is expressed with early kinetics (133). In this same microarray analysis, ORF75A did not exhibit typical kinetics of gene expression, as it did not cluster with any other genes after hierarchical clustering (133). ORF75A was not identified in either of two proteomic analyses for MHV68 virion-associated components, but has been classified as a tegument protein due to homology to the other vFGARAT tegument proteins. Using an antibody to MHV68 ORF75A, Gaspar and colleagues (85) immunoprecipitated ORF75A from MHV68 virions.

Given that multiple gammaherpesvirus genomes encode one or more vFGARATs, we set out to determine if the other vFGARATs encoded by MHV68 retained unique, novel functions or whether they shared functions with ORF75C. Additionally, we were interested in identifying the role of the captured host FGARAT motifs in vFGARAT function. The host FGARAT is part of a larger macromolecular complex known as the purinosome. Interestingly, the purinosome is

tethered to the microtubule network by the host FGARAT and requires host FGARAT for the protein-protein interaction required for purinosome formation (101). Examining whether these captured FGARAT motifs drive attachment to the cell cytoskeleton or mediate vFGARAT interactions with binding partners is long-term aim of this project.

We hypothesize that ORF75A and ORF75B encode functions distinct from ORF75C and that these functions are dependent on the captured FGARAT motifs**.**

Chapter 2: Identification of transposon-disrupted ORF75A and ORF75B as modulators of MHV68 replication

Introduction

NF-κB signaling is hijacked by the gammaherpesviruses to promote the establishment of viral latency and the survival of host cells (134-136). The role of NF-κB signaling in MHV68 is complex. Loss of NF-κB signaling does not impact MHV68 replication within fibroblast or lung epithelial cells in culture (132, 137, 138). In contrast, either the infection of WT mice with a recombinant MHV68 virus expressing a dominant inhibitor of the NF-κB signaling pathway or infection of mice lacking the host p50 NF-κB subunit resulted in reduced latency establishment (132, 137, 138). Additionally, mice lacking the p50 NF-κB subunit also exhibited higher acute lung replication after intranasal infection (137). Thus NF-κB signaling is dispensable for MHV68 replication in fibroblasts and immortalized lung epithelial cells, but is critical for control of virus replication in the lung and latency establishment in the spleen (132, 137, 138).

The studies utilizing dominant negative inhibitors of NF-κB signaling or cells lacking the p50 NF-κB subunit indicated that the disruption of the NF-κB signaling pathway at the level of subunit activation did not lead to deleterious effects on MHV68 replication. Recently, a collection of studies from the Feng laboratory supports a model wherein MHV68 utilizes the ORF75C tegument protein to hijack the RIG-I/MAVS signaling cascade to activate the upstream NF-κB kinase, IKK2 (125-127). Of note, while typical engagement of this signaling axis results in the activation of host innate immunity to restrict viral replication (129, 139), MHV68 utilizes this pathway to activate the viral lytic transactivator, RTA to drive the degradation of the p65 NF-κB subunit (126, 127) and promote viral transcription. Loss of MAVS or impairment of the E3-ligase domain of RTA stabilizes the p65 subunit in infected cells and results in increased cytokine production in fibroblasts and murine lungs (126, 127). Taken together, early during lytic infection MHV68 activates upstream NF-κB signaling to drive lytic gene expression, but

limits downstream NF-κB subunit activation to prevent inflammatory cytokines and host immune activation. Interestingly, studies from our laboratory observed NF-κB subunit activation in MHV68-infected fibroblasts at late timepoints, from 12-24 hpi (137, 138). Whether this late activation indicates a positive role for NF-κB signaling driven by a MHV68 factor or rather represents the response by the host to infection remains to be answered. Additionally, although NF-κB subunits are dispensable for replication in fibroblasts, this late activation might imply uncharacterized roles for NF-κB signaling in other cell types infected by MHV68 (e.g. endothelial cell, dendritic cells and macrophages). Indeed, KSHV utilizes two viral proteins, the viral G protein coupled receptor (vGPCR) and the viral-flice inhibitory protein (vFLIP) to drive the constitutive activation of NF-κB signaling and promote cell survival and inflammatory responses in endothelial cells (140, 141). No constitutive activators of NF-κB signaling have been identified in MHV68; the MHV68 vGPCR activates NF-κB signaling in response to the addition of chemokines (142).

To identify MHV68 genes important for the activation of the NF-κB signaling pathway at late timepoints, we developed a rapid, high-throughput assay to measure NF-κB activation in infected cells by the quantification of firefly luciferase expressed under the control of an NF-κB dependent promoter. Using this assay we screened a transposon (TN) library of 32 recombinant MHV68 mutant viruses previously identified to be dispensable for replication in culture (94). We identified two recombinant viruses encoding TN insertions in ORF75A or ORF75B that were impaired for NF-κB signaling. ORF75A and ORF75B belong to a family of tegument proteins conserved in the gammaherpesviruses. There are three members of this family in MHV68: ORF75A, ORF75B and ORF75C. ORF75C is essential for replication and promotes PML degradation, NF-κB signaling and nuclear-cytoplasmic trafficking of the incoming virion (85, 106, 125). Roles for ORF75A and ORF75B had not been described.

We examined the ability of ORF75A.TN and ORF75B.TN viruses to replicate in primary fibroblasts and observed distinct growth defects. ORF75A.TN was defective early in infection while ORF75B.TN exhibited a late replication defect. Coupled with these *in vitro* defects, intranasal inoculation of mice led to significant defects in acute lung replication and the

establishment of latency in the mouse spleen. Thus, we identified roles for two previously uncharacterized viral genes in productive replication in culture and in the establishment of latency *in vivo*. It remains to be determined whether defects in NF-κB signaling account for the observed phenotypes. Moreover, the phenotypes of the TN disrupted viruses described in this chapter will be compared to the stop-disrupted mutant phenotypes defined in Chapters 3 and 4.

Materials and Methods

Mice, cells, and viruses. WT C57BL/6 mice were purchased from Jackson laboratories (Bar Harbor, Maine) or bred at the Stony Brook University Division of Laboratory Animal Research (DLAR) facility. All protocols were approved by the Institutional Animal Care and Use Committee of Stony Brook University**.** Primary murine embryonic fibroblast (MEF) cells were isolated from C57BL/6 mice and maintained in Dulbecco's modified Eagle's medium supplemented with 10% fetal calf serum, 100 U of penicillin per ml and 100 mg of streptomycin per ml at 37^{o}C in 5% CO_2. Immortalized murine fibroblast cells (NIH 3T12) were maintained in Dulbecco's modified Eagle's medium (DMEM) supplemented with 8% fetal calf serum, 100 U of penicillin per ml and 100 mg of streptomycin per ml at 37^{o}C in 5% CO_2. The transposon-disrupted viruses were a kind gift from Ren Sun, UCLA (94).

Screen for MHV68 modulators of NF-κB signaling. 8 x 10^5 3T12 cells were seeded into a 100-mm cell culture dish one day prior to transfection with 10 μg of the pGL4.32 NF-κB luciferase reporter plasmid (Promega Corporation, Madison, WI) or p57luc a luciferase reporter plasmid that contains the promoter region of MHV68 ORF57, an immediate-early lytic gene responsive the viral lytic transactivator RTA (kindly provided by Dr. Samuel H. Speck). Twenty-four hours post-transfection, the cells were seeded at 0.9 x 10^5 cell per well into 12-well plates and then infected with MHV68 at a multiplicity of infection (MOI) of 5 plaque-forming units per cell the next day. 24 hours post-infection, triplicate cell lysates were harvested in 100 μl of 1X passive lysis buffer (Promega Corporation, Madison, WI). Firefly luciferase activity was measured per manufacturer recommendations (Lumat LB9507 luminometer, EG&G Berthold, Bad Wildbad, Germany)

Virus growth curves. To measure virus replication, 0.9 x 10^5 primary murine embryonic fibroblasts were seeded into each well of a 12-well tissue culture plate one day prior to infection with recombinant MHV68 at an MOI of 5. Triplicate wells were harvested for each timepoint, and the cells with the conditioned medium were stored at -80°C. Serial dilutions of cell

homogenate were used to infect NIH 3T12 cells and then overlayed with 1.5% methylcellulose in DMEM supplemented with 5% FBS. One week later, the methylcellulose was removed and cells were washed twice with PBS prior to methanol fixation and staining with a 0.1% crystal violet solution in 10% methanol.

Efficiency of plating. To assay the efficiency of plating on different cell types, 0.9×10^5 of immortalized NIH 3T12 fibroblasts stably expressing MHV68 LANA (ORF73) or the empty plasmid (143) were seeded in 12-well tissue culture plates one day prior to infection with recombinant MHV68 at a multiplicity of infection (MOI) of 5.

Infections and organ harvests. 8 to 10 week old WT C57BL/6 mice were infected by intranasal inoculation with 1000 PFU of MHV68 in a 20 µl bolus under isoflurane anesthesia. The inoculum was back-titered to confirm the infectious dose. Mice were sacrificed by terminal isoflurane anesthesia. For acute titers, mouse lungs were harvested in 1 ml of DMEM supplemented with 10% FBS and stored at -80^0C prior to disruption in a Mini-BeadBeater (BioSpec, Bartlesville, OK). The homogenates were titered by plaque assay. For latency and reactivation experiments, mouse spleens were homogenized, treated to remove red blood cells, and then filtered through a 100 µm nylon filter. For peritoneal cells, 10 ml of media was injected into the peritoneal cavity and an 18-gauge needle was used to withdraw approximately 7 ml of media from each mouse. The peritoneal exudate cells were pelleted by centrifugation and then resuspended in 1 ml of DMEM supplemented with 10% FBS.

Limiting dilution PCR detection of genome positive cells. To determine the frequency of cells harboring the viral genome, single cell suspensions were prepared and used in a single-copy nested PCR reaction. Six three-fold serial dilutions of cells were plated in a 96-well PCR plate in a background of NIH 3T12 cells and lysed overnight at 56^0C with proteinase K. The plate was subjected to an 80-cycle nested PCR with primers specific for MHV68 ORF50 (58). Twelve

replicates were analyzed at each serial dilution and plasmid DNA at 0.1, 1 and 10 copies was included to verify the single-copy sensitivity of the assay.

Limiting dilution *ex vivo* reactivation assay. To determine the frequency of cells harboring latent virus capable of reactivation upon explant, single cell suspensions were prepared from mice 16 or 18 dpi, resuspended in DMEM supplemented with 10% FBS and plated in twelve serial two-fold dilutions onto a monolayer of MEFs prepared from C57BL/6 mice in 96-well tissue culture plates. Twenty-four replicates were plated per serial dilution. The wells were scored for cytopathic effect (CPE) two and three weeks after plating. To differentiate pre-formed infectious virus from virus spontaneously reactivating upon cell explant, parallel samples were mechanically disrupted using a mini-bead beater prior to plating on the monolayer of MEFs to release preformed virus that is scored as CPE (58).

Statistical analyses. Data were analyzed using GraphPad Prism Software (Prism 5, La Jolla CA). Statistical significance was determined using a non-paired two-tailed t-test. Under Poisson distribution analysis, the frequencies of latency establishment and reactivation from latency were determined by the intersection of nonlinear regression curves with the line at 63.2.

Results

Development of a screen for viral activators of NF-κB signaling

NF-κB subunits are activated in latent B cells and late during a productive fibroblast infection (137). NF-κB signaling promotes MHV68 latency in B cells (132, 144-146). To identify MHV68 factors that may modulate the NF-κB signaling pathway, we set up a screen of a library of transposon-insertion mutants (94). NIH 3T12 fibroblasts that had been previously transfected with an NF-κB dependent luciferase reporter were infected and assayed for changes in firefly luciferase. Infection with WT MHV68 at an MOI of 5 led to a steady increase in firefly luciferase after 12 hpi that continued through 36 hpi (**Fig. 2.1A**). To confirm that the luciferase readings corresponded to NF-κB signaling in the cell, we compared readings from cells transfected with a known activator of NF-κB signaling, MEKK1. In addition, we also infected the cells with a mutant virus encoding a repressor of NF-κB, MHV68 IκBαM, or the marker rescue virus, MHV68 IκBαM.MR, where the mutation has been repaired back to WT (138). MEKK1 transfection results in a potent activation of NF-κB signaling as evidenced by high levels of firefly luciferase in these cell lysates. In contrast, we did not measure any significant luciferase readings from MHV68.IκBαM-infected lysates. Infection with the IκBαM.MR virus restores NF-κB activation levels comparable to WT. However, lysates harvested from cells infected with UV-inactivated MHV68 failed to activate NF-κB signaling over mock (**Fig 2.1B)**. This indicates that virus gene expression or genome replication is required to trigger NF-κB activation.

Given that UV-inactivated viruses are unable to activate NF-κB signaling, we performed a secondary screen to distinguish between viruses that are attenuated for lytic replication from replication-competent viruses. To this end, we infected fibroblast cells expressing a luciferase plasmid driven by activation of the ORF57 promoter. ORF57 encodes an immediate early gene that is directly regulated by the MHV68 master lytic transactivator, RTA. Viruses with competent RTA activation will drive potent ORF57-luc expression. Transfection of an RTA expressing plasmid or infection with WT virus leads to ORF57-luc expression. As expected,

infection with the UV-inactivated WT virus fails to activate the ORF57-luc reporter. Infection with the MHV68.IκBαM does not impair ORF57-luc levels but rather seems to increase luciferase levels (**Fig. 2.1C**).

In MHV68-infected cells, we found that NF-κB signaling is dependent on virus gene expression as UV inactivated viruses fail to drive NF-κB signaling. Using the ORF57-luciferase reporter as a secondary screen, we are able to distinguish mutant viruses that fail to activate NF-κB signaling due to a failure in replication from viruses that have lost a *bona fide* NF-κB activator.

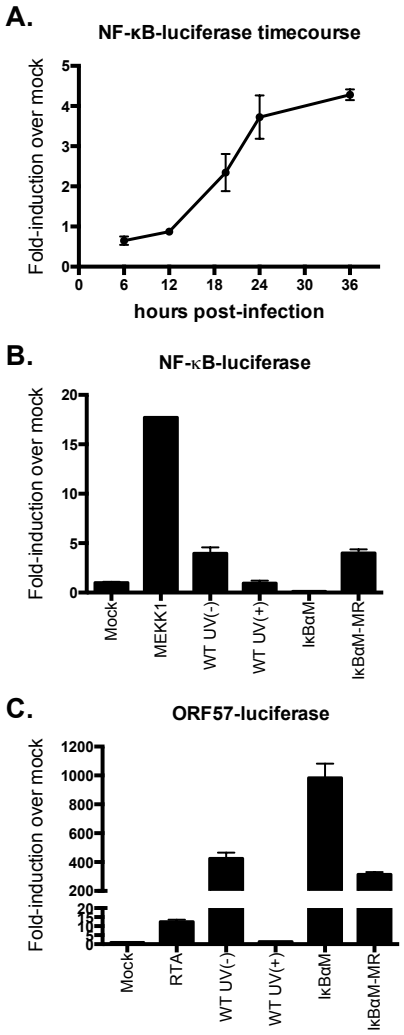

Figure 2.1. Characterization of NF-κB signaling in MHV68 infected fibroblasts. NIH 3T12 fibroblast cells were transfected with either the pGL4.32 NF-κB luciferase reporter (A&B) or p57luc (C), a plasmid that contains the promoter region of MHV68 ORF57 prior to infection with WT or the recombinant viruses IkBaM or IkBaM.MR, MOI 5**. (A)** Timecourse of NF-κB activation in immortalized fibroblasts infected with WT MHV68. **(B)** Examination of NF-κB activation with a transfected NF-κB activator, MEKK1, a UV inactivated virus, a recombinant virus harboring a dominant inhibitor of NF-κB signaling (IκBαM) or the repaired virus, IκBαM.MR **(C)** Examination of ORF57-luc activation upon transfection with the viral lytic transactivator, RTA, a UV inactivated virus, a recombinant virus harboring a dominant inhibitor of NF-κB signaling (IκBαM) or the repaired virus, IκBαM.MR.

ORF75A.TN and ORF75B.TN viruses are defective in NF-κB signaling.

To identify viral determinants of NF-κB signaling, we employed a library of mutant MHV68 viruses whereby each open reading frame is disrupted with the insertion of a 1.2 kb transposon (TN) construct (94). Given our previous observation that the absence of virus replication renders MHV68 unable to activate NF-κB signaling (Fig. 2.1A), we utilized the 32 replication-competent TN mutants (94). We infected NIH 3T12 cells expressing the NF-κB-dependent luciferase reporter with the TN-disrupted viruses and measured firefly luciferase from lysates harvested 24 hpi. Infection with two viruses, ORF75A.TN or ORF75B.TN led to a significant two-fold reduction in firefly luciferase as compared to the WT viruses (**Fig. 2.2A blue and red boxes**). An additional test of the two viruses with WT MHV68 confirmed the defect in NF-κB luciferase levels. The ORF75A.TN mutant, but not the ORF75B.TN mutant, had a defect in the activation of the ORF57 promoter-reporter, suggesting a potential loss of lytic transactivation and defect in virus replication **(Fig. 2.2B).** Thus we conclude that both ORF75A.TN and ORF75B.TN viruses are unable to activate NF-κB signaling. ORF75B might play a specific role in the engagement of NF-κB signaling, but we suspect that the defect in NF-κB signaling for an ORF75A.TN virus is likely secondary to the defect in replication

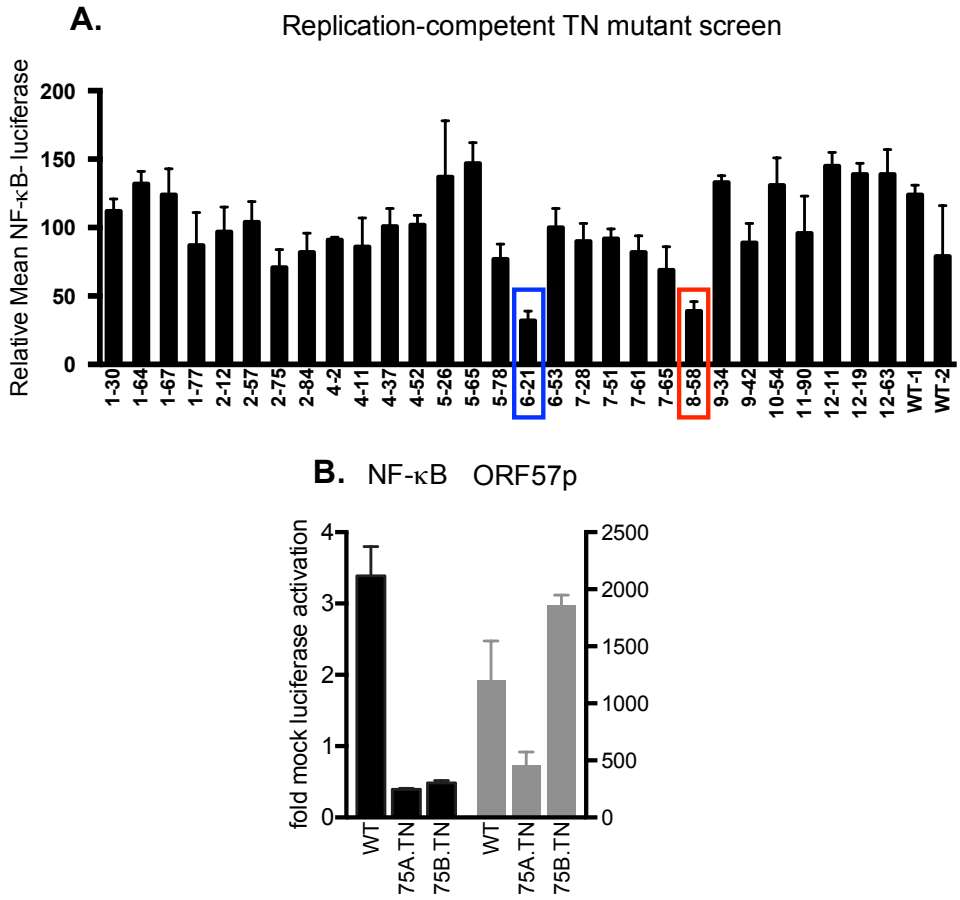

Figure 2.2. Screen of replication-competent transposon mutants identified two open reading frames (ORF75A and ORF75B) that when disrupted lead to a loss in NF-κB activation. NIH 3T12 fibroblast cells were transfected with either pGL4.32, an NF-κB luciferase reporter or p57luc, a plasmid that contains the promoter region of MHV68 ORF57, an immediate-early lytic gene activated by the viral transactivator, RTA prior to infection with the indicated viruses at a Multiplicity of Infection (MOI) of 5 for 24hrs. **(A)** 29 MHV68 viruses with unique transposon (TN) insertions in various open reading frames (ORFs) were screened for their ability to activate NF-κB. **(B)** Validation of the two strongest hits. 6-21(ORF75A TN mut) and 8-58 (ORF75B TN mut) were re-screened using concentrated stocks to confirm the NF-κB activation defect.

ORF75A.TN and ORF75A.TN mutant viruses exhibit distinct defects in fibroblast replication.

Our screen identified two viruses with defects in NF-κB signaling that exhibited distinct profiles in lytic ORF57 gene expression. ORF75A and ORF75B belong to a family of genes encoding tegument proteins unique to the gammaherpesvirus family of herpesviruses. These proteins all encode regions of similarity to a host enzyme involved in *de novo* purine biosynthesis (85, 106). MHV68 encodes three members of this family: ORF75A, ORF75B and ORF75C. ORF75C is essential for replication (85, 94, 106). The TN-disrupted ORF75A and ORF75B viruses were dispensable for replication in immortalized fibroblasts in culture (94). In the original paper describing the TN mutants, the authors also noted a defect in acute lung replication with the ORF75A.TN virus (94). In these next experiments, we set out to examine the replication of ORF75A.TN and ORF75B.TN viruses in primary murine embryonic fibroblasts (MEFs) upon a high MOI of 5. In single-step growth curves, ORF75A.TN and ORF75B.TN had significant replication defects (**Fig. 2.3**). Notably, the ORF75A.TN mutant replication defect was apparent at the earliest stages of infection as an extended eclipse phase and a delay in exponential growth, resulting in only a 1.5 log increase in virus output over the input (**Fig. 2.3**). The ORF75B.TN mutant seemed fairly normal until 24 hpi when virus growth reached a plateau leading to a 1.5 log defect in virus production compared to the MHV68-WTBAC control virus. Therefore, although both the ORF75A and ORF75B genomic regions are critical to MHV68 replication in culture, they likely play different roles in virus replication. We concluded that ORF75A functions early in infection, while ORF75B plays a role in the late stages of replication.

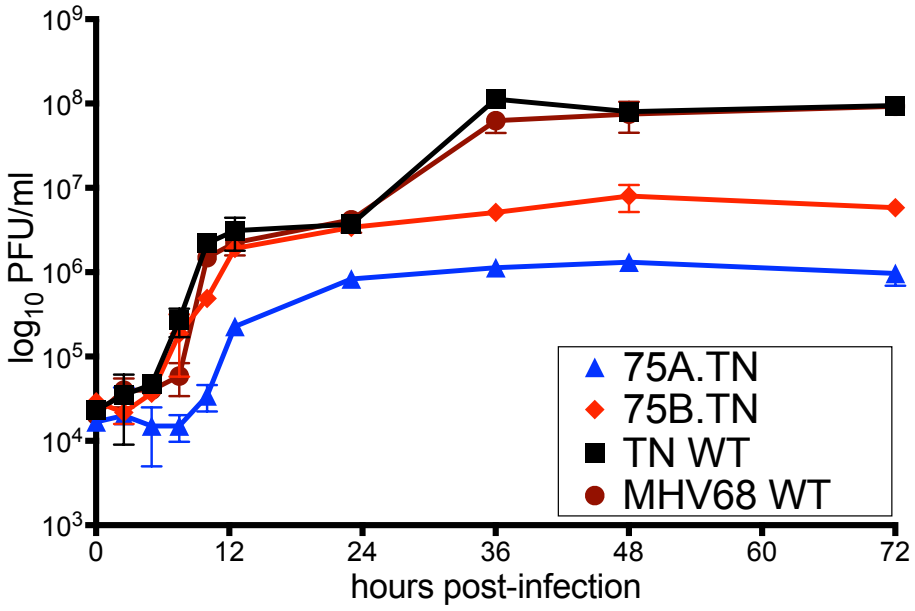

Figure 2.3. ORF75A.TN and ORF75B.TN viruses exhibit distinct defects in virus growth in primary MEFs. Single-step growth curve in primary murine embryonic fibroblasts (MEFs) at an MOI of 5.0 with WT MHV68, TN WT (WT virus generated from the same BAC as the mutants used in the transposon screen), 75A.TN and 75B.TN.

ORF75A.TN and ORF75A.TN mutant viruses exhibit distinct defects in pathogenesis in the mouse.

We next sought to examine the role of ORF75A and ORF75B in the replication of MHV68 in the murine host. Intranasal inoculation of mice with MHV68 leads to a period of acute replication in the lungs of infected mice that peaks between 7 to 9 dpi. We infected mice with WT, ORF75A.TN and ORF75B.TN viruses and quantified the infectious virus output in the lungs of infected mice at 7 dpi (ORF75A.TN) or 9 dpi (ORF75B.TN). The ORF75A.TN virus exhibited a severe 2.5-log replication defect as compared to titers from the lungs of WT-infected mice. Loss of ORF75B also resulted in about a 1 to 1.5-log defect in replication at 9 dpi (**Fig. 2.4**). Two weeks after intranasal infection, the virus is cleared from the lungs and traffics to the spleen to establish latency predominantly in B-lymphocytes (60). In the MHV68 pathogenesis system, peak latency occurs between 14 and 18 dpi. Latency is defined as the frequency of intact cells that harbor the MHV68 genome, upon an 80-cycle, nested limiting dilution PCR analysis with single copy sensitivity. Our method is distinct from the determination of latency using the genome load in a whole organ as it eliminates the impact of cells undergoing productive replication on the latent virus measure. We compared the frequency of splenic cells harboring virus genomes in WT, ORF75A.TN and ORF75B.TN infected spleens and observed that the spleens of mice infected with ORF75B.TN exhibited a ten-fold reduction in genome-positive cells as compared to WT (WT-1/131 vs. 75BTNmut- 1/1710), while spleens from mice infected with ORF75A.TN virus exhibited nearly a two-log reduction in latency establishment (WT-1/131 vs. 75ATNmut- 1/9660) (**Fig.2.5A**). Splenocytes from mice infected with either ORF75A.TN or ORF75B.TN had a similar decrease of approximately one log as compared to WT in the frequency of reactivation (WT-1/12031 vs. 75A-/75BTNmut ~1/100,000) (**Fig.2.5B and Fig.2.5C**). To determine the level of preformed infectious virus, we examined the cytopathic effect (CPE) in wells infected with disrupted splenocytes. No substantial levels of pre-formed virus were observed upon ORF75A.TN or ORF75B.TN infection (**Fig.2.5B and Fig.2.5C**). As such we can conclude that the observed cytopathic effect was a measure of *bona fide* reactivation from latent splenocytes. Taken together, these defects indicate that the ORF75A and ORF75B

genomic regions are critical for the establishment of chronic gammaherpesvirus infection in the host.

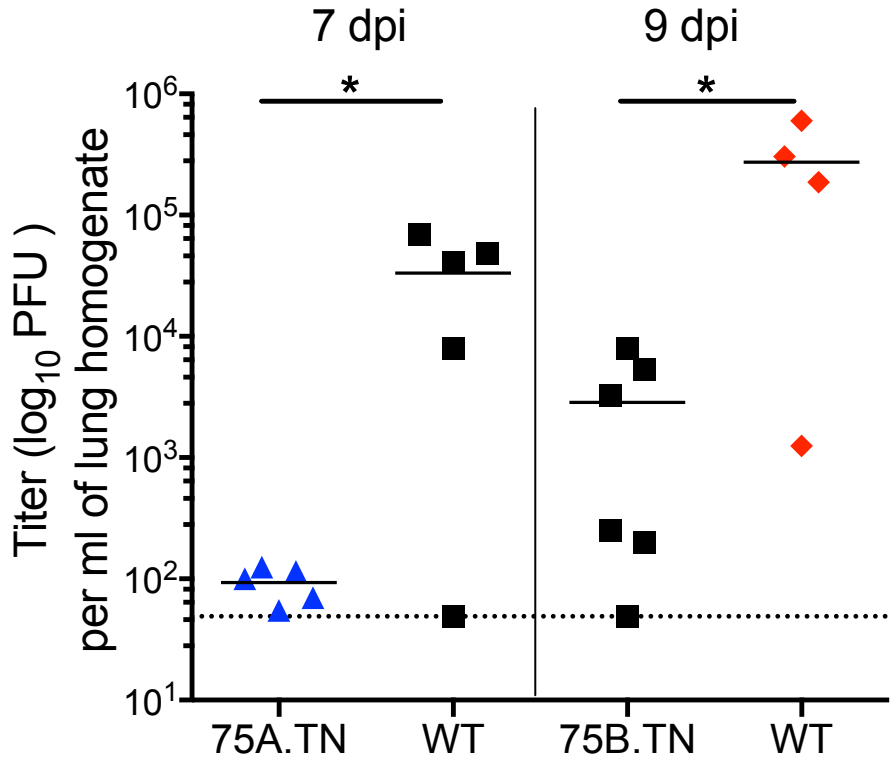

Figure 2.4: ORF75A.TN and ORF75B.TN are defective for replication in the lungs of infected mice. C57BL/6 mice were infected at 1000 PFU by the intranasal route with viruses with TN insertions in either ORF75A or ORF75B (75A.TN and 75B.TN) or WT MHV68. Lung homogenates from mice were titered by plaque assay. Line indicates geometric mean titer. Each symbol represents an individual mouse. The dashed line depicts the limit of detection at 50 PFU/ml of lung homogenate (log_{10} of 1.7), * $p \leq 0.05$.

A. Latency, splenocytes

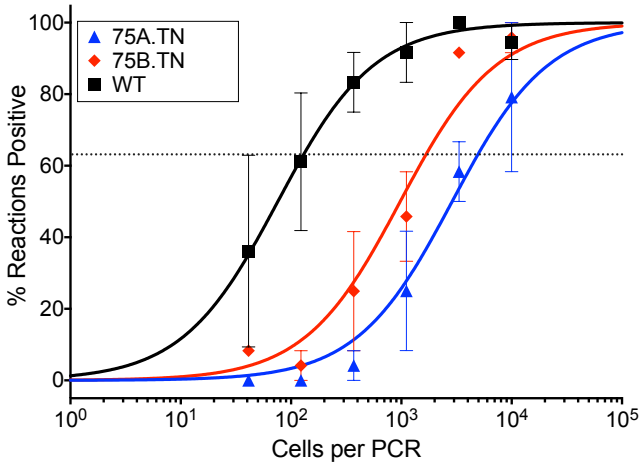

B. Reactivation, intact splenocytes

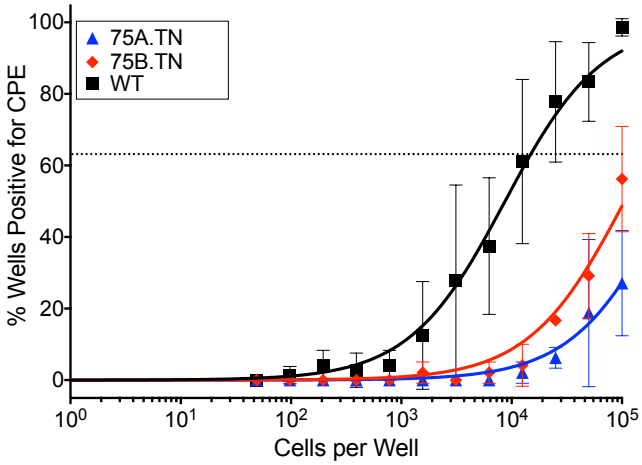

C. Reactivation, disrupted splenocytes

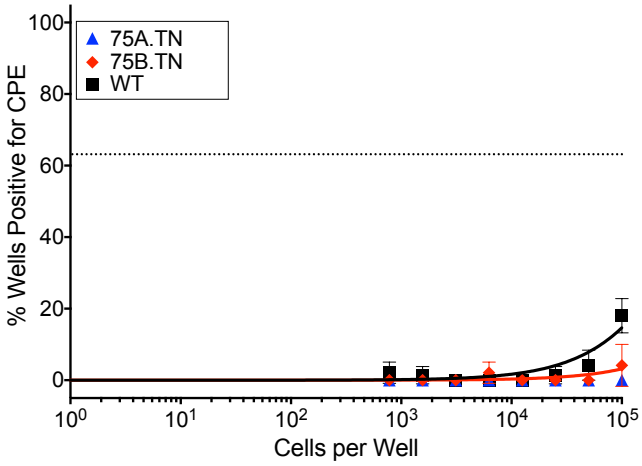

Figure 2.5: ORF75A.TN and ORF75B.TN exhibit severe defects in the establishment of splenic latency after intranasal infection. C57BL/6 mice were infected with 1000 PFU by the intranasal route with the indicated viruses. (**A**) Frequency of splenocytes harboring latent genomes. (**B**) Frequency of splenocytes undergoing reactivation from latency upon explant. (**C**) Frequency of disrupted splenocytes undergoing reactivation from latency upon explant. For the limiting dilution analyses, curve fit lines were determined by nonlinear regression analysis. The dashed lines represent 63.2%. Using Poisson distribution analysis, the intersection of the nonlinear regression curves with the dashed line was used to determine the frequency of cells that were either positive for the viral genome or reactivating virus. Data is generated from two independent experiments.

ORF73/LANA expression does not rescue ORF75A.TN or ORF75B.TN for replication.

ORF75A.TN and ORF75B.TN viruses exhibit distinct defects in replication in culture and pathogenesis in the mouse. However, given the size of the transposon construct (1.2 kb) we were concerned about the influence of this large insertion on the transcription of neighboring genes. One gene of particular interest is the MHV68 latency associated nuclear antigen (mLANA/ORF73). ORF73 mutants exhibit a slight reduction in virus replication upon high MOI that is exacerbated in low-MOI infection (143, 147). Moreover loss of the MHV68 LANA protein impairs the establishment of splenic latency and reactivation from latency (148). ORF73 transcripts splice across the ORF75A/ORF75B/ORF75C genomic region, leading us to examine whether the ORF75A.TN and ORF75B.TN replication defects could be attributed to a loss of ORF73. Our collaborator Dr. J. Craig Forrest, performed an efficiency of plating experiment by infecting NIH 3T12 fibroblast stably expressing ORF73 or control cells expressing an empty vector with our mutant viruses and examined virus production 24 hpi. ORF73 expression trans-complemented an ORF73null MHV68 for replication. ORF75A.TN and ORF75B.TN virus production was at similar levels in either the control or ORF73-expressing cells (**Fig. 2.6**). The lack of rescue by ORF73 expression indicates that the ORF75A.TN and ORF75B.TN phenotypes are not attributable to a defect in ORF73 expression.

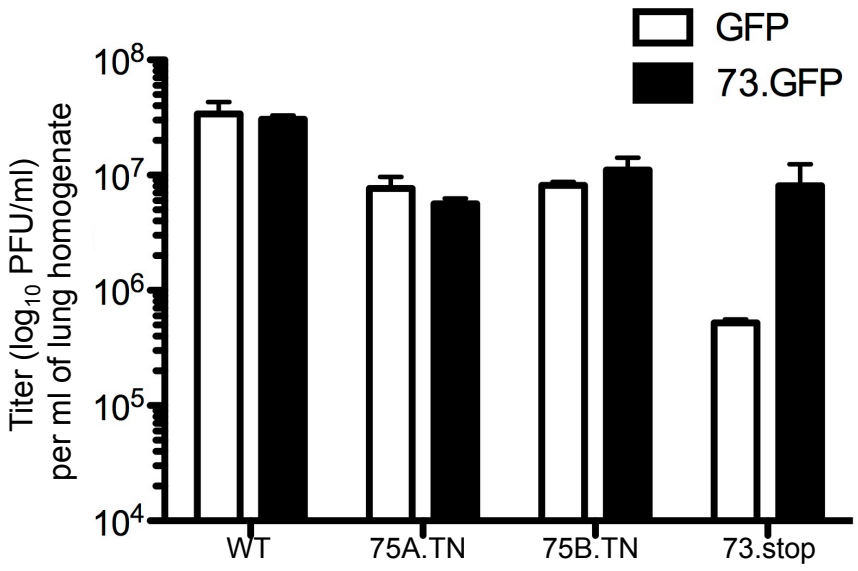

Figure 2.6: ORF75A and ORF75B transposon mutant virus replication defects are not complemented by exogenous mLANA/ORF73 expression. Titers from immortalized 3T12 fibroblasts stably transduced with GFP- or mLANA-GFP-expressing retroviruses and subsequently infected with WT, ORF73.stop, 75A.TN and 75B.TN viruses (data kindly provided by Dr. J. Craig Forrest of the University of Arkansas Medical Science).

Discussion

The MHV68 genome encodes 3 genes, ORF75A, ORF75B and ORF75C, with regions of homology to a host enzyme involved in *de novo* purine synthesis. Initially identified as genes of interest in a screen of mutant viruses for changes in NF-κB signaling, this study describes our initial characterization of the consequences of TN insertion in the 75A and 75B genomic regions for virus replication and pathogenesis. We observed distinct defects in *in vitro* replication with loss of OR75A impacting an early stage in replication while ORF75B loss influences a late stage of replication in cell culture. This *in vitro* defect hindered pathogenesis. ORF75A.TN and ORF75B.TN viruses exhibited defects in acute lung replication and in both the establishment of latency and reactivation from latency in the spleen at 16 dpi in mice.

The loss in NF-κB signaling observed with the ORF75A.TN and ORF75B.TN viruses is intriguing as a previous report examining KSHV proteins necessary for NF-κB signaling identified KSHV ORF75 as an activator of NF-κB signaling (124). This might indicate a conserved function of ORF75 family members. In support of this idea, a recent publication also identified a role for ORF75C in the activation of upstream NF-κB signaling via the deamidation of RIG-I (125). In this study the authors observed a lack of NF-κB activation with the overexpression of ORF75A and ORF75B. We have made similar observations and have confirmed that while overexpression of KSHV75 or MHV68 ORF75C is sufficient to drive NF-κB signaling in 293T cells, ORF75A and ORF75B are not sufficient (data not shown). We propose that the defect in NF-κB signaling during ORF75A.TN infection is related to an early defect in lytic replication. ORF75B.TN exhibits a slight replication defect later during infection, thus it is possible that this is the reason behind its inability to drive NF-κB signaling. Alternatively, ORF75B.TN viruses might be impaired for another aspect of infection that influences host cell signaling that in turn feeds into the IKK signalosome to influence NF-κB signaling, such as PI3K signaling (149). Lastly, ORF75B might interact with another viral protein to drive NF-κB signaling in the context of infection such that overexpression of ORF75B alone is not sufficient to drive signaling. Identification of ORF75B binding partners or host

signaling pathways impacted by ORF75B.TN infection compared to WT infection might reveal a role for this protein in NF-κB signaling.

Several groups have identified roles for ORF75C in NF-κB signaling, PML degradation and the cytoplasmic-nuclear trafficking of MHV68 genome to the nuclear periphery (85) yet no roles had been described for ORF75A or ORF75B. In this study, we identified distinct roles for the genomic regions encompassing ORF75A and ORF75B in promoting replication in cell culture and in the mouse. However, given the possibility that the TN disruption also influences the transcription of neighboring genes or even non-coding RNAs on the opposite strand, these observations need to be confirmed with stop mutations in ORF75A and ORF75B.

Our data indicates that the ORF75A.TN and ORF75B.TN replication defects are not due to a defect in ORF73. However another gene, ORF72, which encodes the viral cyclin has splice variants that splice across the ORF75A to ORF75C locus. A spliced transcript for MHV68 ORF72 initiates in the M12/M13 region upstream of the predicted ORF75A start site to terminate in ORF72 (150). Disruption of ORF72/viral-cyclin gene has no effect on replication in cell culture, but reduces acute replication in the lungs and the establishment of latency and reactivation from latency after intranasal inoculation (150, 151). The *in vivo* phenotypes of ORF75A.TN and ORF75B.TN virus phenotypes might be influenced by a transcriptional reduction in ORF72.

Recent analyses of viral transcripts have identified even more complexity in the gammaherpesvirus transcriptome (118, 133, 152-157). Microarray analyses from our laboratory and others have revealed that similar to HCMV and KSHV, a large portion of the MHV68 genome, both outside of and antisense to annotated ORFs, is transcribed in a productive fibroblast infection (133, 158). These transcripts have been named Expressed Genomic Regions (EGRs) and are predicted to be non-coding RNAs. However, in KSHV some of these antisense transcripts encode small regulatory peptides important for replication (159). MHV68 EGR 30 is transcribed antisense to ORF75A and ORF75B (160). It remains to be determined whether the insertion of the TN constructs into ORF75A or ORF75B influences the transcription of neighboring ORFs or antisense non-coding RNAs.

Our data identified roles for the genomic regions that comprise ORF5A and ORF75B in MHV68 replication. However given the complexity of MHV68 transcription and the potential for the TN insertion to disrupt neighboring transcripts, stop-codon disrupted ORF75A and ORF75B viruses were generated to test for ORF75A and ORF75B-specific contributions to MHV68 replication. These are reported in Chapter 3 and Chapter 4.

Chapter 3: An ORF75A.stop virus is impaired for pathogenesis in the mouse.

Introduction

All gammaherpesviruses encode tegument proteins with regions of similarity to host enzymes involved in *de novo* purine biosynthesis. ORF75 genes are often duplicated in gHV(85). MHV68 and the recently described wood mouse herpesvirus (WMHV), have two ORF75 duplications. MHV68 ORF75A, ORF75B, and ORF75C have amino acid identities of 75%, 88%, and 89%, respectively with their WMHV counterparts. However, there has been significant divergence. In a phylogenetic analysis each MHV68 ORF75 gene is nearly equidistant from each other and the primate ORF75 homologs, with ~25% amino acid identity in each pairwise comparison. Very limited functional data exists for the gHV ORF75 proteins. KSHV ORF75 activates a NF-κB reporter in transfected 293T cells (124) and antagonizes ND10 components (121). EBV BNRF1 is thought to be involved in endosomal to nuclear transport of the capsid and disrupting Daxx-ATRX binding (119). ORF75C is critical for MHV68 replication, targets PML for degradation and plays a critical role in capsid transport to the nucleus(85). Interestingly, these functions are not conserved by ORF75A and ORF75B and they do not complement the replication defect of an MHV68-ΔORF75C(85). ORF75A and ORF75B were deemed dispensable for lytic replication in culture in a transposon mutant screen, but one of two ORF75A transposon mutants had a log defect in lung replication. These viral FGARATs do not retain enzymatic activity and have been implicated in the antagonism of the host antiviral ND10 nuclear complex (85, 106, 119, 121, 122). In the previous chapter we developed a screen for viral modulators of NF-κB signaling, and identified transposon-disrupted ORF75A and ORF75B mutant viruses as defective in NF-κB signaling. These viruses had distinct defects in replication and pathogenesis *in vivo*. However, given the potential for the large transposon insertion to impair transcription of neighboring genes and preclude the identification of ORF-specific roles,

we set out to design and generate new recombinant viruses wherein either ORF75A or ORF75B is disrupted by the insertion of a series of stop codons.

Here we report that we did not observe any influence of ORF75B disruption on either replication in cell culture or in mice infected with ORF75B-stop viruses. On the other hand, loss of ORF75A transiently reduced replication in the lungs of infected mice and led to a severe defect in latency establishment after intranasal infection. Although we could partially rescue this latency defect with a direct intraperitoneal inoculation, there remained a significant reduction in the frequency of cells harboring MHV68 with loss of ORF75A. We conclude that MHV68 ORF75A and ORF75C have diverged and have non-overlapping roles in replication. ORF75B on the other hand may share functions with ORF75A and/or ORF75C, or retain a unique function not identified by our assays.

Materials and Methods

Mice and Cells. WT C57BL/6 mice were purchased from Jackson laboratories (Bar Harbor, Maine) or bred at the Stony Brook University Division of Laboratory Animal Research (DLAR) facility. All protocols were approved by the Institutional Animal Care and Use Committee of Stony Brook University**.** Primary murine embryonic fibroblast (MEF) cells were isolated from C57BL/6 mice and maintained in Dulbecco's modified Eagle's medium supplemented with 10% fetal calf serum, 100 U of penicillin per ml and 100 mg of streptomycin per ml at 37^{o}C in 5% CO_2. Immortalized murine fibroblast cells (NIH 3T3 or NIH 3T12) were maintained in Dulbecco's modified Eagle's medium (DMEM) supplemented with 8% fetal calf serum, 100 U of penicillin per ml and 100 mg of streptomycin per ml at 37^{o}C in 5% CO_2.

Generation of recombinant viruses. The modified MHV68-H2bYFP genome cloned into a BAC was a kind gift from the Speck laboratory (161). MHV68-H2bYFP-ORF75A-stop viruses (ORF75A.stop1, ORF75A.stop2 and ORF75A.dblstop) and the MHV68-H2bYFP-ORF75B-stop viruses (ORF75B.stop1 and ORF75B.dblstop) were all generated using *en passant* mutagenesis (45). Briefly, forward and reverse primers (**Table 3.1**) containing each ORF75 mutation mutation (underlined), flanking WT ORF75A or ORF75B sequences on either side of the mutation and sequences complementary to the kanamycin selection marker were used to amplify the kanamycin (kan) selection marker from plasmid pEPKanS2 (45) by PCR (One Taq DNA polymerase, New England Biolabs, Ipswich MA). This PCR product was excised from the gel, digested with *Dpn*I to remove input template, and transformed into freshly prepared electrocompetent *E. coli* harboring the MHV68-H2bYFP BAC. After recovery, the bacterial cells were plated on dual chloramphenicol (34 μg/ml) and kan (50 μg/ml) plates and incubated at 30°C for 48 hrs. DNA was prepared from isolated colonies and the kan selection marker in *Orf75A* or *Orf75B* was PCR amplified to verify the insertion of the mutagenesis cassette into the MHV68-H2bYFP BAC. The kanamycin selection marker was removed, leaving behind the desired ORF75A, ORF75B or ORF75C mutation. The *Orf75A* or *Orf75B* gene was PCR amplified from

the putative mutant BAC, digested with a restriction enzyme unique to each mutation to confirm the presence of each stop codon. To generate marker rescue viruses, primers flanking WT ORF75A or ORF75B sequence were used to generate a targeting construct, that was then used to repair the ORF75A-stop or ORF75B-stop disrupted viruses described above. Virus passage and titer determination were performed as previously described (58).

Analysis of recombinant viral BAC DNA. BAC DNA was prepared by Qiagen column purification. For restriction analysis. 10 μg of BAC DNA was digested overnight with the desired enzyme and then resolved in a 0.8% agarose gel in 1X TAE. For complete genome sequencing, the BAC DNA samples were prepared for multiplex, 50 cycle single-end read sequencing on an Illumina HiSeq2000 by the SUNY-Buffalo Next Gen Sequencing Core. Reads were demultiplexed using the CASAVA 1.8.2 utility program. Whole genome sequencing data were analyzed for mutations using CLC Genomics Workbench 6.0.2 (CLC bio, Aarhus, Denmark). Illumina sequence data was analyzed using CLC Genomics Workbench 6 (CLCbio/Qiagen, Aarhus, Denmark). Reads were aligned to a modified reference genome based on the WUMS Sequence (Genbank U97553) where the Kozinowski BAC sequence compiled by manual Sanger sequencing was appended to the left end. In order to spot any larger indels, contigs were generated using the CLC denovo assembler and aligned using Sequencher 5 (Genecodes). The reference sequence was modified based on actual sequencing data. Variants from the reference sequence comprising at least 5% of reads were found by using the Quality-based Variant detection algorithm in CLC Genomics Workbench, using a neighborhood radius of 5, minimum neighborhood quality score of 25, and a minimum central quality score of 29. Variants had to be present in both read directions, and had to be contained in uniquely mapped reads. Importantly, engineered mutations were found in >93% of reads.

Virus growth curves. To measure virus replication, 0.9×10^5 NIH 3T12 cells were seeded into each well of a 12-well tissue culture plate one day prior to infection with recombinant MHV68 at an MOI of 5. Triplicate wells were harvested for each timepoint, and the cells with the

conditioned medium were stored at -80°C. Serial dilutions of cell homogenate were used to infect NIH 3T12 cells and then overlayed with 1.5% methylcellulose in DMEM supplemented with 5% FBS. One week later, the methylcellulose was removed and cells were washed twice with PBS prior to methanol fixation and staining with a 0.1% crystal violet solution in 10% methanol.

Infections and organ harvests. 8 to 10 week old WT mice were either infected by intranasal inoculation with 1000 PFU of MHV68 in a 20 µl bolus or by intraperitoneal injection of 0.5 ml with 1000 PFU of MHV68 under isoflurane anesthesia. The inoculum was back-titered to confirm the infectious dose. Mice were sacrificed by terminal isoflurane anesthesia. For acute titers, mouse lungs were harvested in 1 ml of DMEM supplemented with 10% FBS and stored at -80°C prior to disruption in a Mini-BeadBeater (BioSpec, Bartlesville, OK). The homogenates were titered by plaque assay. For latency and reactivation experiments, mouse spleens were homogenized, treated to remove red blood cells, and then filtered through a 100 µm nylon filter. For peritoneal cells, 10 ml of media was injected into the peritoneal cavity and an 18-gauge needle was used to withdraw approximately 7 ml of media from each mouse. The peritoneal exudate cells were pelleted by centrifugation and then resuspended in 1 ml of DMEM supplemented with 10% FBS.

Limiting dilution PCR detection of MHV68 genome positive cells. To determine the frequency of cells harboring the viral genome, single cell suspensions were prepared and used in a single-copy nested PCR. Six three-fold serial dilutions of cells were plated in a 96-well PCR plate in a background of NIH 3T12 cells and lysed overnight at 56°C with proteinase K. The plate was subjected to an 80-cycle nested PCR with primers specific for MHV68 ORF50 (58). Twelve replicates were analyzed at each serial dilution and plasmid DNA at 0.1,1 and 10 copies was included to verify the sensitivity of the assay.

Limiting dilution *ex vivo* reactivation assay. To determine the frequency of cells harboring latent virus capable of reactivation upon explant, single cell suspensions were prepared from mice 16 or 18 dpi, resuspended in DMEM supplemented with 10% FBS and plated in twelve serial two-fold dilutions onto a monolayer of MEFs prepared from C57BL/6 mice in 96-well tissue culture plates. Twenty-four replicates were plated per serial dilution. The wells were scored for cytopathic effect (CPE) two and three weeks after plating. To differentiate between pre-formed infectious virus and virus spontaneously reactivating upon cell explant, parallel samples were mechanically disrupted using a mini-bead beater prior to plating on the monolayer of MEFs to release preformed virus that is scored as CPE (58).

Statistical analyses. Data were analyzed using GraphPad Prism Software (Prism 5, La Jolla CA). Statistical significance was determined using either an ANOVA test followed by a Bonferroni correction or a non-paired two-tailed t-test. Under Poisson distribution analysis, the frequencies of latency establishment and reactivation from latency were determined by the intersection of nonlinear regression curves with the line at 63.2.

Results

Disruption of ORF75A or ORF75B does not significantly impair replication in transformed fibroblasts.

Using transposon-disrupted viruses we observed significant and distinct defects in MHV68 replication upon loss of either ORF75A or ORF75B (Chapter 2). The transposon (TN) was inserted 351 aa downstream of the first methionine in ORF75A and 428 aa downstream of the first methionine in ORF75B. We were concerned that the large 1.2 kbp TN insertion might have adverse effects on neighboring genes or antisense transcripts. Moreover, it is possible that a truncated N-terminal protein made up of the first 351 aa in ORF75A or the first 428 aa in ORF75B might have residual or interfering functions in MHV68 replication. To this end, new recombinant viruses were generated on the MHV68-H2bYFP marking virus platform using allelic exchange (45, 161).

The first set of mutant viruses had either ORF75A or ORF75B disrupted in all frames by the insertion of a stop codon downstream of the first methionine, 101 aa and 78 aa into ORF75A and ORF75B, respectively (**Fig. 3.1A and Fig. 3.2A**). Insertion of the stop-codon into ORF75A results in the formation of a new *Mly*I site whilst the stop-codon insertion in ORF75B leads to the loss of a *Pst*1 site in the gene (**Fig. 3.1A and Fig. 3.2A**). These proximal stop-codon disrupted viruses are herein classified as 75A.stop1 and 75B.stop1. To account for the presence of a downstream methionine in the translation initiation of either ORF75A or ORF75B that is disrupted by the transposon insertion, but not the proximal stop codons discussed above, we generated a second set ORF75A and ORF75B mutant viruses where the stop codon is inserted at exactly the same position in the MHV68 genome as the transposon (i.e 428 aa and 351 aa for ORF75A and ORF75B, respectively) (**Fig. 3.1A and Fig. 3.2A**). The insertion of a stop codon at the TN position in ORF75A results in the addition of a unique *Spe*I site into the ORF75A gene while a stop codon at the TN position of ORF75B results in a loss of an *Ase*1 site (**Fig. 3.1A and Fig. 3.2A)**. These are referred to as 75A.stop2 and 75B.stop2. Finally, we generated ORF75A or ORF75B.stop viruses where either ORF75A or ORF75B harbors both stop codon insertions.

These double stop mutants have been termed 75A.dbl.stop or 75B.dbl.stop (**Fig. 3.1A and Fig. 3.2A).** Using wild-type sequence primers for ORF75A and ORF75B, we repaired the proximal ORF75stop viruses, ORF75A.stop1 and ORF75B.stop1 back to wt ORF75A or ORF75B sequences, respectively. These viruses are herein referred to as 75A.stop1MR and 75B.stop1MR.

The identity of each ORF75A mutant was confirmed by the digestion of a 1 kb PCR product amplified from ORF75A with *MlyI* and *SpeI* (**Fig. 3.1B**). The identity of each mutant ORF75B mutant was confirmed by the digestion of a 1 kb PCR product amplified from ORF75A with *PstI* and *AseI* (**data not shown**). We accounted for the absence of additional, unintended mutations in each MHV68 genome by whole genome sequencing and/or analysis of restriction fragment length polymorphisms in the BAC DNA (**Fig. 3.1C and Fig. 3.2B**).

To examine the effects of the ORF75A.stop and ORF75B.stop mutations on MHV68 replication, we compared replication in immortalized fibroblasts (NIH 3T12) following infection at an MOI of 5. In these single-step growth curves, loss of either ORF75A or ORF75B did not significantly impact MHV68 replication (**Fig. 3.1D and Fig. 3.2C**). Specifically each ORF75A-stop virus (75A.stop1, 75A.stop2 and 75A.dbl.stop) replicated with similar kinetics to the parental MHV68-YFP and 75A.stop1MR virus for the first 24 hrs with the two control viruses (MHV68-YFP and 75A.stop1MR) leading to about 2-3 fold higher titers than the ORF75A-stop viruses from 24 hpi until the end of the experiment (**Fig. 3.1D**). 75B.stop1 and 75B.dbl.stop virus growth was indistinguishable from the kinetics of the 75B.stop1MR virus replication over the course of the experiment (**Fig. 3.2C**). Thus we conclude that ORF75A and ORF75B are largely dispensable for MHV68 replication in immortalized cells.

Table 3.1. Mutagenic primers used in the generation of the ORF75.stop viruses		
Mutant	**Forward primer (5' to 3')**	**Reverse primer (5' to 3')**
75A.stop1MR	CACCCACGAAAACCACGAATTGGGCTTTGTGGTCG TTCACACCTCGACCACTTCCTCATTTAGGGATAACA GGGTAATCGATTT	GTCTCGTGGCAGTTTCGATCAAATGAGGAAGTGGTCGA GGTGTGAACGACCACAAAGCCCAAGCCAGTGTTACAA CCAATTAACC
75A.stop1	GTTCTTGCAGCGCTGTAGCTGGAGGCAAGCTTTGC AGGTGAGAGTCATGCAAAATCCAGCAATTCGGGCC TTCTGGGGAACCCCCTGGGGC	CGAGACGAATTAGGCGATGGATACAGGTGGCAGCACG CCTCACCTAGCAGCGATCTCACGCTTGATAGCACCAGA GAGCCCCCAGATGATG
75A.stop2	CACCCACGAAAACCACGAATTGGGCTTTGTGGTCG TTCACTAGTAACCTCGACCACTTCCTCATTTTAGGG ATAACAGGGTAATCGATTT	GTCTCGTGGCAGTTTCGATCAAATGAGGAAGTGGTCGA GGTTACTAGTGAACGACCACAAAGCCCAGCCAGTGTTA CAACCAATTAACC
75A.dbl.stop	GTTCTTGCAGCGCTGTAGCTGGAGGCAAGCTTTGC AGGTGAGAGTCATGCAAAATCCAGCAATTCGGGCC TTCTGGGGAACCCCCTGGGGC	CGAGACGAATTAGGCGATGGATACAGGTGGCAGCACG CCTCACCTAGCAGCGATCTCACGCTTGATAGCACCAGA GAGCCCCCAGATGATG
	CACCCACGAAAACCACGAATTGGGCTTTGTGGTCG TTCACTAGTAACCTCGACCACTTCCTCATTTTAGGG ATAACAGGGTAATCGATTT	GTCTCGTGGCAGTTTCGATCAAATGAGGAAGTGGTCGA GGTTACTAGTGAACGACCACAAAGCCCAGCCAGTGTTA CAACCAATTAACC
75B.stop1MR	AAGAAATACTCACTGAACTHTTATCTCCCATGGGAG CATTGACATCAATGATTTGCTAGGGATAACAGGGTA ATCGATTT	ACCATGACATACTGGATCTGGCAAATCATTGATGTCAAT TAATGCTCCCATGGGAGATAAGCCAGTGTTACAACCAA TTAACC
75B.stop1	CGAGACGAATTAGGCGATGGATACAGGTGGCAGCA CGCCTCACCTAGCAGCGATCTCACGCTTGATAGCA CCAGAGAGCCCCCAGATGATG	CATCATCTGGGGGCTCTCTGGTGCTATCAAGCGTGAGA TCGCTGCTAGGTGAGGCGTGCTGCCACCTGTATCCAT CGCCTAATTCGTCTCG
75B.dbl.stop	CGAGACGAATTAGGCGATGGATACAGGTGGCAGCA CGCCTCACCTAGCAGCGATCTCACGCTTGATAGCA CCAGAGAGCCCCCAGATGATG	CATCATCTGGGGGCTCTCTGGTGCTATCAAGCGTGAGA TCGCTGCTAGGTGAGGCGTGCTGCCACCTGTATCCAT CGCCTAATTCGTCTCG
	AAGAAATACTCACTGAACTGTTATCTCCCATGGGAA GCATTTTGATAATTGACATCAATGATTTGCCATAGG GATAACAGGGTAATCGATT	AGACCATGACATACTGGATCTGGCAAATCATTGATGTC AATTATCAAAATGCTCCCATGGGAGATAAGCCAGTGTT ACAACCAATTAACC

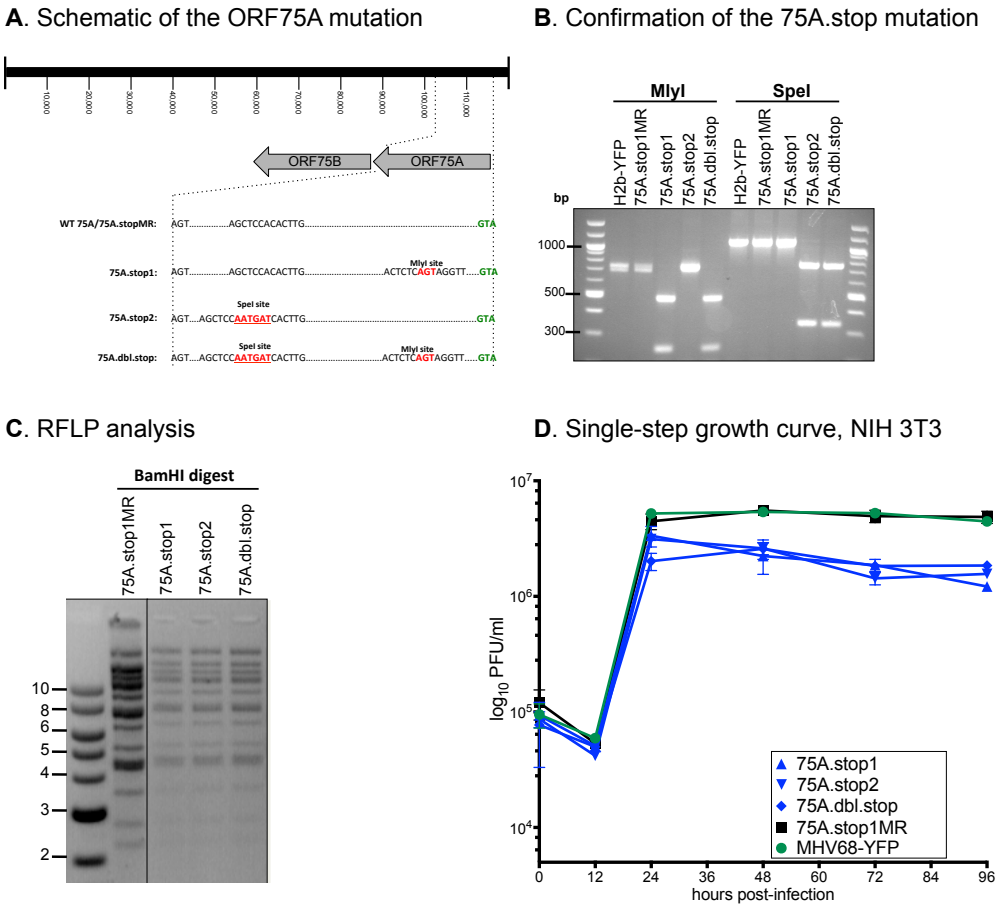

Figure 3.1 Characterization of the ORF75A mutants. (**A**) Schematic of the ORF75A mutation (**B**) Agarose gel showing digestion of a PCR amplified targeting sequence in ORF75A. (**C**) Agarose gel of ORF75A-BAC DNA digested with BamHI. No aberrant bands are observed. (**D**) Single-step growth of ORF75A.stop mutants and WT viruses in the immortalized murine fibroblast line, NIH 3T3.

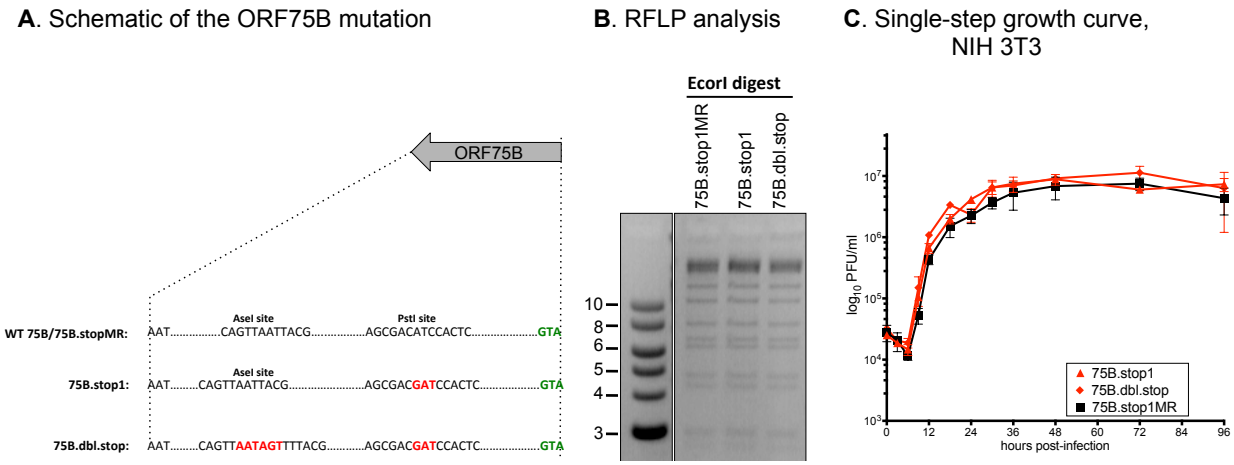

Figure 3.2 Characterization of the ORF75B mutants. (**A**) Schematic of the ORF75B mutation. (**B**) Agarose gel of ORF75B-BAC DNA digested with BamHI. No aberrant bands are observed. (**C**) Single-step growth of ORF75A.stop mutants and WT viruses in the immortalized murine fibroblast line, NIH 3T3.

Loss of the MHV68 ORF75A reduces acute viral replication in the lungs.

The absence of a significant replication defect for the ORF75A.stop and ORF75B.stop viruses in cell culture does not preclude a possible role for these genes in *in vivo* pathogenesis. To identify a role for either ORF75A or ORF75B in replication in the infected animal, we examined acute replication in the lungs of mice infected intranasally using 1000 PFU of each mutant and the respective marker rescue virus. At early timepoints post-infection (4 dpi), we observed robust replication of the 75A.stop1MR viruses in the lung with a mean titer of ~1000 PFU per ml of lung homogenate. In contrast, virus titers from lung homogenate prepared from all five mice infected with 75A.stop1 was below the limit of detection. By 7 dpi, virus replication in the lungs of mice infected with the 75A.stop1MR virus had increased by thirty-five-fold, leading to a mean titer ~2.6 x 10^4 PFU/ml. In contrast, mean titers from the lungs of mice infected with either 75A.stop1, 75A.stop2 and 75A.dbl.stop were much lower, resulting in mean titers of 1.3 x 10^3 PFU/ml, 4.2 x 10^3 PFU/ml and 9.6 x 10^2 PFU/ml, respectively. Interestingly while the 75A.stop1 and 75A.dbl.stop viruses both exhibited about a 20-fold defect in replication within the mouse lung, we only observed a 6-fold reduction in 75A.stop2 lung replication as compared to the 75A.stop1MR virus at 7 dpi. At 9 dpi, we observed comparable levels of virus replication in the lungs of mice infected with either 75A.stop1 or the repaired virus, 75A.stop1MR and by day 12 both 75A.stop1 and 75A.stop1MR had been cleared from the lungs of infected mice. In contrast to the ORF75A mutants, the 75B.stop1 and 75B.dbl.stop viruses replicated to similar levels as the 75B.stop1MR viruses at 7 dpi. Of note, we did not observe any significant difference between peak titers at 7 dpi between our two repaired viruses, 75A.stop1MR and 75B.stop1MR (**Figure 3.3**). Taken together, we conclude that ORF75A promotes replication in the lung while ORF75B is dispensable for replication.

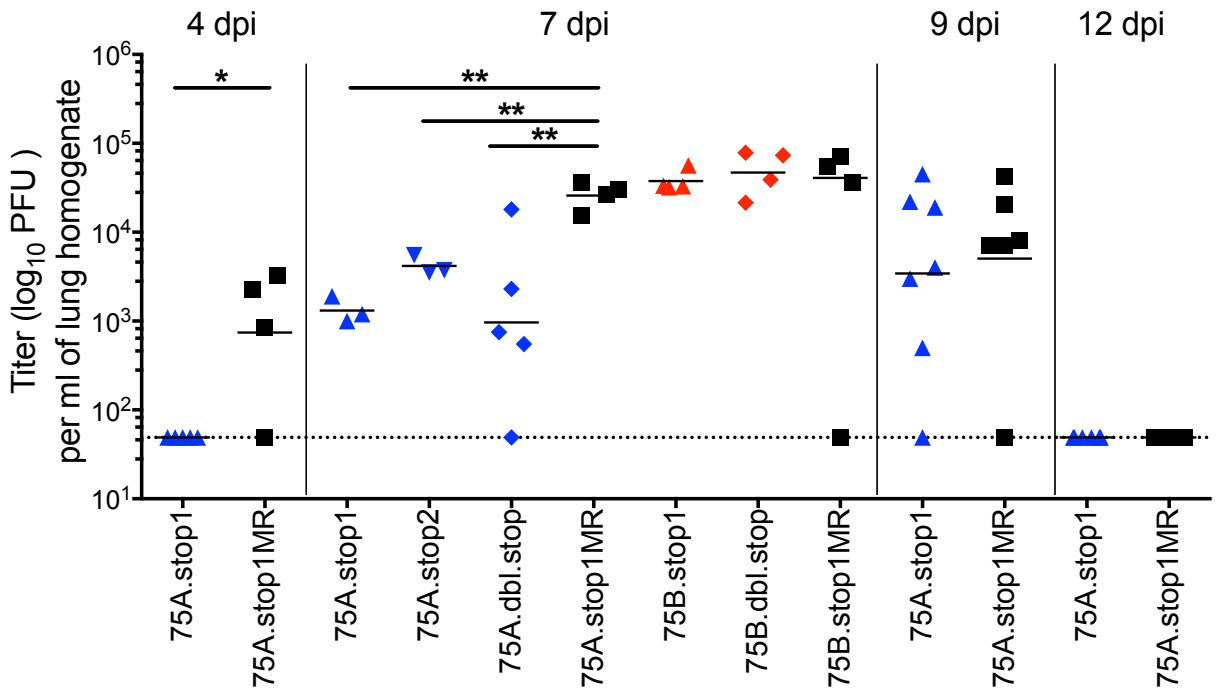

Figure 3.3 ORF75A-stop viruses exhibit a transient defect in acute lung replication. C57BL/6 mice were infected at 1000 PFU by the intranasal route with the indicated viruses. Lung homogenates from mice were titered by plaque assay. Line indicates geometric mean titer. Each symbol represents an individual mouse. WT control viruses are black, ORF75A mutants are blue, and ORF75B mutants are red. The dashed line depicts the limit of detection at 50 PFU/ml of lung homogenate (log_{10} of 1.7), * $p \leq 0.05$. and ** $p \leq 0.005$.

ORF75A is required for the establishment of latency upon intranasal inoculation.

Within two weeks of intranasal infection, virus replication in the lung is fully resolved and the virus transits to the spleen where it targets B lymphocytes. The peak in splenic latency occurs between 14 and 18 dpi and coincides with splenomegaly, which is driven mainly by the expansion of CD4+ T cells (162). Mice infected with the 75A.stop1MR virus exhibited a two-fold increase in splenomegaly at 16 dpi. Mice infected with the 75A.stop1, 75A.stop2 and the 75A.dbl.stop viruses did not exhibit significant splenomegaly as compared to the naïve mice (**Fig. 3.4A**). This defect in splenomegaly correlated with a severe two-log reduction in the frequency of splenocytes that harbor the viral genome in mice infected with the 75A.stop viruses as compared to 75A.stop1.MR (**Fig. 3.4B**). This impairment in latency establishment was accompanied by a similar reduction in the frequency of reactivation from latency upon explant (**Fig. 3.4C, summarized in Table 3.2**). The severity of the defect in the establishment of latency precluded a determination of whether ORF75A plays a role in splenic reactivation. In spite of a severe latency defect at 16 dpi, the frequency of genome-positive splenocytes six weeks after infection with the 75A.stop1 virus was nearly equivalent to 75A.stop1MR (**Fig. 3.4D, summarized in Table 3.3**). In contrast, infection of mice with either 75B.stop1 or 75B.dbl.stop did not significantly influence latency establishment. We observed no difference in the frequency of cells harboring MHV68 genomes between 75B.stop1 and 75B.stop1MR infections. Spleens from 75B.dbl.stop-infected mice exhibited a slight 2.4-fold reduction in the frequency of cells positive for the genome (**Fig. 3.5**). Taken together, this data implicates a role for ORF75A in the establishment but not the maintenance of latency in the spleen after intranasal inoculation of mice. Coupled with the absence of a requirement for ORF75B in acute replication in the lung, we did not observe a role for ORF75B in the establishment of splenic establishment after intranasal infection.

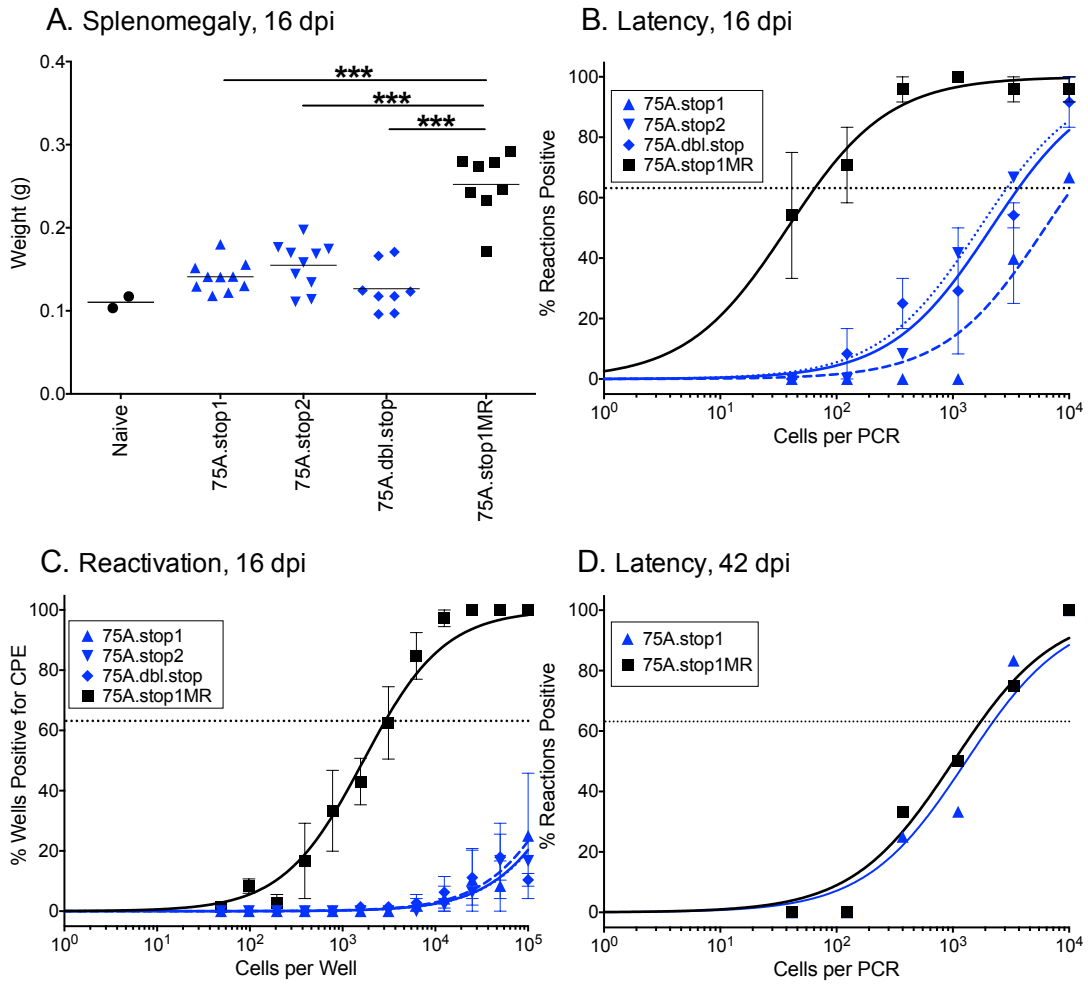

Figure 3.4 MHV68 ORF75A is essential for the establishment of latency in the spleen at early, but not late times during chronic infection after intranasal inoculation. C57BL/6 mice were infected at 1000 PFU by the intranasal route with the indicated viruses. (**A**) Weights of spleens harvested 16 dpi, *** $p \leq 0.001$. (**B**) Frequency of splenocytes harboring latent genomes at 16 dpi. (**C**) Frequency of splenocytes undergoing reactivation from latency upon explant. (**D**) Frequency of splenocytes harboring latent genomes at six weeks post-infection. For the limiting dilution analyses, curve fit lines were determined by nonlinear regression analysis. The dashed lines represent 63.2%. Using Poisson distribution analysis, the intersection of the nonlinear regression curves with the dashed line was used to determine the frequency of cells that were either positive for the viral genome or reactivating virus. Data is generated from at least 2 independent experiments for 16 dpi and one for 42 dpi.

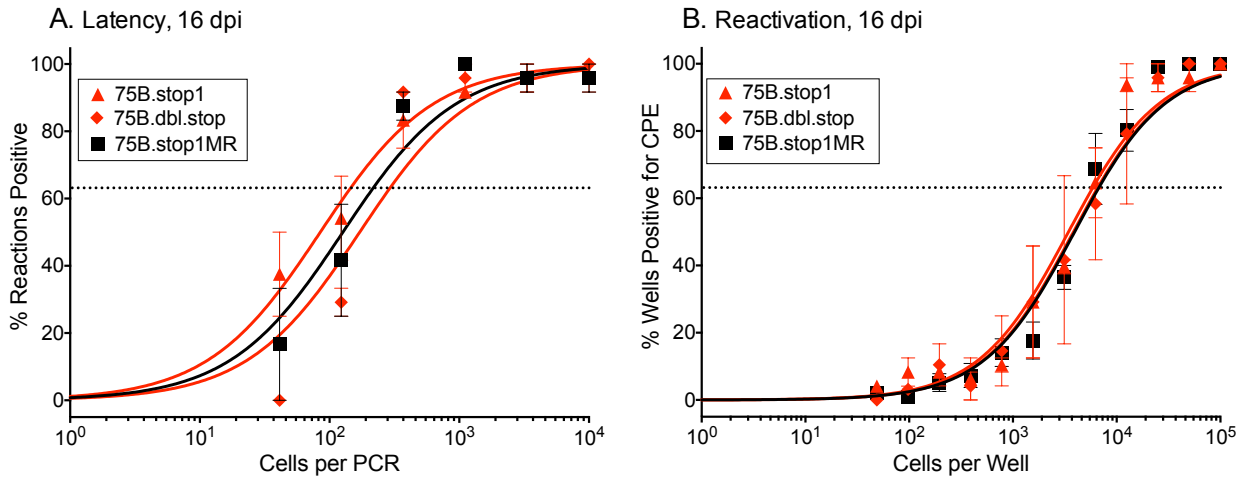

Figure 3.5 MHV68 ORF75B is dispensable for the establishment of latency in the spleen. C57BL/6 mice were infected at 1000 PFU by the intranasal route with the indicated viruses. (**A**) Frequency of splenocytes harboring latent genomes at 16 dpi. (**B**) Frequency of splenocytes undergoing reactivation from latency upon explant. The limiting dilution analyses curve fit lines were determined by nonlinear regression analysis. The dashed lines represent 63.2%. Using Poisson distribution analysis, the intersection of the nonlinear regression curves with the dashed line was used to determine the frequency of cells that were either positive for the viral genome or reactivating virus. Data is generated from at least 3 independent experiments for 16 dpi.

Bypassing the lung via intraperitoneal inoculation rescues the splenic latency defect of murine gammaherpesvirus lacking ORF75A.

The intranasal route of infection identified a critical role for ORF75A in seeding the spleen. We next bypassed lung replication using direct administration of virus by intraperitoneal (IP) inoculation. We observed an increase in spleen weights in mice infected with 75A.stop1 or 75A.stop1MR. However, while spleens harvested from 75A.stop1MR-infected mice were four-fold larger than naïve mouse spleens, we observed only a two-fold increase in spleen weight in 75A.stop1-infected mice (**Fig. 3.6**).

In agreement with the reduced splenomegaly in 75A.stop1-infected spleens, we observed a five-fold reduction in the frequency of splenic cells harboring the viral genome upon 75A.stop1 infection as compared to 75A.stop1MR infection (1/705 vs. 1/139). The frequency of cells reactivating virus was also reduced by four-fold in 75A.stop1 infections (1/54,005 vs. 1/12,202 respectively) (**Fig. 3.6**). At six weeks post infection, we did not observe any differences in spleen weight or the frequency of genome-positive cells after 75A.stop1 or 75A.stop1MR infection (**Fig. 3.7**). Thus, although the defect in splenic latency establishment after intranasal 75A.stop1 infection is reduced upon a change in the route of virus administration to a direct intraperitoneal inoculation, a significant role for ORF75A in the establishment of splenic latency remained.

A. Splenomegaly, 18 dpi

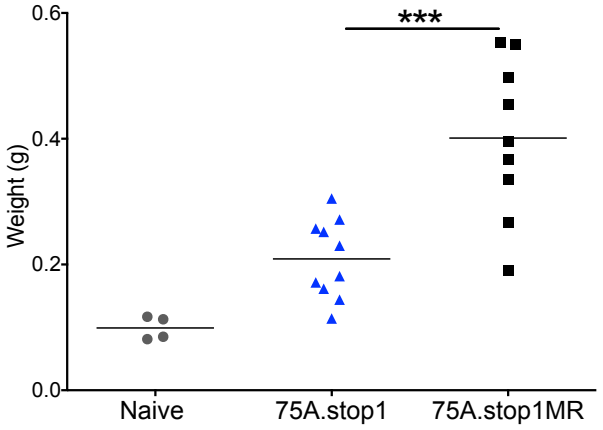

B. Latency, 18 dpi

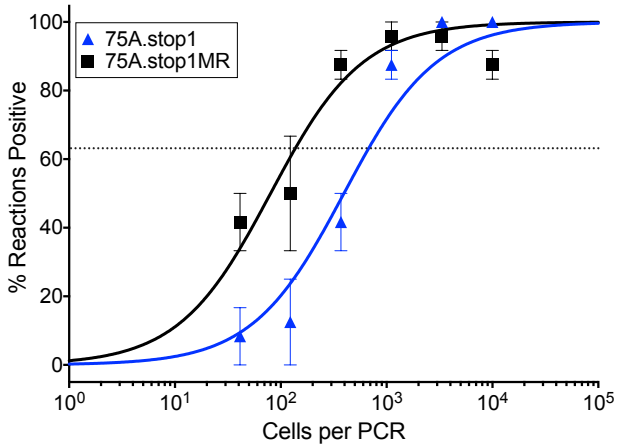

C. Reactivation, 18 dpi

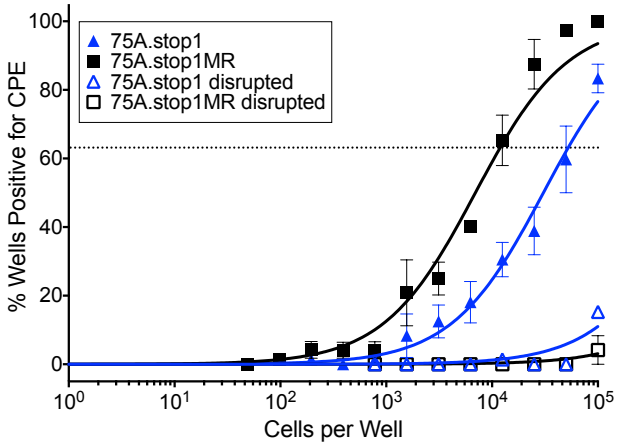

Figure 3.6 Intraperitoneal administration of MHV68 largely rescues the ORF75A.stop1 latency establishment defect. (A) Weights of spleens harvested from the indicated infections 18 dpi. Each symbol represents an individual mouse, t-test *** $p \leq 0.001$. **(B)** Frequency of splenocytes harboring latent genomes 18 dpi. **(C)** Frequency of splenocytes spontaneously reactivating from latency 18 dpi. For the limiting dilution analyses, curve fit lines were determined by nonlinear regression analysis. The dashed lines represent 63.2%. Using Poisson distribution analysis, the intersection of the nonlinear regression curves with the dashed line was used to determine the frequency of cells that were either positive for the viral genome or reactivating virus. Data is generated from three independent experiments for 18 dpi.

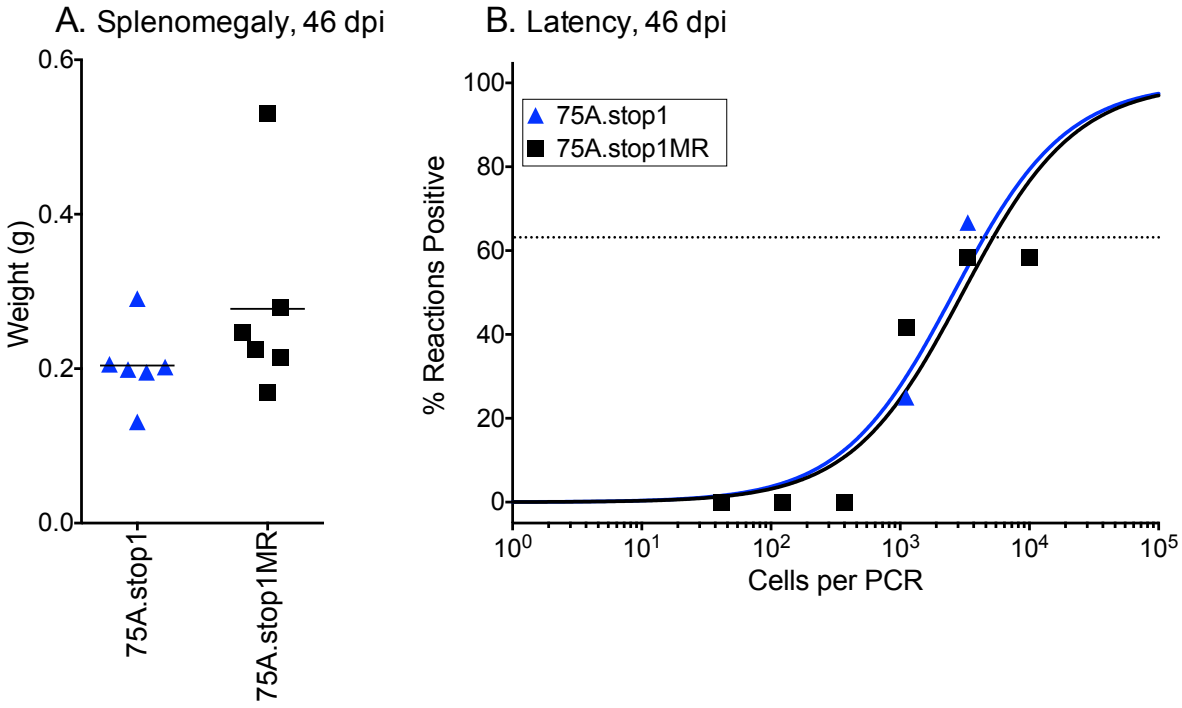

Figure 3.7 Loss of ORF75A does not impact maintenance of latency after intraperitoneal inoculation. (A) Weights of spleens harvested from the indicated infections 46 dpi. Each symbol represents an individual mouse. **(B)** Frequency of splenocytes harboring latent genomes 46 dpi. For the limiting dilution analyses, curve fit lines were determined by nonlinear regression analysis. The dashed lines represent 63.2%. Using Poisson distribution analysis, the intersection of the nonlinear regression curves with the dashed line was used to determine the frequency of cells that were either positive for the viral genome or reactivating virus.

ORF75A is dispensable for latency in peritoneal exudate cells.

In addition to the major latency reservoir, B lymphocytes, MHV68 latency is also established in macrophages and dendritic cells (60). We examined the role for ORF75A in latency establishment in peritoneal exudate cells (PEC), which are comprised largely of macrophages. Loss of the ORF75A did not influence the frequency of genome positive cells 18 days after IP inoculation. Additionally, we did not observe a reduction in explant reactivation from PECs following infection with 75A.stop1 as compared to 75A.stop1MR **(Fig. 3.9, summarized in Table 3.2 and Table 3.3)**. We conclude that MHV68 latency establishment and reactivation from latency in the peritoneal compartment is independent of ORF75A.

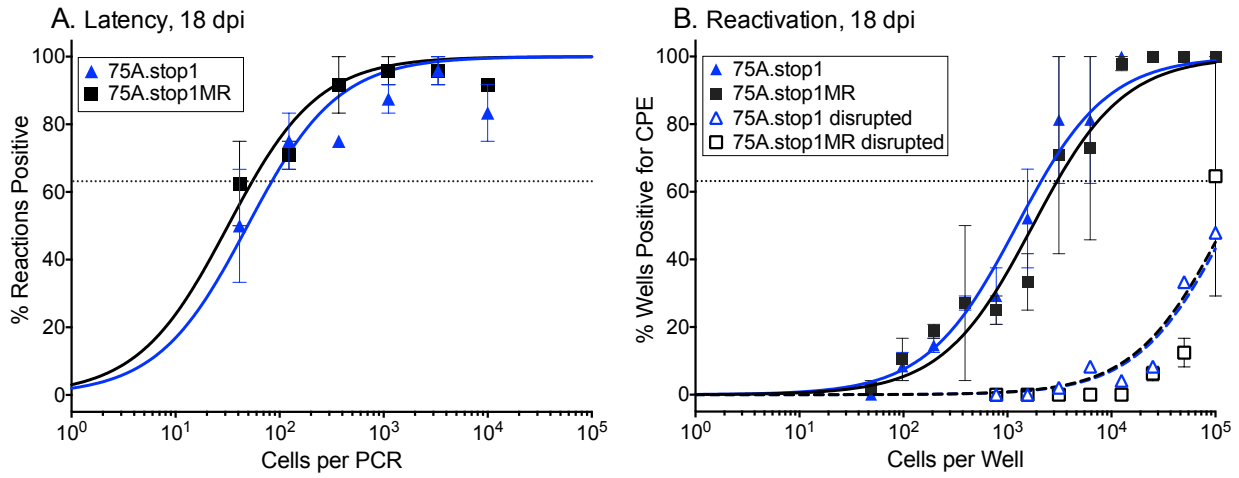

Figure 3.8 MHV68 ORF75A is not required for the establishment or reactivation of latency in the peritoneal exudate compartment after intraperitoneal inoculation. C57BL/6 mice were infected at 1000 PFU by the intraperitoneal route with the indicated viruses. (A) Frequency of peritoneal exudate cells harboring latent genomes 18 dpi (B) Frequency of splenocytes spontaneously reactivating from latency 18 dpi. For the limiting dilution analyses, curve fit lines were determined by nonlinear regression analysis. The dashed lines represent 63.2%. Using Poisson distribution analysis, the intersection of the nonlinear regression curves with the dashed line was used to determine the frequency of cells that were either positive for the viral genome or reactivating virus. Data is generated from at least 2 independent experiments

Table 3.2. Frequencies of cells harboring viral genomes in C57BL/6 mice.

Virus[a]	Route of infection[b]	Organ[c]	dpi	Total # of cells harvested	Frequency of genome-positive cells (one in) [d]	Total # of cells positive for latent virus [e]
75A.stop1MR	i.n.	Spleen	16	1.7×10^9	65	2.6×10^7
			42	7.5×10^8	1760	4.3×10^5
75A.stop1	i.n.	Spleen	16	0.6×10^9	10841	5.5×10^4
			42	7.5×10^8	2282	3.3×10^5
75A.stop2	i.n.	Spleen	16	0.6×10^9	2960	2.0×10^7
75A.dbl.stop	i.n.	Spleen	16	0.7×10^9	3727	1.9×10^5
75A.stop1MR	i.p.	Spleen	18	1.2×10^9	138	8.7×10^6
	i.p.		46	4.3×10^8	5269	8.2×10^4
75A.stop1	i.p.	Spleen	18	0.8×10^9	699	1.1×10^6
	i.p.		46	4.1×10^8	4561	9.0×10^4
75A.stop1MR		PEC	18	4.4×10^7	55	8.0×10^5
75A.stop1	i.p.	PEC	18	3.5×10^7	85	4.1×10^5
75B.stop1	i.n.	Spleen	16	1.3×10^9	147	8.8×10^6
75B.dbl.stop	i.n.	Spleen	16	0.9×10^9	404	2.2×10^6
75B.stop1MR	i.n.	Spleen	16	1.5×10^9	123	1.2×10^7

[a] Infection with recombinant MHV68 viruses
[b] i.n., intranasal; i.p., intraperitoneal
[c] Organ harvested for limiting dilution analysis
[d] The frequency data were determined from the mean of at least two independent experiments with cells from the indicated organs. Organs were pooled from three to five mice per experiment.
[e] The total number of genome positive cells per mouse was extrapolated using the frequency value generated from the limiting dilution analysis together with the total number of splenocytes or PEC cells harvested.

Table 3.3. Frequencies of cell populations reactivating viral genomes in C57BL/6 mice.

Virus[a]	Route of infection[b]	Organ[c]	dpi	Total # of cells harvested	Frequency of genome-positive cells (one in) [d]	Total # of cells reactivating latent virus [e]
75A.stop1MR	i.n.	Spleen	16	1.7×10^9	2,894	5.9×10^6
			42	7.5×10^8	n.d	n.d
75A.stop1	i.n.	Spleen	16	0.6×10^9	<100,000	$<6.4 \times 10^4$
			42	7.5×10^8	n.d	n.d
75A.stop2	i.n.	Spleen	16	0.6×10^9	<100,000	$<6.4 \times 10^4$
75A.dbl.stop	i.n.	Spleen	16	0.7×10^9	<100,000	$<7.0 \times 10^4$
75A.stop1MR	i.p.	Spleen	18	1.2×10^9	12,030	9.9×10^4
	i.p.		46	4.3×10^8	n.d	n.d
75A.stop1	i.p.	Spleen	18	0.8×10^9	54,005	1.5×10^4
	i.p.		46	4.1×10^8	n.d	n.d
75A.stop1MR		PEC	18	4.4×10^7	3,007	1.5×10^4
75A.stop1	i.p.	PEC	18	3.5×10^7	2,126	1.6×10^4
75B.stop1	i.n.	Spleen	16	1.3×10^9	6,095	2.1×10^5
75B.dbl.stop	i.n.	Spleen	16	0.9×10^9	6,751	1.3×10^5
75B.stop1MR	i.n.	Spleen	16	1.5×10^9	6,751	2.2×10^5

[a] Infection with recombinant MHV68 viruses
[b] i.n., intranasal; i.p., intraperitoneal
[c] Organ harvested for limiting dilution analysis
[d] The frequency data were determined from the mean of at least two independent experiments with cells from the indicated organs. Organs were pooled from three to five mice per experiment.
[e] The total number of cells reactivating latent virus per mouse was extrapolated using the frequency value generated from the limiting dilution analysis together with the total number of splenocytes or PEC cells harvested.

Discussion

We previously identified roles for transposon-disrupted ORF75A and ORF75B mutants in cell culture replication and pathogenesis in mice (**see Chapter 2**). However, there were concerns about the influence of the large transposon insertion on the integrity of neighboring genes and uncharacterized transcripts antisense to the ORF75 locus. We disrupted ORF75A and ORF75B with the insertion of a series of all frame stops into the protein coding sequences of either ORF75A or ORF75B. Disruption of ORF75B did not influence replication in cell culture or pathogenesis in the infected mouse. ORF75A was largely dispensable for replication in immortalized fibroblasts in cell culture, yet intranasal infection of mice with the ORF75A.stop viruses led to a transient replication defect in the lungs of infected mice and a delay in latency establishment and reactivation in the spleen. By six weeks post-infection, the severe defect in the initial latency establishment at 16 dpi was not observed. A bypass of the respiratory tract infection by a direct intraperitoneal inoculation partially rescued the defect in latency establishment observed with the ORF75A mutant. Thus we identified route-dependent roles for ORF75A in MHV68 replication and latency in the host. These are the first *in vivo* roles identified for a member of the gammaherpesvirus vFGARAT tegument proteins.

Intranasal infection with MHV68 ΔORF75A resulted in a transient reduction in replication in lung tissues that impaired latency establishment in the spleen. However, this latency defect was partially rescued by changing the route of virus administration to intraperitoneal inoculation to bypass the lung. This observation supports a role for ORF75A in MHV68 dissemination from initial sites of virus entry or replication to seed latent reservoirs. However, this finding is not limited to ORF75A. The influence of acute replication defects in the lung on the establishment of latency after intranasal inoculation is well documented. Indeed MHV68 genes necessary for gene expression (163, 164) or DNA replication (165-170) all fail to establish WT levels of latency in the spleens of infected mice after intranasal inoculation. Similar to the observation with ORF75A.stop infected mice, splenic latency could be partially (164) or fully restored (165-169) after altering the route of infection or dramatically increasing virus dose. Together, these observations imply a critical role for lytic replication in seeding the latent splenic

reservoir after intranasal inoculation. It remains to be determined if these phenotypes simply represent an inability to replicate in mucosal tissues at sites of entry or represent an inability to efficiently infect immune cells critical for the dissemination of MHV68 to the B cells in the spleen.

MHV68 infection *in vivo* does not result in high levels of cell-free virus (162), and the virus depends on cell-to-cell spread for efficient propagation (171). Recent studies have extended these observations further to demonstrate that MHV68 exploits normal immune cell trafficking routes to seed the latent lymphoid reservoir. Using recombinant viruses that enabled the cell-types that the MHV68 infects to be tracked over time, the authors found that virus recovered from the spleen after intranasal infection had passed through $lysM^+$, $CD11c^-CD11b^+$ and $CD11c^+$ myeloid cells (56, 172). Thus MHV68 utilizes dendritic cells and macrophages for dissemination from mucosal epithelia to B cells in secondary lymphoid tissues. Future experiments are required to determine whether the ORF75A latency defect in the spleen is mediated by defects in replication within specific subsets of cells in the lung or the draining mediastinal lymph node.

The frequency of splenocytes harboring the viral genome was severely reduced with loss of ORF75A at 16 dpi. However by 42 dpi, we did not observe any differences in latency between 75A.stop1 and 75A.stop1MR-infected spleen. Given the defects in latency establishment at 16 days post-intranasal infection with 75A.stop viruses, it was surprising that the maintenance of latency was not influenced as well. Like EBV and KSHV, MHV68 persists in germinal center derived B cells and establishes long term latency in immunoglobulin isotype-switched memory B cells (60). Given the absence of a defect in the maintenance of viral latency we predict that loss of ORF75A does not influence MHV68 residency in these B cell subsets. Future experiments will require isolation of specific subsets by flow cytometry for latency analysis.

While intraperitoneal infection partially rescued the ORF7A.stop splenic latency defect, the frequency of cells harboring MHV68 genomes was five-fold lower in spleens infected with the 75A mutant as compared to the marker rescue/WT virus. This observation of reduced latency implicates a role for ORF75A in promoting productive replication in B cells or a cell type that precedes B cell infection in the spleen. Prior studies with viruses mutated in genes essential for

lytic replication, reported a defect in the establishment of splenic latency after intraperitoneal infection (163, 170). This has established a working model in which early gene expression or early events in productive replication are required to seed the latency reservoir in the spleen. MHV68 may utilize cell-to-cell spread to disseminate from the lungs to the spleen. Moreover, once in the spleen, the virus is thought to exploit the normal routes of interaction between immune cells in the spleen to access germinal center B cells to establish latency. Specifically, upon entering the spleen, MHV68 infects marginal zone macrophages, which then transfer the virus to marginal zone B cells. The movement of the marginal zone B cells into the white pulp of the spleen enables the transfer of virus to follicular dendritic cells (55). Finally, the follicular dendritic cells are responsible for the transfer of MHV68 from the marginal zone B cells to germinal center B cells. Interestingly, an ORF50-null virus (replication-defective virus) is impaired in the seeding of marginal zone macrophages, implying a role for lytic replication at this early step of splenic colonization by MHV68 (55). On the other hand, a virus mutated in the ORF27 glycoprotein is slightly attenuated for lytic replication in cell culture, but after intraperitoneal inoculation remains in the marginal zone and does not seed B cells in the white pulp and is impaired for latency establishment (55). ORF27 encodes a glycoprotein that facilitates intercellular spread, implying a requirement for cell to cell spread in the establishment of latency (171). Thus, defects in lytic replication and intercellular spread can impact latency establishment in the spleen even after direct intraperitoneal infection. Future experiments might determine whether ORF75A.stop viruses exhibit any defects in transmission between the lymphoid and myeloid cell reservoirs, a process that is necessary for the efficient establishment of latency in the spleen.

Interestingly, latency establishment in peritoneal exudate cells was not impacted with loss of ORF75A. This was not wholly surprising, as seeding of the PEC latency reservoir has been independent of many MHV68 genes with roles in lytic replication in cell culture or acute replication in the lungs of infected mice. Indeed, apart from the ORF50/RTA null virus, infection with other replication-defective viruses did not impair PEC latency (163, 170). We reason that intraperitoneal inoculation allows direct access to the cells within the peritoneum and so the

requirement for lytic expansion to produce virus to seed the latent reservoir is mostly eliminated. Therefore, only the most defective lytic viruses such as an ORF50/RTA null virus are impacted in this reservoir. As such, the requirements for viral gene expression in a cellular environment conducive to latency establishment may vary with cell-type.

Our data define a role for the MHV68 ORF75A in promoting lytic replication at the site of initial infection in the host to influence the dissemination and establishment of latency in distal reservoirs. Additionally, we also identified a specific role for ORF75A in direct seeding of the splenic reservoir. The requirement for infecting the myeloid or the lymphoid cells in the spleen prior to germinal center B cell infection remains to be determined. Importantly we have identified a role for the gammaherpesvirus vFGARATs apart from ORF75C. We did not observe a role for ORF75B in cell culture replication or in the pathogenesis of mice. We propose that ORF75B may function in a cell-type not assayed thus far or it may posses overlapping functions with ORF75A and/or ORF75C such that its function is compensated by ORF75A or ORF75C. We next undertook a close examination of ORF75A in models of lytic replication in cell culture to elucidate the mechanisms that drive ORF75A.stop virus phenotypes.

Chapter 4: ORF75A.stop viruses exhibit profound defects in replication in Bone Marrow derived macrophages.

Introduction

In the preceding chapter, we generated and tested a panel of recombinant MHV68 viruses to identify roles for ORF75A in pathogenesis. ORF75A-null viruses exhibited a defect in acute replication in the lungs of infected mice that translated to over a 2-log defect in latency establishment after intranasal inoculation. Although we partially rescued this latency defect by intraperitoneal inoculation, we observed a 0.5-log defect in splenic latency upon infection with ORF75A.stop. MHV68 replicates in alveolar epithelial cells (59), traffics to the spleen after replication in myeloid cells and infects splenic macrophages and dendritic cells prior to establishing latency in B cells (55, 56, 172). Given that our largest defect is in latency establishment after intranasal inoculation, we reason that ORF75A is likely required for productive infection in multiple cell types. With respect to ORF75B, we hypothesize that the absence of a phenotype might imply an overlap of function with the other copies of vFGARATs encoded by MHV68.

In this chapter we utilized replication defective ORF75C mutant viruses to examine overlap in function between ORF75B and ORF75C. Of note, ORF75A did not rescue ORF75C defective viruses for gene expression implying at least one unique role for ORF75A in MHV68 replication. We confirmed that ORF75A is a *bona fide* protein made during MHV68 replication and developed a recombinant virus with an epitope tagged ORF75A virus to be used for further characterization. Lastly, we have established that loss of ORF75A impairs virus replication in culture with a concomitant dysregulation of tegument delivery and acceleration in the kinetics and levels of viral proteins. Additionally, in bone marrow derived macrophages, we also observed an enhancement in CPE induced by the ORF75A.stop virus. These data demonstrate that ORF75A is critical for lytic replication and influences both early and late events in MHV68.

Future studies will identify ORF75A binding partners as well as motifs critical for the aforementioned ORF75A.stop phenotypes. Additionally, It remains to be seen if ORF75A and ORF75B share other functions as well.

Materials and Methods

Generation of recombinant viruses. The modified MHV68-H2bYFP genome cloned into a BAC was a kind gift from the Speck laboratory (161). MHV68-H2bYFP-3XFLAG ORF75A and the MHV68-H2bYFP-ORF75C.stop and ORF75CΔFGAM viruses were all generated using *en passant* mutagenesis (45). Briefly, forward and reverse primers (**Table 4.1**) containing each ORF75C mutation were used to amplify the kanamycin (Kan) selection marker from plasmid pEPKanS2 (45) by PCR (One Taq DNA polymerase, New England Biolabs, Ipswich MA). This PCR product was excised from the gel, digested with *Dpn*I to remove input template, and transformed into freshly prepared electrocompetent *E. coli* harboring the MHV68-H2bYFP BAC. After recovery, the bacterial cells were plated on dual chloramphenicol (34 ug/ml) / Kan (50 ug/ml) plates and incubated at 30°C for 48 hrs. DNA was prepared from isolated colonies and the Kan selection marker in *Orf75A* or *Orf75C* was PCR amplified to verify the insertion of the mutagenesis cassette into the MHV68-H2bYFP BAC. The kanamycin selection marker was removed, leaving behind the desired ORF75A or ORF75C mutation. The *Orf75A* or *Orf75C* gene was PCR amplified from the putative mutant BAC, digested with a restriction enzyme unique to each mutation to confirm the presence of each stop codon. Virus passage and titer determination were performed as previously described (58).

Analysis of recombinant viral BAC DNA. BAC DNA was prepared by Qiagen column purification. For restriction fragment length polymorphism analysis, 10 μg of BAC DNA was digested overnight with the desired restriction enzyme and then resolved in a 0.8% agarose gel in 0.5X TAE.

Cell Culture. Primary murine embryonic fibroblast (MEF) cells were isolated from C57BL/6 mice and maintained in Dulbecco's modified Eagle's medium supplemented with 10% fetal calf serum, 100 U of penicillin per ml and 100 mg of streptomycin per ml at 37^{o}C in 5% CO_2. Immortalized murine fibroblast cells (NIH 3T3 or NIH 3T12) were maintained in Dulbecco's

modified Eagle's medium (DMEM) supplemented with 8% fetal calf serum, 100 U of penicillin per ml and 100 mg of streptomycin per ml at 37^{o}C in 5% CO_2. To generate bone marrow-derived macrophages (BMDMs), bone marrow from 8-12 week old mice was flushed from the femur and differentiated for 5 days in DMEM with Glutamax (Life Technologies, Grand Island, NY) containing 10% FBS and 30% L-supplement (BMM-Hi) in non-tissue culture treated plates. Cells were maintained in DMEM with Glutamax containing 10% FBS and 10% L-supplement (BMM-low) in non-tissue culture treated plates.

Plasmids and Transfections.

DNA encoding MHV68 ORF75A, ORF75B and ORF75C were generated by PCR amplification from WT MHV68 BAC DNA. ORF75A was amplified using PCR primers: Forward primer 5'GAGGCGGCCGCATCAGACGACTTTATTTGGACATTGAG3'and Reverse primer 5'CGCCAATTGTCAGGTTTCTCTTGCTGCCAGTGC 3' prior to being cloned into the NotI and EcorI sites of p3XFLAGMyc-CMV-24. ORF75B was amplified using PCR primers: Forward primer 5'GCGAAGCTTGATGAGGACGTCTGGGCAATCCAAG3'and Reverse primer 5'GCGGTCGAC TTACAGACCATCGGTGGATAGTGTCC3' prior to being cloned into the HindIII and SalI sites of p3XFLAGMyc-CMV-24. ORF75C was amplified using PCR primers: Forward primer 5'GCGAAGCTTGCTAGACACTTTGCCTTTATC3'and Reverse primer 5'GCGGTCGACCTAATCTCTAGATGCCAATGAC3' prior to being cloned into the HindIII and SalI sites of the p3XFLAGMyc-CMV-24 expression vector (Sigma, St. Louis MO).

For transient co-transfections, 4 x 10^5 HEK 293T cells were seeded into each well of a 12-well tissue culture plate one day prior to transfection with 50 ng or 100 ng of MHV68-H2bYFP-ORF75C-stop BAC DNA and 500 ng of the vFGARAT expression plasmid. All transient co-transfections were performed using TransIT-LT1 Transfection Reagent according to the manufacturer instructions (Mirus, Madison WI). Seventy-two hours later, the cell lysates were harvested for YFP expression by flow cytometry or for immunoblotting analysis.

Fluorescence microscopy

Virus infection with MHV68-H2bYFP ORF75C.stop or MHV68-H2bYFP ORF75CΔFGAM was visualized by fluorescence microscopy. MHV68-H2bYFP ORF75CΔFGAM imaging was performed with a Zeiss Axiovert S100 inverted microscope (Carl Zeiss Microscopy GmbH, Jena Germany) equipped with a Luminera INFINITY 3-1UR 1.4 megapixel low light CCD digital camera (Lumenera, Ottawa ON Canada). Images were analyzed using Axiovision Software (Axiovision LE Rel.4.3, Carl Zeiss Microscopy GmbH, Jena Germany).

Antibodies and immunoblotting. Total protein lysate was harvested in lysis buffer (150 mM sodium chloride, 1.0% IGEPAL CA-630, 0.5% sodium deoxycholate, 0.1% sodium dodecyl sulfate, 50 mM Tris pH 8.0) supplemented with a protease inhibitor cocktail (Sigma, St. Louis MO) and PMSF. 50 μg of each lysate was separated on a gradient 4-15% SDS PAGE gel (Bio rad, Hercules CA) and transferred to polyvinylidene fluoride membrane. ORF59 and ORF75C were detected using affinity-purified chicken anti-peptide antibodies against MHV68 ORF59 (173) and ORF75C (169). For ORF65 detection, a rabbit polyclonal antibody was used (kind gift from Dr. Ren Sun, UCLA) (174)**.** A rabbit polyclonal antibody to glyceraldehyde 3-phosphate dehydrogenase (GAPDH) (Sigma) was used as a loading control. ORF57 was detected using a rabbit polyclonal antibody generously provided by Dr. Paul Ling, Baylor College of Medicine (106). Mouse PML was detected using a monoclonal antibody generated with a His-tagged PML fusion protein corresponding to amino-acids 1-581 of mouse PML (EMD Millipore Corporation, Temecula CA). FLAG-tagged vFGARAT protein expression was detected with a monoclonal mouse anti-FLAG antibody (F1804) (Sigma). HRP-conjugated secondary antibodies were detected using an enhanced chemiluminescence reagent (ECL, Thermo Scientific, Waltham MA). Immunoblot images were captured using the Image quant LAS 500 chemiluminescence imager (GE Healthcare Biosciences, Pittsburgh PA).

Virus growth curves. To measure virus replication, 0.9×10^5 of primary murine embryonic fibroblasts were seeded into each well of a 12-well tissue culture plate one day prior to infection at a multiplicity of infection (MOI) of 5 or 0.05. For virus growth in bone-marrow derived

macrophages, 2 x 10^5 cells were seeded into each well of a 12-well tissue culture plate two days prior to infection at a MOI of 5. Triplicate wells were harvested for each timepoint, and the cell homogenate was stored at -80°C. Serial dilutions of cell homogenate were used to infect NIH 3T12 cells and then overlayed with 1.5% methylcellulose in DMEM supplemented with 5% FBS. One week later, the methylcellulose was removed and cells were washed twice with PBS prior to methanol fixation and staining with a 0.1% crystal violet solution in 10% methanol.

Statistical analyses. Data were analyzed using GraphPad Prism Software (Prism 5, La Jolla CA). Statistical significance was determined using a non-paired two-tailed t-test.

Results

Expression of MHV68 ORF75B but not ORF75A complements gene expression and replication of ORF75C mutant viruses.

The data in the preceding chapter identified a role for ORF75A but not ORF75B in MHV68 replication and pathogenesis. This observation implies that ORF75A plays a novel role in MHV68 replication that is distinct from ORF75C function. However we cannot rule out the possibility that ORF75A and ORF75C retain redundant functions and the phenotypes we observe for ORF75A.stop are simply due to a specific cell-type or a stage in the virus lifecycle where ORF75C expression is restricted. Moreover the lack of an ORF75B.stop phenotype may be due to an overlapping role with ORF75C.

To examine shared functions in MHV68 replication between ORF75A, ORF75B and ORF75C, we used a trans-complementation assay as reported for the rescue of replication of recombinant MHV68 viruses with mutations in essential genes (50, 90). We examined trans-complementation of replication defective ORF75C mutants upon cotransfection of a BAC clone of the ORF75C mutant viruses with ORF75A and ORF75B expression constructs. The first mutant virus ORF75C.stop was generated based on a prior report (106). For the ORF75CΔFGAM virus, we targeted a region of high sequence conservation between the viral and host FGARATs predicted to encode a nucleotide-binding pocket and mutated this stretch of amino acids to alanines by allelic exchange. We confirmed the insertion of the stop and FGAM motif mutations by amplification and digestion of the target region encoding the mutation with novel restriction sites, BamHI (ORF75C.stop) or NsiI (ORF75CΔFGAM) (data not shown). Consistent with previous reports (85, 106), insertion of either mutation in ORF75C rendered the virus unable to replicate in fibroblasts or African green monkey kidney epithelial Vero cells such that we could not generate virus stocks upon transfection of the ORF75C mutant BAC. These data demonstrate that ORF75C is essential for MHV68 replication.

We transfected HEK 293T cells with 100 ng of either the H2b-YFP ORF75C.stop BAC DNA or H2b-YFP ORF75CΔFGAM BAC DNA and 500 ng of either an empty plasmid or a

plasmid encoding the MHV68 vFGARAT genes, ORF75A, ORF75B and ORF75C. The MHV68 ORF75C.stop and ORF75CΔFGAM viruses were generated on the H2b marking virus background allowing us to visualize infected cells by detection of histone 2B tethered YFP expression (161). YFP expression served as a visual indication of virus replication by fluorescence microscopy and was quantitated by flow cytometry. Protein lysates were examined in immunoblots to monitor the transiently expressed ORF75 proteins and other viral proteins. Cells co-transfected with the ORF75C.stop BAC and the empty vector of ORF75A exhibited limited YFP expression resulting in ~5% of YFP+ cells in the culture 72 hrs after transfection (**Fig. 4.1A second and third panels and Fig. 4.1B**). Co-transfection with either ORF75B or ORF75C rescued YFP expression and increased the number of YFP+ foci implying cell-to-cell spread of MHV68 within the culture (**Fig. 4.3A fourth and 5th panels and Fig. 4.1B**). Viral protein levels by immunoblot supported the YFP data. Lysates prepared from co-transfections with the empty plasmid contained low levels of the immediate early ORF57 that was increased with the expression of ORF75C. The exogenous addition of ORF75B DNA resulted in ORF57 protein expression at levels similar to cells expressing ORF75C. In contrast to the complementation observed for ORF75B and ORF75C, exogenous addition of ORF75A did not complement an ORF75C.stop virus for ORF57 expression (**Fig. 4.1C**).

We observed a similar trend upon trans-complementation of the ORF75CΔFGAM BAC with only the pCMV24-FLAG expression plasmid; the infection was predominatly limited to single YFP+ cells (**Fig. 4.2A, first panel from left**). In contrast, co-transfection with the ORF75C expressing plasmid resulted in multiple foci of YFP+ cells indicating that ORF75C rescues the ability of the virus to replicate and spread to neighboring cells (**Fig. 4.2A, fourth panel**). Co-transfection of ORF75B with the ORF75CΔFGAM BAC DNA also resulted in an increase in YFP+ foci (**Fig. 4.2A,third panel**). In contrast, co-transfection with ORF75A only slightly increased the number of YFP+ single cells and did not significantly increase the number of YFP+ foci in the infection (**Fig. 4.2A, second panel**). In agreement with the fluorescence microscopy data, expression of the early gene ORF59 (DNA polymerase processivity factor) was not detected upon co-transfection of the ORF75CΔFGAM BAC with the empty vector control.

Addition of either ORF75C or ORF75B resulted in detectable ORF59 protein expression. In contrast, the addition of ORF75A did not result in ORF59 protein expression (**Fig. 4.2B**). We identified a role for a region in the conserved FGAM motif of ORF75C and all vFGARAT and host FGARATs in MHV68 replication. Taken together, the trans-complementation of virus spread and lytic protein production by ORF75B implies overlapping roles in virus replication between ORF75B and ORF75C. In contrast, ORF75A does not seem to have conserved ORF75C functions.

Table 4.1. Mutagenic primers used in the generation of the ORF75C mutant viruses		
Mutant	**Forward primer (5' to 3')**	**Reverse primer (5' to 3')**
75C.stop	ATAACAAAACCACCAACAAGAACTGGTCCGTCTCG CCATGTGAGGATCCTTTTGCCTTTATCTATTTTGGT GATAGGATAACAGGGTAATCGATT	CTGTCTCATTATATTGACTATCACCAAAATAGATAA AGGCAAAAGGATCCTCACATGGCGAGACGGACCA GTTGCCAGTGTTACAACCAATTAACC
75CΔFGAM	TCTGGCACATGCTCTGGAGATGTTGACATCACGCA CCGCCGCACTAGCTATGGCCGCTGCAAGCGCCGC CGCTGCAGCTGCCGCCGCCATTTTGGAGATGGCT AGGGATAACAGGGTAATCGATTT	ATCCCTTATTTCCAGCCATGGCCATCTCCAAAATG GCGGCAGCTGCAGCGGCGGCGCTTGCAGCGGCC ATAGCTAGTGCGGCGGTGCGTGATGTCAACAGCC AGTGTTACAACCAATTAACC

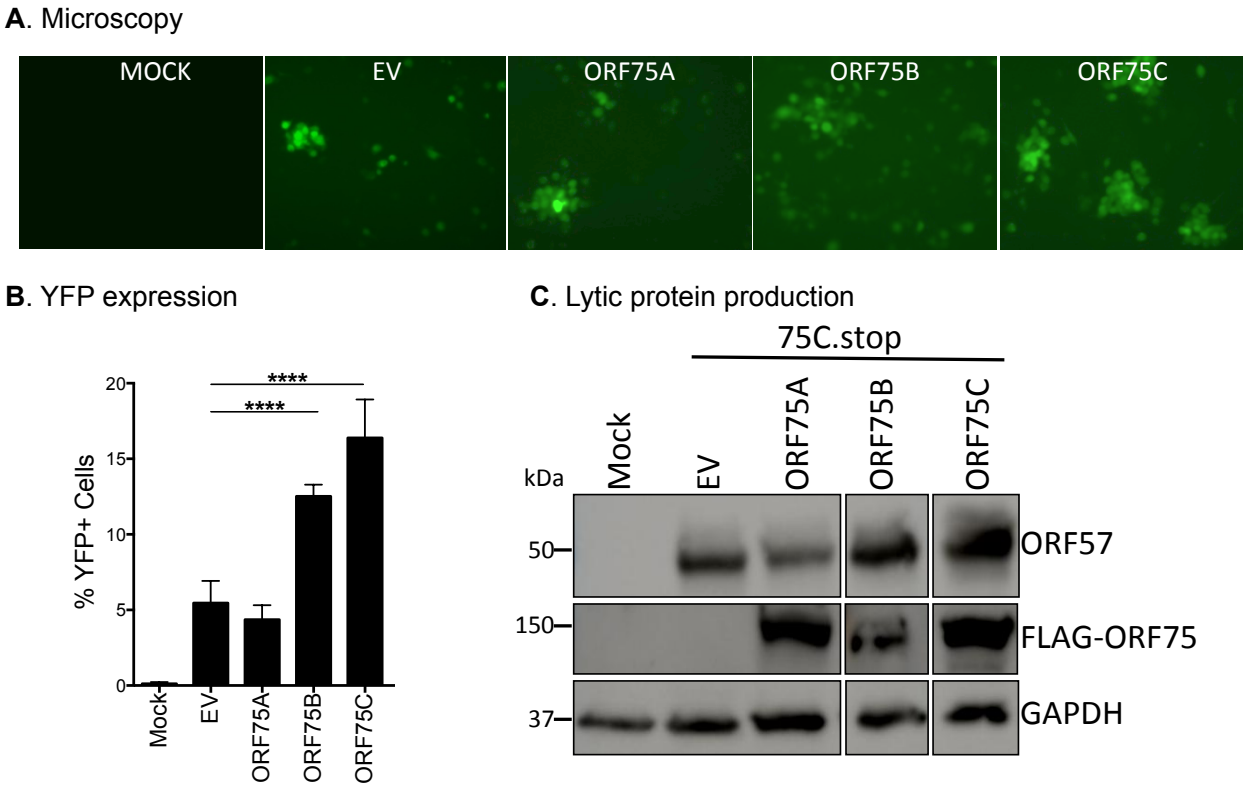

Figure 4.1 Complementation of MHV68 ORF75C.stop by MHV68 vFGARATs.
HEK 293T cells were co-transfected with MHV68 ORF75C.stop BAC and MHV68 vFGARAT expression plasmids or the empty plasmid. **(A)** Fluorescent microscopy of YFP+ cells and foci in co-transfected culture 2 days after transfection. (B) Triplicate flow cytometric analysis of the percentage of YFP+ in the cells cotransfected with the 75C.stop BAC DNA and the MHV68 vFGARAT expression constructs or the empty plasmid control. **** $p < 0.0001$ **(C)** Immunoblot analysis of productive infection by expression of the immediate-early ORF57 gene product and Flag-tagged vFGARAT expression 3 days after co-transfection

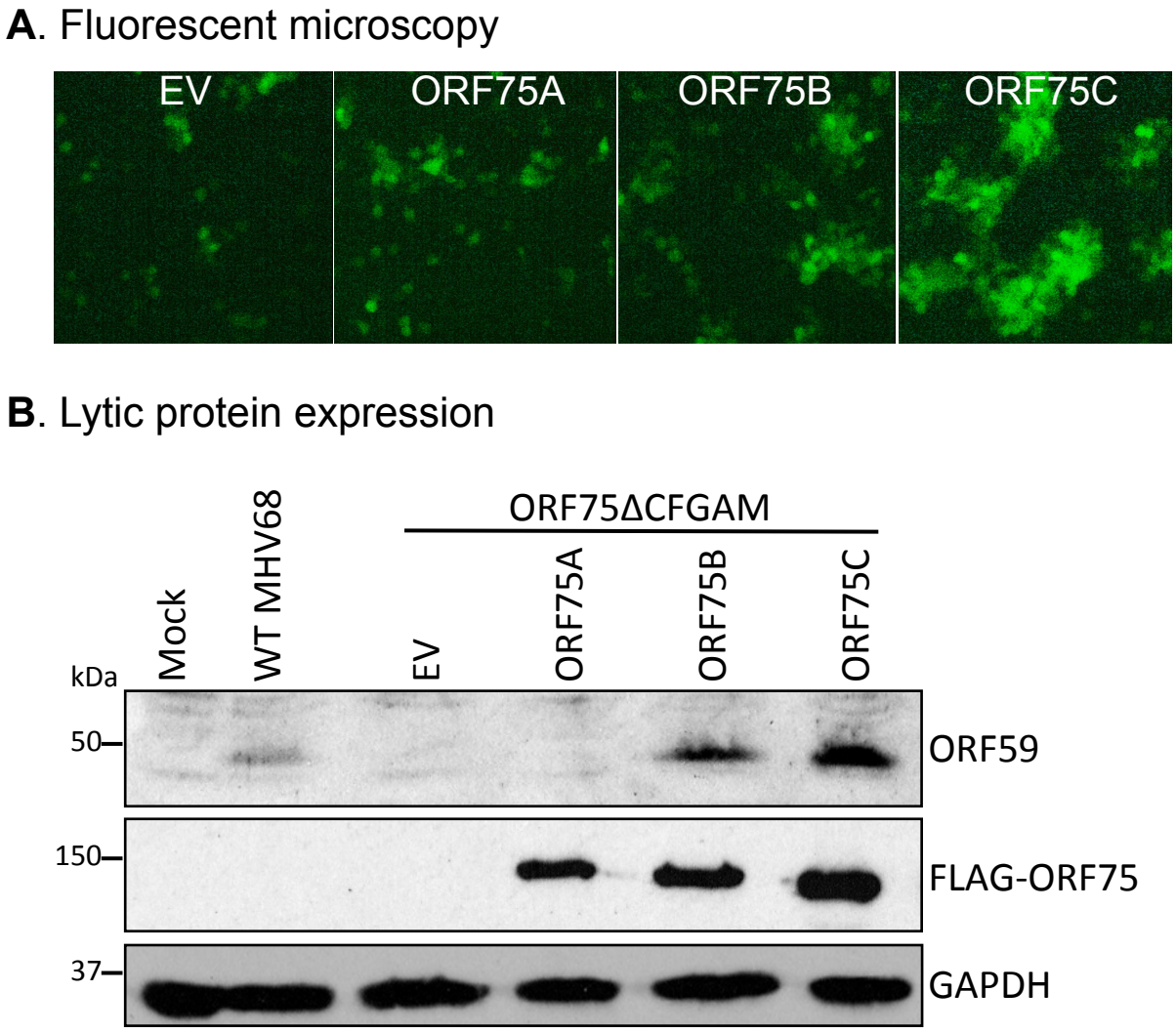

Figure 4.2. Complementation of MHV68 ORF75CΔFGAM by MHV68 vFGARATs. HEK 293T cells were co-transfected with MHV68 ORF75CΔFGAM BAC DNA and MHV68 vFGARAT expression plasmids or the empty vector. **(A)** Fluorescence microscopy of YFP+ cells and foci in co-transfected cultures at 48 hrs. **(B)** Immunoblot analysis of the early ORF59 gene product and Flag-tagged vFGARAT expression at 48 hrs.

ORF75A is expressed during MHV68 infection and increases over time.

Given that both the *in vivo* pathogenesis (Chapter 3) and trans-complementation (**Fig. 4.1 and Fig 4.2**) experiments pointed towards a distinct role for ORF75A in MHV68 replication we set out to characterize the mechanism by which ORF75A influences replication. First, we examined the expression of ORF75A protein during lytic infection. ORF75A had been previously identified as a viral protein expressed during infection and also present in the MHV68 virion (85). However in this study, the authors also noted background staining of ORF75C-transfected cells with their ORF75A antibody, indicating that the antibody could also be recognizing ORF75C (85). Since we were unable to generate an anti-peptide antibody to ORF75A, we constructed a recombinant MHV68 virus on the H2b-YFP MHV68 BAC template where the 3X-FLAG epitope tag is fused to the N terminus of ORF75A. We confirmed this genomic construct by whole genome sequencing. Primary MEFs were infected with the parental MHV68-(H2b) YFP virus and the FLAG-75A virus at an MOI of 5. The kinetics of viral protein expression (**Fig. 4.3A**) and replication (**Fig. 4.3B**) were examined at multiple timepoints after infection. We observed a delay and reduction in the immediate early gene ORF57, the late gene ORF65 and the late/tegument protein ORF75C in cells infected with the FLAG-75A virus as compared to the WT control (**Fig. 4.3A**). FLAG-75A protein was detected at 9 hpi. Similar to the late genes, ORF65 and ORF75C, ORF75A protein expression increased between 9 hpi and 18 hpi (**Fig. 4.3A**). Although the FLAG-75A virus exhibited reduced ORF65 and ORF75C levels, we did not observe any defects in virus replication in primary MEFs (**Fig. 4.3B**). In contrast FLAG-75A virus titers were 1.5 to 2-fold higher at almost each timepoint tested as compared to the parental MHV68-YFP virus (**Fig. 4.3B**). These data indicate that ORF75A is a *bona fide* protein produced during MHV68 replication in fibroblasts with a kinetic pattern consistent with a late gene class. Moreover, the addition of the FLAG epitope to ORF75A does not impair MHV68 replication in primary fibroblasts.

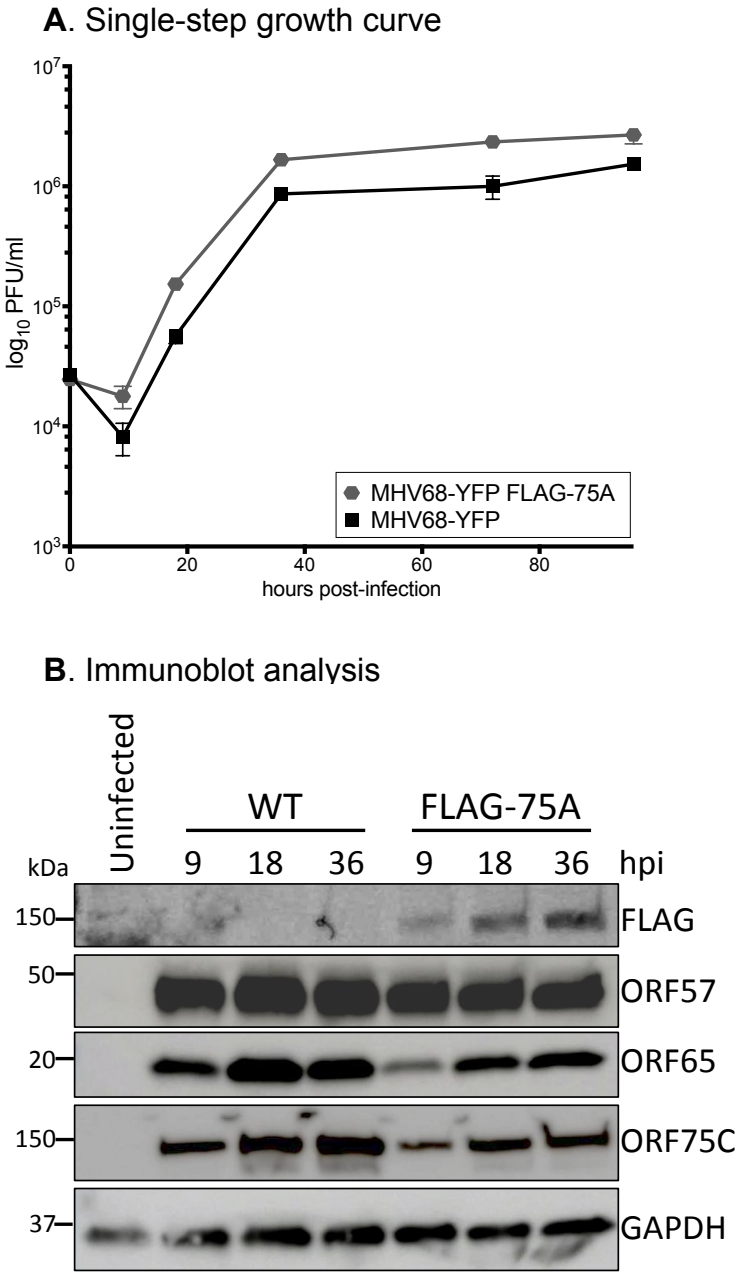

Figure 4.3. Characterization of a recombinant FLAG-75A MHV68. (A) Single-step growth curve in primary MEFs at an MOI of 5 with 75A.stop1 and 75A.stop1MR. **(B)** Timecourse analysis of immediate-early (ORF57) and late (ORF65 and ORF75C) gene products upon a single-step infection of BMDMs.

Loss of ORF75A results in cell specific defects in replication.

In the previous chapter we identified roles for ORF75A in acute replication in the lung and the establishment of latency after intranasal inoculation. Interestingly, this defect in latency establishment was largely rescued by direct intraperitoneal administration of the virus. This indicates a role for ORF75A in the dissemination of virus from the lung to the spleen. Productive MHV68 replication in the lung occurs mainly in alveolar epithelial cells (59). However, dissemination to the spleen after intranasal inoculation is dependent on MHV68 replication in macrophages and dendritic cells **(**56, 172**)**. Initial colonization of the spleen is dependent on lytic replication in marginal zone macrophages and B cells (55). Thus we reasoned that the severity of the ORF75A defect might be dependent on the cell type engaged by the ORF75A.stop virus. To this end we set out to compare ORF75A.stop1 and ORF75A.stop1MR replication in primary murine embryonic fibroblasts (MEFs) and primary bone marrow derived macrophages (BMDMs).

We infected primary MEFs with WT, ORF75A.stop1MR and ORF75A.stop1 viruses at an MOI of 5 and quantified virus titers at multiple timepoints after infection. The WT and ORF75A.stop1MR viruses replicated with similar kinetics and resulted in about a two-log increase over the input inoculum (**Fig. 4.4A**). However we observed a slight, yet significant 2-3-fold defect in virus titers upon infection of MEFs with the ORF75A.stop1 virus as compared to the MR and WT controls. This defect began as early as 12 hpi and was maintained through 96 hpi (**Fig. 4.4A**). Interestingly, an examination of protein expression from the different kinetic classes of viral genes did not reveal defects in any single kinetic class in ORF75A.stop1 infected cells (**Fig 4.4B**). Instead, we observed a noticeable increase in the levels of the immediate early protein ORF57 and the ORF75C tegument protein expression (**Fig. 4.4B**).

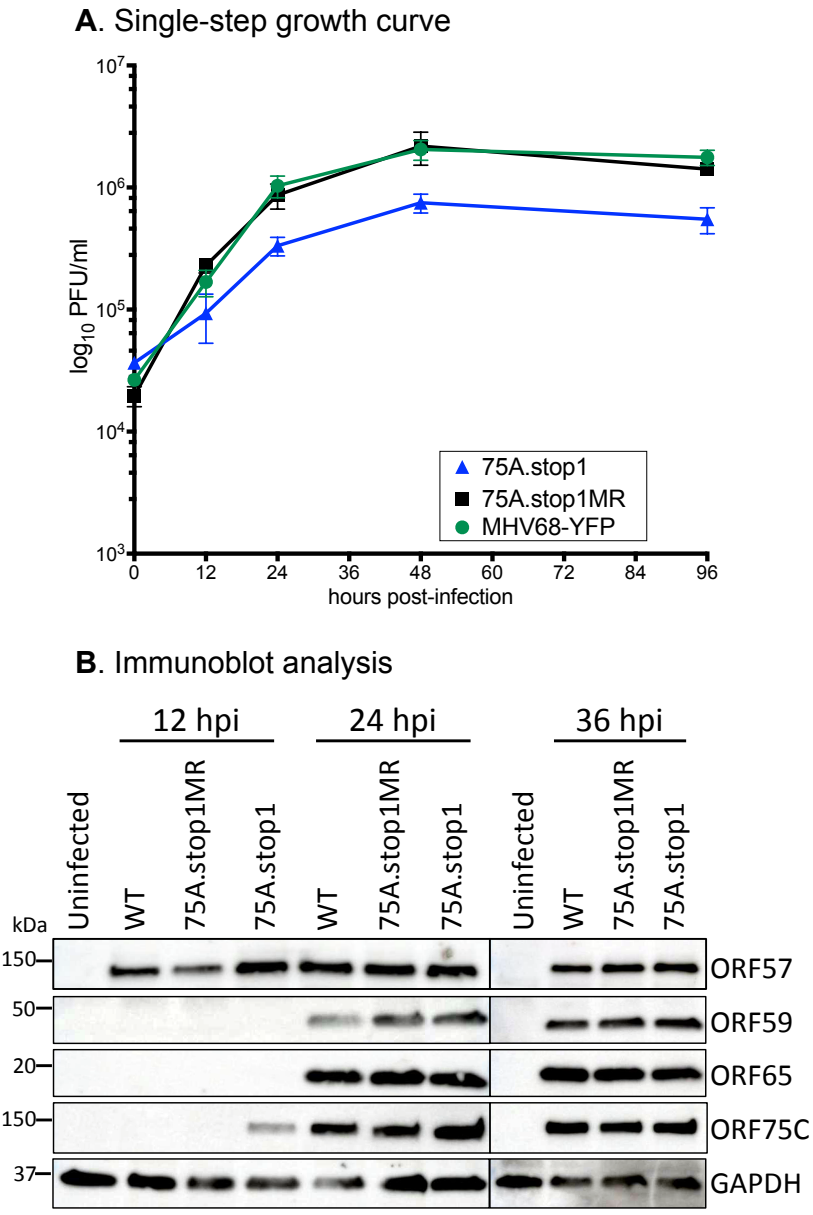

Figure 4.4. Single-step growth of ORF75A.stop in primary MEFs. (A) Single-step growth curve in primary MEFs at an MOI of 5 with 75A.stop1 and 75A.stop1MR. **(B)** Timecourse analysis of immediate-early (ORF57), early (ORF59) and late (ORF65 and ORF75C) gene products upon a single-step infection of primary MEFs.

Next we analyzed single-step replication of the ORF75A.stop1 virus in BMDMs. The kinetics of ORF75A.stop1 and ORF75A.stop1MR replication were comparable for the first 12 hrs of infection. The ORF75A.stop1MR control virus continued exponential growth from 12 to 24 hpi before reaching a plateau between 72 and 96 hpi. In contrast, there was a delay in the replication of ORF75A.stop1. This lag in replication resulted in a log-defect in virus titers for ORF75A.stop1 as compared to ORF75A.stop1MR (2.9×10^5 PFU/ml vs. 2.6×10^6 PFU/ml, respectively) (**Fig. 4.5A**). Additionally, viral protein expression from all kinetic classes was significantly higher in ORF75A.stop1 infected cells as compared to ORF75A.stop1MR-infected cells. Specifically, we observed higher levels of ORF73 (immediate early protein) at 6 hpi, ORF59 (early protein) at 12 and 24 hpi, ORF65 (late protein) at 12 hpi and detection of the ORF75C tegument protein at 6 hpi in the ORF75A.stop1 infected cells compared to the ORF75A.stop1MR infected cells (**Fig. 4.5B**). This acceleration in the kinetics and the levels of viral proteins upon ORF75A.stop1 infection correlated with an increase in cytotoxicity with ORF75A.stop1 infection as measured by a two-fold increase in lactate dehydrogenase (LDH) release at 36 hpi (**Fig 4.6**).

We conclude that ORF75A promotes virus replication. We observed a more severe defect in primary macrophages as compared to primary fibroblasts. ORF75A disruption in infected BMDMs led to a severe dysregulation of viral gene expression, an enhancement of a cytopathic effect and reduced virus titers. This data indicates that ORF75A might provide regulatory functions that enhance virus yield.

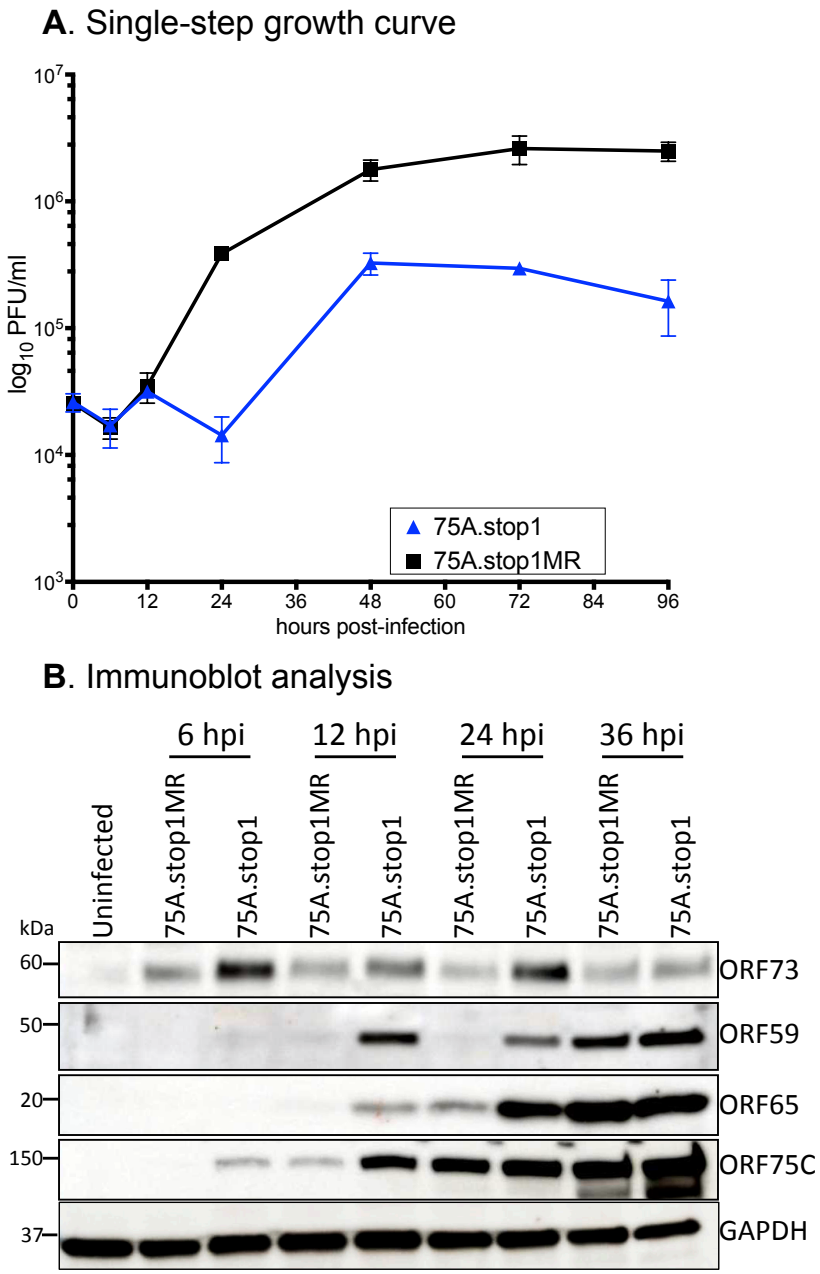

Figure 4.5. Enhanced protein expression upon 75A.stop infection of primary BMDMs. (A) Single-step growth curve in primary BMDM at an MOI of 5 with 75A.stop1 and 75A.stop1MR. **(B)** Timecourse analysis of immediate-early (ORF73), early (ORF59) and late (ORF65 and ORF75C) gene products upon a single-step infection of BMDMs.

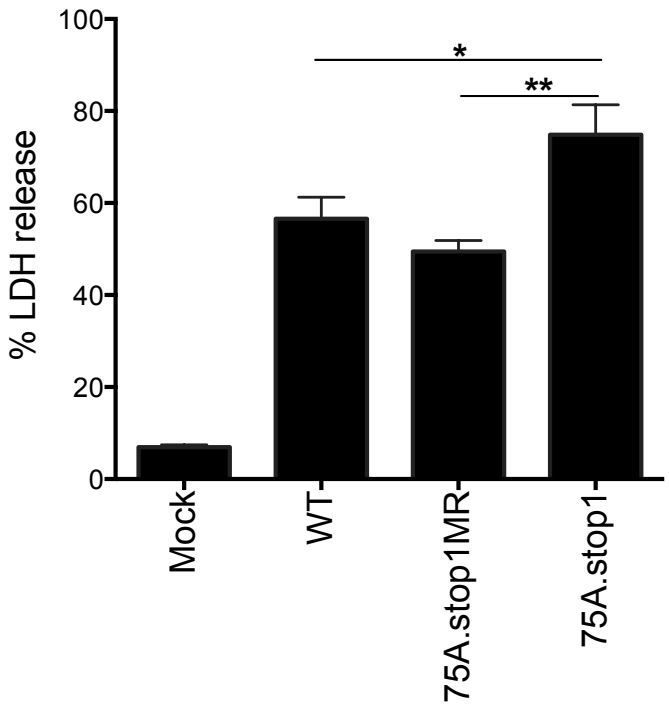

Figure 4.6. Loss of ORF75A promotes a higher cytopathic effect in BMDMs.
Primary BMDMs were infected at an MOI of 5 with the indicated viruses and LDH release was measured 36 hpi. Data is presented as a percentage of LDH release from cells that were freeze-thawed to release LDH.

Enhanced tegument delivery with ORF75A.stop

ORF75C was detected earlier in the absence of ORF75A during MEF infection (**Fig. 4.7A**). In BMDMs, ORF75C in addition to proteins from all kinetic classes were expressed earlier in ORF75A.stop infections. Given that ORF75A is predicted to be a tegument protein, we postulated that loss of ORF75A might influence the packaging and delivery of virion components to the infected cell. We compared ORF75C tegument protein levels in primary MEFs or BMDMs at 3 hpi (**Fig 4.7**). ORF75C is a tegument protein and is also expressed *de novo* late in productive infection (123, 133). Therefore, at early timepoints the bulk of ORF75C that is detected will be derived from the virion. As expected, infection of either cell-type with the ORF75A.stop1 virus led to a greater accumulation of ORF75C tegument protein in the infected culture 3 hpi (**Fig 4.7A and Fig 4.7B**).

Given the observation that ORF75C is present at higher levels by 3 hpi in ORF75A.stop1-infected cultures, we set out to determine if this led to the dysregulation in viral protein expression observed in the BMDMs. ORF75C has been reported to promote the degradation of the ND10 antiviral component, PML (85, 106). Multiple studies have identified roles for ND10 nuclear bodies in the transcriptional repression of herpesvirus genomes (113, 175-180). In these studies, depletion of PML enhanced ICPO-null HSV-1 replication (177, 181), HCMV replication (182) and MHV68 gene expression and titers (106). Thus it is possible that the enhanced viral protein expression upon ORF75A.stop1 infection is simply due to the increase in the levels of ORF75C deposition in these cells. We compared the kinetics of PML degradation in BMDMs infected with ORF75A.stop1 to ORF75A.stop1MR-infected cultures. As previously observed, ORF75A.stop1-infected cultures exhibited higher ORF75C expression, yet we did not observe an enhancement in PML degradation in the ORF75A.stop1 infected cultures as compared to the GAPDH loading control (**Fig 4.7C**).

Taken together, the loss of ORF75A results in greater amounts of virion delivered ORF75C at early timepoints in infection. However, greater deposition of ORF75C did not correlate with accelerated PML degradation. Thus, the dysregulation in viral gene expression in ORF75A.stop infection is not attributed to increased ORF75C antagonism of PML.

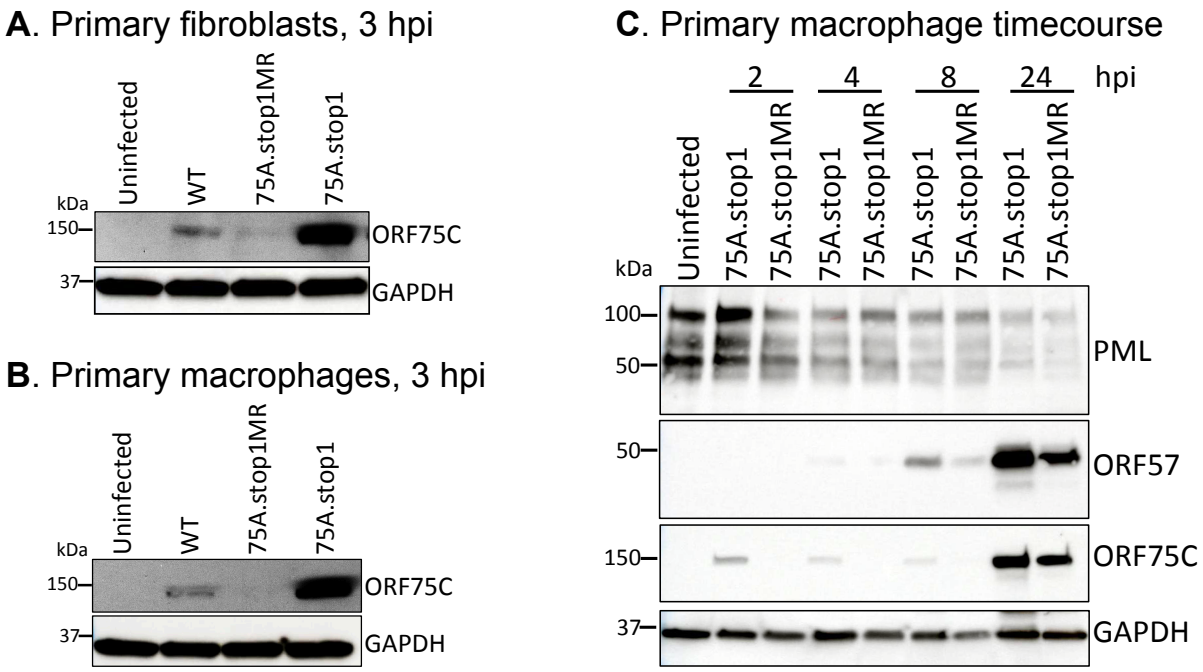

Figure 4.7 Higher levels of ORF75C deposition does not correlate to enhanced kinetics of PML degradation in ORF75A stop infections. Primary MEFs or BMDMs were infected at an MOI of 5 with the indicated viruses (**A**) Immunoblot analysis of ORF75C tegument protein levels 3 hpi of primary MEFs. (**B**) Immunoblot analysis of ORF75C tegument protein levels 3 hpi of primary macrophages (C) Timecourse analysis of PML degradation, Immediate-early protein expression (ORF57) and tegument/late (ORF75C) gene products upon a high MOI infection of primary BMDMs.

Low MOI MEF infection recapitulates high MOI BMDM infection

We observed a more severe replication defect in BMDMs as compared to the MEFs in the absence of ORF75A (**Fig. 4.4 vs. Fig. 4.5 and 4.6**). We predicted that since BMDMs are refractory to infection, and exhibit a higher sensitivity to MHV68 infection, it was likely that a low MOI infection of MEFs would recapitulate the BMDM phenotype. To this end, we examined virus replication as well as intracellular levels of viral proteins in a multi-step growth curve in primary MEFs at a low MOI (0.05). Similar to the high MOI BMDM infection, low MOI infection of primary MEFs with ORF75A.stop1 led to higher levels of ORF57, ORF65 and ORF75C (**Fig. 4.8A**). Additionally, we observed a more pronounced defect in ORF75A.stop1 replication upon low MOI infection. Specifically, ORF75A.stop1 and ORF75A.stopMR replicated with similar kinetics for the first 24 hrs. However, from 48 hpi to 96 hpi, ORF75A.stop1 titers plateaued while we observed a further log increase with the ORF75A.stop1MR virus (**Fig. 4.8B**). These data indicate that the dysregulation of gene expression and replication defects are not limited to BMDMs. The loss of ORF75A impacts MHV68 replication in multiple cell types.

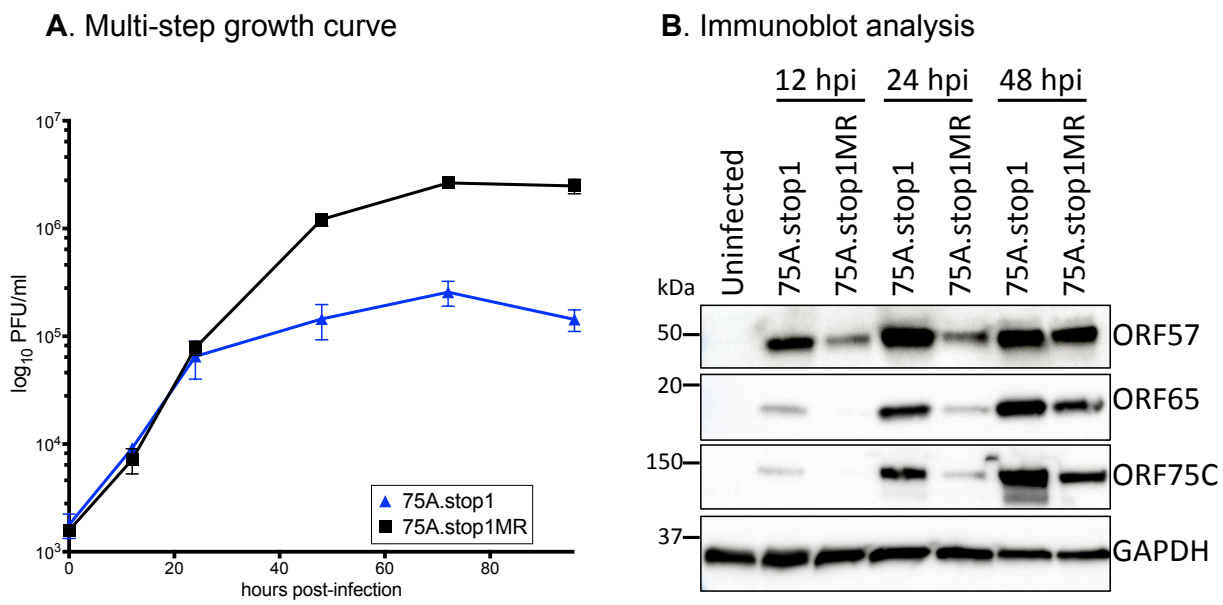

Figure 4.8 Low multiplicity of infection in primary MEFs recapitulates ORF75A.stop1 in primary BMDMs. (A) Multi-step growth curve in primary MEFs at an MOI of 0.05 with 75A.stop1 and 75A.stop1MR. **(B)** Timecourse analysis of immediate -early (ORF57) and late (ORF65 and ORF75C) gene products upon a low MOI infection of MEFs.

Discussion

In the previous chapter, ORF75A was found to be critical for pathogenesis while no role for ORF75B was observed. In this chapter, we found that ORF75B complemented replication-defective ORF75C mutant viruses for virus spread and lytic protein expression indicating an overlap of function between ORF75B and ORF75C. ORF75A did not complement replication-defective ORF75C viruses. This demonstrates non-overlapping roles for ORF75A in MHV68 replication. ORF75A was confirmed as a *bona fide* protein expressed late in lytic infection. We identified reduced viral replication in cells infected with ORF75A.stop. This defect in virus replication was characterized by greater deposition of the ORF75C tegument protein, an enhancement of intracellular protein levels and increased cell death.

The overexpression of ORF75B complemented gene expression, virus replication and spread in two replication-defective ORF75C mutant viruses. This rescue of ORF75C defects implies ORF75B shares at least some functions with ORF75C. Three functions have been identified for ORF75C in MHV68 replication: capsid transport to the nucleus (85), deamidation of RIG-I and activation of IKK2 to drive RTA and evade cytokine production in the cell (125) and PML degradation (85, 106). We originally identified ORF75B in a screen for activators of NF-κB (**Chapter 2**) yet overexpression of ORF75B did not significantly drive an NF-κB dependent luciferase reporter (data not shown). Moreover, in a recent study identifying the role of ORF75C in the deamidation of RIG-I and activation of IKK2, ORF75B expression was not sufficient to either drive NF-κB activation or lead to RIG-I deamidation (125). Thus we conclude that engagement of NF-κB signaling and RIG-I deamidation are not the functions shared between ORF75C and ORF75B.

The observation that ORF75C.stop viruses are impaired for nuclear delivery of infected capsids implicates ORF75C or another viral protein that is dependent on ORF75C protein for efficient packaging into the virion in this process. It is unlikely that ORF75B is required for nuclear trafficking of the viral capsid as we did not observe any early defects in replication of the ORF75B-stop viruses. Lastly, ORF75B expression does not promote PML degradation (106).

Future studies will examine whether ORF75B promotes capsid transport or targets other components of the ND10 antiviral complex.

We made the novel observation that a region of high conservation between the vFGARATs and the host FGARAT is required for ORF75C function and phenocopies an ORF75C.stop mutation in the inability to replicate in fibroblasts. Interestingly, a crystal structure of the *Salmonella typhimurium* FGARAT identified residues in this conserved region that form hydrogen bonds with ADP (102). As such, our mutation might have uncovered a role for nucleotide binding in ORF75C function. However, given the dramatic mutations made, we cannot exclude the possibility that the ORF75C protein structure was destabilized. Indeed, amino-acids residues within the targeted conserved region lie in a buried helical region. More conservative mutations to impair the nucleotide-binding pocket without the likelihood of impairing protein structure will help address the potential role of this ADP binding pocket to ORF75C function. Of note, Tsai and colleagues also identified that deletion of this region influences BNRF1 displacement of Daxx from its cognate binding partner ATRX (120).

A striking observation was the difference in phenotypes observed with high MOI infection of BMDMs and MEFs. While the high MOI BMDM infection with ORF75A.stop led to higher intracellular viral protein levels, cell death and a log defect in virus replication as compared to control viruses, there was only a two-fold defect in MEFs infected at an MOI of 5. We only recapitulated the high MOI BMDM phenotypes with a low MOI MEF infections. We reason that BMDMs might be refractory to MHV68 entry and productive infection, thus resulting in a much lower efficiency of infection than the high MOI infection of MEFs. Our laboratory has observed that only about 30-40% of BMDMs are positive for YFP expression 12-24hrs after MHV68-YFP infection (Qiwen Dong, unpublished data). BMDMs are a well-established system to examine the pathogen interaction with the innate immune system. These primary macrophages have been used extensively in the identification of virus and host factors responsible for the modulation of MHV68-specific inflammatory responses (183-186). Therefore the larger replication defect in BMDMs after high MOI infection compared to MEFs is likely influenced

both by the absence of ORF75A and increased intrinsic and innate responses to infection in the primary macrophage cell.

Our data implicates a role for ORF75A in MHV68 replication that is characterized by enhanced delivery of the viral tegument at early timepoints in infection and a reduction in virus titers that manifests late in replication (24 hpi in BMDMs and 48 hpi in low MOI MEFs). Given that loss of ORF75A results in higher levels of the late proteins ORF75C and ORF65, it is unlikely that the defect in ORF75A.stop1 replication is due to a defect in either DNA replication or the transcription and translation of late genes. Rather, ORF75A may be required for the latter stages in the virus life cycle including the assembly, packaging or egress of the virion through the cell and that loss of ORF75A influences the proportion and/or delivery of a virion component that, in turn, influences the dysregulation of viral gene expression in the next round of infection. In support of this idea, a yeast two-hybrid study examining interactions between KSHV virion components identified KSHV ORF52 and KSHV ORF45 as KSHV ORF75 binding partners (91). Moreover KSHV ORF45 is required for the kinesin-2 dependent movement of newly packaged KSHV capsids to the cell periphery (88). Roles for MHV68 ORF45 in assembly and egress have not been identified. However, expression of KSHV ORF45 rescues the replication defects of an MHV68 ORF45 null virus implying conservation of function (89). Although KSHV ORF52 has not been studied, recombinant viruses with defects in MHV68 ORF52 exhibit defects in secondary envelopment as well as the absence of the MHV68 ORF45 and ORF42 tegument proteins in the virion (50, 187). We propose that ORF75A is involved in the tegumentation of MHV68.

Infection of BMDMs or MEFs (low MOI) with ORF75A.stop led to increased intracellular protein levels across all kinetic classes. ORF75C degrades the antiviral molecule PML and relieves repression of virus gene expression (106). Infection of PML-null MEFs with WT virus results in higher titers and increased gene expression (106). We examined whether increased ORF75C tegument deposition correlated with faster PML degradation in infected BMDMs. However, similar rates of PML degradation were observed in 75A.stop1 and 75A.stop1MR infections. Thus, PML degradation is unlikely to be the explanation for increased

intracellular protein levels. A recent report suggests that ORF75C promotes RTA function by the activation of IKK2 through the engagement of RIG-I/MAVS signaling (125). Our finding of increased viral gene expression is consistent with an increase in RTA activity. However, the expression of LANA, a gene whose transcription is independent of RTA function (183), is also increased with the ORF75A mutant. Another tegument protein, ORF49, displaces a negative regulator of RTA (84). Therefore the enhanced viral protein levels in ORF75A.stop might be due to an increased packaging of ORF49 in the virion or increased deposition of ORF49 into newly infected cells, much like the phenotype observed for ORF75C.

The enhancement in viral tegument deposition and the intracellular protein levels in ORF75A.stop1 infection led to the unexpected decrease in virus production. However, ORF75A is not the only viral gene whose absence results in an enhancement in lytic induction that does not correlate with higher titers. The MHV68 host shutoff protein, muSOX is required for the global dampening of host and viral mRNA (188), (189)} and the muSOX-null virus exhibits enhanced binding and entry into target cells, as well as elevated intracellular protein levels (189). Interestingly, there were higher levels of some tegument proteins in virions isolated from muSOX-infected cells (189). This suggests that the absence of muSOX or some other viral protein regulated by muSOX regulates tegumentation. Future studies will determine whether the ORF75A.stop mutation impairs muSOX levels in the cell or if ORF75A directly plays a role in optimal tegumentation.

We have identified a novel role for a vFGARAT tegument protein in MHV68 replication and pathogenesis. Given the dysregulation in tegument delivery and intracellular viral protein levels, we propose that ORF75A is required for efficient packaging of virion components in newly produced MHV68 virions. KSHV ORF75 is found to interact with two other tegument proteins required for virion assembly (91). Recent findings imply that tegumentation is a decidedly ordered process. This process is dependent on distinct interactions between virus capsid and tegument proteins. Future studies on the MHV68 ORF75A tegument protein may inform roles for gammaherpesvirus ORF75/vFARAT homologs distinct from their previously reported ND10 antagonistic functions.

Chapter 5: Conclusion

I. **Summary**

In this study, I constructed mutant MHV68 viruses disrupted by the insertion of all-frame stop codons into either ORF75A or ORF75B to examine the contributions of the ORF75A and ORF75B gene products to MHV68 pathogenesis. Disruption of ORF75B did not influence productive replication in culture or pathogenesis *in vivo*. However, I utilized cell-culture models of lytic replication to show that ORF75B shares overlapping functions with the third member of the MHV68 vFGARAT family of proteins, ORF75C. This overlap of function between ORF75B and ORF75C likely explains the lack of an ORF75B.stop phenotype.

ORF75A, on the other hand, encodes a function distinct from ORF75C. To this end, I identified a route-dependent role for ORF75A in pathogenesis as well as roles in tegument delivery, viral gene expression and lytic virus production in cell culture. Interestingly, the ORF75A replication defect was more pronounced in macrophages, a cell-type critical for the dissemination of MHV68 replication from the lung to the latent B cell reservoir in the spleen. Additionally, low MOI infection of primary fibroblasts unveiled larger defects in virus replication not observed upon a high MOI, synchronous infection of primary fibroblasts. This indicates that ORF75A is critical for cell-to-cell spread and/or the antagonism of host immune response to infection.

Overall, this dissertation has identified roles for two previously uncharacterized genes in MHV68 replication. These data have also raised some interesting questions that need to be addressed in future experiments to fully understand the mechanism of ORF75A and ORF75B function and link replication defects to changes in the pathogenesis upon infection with mutant viruses. These genes are part of a family of tegument associated proteins unique to the gammaherpesviruses, linked by the intriguing evolutionarily distant capture and conservation of a domain from the host purine biosynthetic enzyme FGARAT. Their functions will likely inform their unique lifecycle and niche in the host that have etiological associations with cancer.

II. Modulation of NF-κB signaling by the gammaherpesvirus vFGARATs.

Our laboratory found that MHV68 infection of fibroblasts in culture resulted in a late, sustained activation of NF-κB signaling. However, inhibition of canonical NF-κB signaling with a dominant inhibitor had no influence on lytic replication in culture, but impaired the establishment of splenic B cell latency *in vivo* (138). Infection of mice lacking the p50 NF-κB subunit also reduced splenic latency establishment (137). Interestingly, these $p50^{-/-}$ mice also exhibited increased virus replication in the mouse lung without an effect on virus replication in primary fibroblasts, consistent with a role for the NF-κB p50 subunit in mediating host immune control of virus expansion in the respiratory tissue. We hypothesized that late-stage activation may lead to the recruitment of macrophage, dendritic, or B cells needed to promote dissemination from the lung to secondary lymphoid tissues where the virus established latency. However, the manner of the late NF-κB activation had not been determined. KSHV and EBV encode viral proteins critical for the constitutive activation of NF-κB signaling in infected cells (140, 141, 190, 191), but constitutive activators of NF-κB had not been identified for MHV68.

My dissertation project began with a screen to identify and characterize viral genes responsible for NF-κB activation late during infection. We identified two viruses with disruption in the ORF75A and ORF75B genomic regions that were defective in NF-κB activation. Further characterization of these two TN-disrupted viruses identified distinct defects in lytic replication in culture and pathogenesis *in vivo* (Chapter 2). We propose that the defect in NF-κB signaling observed upon infection with the 75.TN viruses is likely due to an inability to efficiently replicate as opposed to a direct role of ORF75A or ORF75B in NF-κB activation. Consistent with a report by He et al. (125), our laboratory determined that overexpression of ORF75A or ORF75B alone is not sufficient to drive NF-κB signaling (data not shown).

A recent study identified a role for ORF75C in promoting NF-κB signaling to drive lytic replication. In this study, the authors have developed a model whereby ORF75C usurps the RIG-I/MAVS/IKK2 axis to promote the transcriptional activation of the viral lytic transactivator RTA. RTA then degrades the NF-κB subunit p65 to limit cytokine production, allowing MHV68

to evade innate immune signaling (127),(126),(192),(125). However, we have observed that overexpression of ORF75A reduced the levels of NF-κB induced by the NF-κB subunit p65 or the upstream activator MyD88 (data not shown). This indicates that MHV68 utilizes another viral factor to limit host activation of innate immune signaling. An examination of the NF-κB-dependent transcriptome and profiling subunit translocation signaling events in 75A.stop and 75A.stopMR infected cells, untreated or challenged with NF-κB activating stimuli, may unveil a novel target for ORF75A in NF-κB signaling.

III. Basis for TN phenotypes.

The phenotypes observed with the TN-disrupted viruses were distinct from the phenotypes of the stop-codon mutant viruses. This was also observed in the comparison of ORF54.TN and ORF54.stop viruses. TN disrupted ORF54 virus (54.TN) exhibited nearly a 2-log replication defect in the lung of infected mice (94). In contrast, an ORF54.stop virus exhibited less than a 0.5-log defect in acute lung replication (186). This implies that the large TN insertions likely adversely impact neighboring transcripts in the compact MHV68 genome. It remains to be determined whether other transcripts within the ORF75A-ORF75B genomic region are impaired by the TN insertion.

Transcripts of ORF73/LANA and ORF72/v-cyclin initiate in the right terminal repeats of the genome and splice across the ORF75A-ORF75C region (148). Both genes play roles in lytic replication and their absence might explain the larger defects observed with the TN viruses. Expression of the MHV68 ORF73 protein in trans did not rescue the ORF75A.TN or ORF75B.TN replication defects, indicating that ORF73 expression is likely not impaired in the ORF75A- and ORF75B.TN viruses (Chapter 2). However, potential complementation of the ORF75.TN defects by ORF72 expression has not been explored. Additionally, studies from our lab (133) and others (160) have described the presence of an antisense non-coding transcript in the ORF75A-ORF75B genomic region termed expressed genomic region 30 (EGR 30) . EBV encoded small non-coding RNAs (EBERs) upregulate Il-6 and STAT3 signaling to modulate cell cycle progression (193) and recruit the cellular transcription factor, PAX5 to the EBV genome to

upregulate latent gene transcription in the B cell to promote B cell latency (155). Lastly, viral long noncoding RNAs in the EBV latent origin of replication, OriP, antagonize host innate immunity to promote global viral gene expression and lytic replication (194). Given the potential for EGR 30 to influence MHV68 replication, future experiments should utilize strand-specific Northern blot analysis to compare transcript differences between the ORF75.TN and ORF75.stop viruses. Any differences in EGR 30 expression might result in the identification of the source of the 75.TN phenotypes. Identification and disruption of RNA polymerase II promoter elements upstream of EGR 30 would confirm the role of this transcript in MHV68 replication.

IV. Characterization of ORF75A.

Using an epitope-tagged ORF75A recombinant virus, we have confirmed the expression of ORF75A in MHV68 infection. ORF75A is expressed at low levels and increased slightly between 9 hpi and 18 hpi. The kinetic increase in ORF75A protein was similar to that observed for the late proteins, ORF65 and ORF75C. This observation is in agreement with previous MHV68 transcriptome studies (195),(160). To more carefully examine the kinetics of ORF75A protein expression, future experiments will utilize treatment with the protein synthesis inhibitor, cyclohexamide (CHX) and the DNA synthesis inhibitor, phosphonoacetic acid (PAA) to arrest virus infection and then examine for ORF75A protein expression. Treatment with the fusion inhibitor, bafilomycin will determine if ORF75A protein detected at early time points is due to tegument-delivered ORF75A. Moreover, future studies are needed to examine the subcellular localization of ORF75A. Previous studies imply that transfected ORF75A is restricted to the host cell nucleus (85, 106). However, in MHV68-infected cells, ORF75A protein was also detected in the cytoplasm (85). In addition, nuclear ORF75A staining was weak, likely to due to the low abundance of the ORF75A protein coupled with a high level of background for the polyclonal ORF75A antibody utilized in these assays (85). We generated a recombinant MHV68 expressing an epitope-tagged ORF75A to enable better characterization of ORF75A localization in the context of infection by immunofluorescence and subcellular fractionation.

To better characterize the biological properties of the MHV68 ORF75A protein, proteomic studies can be designed where cells are infected with FLAG-75A and FLAG-75A.stop viruses, and cell lysates are subjected to immunoprecipitation. After SDS-PAGE analysis, bands unique to the FLAG-75A infection can be analyzed by mass spectrometry to identify novel ORF75A binding partners and examine the mechanisms underlining the ORF75A.stop phenotypes presented in this dissertation.

V. Impact of vFGARATS on ND10 components and the roles of ND10 components in MHV68 replication.

As previously outlined, gammaherpesviruses encode homologs of the host biosynthetic enzyme, FGARAT, and are hence termed viral FGARATs (vFGARATs) in this dissertation. MHV68 encodes three vFGARATs. An intriguing question is whether the three MHV68 vFGARATs encode three independent functions that are each conserved in the single human gammaherpesvirus vFGARATs, or whether they have diverged to encode host-specific roles distinct from conserved vFGARAT functions. To date, studies on vFGARATs from multiple γHVs have identified the antagonism of the host ND10 antiviral complex as a conserved feature of vFGARATs (85, 106, 119, 121, 122). However, each vFGARAT may encode other functions as well. ORF75C degrades PML, but targeting PML is not the essential function that ORF75C provides for MHV68 replication. ORF75C hijacks RIG-I/MAVS signaling to activate NF-κB signaling, again a non-essential function for replication in culture. The role of ORF75C in promoting the cytoplasmic to nuclear trafficking of incoming MHV68 virions is not well characterized, but may be the essential role it provides.

We developed a trans-complementation system and determined that while ORF75A function is distinct from that of ORF75C, ORF75B rescues virus gene expression in an ORF75C mutant infection. Together, with the observation that ORF75B.stop viruses replicate as efficiently as WT viruses, we propose that loss of ORF75B is compensated for by the presence of ORF75C in the ORF75B.stop viruses. Moreover, given that transfected ORF75B is strictly nuclear (106), we predict that the rescue by ORF75B implies overlap of the nuclear ND10

antagonism function and not the cytoplasmic functions (RIG-I/MAVS hijack or virion trafficking).

The antiviral ND10 nuclear body consists of multiple transient and permanent host proteins (107, 108). The three most characterized members are PML and the chromatin remodeling proteins, Sp100 and hDaxx (109, 110). PML is the nucleating protein in this complex and is required for maintaining the integrity of the ND10 complex (111). Thus, degradation of PML leads to the disruption of the complex, thereby limiting the antiviral properties of the ND10 complex. However, recent accumulating evidence proposes antiviral roles for individual ND10 components in the absence of a competent ND10 signaling complex. The HSV-1 immediate early protein, ICP0, degrades PML and Sp100, yet infection of cells lacking PML, Sp100 or hDaxx does not restore replication of ICP0-null HSV-1 viruses to WT levels (176, 177, 179). In contrast, ICP0-null HSV-1 virus replication is almost fully rescued in cells depleted for all 3 permanent ND10 components (196).

Herpesviruses encode multiple ND10 antagonists in their genomes or target multiple components with a single antagonist. HSV-1 ICP0 degrades PML and Sp100 (196). HCMV antagonizes PML and Sp100 with the immediate early protein, IE1 (113), and hDaxx is degraded by the tegument protein pp71 (114). EBV utilizes EBNA1 to drive the phosphorylation, polyubiquitination and subsequent degradation of PML (115), BZLF1 to disperse PML (116) and the vFGARAT BNRF1 to disperse hDaxx from its cognate partner ATRX (119). KSHV also encodes multiple ND10 antagonists. The vFGARAT K75 depletes ATRX and disperses Sp100 and PML from ND10 bodies (121). The vIRF3 degrades PML and displaces Sp100 from ND10 bodies (117). Lastly k-RTA retains SUMO-targeting Ubiquitin ligase (STUBL) function to degrade SUMO-modified PML (118). Only two viral antagonists of ND10 bodies have been identified in MHV68 thus far: the vFGARAT ORF75C degrades PML (85, 106) and the ribonucleotide reductase small/large subunit encoded by the early gene ORF61 (197) relocalizes PML into track-like structures reminiscent to that observed for the adenovirus E4-ORF3 protein (198).

Interestingly, MHV68 infection of human foreskin fibroblasts leads to the depletion of higher molecular weight Sp100 species as well as a slight reduction in hDaxx levels (122, 199). It remains to be determined if ORF75B is the virus factor responsible for the depletion of the lower mobility Sp100 isoforms or Daxx. It is also possible that ORF75B is encoded to antagonize an as yet unidentified host repressor. An analysis of ORF75B binding partners together with the examination of host proteins modulated during WT MHV68 and ORF75B.stop infections will likely shed more light on other host repressors targeted by ORF75B. Another informative experiment might be to compare the status of ND10 components in infections with viruses where the ORF75B.stop mutations discussed in this dissertation are layered on the predicted E3-ligase domain of ORF75C. Sewatonon and colleagues (123) determined that the 75C-E3 ligase null virus is impaired for PML degradation yet unperturbed in virus replication. This suggests redundancy in ND10 antagonism by MHV68. The 75C-E3 ligase null virus was used to identify MHV68 ORF61, a homolog of the large subunit of host ribonucleotide reductase large subunit, as a second PML antagonist encoded by MHV68 (197). An examination of the kinetics and levels of MHV68 replication in cells depleted for individual ND10 components might also be useful in identifying the influence of individual ND10 components in MHV68 replication.

In data not presented in this dissertation, we have found that the sole EBV vFGARAT, BNRF1, complements gene expression in an ORF75C mutant virus while KSHV ORF75 and MHV68 ORF75A do not complement ORF75C mutants for virus spread or gene expression. We propose that BNRF1 shares functions with MHV68 ORF75C. Whether this rescue is simply due to their conserved ND10 antagonism functions or signifies additional unknown roles for BNRF1 remains to be determined. Using the trans-complementation assay we are now exploring whether any of the other vFGARATs shares overlapping functions with MHV68 ORF75A. Given the enhancement in tegument delivery, we predict that ORF75A likely plays a role in the assembly and packaging of virion components. Interestingly, KSHV ORF75 interacts with two tegument proteins that promote virion assembly and egress (91). As such we will test if KSHV ORF75

rescues the MHV68 ORF75A replication defect. The trans-complementation assay will also determine if either ORF75B or EBV BNRF1 share functions with MHV68 ORF75A

VI. Impact of 75A on viral gene regulation, tegumentation, and virus production

The dysregulation of the levels and kinetics of intracellular protein expression in the absence of ORF75A requires a determination of whether ORF75A directly regulates viral gene expression or exerts regulatory functions in an indirect manner via host or viral factors. MHV68 viruses lacking either ORF73/LANA or ORF37 exhibit similar phenotypes to the MHV68 ORF75A.stop virus. They have higher lytic protein expression that leads to decreased infectious particle production (143, 189). Here, we find that ORF73 levels were not reduced, but rather elevated in 75A.stop infections or primary BMDM macrophages. Thus the ORF75A.stop phenotype is not likely attributed to the absence of LANA. MHV68 ORF37/muSOX encodes a homolog of the gammaherpesvirus viral nuclease that degrades viral and host mRNA during productive lytic replication (188, 189). ORF37 is not a tegument protein but is expressed with immediate early kinetics similar to MHV68 RTA or MHV68 ORF73 in *de novo* infected fibroblasts(133). MuSOX transcript or protein levels will be analyzed to determine if loss of ORF75A influences the levels of muSOX in the infected cell. To confirm that the enhancement of protein expression is due to a dysregulation of transcription and examine if this extends beyond muSOX, we will analyze whole genome transcription in 75A.stop1MR and 75A.stop1 infected cultures by microarray. These studies will aid in determining whether subsets of genes/transcripts escape dysregulation upon ORF75A loss. Finally, to determine if ORF75A directly regulates viral gene expression, we will examine the ability of ORF75A to repress the activation of lytic promoter-driven luciferase reporter constructs that are known to be responsive to the lytic transactivator RTA.

VII. Current model and experiments to address the model

From the data generated in this dissertation, we propose that ORF75A plays a role in negatively regulating the kinetics of ORF75C delivery and viral protein expression. The

enhanced protein production in turn triggers innate immune signaling. This innate response or other intrinsic defense in turn drives the observed increase in cell death such that the proportion of cells that produce infectious particles in the culture is reduced. The innate immune response to herpesvirus infections is dependent on host recognition of viral proteins, DNA and RNA (200). We established that loss of ORF75A results in an increase in both ORF75C tegument protein as well as intracellular proteins from each viral kinetic class. We will examine whether the production of viral transcripts and the viral DNA are also enhanced with ORF75A.stop virus infection. An increase in these pathogen-associated molecular patterns (i.e viral DNA, RNA and protein) will likely result in enhanced recognition by the cell. To confirm this, we will analyze the induction of innate immune signaling including the activation of type I interferon (IFN) signaling and the production of pro-inflammatory cytokines including TNFα, IL-1β and IL-18 upon infection of BMDMs or MEFs with the ORF75A.stop virus. We will also identify the upstream sensors required for the induction of IFN signaling by examining IFN induction or cytokine release in primary macrophage or fibroblast cells lacking pattern recognition receptors. A comparison of 75A.stop virus titers in WT and mutant primary fibroblasts or macrophages will test the influence of IFN signaling on the 75A.stop replication replication defect. *In vivo*, an examination of the immune infiltrate within the bronchial lung lavage would identify whether enhanced recognition by the innate immune system results in enhanced recruitment of innate immune cells such as natural killer cells to the MHV68 infected lung. To examine the manner of cell death, immunoblot analysis of caspase activation in ORF75A.stop and ORF75A.stopMR infected cells is needed. We would also couple these immunoblots with drug treatment of infected cells with cell death inhibitors to further confirm the manner of cell death.

ORF75A may serve as a rheostat to limit viral gene expression. This hypothesis is intriguing in that it implies that the virus limits protein expression to impair engagement of host innate immune defenses. If this is true, then it is not necessarily the absence of ORF75A, but rather the host response to the infection that is responsible for the majority of the ORF75A.stop replication defect. Eliminating the innate host response to infection might also unveil other novel functions of the ORF75A tegument protein that would not otherwise be revealed.

VII. Impact of these studies.

The experiments described above may uncover novel functions of host components of host immunity in regulating the response to gammaherpesvirus infection. Moreover, we predict that that these studies will aid in the identification of viral and host determinants critical for regulating viral gene expression to maximize virus output. An ORF75A function in virion assembly and tegumentation will expand our understanding on which viral factors control and regulate this crucial step in herpesvirus replication. This might lead to the identification of virus-host interactions that promote assembly. We developed a trans-complementation assay to examine roles for the other MHV68 vFGARATs in ORF75C defective viruses. This assay will be used to examine whether human vFGARATs retain similar functions. We predict that these studies will be crucial in strengthening our understanding of the roles played by these gammaherpesvirus-specific proteins in chronic infection and possibly the oncogenic events associated with this family of herpesviruses. Lastly, these studies may lead to novel antiviral strategies that target vFGARAT-specific motifs or their host binding partners to block virus.

Appendix 1. Host Restriction of Murine Gammaherpesvirus 68 Replication by Human APOBEC3 Cytidine Deaminases but Not Murine APOBEC3

Nana Minkah[1], Kevin Chavez[1], Parth Shah[2], Thomas MacCarthy[2], Hui Chen[3,*], Nathaniel Landau[3], Laurie T. Krug[1]

[1]Department of Molecular Genetics and Microbiology, [2]Department of Applied Mathematics and Statistics, Stony Brook University, Stony Brook, NY 11794; [3]Department of Microbiology, NYU Langone Medical Center, New York, NY 10016

*, current address for Hui Chen: Cornell University, Ithaca, NY 14850

ABSTRACT

Humans encode seven APOBEC3 (A3A-A3H) cytidine deaminase proteins that differ in their expression profiles, preferred nucleotide recognition sequence and capacity for restriction of RNA and DNA viruses. We identified APOBEC3 hotspots in numerous herpesvirus genomes. To determine the impact of host APOBEC3 on herpesvirus biology *in vivo*, we examined whether murine APOBEC3 (mA3) restricts murine gammaherpesvirus 68 (MHV68). Viral replication was impaired by several human APOBEC3 proteins, but not mA3, upon transfection of the viral genome. The restriction was abrogated upon mutation of the A3A and A3B active sites. Interestingly, virus restriction by A3A, A3B, A3C, and A3DE was lost if the infectious DNA was delivered by the virion. MHV68 pathogenesis, including lung replication and splenic latency, was not altered in mice lacking mA3. We infer that mA3 does not restrict wild type MHV68 and restriction by human A3s may be limited in the herpesvirus replication process.

INTRODUCTION

*A*polipoprotein *B* mRNA editing enzyme catalytic polypeptide-like editing complex 3 (APOBEC3) proteins belong to a family of host cytidine deaminases with a wide array of biological functions, subcellular localization and tissue expression profiles (201, 202). Eleven members of this enzyme family have been discovered in humans; APOBEC1, APOBEC2, APOBEC3, APOBEC4 and *a*ctivation induced deaminase (AID). APOBEC1 (A1), the founding member of this family, is an mRNA editing enzyme that deaminates Apolipoprotein B mRNA to produce two isoforms of apolipoproteins that are required for low-density lipid formation(203, 204). APOBEC2 (A2) is a more recently discovered member detected predominantly in the heart and skeletal muscle (205). Mice transgenic for human A2 develop lung and liver tumors (206). APOBEC4 (A4) was discovered by computational searches for genes homologous to A1 and, like A2, has no ascribed function. The most widely studied members are AID, which is critical for generating antibody diversity through ssDNA deamination of the immunoglobulin locus, and APOBEC3 (A3) proteins, which act as innate immune barriers to the replication of viruses and endogenous retroelements (207, 208).

APOBEC3 genes have undergone duplication events in the course of mammalian evolution. Murid rodents encode the single APOBEC3, mA3, while felines encode four APOBEC3s (209) and the equine genome encodes six (210). Primates have an expanded repertoire of seven APOBEC3 proteins; A3A, A3B, A3C, A3DE, A3F, A3G and A3H with each having slightly different target sequences. A3s have been widely studied since the identification of human A3G (hA3G) as a host restriction factor of viral infectivity factor (Vif)-deficient HIV (211). In Vif-deficient HIV infections, hA3G is packaged into viral cores through interactions with both the HIV nucleopcapsid protein and the viral genomic RNA. A3G deaminates cytosine residues to uracils in the newly synthesized strand. Vif enhances HIV replication by binding to hA3G and either targeting it for degradation or preventing packaging into the HIV core (212, 213).

Retroviruses, retroelements and more recently DNA viruses have emerged as targets of hA3 proteins (214-223). Human A3A and A3C have been reported to restrict herpes simplex virus type 1 (HSV-1) replication in transient expression studies (224). Additionally, Suspene et al.

reported the detection of virus variants consistent with cytidine deamination in clinical specimens positive for either HSV-1 or Epstein-Barr virus (EBV) (224). However, in most cases the impact of hA3 activity on the *in vivo* pathogenesis of a given virus in the host has not been extensively studied. The murine APOBEC3 exhibits antiviral activity against multiple murine and human retroviral targets, (225-228) implying that mA3 retains the retroviral targeting function of the human A3. However, the antiviral function of mA3 against herpesviruses is not known. In this report, we examined the ability of mA3 to restrict murine gammaherpesvirus 68 (MHV68), a natural pathogen of murid rodents that has strong genetic colinearity with, and biological similarities to, the human gammaherpesviruses, Kaposi's sarcoma-associated herpesvirus (KSHV/HHV-8) and Epstein Barr Virus (EBV). We determined the distribution of A3 hotspots in the MHV68 genome, queried the effect of A3 overexpression on viral replication and the finally ascertained the impact of loss of A3 on *in vivo* pathogenesis. Although we observed restriction of MHV68 replication with co-expression of several hA3s, the murine APOBEC3 did not alter MHV68 replication and pathogenesis.

MATERIALS AND METHODS

Viruses, cells and mice. The recombinant marking virus, MHV68-H2BbYFP was used the for cell-culture experiments. This virus encodes a histone 2b (H2b)-enhanced yellow fluorescent protein (eYFP) fusion protein that tethers the YFP protein to nucleosomes and eliminates the passive diffusion of the fluorescent YFP signal out of the nucleus to enhance infected cell imaging by microscopy (161). Mice were infected with MHV68 WUMS (ATCC VR1465) as the wild-type virus. Virus passage and titer determination were performed as previously described (57, 229).

Human epithelial kidney cells (HEK 293T) were maintained in Dulbecco's modified Eagle's medium (DMEM) supplemented with 10% fetal bovine serum, 1% penicillin, and streptomycin at 37^{o}C in 5% CO_2. Murine fibroblast cells (NIH 3T12) were maintained in Dulbecco's modified Eagle's medium (DMEM) supplemented with 8% fetal calf serum, 100 U of penicillin per ml and 100 mg of streptomycin per ml at 37^{o}C in 5% CO_2

Murine APOBEC3 KO (mA3$^{-/-}$) mice were generated by blastocyst injection of 129P2/OlaHsd embryonic stem cell clone XN450 (Baygenomics, San Francisco) that contained an 8 kb galactosidase-neomycin fusion (β-geo) gene trap insertion retroviral vector between exons 4 and 5 of *mA3*. The mice were crossed for several generations onto a C57/Bl6 background and genotyped by PCR using primers spanning the insertion site. The WT genotype was amplified with primer 21 (5' CTGTAACCTGGTATCTCCCGTC 3') and primer 22 (5' GGAAAAACTGCTTGCCAGGCTC 3'). The mA3$^{-/-}$ genotype was amplified with primer 21 (5' CTGTAACCTGGTATCTCCCGTC 3') and primer 23 (5' CACAAGGTTCATATGGTGCCGT 3'). The mA3$^{-/-}$ mice and their WT C57BL6 counterparts were maintained at the Stony Brook University Division of Laboratory Animal Research (DLAR) facility in accordance with protocols approved by the Institutional Animal Care and Use Committee of Stony Brook. Eight- to twelve-week old WT and mA3$^{-/-}$ mice were infected intranasally with 1000 PFU of MHV68

under isoflurane anesthesia. At the indicated times post infection, organs were harvested and processed as described below.

Transfections. For transient co-transfections, 4 x 10^5 HEK 293T cells were seeded per well of a 12-well tissue culture plate one day prior to transfection with 2.5 μg of APOBEC3 expression plasmids and 1.55 μg of MHV68 BAC DNA. All transient co-transfections were performed using TransIT-LT1 Transfection Reagent according to the manufacturer's instructions (Mirus, Madison WI). Forty-eight hrs later, the cells were subjected to multiple freeze-thaw cycles to release infectious virus that was then titered by plaque assay on a NIH 3T12 cell monolayer.

For the transfection followed by infection experiments, HEK 293T cells were transfected with the desired human and mouse APOBEC3 proteins as outlined above. Twenty-four hrs post-transfection, cells were infected with MHV68-H2bYFP virus at an MOI of 0.01. Forty-eight hrs after the infection virus output was quantified by a plaque assay.

Fluorescence microscopy. Virus infection with MHV68-H2bYFP was visualized by fluorescence microscopy. Imaging was performed with a Zeiss Axiovert S100 inverted microscope (Carl Zeiss Microscopy GmbH, Jena Germany) equipped with a Luminera INFINITY 3-1UR 1.4 megapixel low light CCD digital camera (Lumenera, Ottawa ON Canada). Images were analyzed using Axiovision Software (Axiovision LE Rel.4.3, Carl Zeiss Microscopy GmbH, Jena Germany).

Plaque assay. 1.8 x 10^5 NIH 3T12 cells were seeded per well in a 6-well tissue culture plate one day prior to infection. The next day, the NIH 3T12 cells were infected with serial dilutions of cell homogenate and overlayed with 1.5% methylcellulose in DMEM containing 5% FBS. One week later, the methylcellulose was removed and cells were washed twice with PBS prior to methanol fixation and staining with a 0.1% crystal violet solution in 10% methanol.

Immunoblot. Total protein lysate was harvested in lysis buffer (150 mM sodium chloride, 1.0% IGEPAL CA-630, 0.5% sodium deoxycholate, 0.1% sodium dodecyl sulfate, 50 mM Tris pH 8.0) supplemented with a protease inhibitor cocktail (Sigma, St. Louis MO). Fifty micrograms of each lysate were separated in a 12% SDS PAGE gel and transferred onto polyvinylidene fluoride (PVDF) membrane. APOBEC3 proteins were detected using a mouse monoclonal antibody specific for the HA-epitope (Cell signaling, Danvers MA) on mA3, A3B, A3C, A3F, and A3G constructs, a V5 epitope (Santa Cruz biotechnology, Dallas Texas) for A3DE and a rabbit monoclonal specific for human A3A (230). A rabbit monoclonal antibody to human glyceraldehyde 3-phosphate dehydrogenase (GAPDH) was used as a loading control. HRP-conjugated secondary antibodies were detected using an enhanced chemiluminescence reagent (ECL, Thermo Scientific, Waltham MA).

Quantitative PCR. Total cell DNA from the co-transfection experiments was column-purified (Qiagen, Limburg, Netherlands) and digested with 20 units of *Dpn*1 (New England Biolabs, Ipswich MA) for 12 hours at 37^{o}C to remove input MHV68 BAC DNA. One ng of DpnI-digested DNA was input into a quantitative PCR reaction (Quanta Biosceinces- Perfecta SYBR GREEN, Gaithersburg MD) using primers specific to a region of MHV68 ORF12 (forward primer, 5' GTCTACAACAGGATCTGCATTT 3', reverse primer 5' AAAACTCTACCGTGACTGTGAA 3') and primers for human GAPDH (forward primer, 5' GTATGACTGGGGGTGTTGGG 3', reverse primer 5' GCGCCCAATAGGACCAAATC 3'). The relative level of viral genome copy number was determined by ΔΔCt.

Sequencing. Total cell DNA from the co-transfection experiments was extracted as outlined above. The DNA was digested with 20 units of *Dpn*1 (New England Biolabs, Ipswich MA) for 12 hours at 37^{o}C to remove input MHV68 BAC DNA. Two regions in the MHV68 genome (bp 69,873- 70,761 and bp 88,884 to 89,613) were amplified with Dynazyme II DNA polymerase (Thermo Scientific, Waltham MA), cloned into the TOPO TA cloning vector (Life Technologies, Carlsbad, CA) and sequenced to identify mutations that arose during infection.

Pathogenesis. For acute titers, the right and left lungs of mice were removed 4 and 9 days post infection and disrupted with a Mini-Beadbeater (Biospec, Bartlesville OK). The homogenates were titered by plaque assay. Spleens were harvested to determine viral latency establishment and reactivation from latency 16 dpi.

To determine the frequency of cells harboring the viral genome, a single cell suspension of splenocytes was prepared and analyzed by limiting dilution PCR. Six, three-fold serial dilutions of splenocytes were plated in a 96-well PCR plate in a background of NIH 3T12 cells and lysed overnight at 56^0C with Proteinase K. The plate was then subjected to an 80-cycle nested PCR with primers specific for MHV68 ORF50. Twelve replicates were analyzed at each serial dilution and plasmid DNA at 0.1,1 and 10 copies was included to verify the sensitivity of the assay.

To determine the frequency of cells harboring latent virus capable of reactivation upon explant, single cell splenocytes were prepared from mice 16 dpi, resuspended in DMEM containing 10% fetal bovine serum and plated in twelve serial two-fold dilutions onto a monolayer of mouse embryonic fibroblast (MEF) cells prepared from C57BL6J mice in 96-well tissue culture plates. Twenty-four replicates were plated per serial dilution. The wells were scored for cytopathic effect (CPE) two to three weeks after plating. To differentiate between pre-formed infectious virus and virus spontaneously reactivating upon cell explant, parallel samples were mechanically disrupted using a Mini-Beadbeater prior to plating on the monolayer of MEFs to release preformed virus that is scored as CPE.

Bioinformatic analysis. To measure under- and over-representation of APOBEC3 hotspots, we compared the observed frequency of each APOBEC consensus motif (TC for hA3A, hA3B, hA3F and hA3H, TTC for hA3C, CCC for hA3G and TCC for mA3) to a random expectation null model. To assess the effects throughout the viral genomes we used sliding 1 kilobase windows to scan each genome at intervals of 100 nucleotides (i.e. first window from position 1-1000, second window from 101-1100, and so on). The null model was generated using 1,000

randomly shuffled versions of each genome. The number of occurrences of the motif (TC, TTC, etc) in each randomly shuffled sequence was used to build a null model distribution for that window. If the true frequency that was observed in the unshuffled sequence was within the lowest 5^{th} percentile of this distribution, we labeled that window as being underrepresented. Conversely, if the true frequency was in the highest 5^{th} percentile, the window was labeled as overrepresented for that motif. The NCBI accession numbers for the genomes analyzed are: Human papilloma virus type 16(NC_001526), Herpes simplex virus 1(NC_001806), Herpes simplex virus 2(NC_001798), Varicella-zoster virus (NC_001348), Epstein-Barr virus (NC_007605), Human cytomegalovirus (NC_006273), Human herpesvirus 6A (NC_001664), Human herpesvirus 6B (NC_000898), Human herpesvirus 7(NC_001716), Kaposi's sarcoma-associated herpesvirus (NC_009333) and Murine gammaherpesvirus 68 (NC_001826).

Statistical analyses.

Data was analyzed using Graphpad Prism Software (Prism 5, La Jolla CA). The statistical significance of differences between groups was tested using a non-paired two-tailed t test. Under Poisson distribution analysis, the frequencies of latency establishment and reactivation from latency were determined by the intersection of nonlinear regression curves with the line at 63.2%.

RESULTS

APOBEC3 hotspots are prevalent in herpesvirus genomes.

In a single report outlining the impact of APOBEC3 cytidine deaminase on herpesviruses, HSV-1 replication was reduced 4-10 fold upon transient expression of hA3C. In addition, hyperedited HSV-1 and EBV sequences consistent with hA3 deamination were detected in patient samples using a sensitive, but non-quantitative PCR detection method (224). However, the natural occurrence of APOBEC3-mediated cytidine deamination and the consequence of this selective pressure are not known. We utilized an *in silico* approach to predict the distribution of APOBEC3 recognition sites in herpesvirus genomes. The 'hotspot' or consensus recognition sequence is TC (where the underlined C represents the targeted cytidine) for hA3A, hA3B, hA3F and hA3H, (231-235) TTC for hA3C (236), CCC for hA3G (237), and TCC for mA3 (238). To determine whether particular A3 hotspot motifs were over- or under-represented throughout the viral genomes we measured the frequency of each A3 hotspot motif (TC, TTC, CCC and TCC) within a 1 kb sliding window across each genome at intervals of 100 nt. The observed frequencies in each window were then compared to a null model based on randomly shuffled versions of that genome sequence, allowing us to statistically evaluate overrepresentation and underrepresentation.

Viruses that are susceptible to various A3 enzymes would likely have evolved to limit hotspot motifs in their genomes. Viruses that do not encounter certain A3 proteins or those with a viral countermeasure might have an overrepresentation of motifs in their genomes, especially if they have evolved under pressures to avoid a different A3 protein. For example. an under-representation of TTC (the motif for hA3C) will increase the relative frequency of other motifs such as CCC (the motif for hA3G) assuming that there are no additional selective pressures against the other motifs. We evaluated the predictive ability of our model by examining the APOBEC3 hotspot distribution in human papilloma virus 16 (HPV16). HPV genomes are targets for deamination upon overexpression of hA3A, hA3C, and hA3H, and mutation signatures that are consistent with deamination at TC hotspots are detected by a sensitive PCR assay in clinical

wart specimens (222). Human A3A, hA3B and hA3H are expressed in dermal epithelial cells, the preferred site of infection and viral replication of HPV (239-242). Taken together, HPV is subjected to the selective pressures of hA3s with TC hotspots (222). In agreement, our computational analysis determined that TC hotspots were largely underrepresented in the HPV genome (Figure 1A). This depletion of TC hotspots in the genome is consistent with evasion from the antiviral pressures of hA3A, hA3B, hA3F or hA3H (A3A/A3B/A3F/A3H). Moreover, the HPV genome had an underrepresentation of TTC hotspots favored by the ubiquitously expressed hA3C. In contrast, the HPV genome was largely neutral with some enrichment for CCC hotspots recognized by hA3G, which is expressed predominantly in lymphocytes, a cell type not known as a reservoir for HPV. Finally, the HPV genome was predominately neutral with some occurrences of mA3 enriched regions. This is consistent with a human pathogen that would not have been under selective pressure to limit mA3 sites in the genome.

An analysis of multiple herpesviruses revealed similar trends in the profile of human and mouse APOBEC3 hotspots among members within the alpha, beta, and gammaherpesvirus subfamilies. As depicted in Figure 1A, the alphaherpesvirus HSV-1 genome is enriched for A3C and A3G hotspots. The VZV genome also has regions with overrepresentation of A3G hotspots. However, the underrepresentation of A3A/A3B/A3F/A3H and A3C hotspots suggests selective pressure to limit APOBEC3 recognition. Within the betaherpesviruses, the HCMV genome had regions overrepresentated with A3C and A3A/A3B/A3F/A3H hotspots, but was largely underrepresented for A3G and mA3 hotspots. The HHV-6A genome was enriched for A3A/A3B/A3F/A3H and A3C hotspots. The human gammaherpesvirus EBV and KSHV genomes are enriched for A3G sites. The KSHV genome was underrepresented for A3A/A3B/A3F/A3H hotspots. The MHV68 genome was enriched for hA3G and mA3 hotspots. In Figure 1B, the heatmap representation of the percentage of overrepresented regions (left panel) and underrepresented regions (right panel) in the genomes of each human herpesvirus and MHV68 illustrates commonalities in the hotspot profile within the betaherpesvirus and gammaherpesviruses. With the exception of HCMV, mA3 sites (TCC) were overrepresented in each herpesvirus genome analyzed. Lastly, we examined the distribution of hotspots in the

MHV68 genome. With the exception of the internal repeats at nt positions 26,778-28,191 and 98,981-101,170, the regions of overrepresented hotspots were evenly distributed along the MHV68 genome (Figure 1C). Taken together, our analysis predicts that herpesvirus genomes are susceptible to APOBEC3 deamination.

Human APOBEC3 restriction of MHV68 replication.

Given the identification of A3 hotspots in the MHV68 genome, we next examined the impact of A3 expression on lytic replication. We co-transfected A3 expression constructs with infectious MHV68+ BAC DNA that encodes the YFP marker to monitor viral replication by fluorescent microscopy. Expression of hA3A limited the infection to single YFP+ cells (Figure 2, top panel). In contrast, co-transfection of the empty vector or the A3A E72A active site mutant resulted in foci of 10-20 YFP+ cells, indicating no impairment of virus spread. Expression of wild type mA3 did not impair the formation of YFP+ foci in the infection (Figure 2, bottom panel).

These observations of virus restriction by hA3 but not mA3 were confirmed and extended to other human APOBEC3s upon quantitation of virus yield by plaque assay (Figure 3A). Human A3A inhibited viral replication by nearly 4 logs while co-transfection with hA3B and hA3C proteins resulted in a 2.5 log-fold reduction in replication. Co-transfection of either hA3DE or hA3H resulted in a lesser 5-fold reduction in virus output while hA3F and hA3G did not impair MHV68 replication. In agreement with our previous observation that mA3 overexpression did not impact virus spread in the culture, co-transfection with mA3 did not impact MHV68 yield (Figure 3B). Expression of the human and mouse APOBEC3 proteins was verified by immunoblot (Figure 3A and 3B, respectively). We conclude that hA3A, hA3B and hA3C are restrictive against MHV68 while mA3 is not.

Human APOBEC3 restriction of MHV68 replication is dependent on A3 active sites.

Given the observation that several human APOBEC3 proteins impair MHV68 replication, we next examined if APOBEC3 enzymatic activity is required by comparing

restriction of MHV68 by the WT and active site mutant forms of hA3A and hA3B. Similar to other APOBEC proteins, A3 enzymes have retained a conserved active site sequence consisting of His-X-Glu-X_{23-28}-Pro-Cys-X_{2-4}-Cys. The histidine and cysteine residues coordinate a Zinc ion while the glutamic acid serves as a proton shuttle in catalysis (207). Mutation of either the cysteine or the glutamic acid abolishes the cytidine deaminase function of A3 enzymes (223, 230). The hA3A E72A active mutant did not restrict MHV68 yield compared to WT hA3A (Figure 4A). Restriction by hA3B was lost with the N-terminal E68A single active site mutant and the E68A/E255A double mutant. However, the C-terminal single hA3B E255A mutant retained restrictive function by reducing virus yield by 4.5-fold, albeit 56% less than the WT hA3B (Figure 4A). The changes in restriction were not attributed to differences in expression levels of the WT and active site hA3 mutants (Figure 4A, lower panel). Since hA3A reduced MHV68 DNA copy number by greater than 50-fold compared to the empty vector and A3A E72A mutant controls (Figure 4B), we examined two regions of the MHV68 genome for C to T or G to A transition mutations. In samples derived from A3A and A3B cotransfections, the incidence of mutation was extremely low in 18 and 11 respective clones of a GC-rich region of the genome (bp 69,873 to 70,761) and 24 and 23 respective clones of a second region of the genome that is enriched for TC hotspots (bp 88,884 to 89,613) (Table 1). While three transition mutations were observed for region two in A3A-restricted samples, these led to silent or conservative aa changes. We also found a similar number of transition mutations in the viral DNA of samples derived from the empty control vector cotransfections. The mean mutation frequency for MHV68-infected samples restricted by A3A (0.15%) and A3B (0.06%) contrasts sharply with the mutation frequencies reported for HSV-1 and EBV (6-20% by Suspene et al. 2001) and hepatitis B virus (25-50% by Vartanian et al. 2008). Taken together, the active sites of hA3A and hA3B are required for MHV68 restriction, but we found no strong evidence for hA3A or hA3B deamination of the genome.

Human APOBEC3 restriction of MHV68 replication is lost upon *de novo* infection.

Several human APOBEC3 proteins were identified as potent inhibitors of MHV68 replication, the nuclear localized hA3B (243), the predominantly cytoplasmic hA3DE (244), and hA3A, hA3C and hA3H, which shuttle between the nucleus and cytoplasm (244-246). The MHV68 genome delivered by transfection would likely be susceptible to APOBEC3s in both the nucleus and cytoplasm. However, we reasoned that the encapsidated genome would be protected from cytoplasmic A3s in a *de novo* infection with intact particles. As such, we transfected the panel of APOBEC3 constructs one day prior to infection with MHV68 at a multiplicity of infection (MOI) of 0.01. We unexpectedly found that the APOBEC3 proteins with potent restrictive function in the co-transfection experiment were no longer restrictive against infection initiated by virion particles (Figure 5). Thus, the method of viral genome delivery and initiation of lytic infection influences the restrictive capacity of the APOBEC3 enzymes. This suggests that either compartmentalization of the herpesvirus genome or counter-functions imparted by virion-associated factors result in a replicative process that is impervious to antiviral APOBEC3 function.

Murine APOBEC3 does not impact MHV68 replication *in vivo*.

Murine A3 overexpression in 293T cells did not significantly restrict MHV68 replication. However transient expression studies cannot be relied upon as an absolute indicator of the capacity of an antiviral molecule to restrict a pathogen in the host. Thus, we determined the impact of murine A3 on MHV68 pathogenesis in mice with a disruption in the mA3 gene (Figure 6A). The galactosidase-neomycin fusion (*β-geo*) stop cassette that is inserted between exons IV and V of mA3 in murine APOBEC3 knock-out mice ($mA3^{-/-}$ mice) was confirmed by PCR and amplimer sequencing (Figure 6B). Additionally, mA3 protein was not detected in the spleens or thymus of $mA3^{-/-}$ mice (Figure 6C). Okeoma et al. (2007) generated $mA3^{-/-}$ mice as described here; a truncated protein in $mA3^{-/-}$ tissues was not observed. Furthermore, a truncated mA3 protein generated from exons 1-4 was devoid of deaminase function upon *in vitro* expression (226).

Infection of mice with MHV68 by intranasal inoculation is followed by a period of acute replication in the lung. To examine the influence of mA3 on acute replication, the levels of virus replication in the lungs of infected WT or mA3$^{-/-}$ mice were measured at 4 and 7 dpi. Although there is a slight, non-statistically significant difference between the two groups at 4 dpi, viral titers were indistinguishable between WT and mA3$^{-/-}$ mice at 7 dpi, indicating that the loss of murine APOBEC3 did not enhance MHV68 replication in the lung (Figure 6D).

Active MHV68 replication is typically cleared from the lung within two weeks prior to virus dissemination to the spleen. MHV68 establishes a latent infection primarily in B cells of the spleen with the peak of latency 16-18 dpi, a timepoint closely corresponding to germinal center expansion (57, 229). We observed a robust two-fold increase in splenomegaly as expected, yet there was no difference between the degree of splenic expansion in the infected WT and mA3$^{-/-}$ mice. To examine whether loss of mA3 would impact latency establishment in the spleen 16 dpi, intact splenocytes were analyzed by a limiting dilution PCR assay to determine the frequency of viral genome positive cells. MHV68 established equivalent levels of latency in the spleens of WT (1/156) and mA3$^{-/-}$ mice (1/128) (Figure 6F). The frequency of intact splenocytes that spontaneously reactivated was examined by the observation of CPE upon explant and coculture with MEFs in a limiting dilution reactivation assay. Loss of mA3 had an insignificant two-fold impact on MHV68 reactivation, with splenocytes from infected WT mice and infected mA3$^{-/-}$ mice reactivating at frequencies of 1/19,074 and 1/10,966 cells, respectively (Figure 6G). Moreover, this slight difference in reactivation at 16 dpi had no effect on the maintenance of the frequency of genome positive cells later during chronic infection at 42 dpi (data not shown). Taken together, the absence of mA3 did not impact any aspect of MHV68 pathogenesis up to six weeks following an intranasal infection.

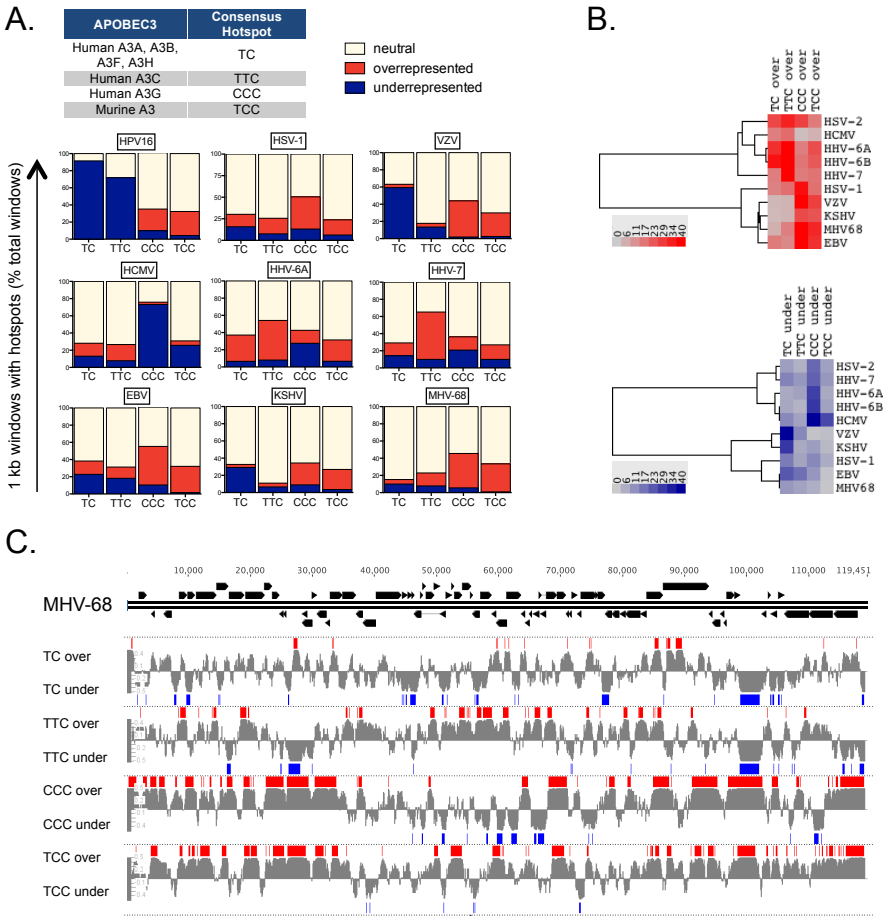

Figure 1: APOBEC3 hotspots in herpesvirus genomes. A. Percentage of 1 kb windows neutral, overrepresented or underrepresented for human and mouse APOBEC3 hotspots in the indicated viral genome. B. Heatmap of A3 hotspots in herpesvirus genomes. Scale indicates the percentage of 1 kb windows of the viral genome with overrepresentation or underrepresentation of hotspots as described in A. C. Distribution of 1 kb regions of the MHV68 genome overrepresented (red bars) or underrepresented (blue bars) for the indicated A3 hotspots. The boundary of each bar corresponds to the midpoint of the first and last 1 kb window represented within the bar. The gray trace represents the distribution of the hotspot occurrence in a region compared to the occurrence in 1,000 randomly shuffled 1 kb genomic regions. The scale of the trace is from -0.5 to 0.5, the numbers on the y-axis indicate the distance from the mean of each distribution (y=0). Genomic regions are significantly overrepresented (red bars) or underrepresented (blue bars) if they are above 0.45 or below -0.45 respectively.

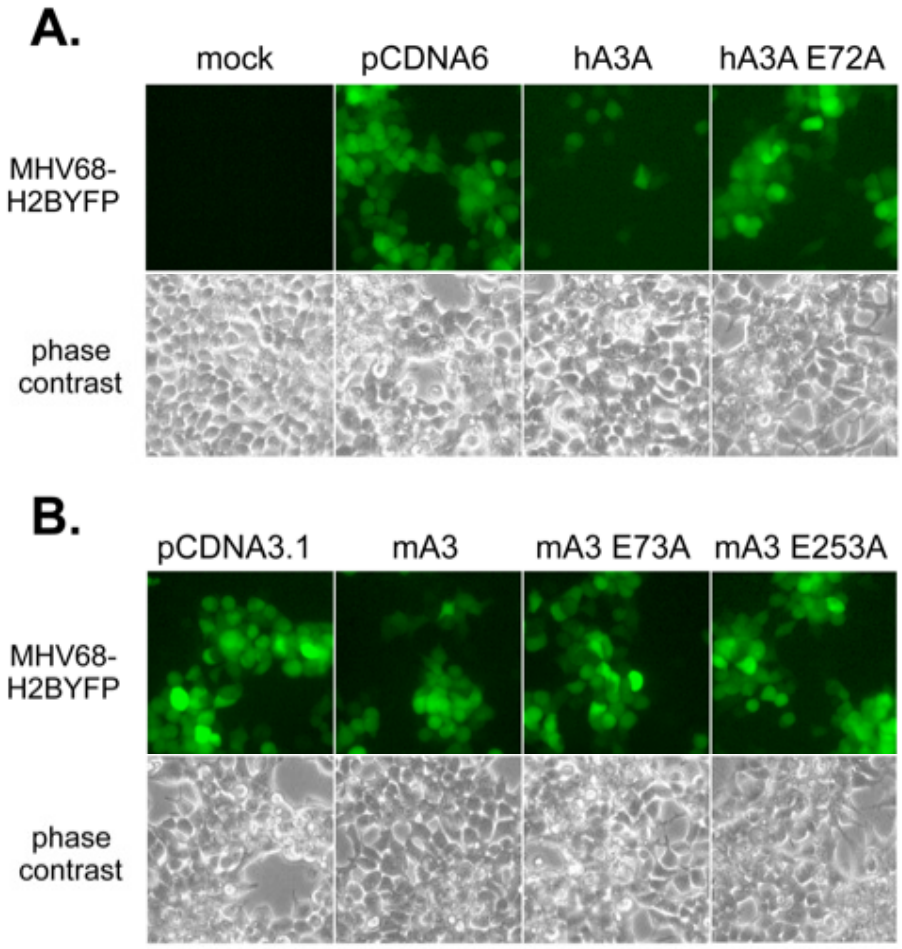

Figure 2: Restriction of MHV68 spread by human APOBEC3A, but not murine APOBEC3. HEK 293T cells were cotransfected with MHV68-H2bYFP BAC and the indicated human (hA3) and murine (mA3) APOBEC3 constructs and virus spread was visualized by fluorescence microscopy (upper panels) and bright field microscopy (lower panels) 48 hrs later. HA3A E72A is an active site mutant of human A3A. MA3 E73A and mA3 E253A are active site mutants of mA3. Images shown are cropped fields of pictures taken at 20X magnification. The images of MHV68-H2bYFP+ foci were false-colored green.

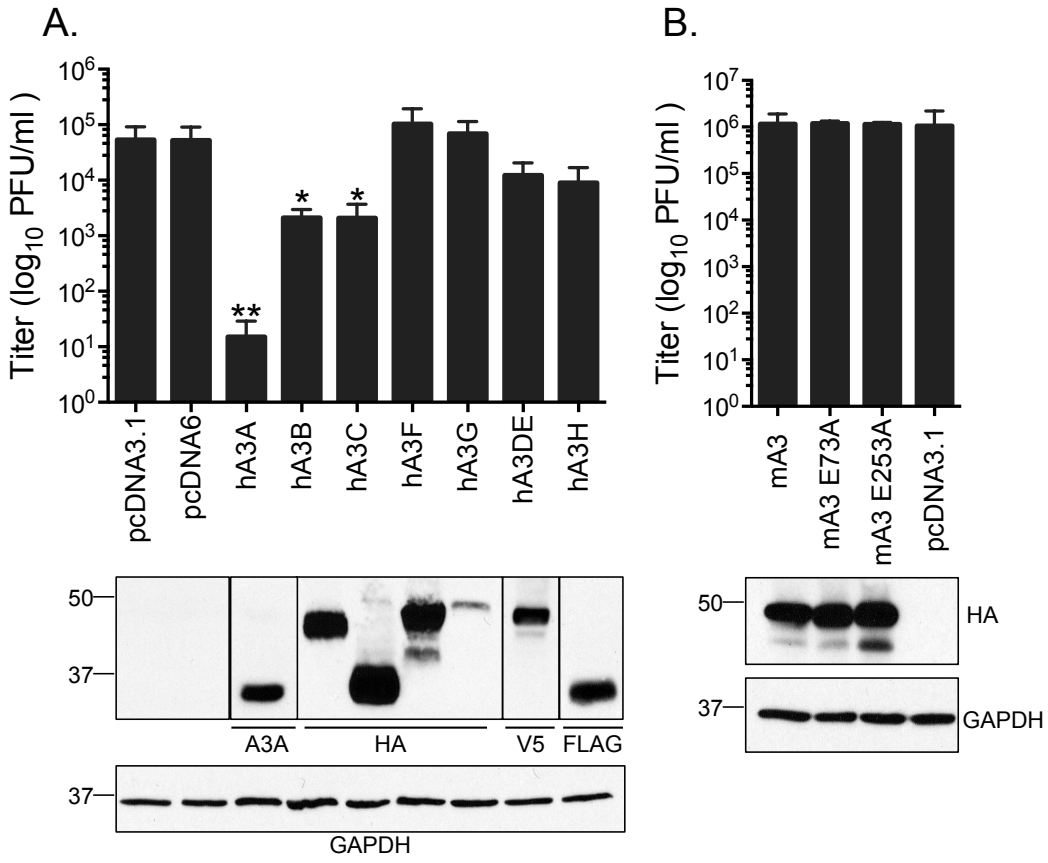

Figure 3: Restriction of MHV68 replication by human APOBEC3. A. Variable restriction by human APOBEC3 constructs as measured by plaque assay 48 hrs after HEK 293T cells were cotransfected with infectious MHV68-H2bYFP BAC DNA and the indicated APOBEC3 constructs. B. Murine A3 did not significantly impair MHV68 replication in HEK293Ts. Below each bar graph, immunoblots using antibodies against the indicated epitopes were used to validate APOBEC3 expression. Lysates from the empty vectors pcDNA3.1 (control vector for hA3B-hA3H) and pcDNA6 (control vector for hA3A and hA3C) were included in each blot and revealed no specific signal. Bars represent the mean +/- standard deviation of three replicates (A) and five replicates (B); *p≤0.05 and **p≤0.005.

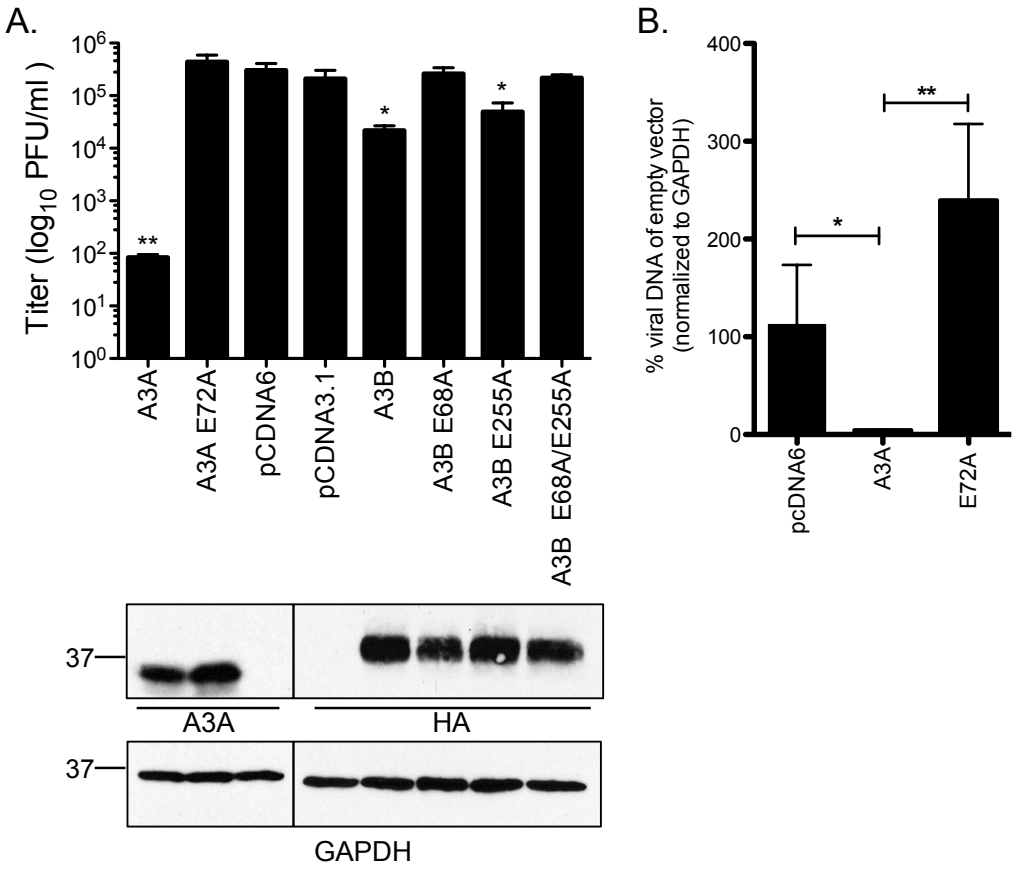

Figure 4: APOBEC3A and APOBEC3B active sites are required for restriction of viral replication and viral DNA synthesis. A. Loss of restriction by mutant human APOBEC3A (hA3) and APOBEC3B (hA3B) constructs as measured by plaque assay and quantitative PCR (hA3B) 48 hrs after HEK 293T cells were cotransfected with infectious MHV68-H2bYFP BAC DNA and the indicated APOBEC3 constructs. Below each bar graph, immunoblots using antibodies against the indicated epitopes were used to validate APOBEC3 expression. Lysates from the empty vectors pcDNA6 (control vector for WT and mutant hA3A) and pcDNA3.1 (control vector for WT and mutant hA3B) were included in each blot and revealed no specific signal. Bars represent the mean +/- standard deviation of three replicates; *p≤0.05 and **p≤0.005. B. Quantitation of MHV68 genomes by qPCR analysis of *Dpn*I-digested DNA. DNA levels were normalized to levels upon cotransfection with the empty vector, pCDNA6; *p≤0.05 and **p≤0.005.

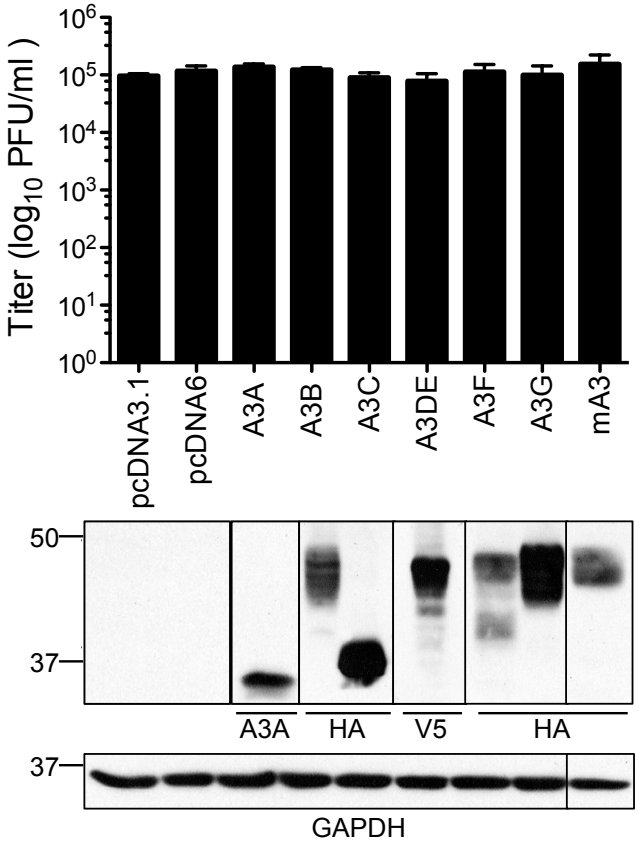

Figure 5: Loss of APOBEC3 restriction in the context of *de novo* infection with virus particles. HEK 293T cells were transfected with the indicated APOBEC3 constructs 24 hrs prior to *de novo* infection with MHV68-H2bYFP virus. MHV68 replication was measured by plaque assay 48 hpi. Below each bar graph, immunoblots using antibodies against the indicated epitopes were used to validate APOBEC3 expression. Lysates from the empty vectors pcDNA3.1 (control vector for hA3B, hA3DE-hA3H) and pcDNA6 (control vector for hA3A and hA3C) were included in each blot and revealed no specific signal.

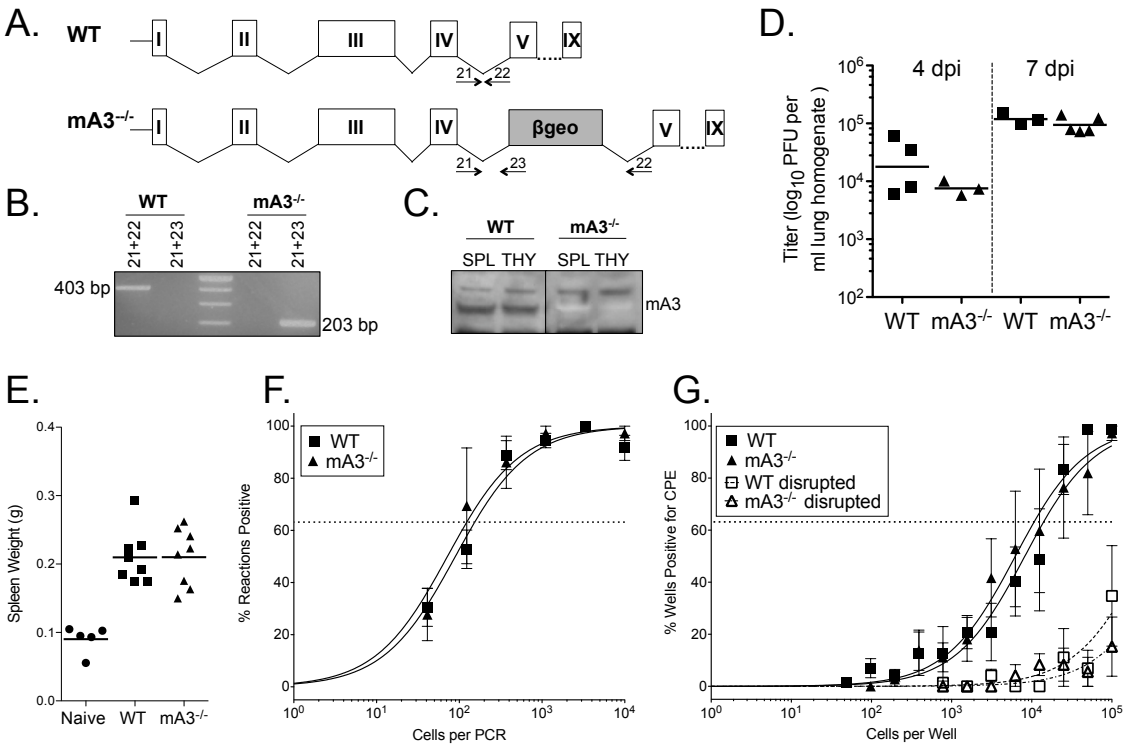

Figure 6: Absence of murine APOBEC3 does not alter MHV68 pathogenesis.
A. Schematic depicting the disruption of murine APOBEC3 (mA3) by the insertion of a β-geo cassette to generate mA3 knockout mice (mA3$^{-/-}$). **B.** Genotype PCR analysis of DNA harvested from the splenocytes of infected WT C57BL/6 or mA3$^{-/-}$ mice. The locations of primers for either the WT or mutant mA3 gene are shown in panel A. **C**. Immunoblot demonstrating expression of mA3 in WT but not mA3$^{-/-}$ mice. **D**. Acute replication in the lungs of WT or mA3$^{-/-}$ lungs 4 and 7 days post intranasal infection with 1000 PFU of WT MHV68. **E.** Spleen weights from naïve WT, infected mA3$^{-/-}$ mice or infected WT mice 16 dpi. **F.** Latency is determined as the frequency of viral genome positive splenocytes determined by limiting dilution PCR. **G.** Frequency of reactivation from intact splenocytes determined by a limiting dilution explant reactivation assay 16 dpi. Open symbols represent preformed infectious virus from mechanically disrupted cells plated in parallel. The data shown represent three independent experiments with splenocytes pooled from three to five mice per experimental group.

DISCUSSION

Targets of human APOBEC3 deaminase activity have been recently expanded to include plasmid DNA (221), small DNA viruses (247) and the large human herpesviruses (224). In this study, we set out to determine if the single APOBEC3 protein, mA3, encoded by the mouse had the ability to restrict the rodent herpesvirus pathogen MHV68. Our *in silico* analysis determined that A3 sites were abundant in MHV68, implying that this genome would be susceptible to A3 mediated deamination. Overexpression of mA3 together with infectious herpesvirus DNA did not significantly impact MHV68 titers compared to a more substantial restriction observed with hA3s. Surprisingly, the hA3 restriction was lost upon *de novo* infection. WT and $mA3^{-/-}$ C57BL6 mice were indistinguishable in the levels of acute MHV68 replication in the lung, latency establishment in the spleen and reactivation from the spleen. Thus, loss of mA3 had no discernable effect on MHV68 replication *in vivo*.

In this study we identified several human APOBEC3s as potent restrictors of MHV68 replication. Additionally, we found that the restriction by hA3A and hA3B is dependent on their previously identified active sites (221, 230). Interestingly hA3B restriction of MHV68 was absolutely dependent on the N-terminal amino acid, E68 and less dependent on the C-terminal E255 residue, possibly indicating a separation of function between the E68 and E255 active sites. The requirement for these hA3 active sites to restrict MHV68 growth and DNA replication is consistent with deamination of the genome as the basis of restriction. However, we have no direct evidence to support this hypothesis since DNA from A3A or A3B cotransfections did not contain widespread levels of C to T or G to A transitions. Although two transitions were present in A3A cotransfected samples, we observed a similar frequency of transitions in DNA from control transfections. The lack of a high mutation frequency in the A3A samples might be attributed to heavily deaminated DNA that is unable to serve as a template for replication or rare events that are below the limit of detection. Alternatively, A3A might impair MHV68 replication using a deamination-independent mechanism that is dependent on the active site. For example,

A3A mutants that were deaminase defective but retained other known functions such as DNA binding and localization to the nucleus were found to restrict parvoviruses (223, 247).

Our *in silico* analysis identified an overrepresentation of TC and TTC hotspots in the HSV-1 genome, consistent with the restriction of HSV-1 replication by the ectopic expression of hA3A and hA3C reported by(224)Interestingly, this study reported a high incidence of edited HSV-1 genomes upon transient transfection of hA3C and a striking frequency of hypereditied HSV-1 and EBV genomes in clinical specimens. These findings relied on the detection of rare deamination events by PCR based amplification at low denaturing temperatures (224). A non-biased quantitative determination of the incidence of herpesvirus deamination in human infections and the impact on pathogenesis warrants further investigation.

Strikingly, hA3 restriction of MHV68 replication was observed upon transfection of nonencapsidated infectious DNA but was lost upon *de novo* infection with virion particles. MHV68 virions may deliver a factor that counteracts the hA3 proteins. Tegument proteins from several herpesviruses families function in either the cytoplasm or the nucleus to limit the antiviral response from the host. KSHV ORF45 inhibits type I interferon signaling by impairing the phosphorylation and nuclear translocation of IRF-7 (Sathish et al., 2011; Zhu et al., 2002). HSV1 ICPO, HCMV pp71, HVS ORF3, EBV BNRF1 and MHV68 ORF75C translocate to the nucleus upon virus infection to degrade or relocalize components of the antiviral nuclear domain 10 structures (ND10) (106, 119, 122, 248, 249). We did not find significant homology of MHV68 virion components including glycoproteins, tegument and capsid proteins to known A3 antagonists. However, we cannot rule out the existence of a novel mechanism by which the virion structural components or even RNA molecules mediates resistance to APOBEC3 proteins.

The loss of MHV68 restriction might also be explained by the compartmental separation of A3 proteins from the MHV68 genome in a natural course of infection. Several of the hA3 proteins that exhibit restriction of MHV68, namely hA3A, hA3B, hA3C and hA3H are targeted to the nucleus (244, 245). We propose that the hA3 proteins might be separated from viral replication centers in the nucleus via either the direct action of a viral factor or indirectly due to viral remodeling of the nucleus. Herpesvirus replication, transcription and the formation of viral

capsids transpires in intranuclear structures known as replication centers that are defined by the presence of key viral replication proteins as well as host proteins (241, 250, 251). Nuclear substructures such as the ND10, as well as nuclear protein localization and abundance are tightly regulated by herpesviruses to maintain optimal viral gene expression and replication (252). The subcellular localization of A3 proteins and herpesvirus replication compartments could provide mechanistic insight for viral evasion of hA3 restriction.

Several human APOBEC3 proteins exhibit restriction of MHV68 replication, but mA3 exhibited no restrictive capacity in the cotransfection experiments. This lack of restriction with mA3 overexpression is not likely due to the absence of a co-factor in the HEK 293T cells. Murine APOBEC3 partially restricts Moloney murine leukemia virus replication and restricts HIV-1 lacking Vif to similar levels as hA3G in 293T cells (253, 254). The absence of restriction with overexpressed mA3 was supported by a lack of enhancement in MHV68 pathogenesis in mA3 knockout mice. Thus, MHV68 might encode a mA3 antagonist that significantly limits antiviral APOBEC3 activity such as HIV Vif (255-257) or Murine Leukemia Virus (MLV) glyco-gag (258). Additionally, a recent report identified a significant role for host uracil DNA glycosylase (UNG) in reducing the effect of hA3G-induced hyperediting of duck hepatitis B virus (259). MHV68, like other herpesviruses encodes a uracil DNA glycosylase (UNG/ORF46). However, we did not observe an increased restriction of MHV68 replication by hA3A, hA3B or mA3 with loss of MHV68 UNG in cell culture (Minkah, Chavez, and Krug, unpublished results).

Infection of mice lacking mA3 did not lead to an enhancement of MHV68 pathogenesis. This may be attributed to a viral countermeasure as described above, a lack of mA3 deamination function in the context of a herpesvirus infection or a yet undiscovered role in a particular aspect of chronic infection in this pathogenesis model. The intranasal route of inoculation is characterized by high levels of productive replication in the lungs, a tissue with lower mA3 expression levels (205). MA3 protein is expressed at high levels in the spleens, but its absence did not influence latency establishment in the spleen or reactivation from latency. Another route of infection, such as intraperitoneal inoculation might reveal the importance of MHV68 replication in peritoneal exudate cells wherein the primary latency reservoir is macrophages (58).

Indeed, the influence of some host proteins such as promyelocytic leukemia nuclear bodies (PML) (260) or viral proteins such as M1 and M2 on MHV68 pathogenesis is dependent on the route of infection (261, 262). Finally, it is possible that another APOBEC protein compensates for the loss of mA3 to limit MHV68 replication. A hyperediting signature similar to murine APOBEC1 deamination was reported in a mouse model of hepatitis B virus infection (263, 264). Furthermore, in a rat model of HSV-1-induced encephalitis, APOBEC1 levels were increased upon HSV-1 infection and overexpression of APOBEC1 both enhanced hyperediting of HSV-1 genomes and reduced viral titers (265).

MHV68 infection of mice provides a tractable model pathogenesis system to dissect the contribution of virus and host factors that influence chronic gammaherpesvirus infection. Primates have diversified their repertoire of A3 cytidine deaminases under the selective pressure of retroelements and viral pathogens. We sought to examine whether the evolutionary distinct yet 'primordial' APOBEC3 encoded by mice shared the restrictive property of the expanded human APOBEC3 molecules against MHV68, with the aim of utilizing $mA3^{-/-}$ mice as a platform for pathogenesis and mechanistic investigations. However, mA3 did not restrict MHV68 replication in cell culture or pathogenesis in mice. The unexpected loss of the hA3 restrictive phenotype when replication was initiated upon *de novo* infection with virus particles leads us to posit that herpesviruses are largely protected from hA3 restriction. Possible evasion mechanisms to explore include a virion-associated countermeasure such as a tegument protein or a block in APOBEC3 access to the viral genome either due to encapsidation of the viral genome during cytoplasmic transport to the nucleus or compartmentalization of the genome in nuclear replication centers.

ACKNOWLEDGMENTS

Kevin Chavez was supported by an NIH-MARC fellowship grant (grant #5T34GM008655). Parth Shah was partly supported by the Stony Brook University Simons Summer Research Program (2013) and Thomas MacCarthy was supported by Stony Brook University startup funds. Nathaniel Landau was supported by NIH grants (AI058864 and AI074967). Laurie Krug was supported by an American Cancer Society research scholar grant, RSG-1-160-01-MPC and NIH AI097875. Special thanks to Steven Reddy for technical support and members of the Krug laboratory for helpful discussions.

Appendix 2. Absence of the Uracil DNA Glycosylase of Murine Gammaherpesvirus 68 Impairs Replication and Delays the Establishment of Latency *In Vivo.*

Nana Minkah[1], Marc Macaluso[2], Darby G. Oldenburg[3], Clinton R. Paden[1,*],

Douglas W. White[3], Kevin M. McBride[2] and Laurie T. Krug[1,]

[1]Department of Molecular Genetics and Microbiology, Stony Brook University, Stony Brook, NY 11790; [2]Department of Molecular Carcinogenesis, Science Park, The University of Texas MD Anderson Cancer Center, Smithville, Texas 78957; [3]Gundersen Health System, La Crosse, Wisconsin 54601

*Current address:
Centers for Disease Control and Prevention
1600 Clifton Road
Atlanta, Georgia 30329-4027

ABSTRACT

Uracil DNA glycosylases (UNG) are highly conserved proteins that preserve DNA fidelity by catalyzing the removal of mutagenic uracils. All herpesviruses encode a viral UNG (vUNG), yet the role of the vUNG in a pathogenic course of gammaherpesvirus infection is not known. First, we demonstrated that the vUNG of murine gammaherpesvirus 68 (MHV68) retains the enzymatic function of host UNG in an *in vitro* class switch recombination assay. Next, we generated a recombinant MHV68 with a stop codon in ORF46/UNG (ΔUNG) that led to loss of UNG activity in infected cells and a replication defect in primary fibroblasts. Acute replication of MHV68ΔUNG in the lungs of infected mice was reduced a hundred-fold and was accompanied by a substantial delay in the establishment of splenic latency. Latency was largely, yet not fully, restored by an increase in virus inoculum or by altering the route of infection. MHV68 reactivation from latent splenocytes was not altered in the absence of the vUNG. A survey of host UNG activity in cells and tissues targeted by MHV68 indicated that the lung tissue has a lower level of UNG enzymatic activity than the spleen. Taken together, these results indicate that the vUNG plays a critical role in the replication of MHV68 in tissues with limited host UNG activity and this vUNG-dependent expansion, in turn, influences the kinetics of latency establishment in distal reservoirs.

IMPORTANCE

Herpesviruses establish chronic life-long infections using a strategy of replicative expansion, dissemination to latent reservoirs, and subsequent reactivation for transmission and spread. We examined the role of the viral uracil DNA glycosylase, a protein conserved among all herpesviruses, in replication and latency of murine gammaherpesvirus 68. We report that the viral UNG of this murine pathogen retains catalytic activity and influences replication in culture. The viral UNG was impaired for productive replication in the lung. This defect in expansion at the initial site of acute replication was associated with a substantial delay of latency establishment in the spleen. Levels of host UNG were substantially lower in the lung compared to the spleen, suggesting that herpesviruses encode a viral UNG to compensate for reduced host enzyme levels in some cell types and tissues. These data suggest that intervention at the site of initial replicative expansion can delay the establishment of latency, a hallmark of chronic herpesvirus infection.

INTRODUCTION

All herpesvirus genomes encode a homolog of the host uracil DNA glycosylase. If not repaired, uracil misincorporation during DNA replication (1,2) or conversion upon cytosine deamination (2,4) will lead to a C:G to T:A transition mutation that may have severe consequences for genomic integrity (266). In the host, the recognition and removal of uracils is mediated by members of the uracil DNA glycosylase (UDG) superfamily. UNG2 is the predominant nuclear enzyme responsible for initiating repair (267-271). The role of a seemingly redundant herpesvirus UNG in viral replication is not well understood.

The viral uracil DNA glycosylases (vUNG) are typically expressed early in the viral lifecycle and their expression correlates with the onset of viral DNA replication (272-275). Viral UNGs (vUNGs) interact with components of the viral DNA replication machinery including viral DNA polymerases and lytic gene transactivators (276-278). Mutation of the HCMV vUNG (UL114) delays HCMV replication in cell culture (279, 280). Epstein-Barr virus (EBV) DNA synthesis is reduced upon reactivation from latency in the absence of the vUNG (BKRF3) (278). Moreover, herpes simplex virus type 1 (HSV-1) vUNG (UL2) mediates base-excision repair *in vitro* (281) and loss of UL2 alone or together with loss of the HSV-1 dUTPase results in increased mutation rates upon serial passaging in culture (274). Similarly, loss of HCMV vUNG increases uracil frequency in the viral genome (280). Thus, vUNGs promote viral DNA replication and safeguard against uracil misincorporation, consistent with a role in maintaining the integrity of the viral genome.

The viral genes involved in nucleotide metabolism and DNA repair, the viral ribonucleotide reductase (RNR), thymidine kinase (TK), viral dUTPase and the viral UNG (282), are considered accessory proteins. These proteins are dispensable for viral replication in proliferating cells, yet are required in primary, quiescent or terminally differentiated cells. Herpesviruses typically replicate within mucosal tissues at the site of infection and disseminate to distal latency reservoirs, from which the virus reactivates periodically to maintain life-long infection. The role of a herpesvirus-encoded UNG *in vivo*, where the virus has to navigate both

quiescent and proliferating cells, has only been described for a mouse model of HSV-1 infection. HSV-1ΔUNG was impaired in viral replication at the sites of infection and led to a reduction in virus titers in both the central and peripheral nervous system (283). Moreover, *ex vivo* reactivation of HSV-1 from trigeminal ganglia was defective in the absence of the vUNG (283).

The role of the gammaherpesvirus vUNG in virus replication and pathogenesis in the host is not well-defined. We utilized murine gammaherpesvirus 68 (MHV68), a natural pathogen of murid rodents, to examine the influence of the viral UNG on gammaherpesvirus infection. We constructed recombinant MHV68 viruses with a stop codon in ORF46 and observed that loss of the vUNG reduced viral replication in fibroblasts and led to a severe impairment in viral replication within the lung. This defect in acute replication altered the kinetics of the establishment of latency in the spleen that could be largely overcome by an increase in virus dose or a change in the route of infection. Moreover, we observed a near absence of host UNG activity in the lungs that correlated with the requirement for vUNG in acute lung replication. Taken together, these data suggest that MHV68 requires the vUNG to overcome the restrictive environment of host tissues that lack adequate UNG activity.

MATERIALS AND METHODS

Mice and Cells. Female WT C57BL/6 mice were purchased from Jackson laboratories (Bar Harbor, Maine) or bred at the Stony Brook University Division of Laboratory Animal Research (DLAR) facility. All protocols were approved by the Institutional Animal Care and Use Committee of Stony Brook University**.** UNG-/- mice were obtained from the Jaenisch lab and bred at the MD Anderson Cancer Center animal facility in compliance with the Institutional Animal Care and Use Committee policies of MD Anderson Cancer Center**.** Primary murine embryonic fibroblast (MEF) cells were isolated from C57BL/6 mice and maintained in Dulbecco's modified Eagle's medium supplemented with 10% fetal calf serum, 100 U of penicillin per ml and 100 mg of streptomycin per ml at 37^{o}C in 5% CO_2. Immortalized murine fibroblast cells (NIH 3T3 or NIH 3T12) were maintained in Dulbecco's modified Eagle's medium (DMEM) supplemented with 8% fetal calf serum, 100 U of penicillin per ml and 100 mg of streptomycin per ml at 37^{o}C in 5% CO_2.

Class switch recombination assay. B cell isolation and the pMX retroviral infection have been previously described (284, 285). In brief, primary naïve B-lymphocytes from WT and UNG-/- mouse spleens were purified by negative selection with anti-CD43 beads (Miltenyi Biotec, Auburn CA) and cultured with 25 μg/ml LPS and 5 ng/ml IL-4 (Sigma-Aldrich). Retrovirus for cultured B cells was produced in BOSC23 cells by co-transfection with retroviral pMX and pCL-ECO plasmids. Supernatants were harvested 2-3 days after transfection and used to infect purified naïve B cells following 16 hr of culture in LPS and IL-4. To determine relative class switching to IgG_1, naïve and/or retrovirally transduced primary B cells were cultured, stained with anti-mouse IgG_1 antibodies (Becton Dickinson) and analyzed by flow cytometry as previously described (284, 285).

Generation of recombinant viruses. The modified MHV68-H2bYFP genome cloned into a BAC was a kind gift from the Speck laboratory (161). MHV68-H2bYFP-ORF46-stop (ΔUNG) virus was generated using *en passant* mutagenesis (45). Briefly, primers containing the ORF46-stop mutation (underlined), flanking WT ORF46 sequences on either side of the mutation and

sequences complementary to the kanamycin selection marker (forward primer 5'TTTTCTACCTCAATCCTGGATAGACTACTTACAACTCTCCGCGTTTTAAATCCAAGAAGCTTGAGCAGATTATGGCTGCATAGGGATAACAGGGTAATCGATTT3' and reverse primer 5'TGTTTTCTTCTGTTTTCTACTGCAGCCATAATCTGCTCAAGCTTCTTGGATTTAAAACGCGGAGAGTTGTAAGTAGTCTAGCCAGTGTTACAACCAATTAACC3') were used to amplify the kanamycin (Kan) selection marker from plasmid pEPKanS2 (20) by PCR (One Taq DNA polymerase, New England Biolabs, Ipswich MA). This PCR product was excised from the gel, digested with *Dpn*I to remove input template, and transformed into freshly prepared electrocompetent *E. coli* harboring the MHV68-H2bYFP BAC. After recovery, the bacterial cells were plated on dual chloramphenicol (34 ug/ml) / Kan (50 ug/ml) plates and incubated at 30°C for 48 hrs. DNA was prepared from isolated colonies and the Kan selection marker in *Orf46* was PCR amplified to verify the insertion of the mutagenesis cassette into the MHV68-H2bYFP BAC. Following the protocol outlined in reference 20, the kanamycin selection marker was removed, leaving behind the desired ORF46 stop mutation. The *Orf46* gene was PCR amplified from the putative mutant BAC, digested with *Dra*I to confirm the presence of the stop codon and then PCR products harboring the newly introduced *Dra*I site were sequenced (Laragen Inc, Culver City, CA). To generate marker rescued viruses, primers flanking WT *Orf46* sequence were used to generate a targeting construct, that is then used to repair the ORF46-stop disrupted virus as described above. Virus passage and titer determination were performed as previously described (57, 229).

Analysis of recombinant viral BAC DNA. BAC DNA was prepared by Qiagen column purification. For restriction analysis. 10 ug of BAC DNA was digested overnight with *Dra*I and then resolved in a 0.8% agarose gel in 1X TAE. For complete genome sequencing, the BAC DNA samples were prepared for multiplex, 50 cycle-single-end read sequencing on an Illumina HiSeq2000 by the SUNY-Buffalo Next Gen Sequencing Core. Reads were demultiplexed using the CASAVA 1.8.2 utility program. Whole genome sequencing data were analyzed for mutations

using CLC Genomics Workbench 6.0.2 (CLC bio, Aarhus, Denmark). Illumina sequence data was analyzed using CLC Genomics Workbench 6 (CLCbio/Qiagen, Aarhus, Denmark). Reads were aligned to a modified reference genome based on the WUMS Sequence (Genbank U97553) where the Kozinowski BAC sequence compiled by manual Sanger sequencing was appended to the left end. In order to spot any larger indels, contigs were generated using the CLC denovo assembler and aligned using Sequencher 5 (Genecodes). The reference sequence was modified based on actual sequencing data.Variants from the reference sequence comprising at least 5% of reads were found by using the Quality-based Variant detection algorithm in CLC Genomics Workbench, using a neighborhood radius of 5, minimum neighborhood quality score of 25, and a minimum central quality score of 29. Variants had to be present in both read directions, and had to be contained in uniquely-mapped reads. Importantly, engineered mutations were found in >93% of reads.

Virus growth curves. To measure virus replication, 2 x 10^5 MEFs or 1.8 x 10^5 NIH 3T12 cells were seeded in 6-well tissue culture plates one day prior to infection with recombinant MHV68 at a multiplicity of infection (MOI) of 5. Triplicate wells were harvested for each timepoint, and the cells with the conditioned medium were stored at -80°C. Serial dilutions of cell homogenate were used to infect NIH 3T12 cells and then overlayed with 1.5% methylcellulose in DMEM supplemented with 5% FBS. One week later, the methylcellulose was removed and cells were washed twice with PBS prior to methanol fixation and staining with a 0.1% crystal violet solution in 10% methanol.

Real time PCR. Total cell DNA from the MHV68 infected or mock infected MEF cells was column-purified (Qiagen, Limburg, Netherlands). 50 ng of DNA was input into a quantitative PCR reaction (Thermo scientific-SYBR Green low ROX mix, Waltham MA) using primers specific to a region of MHV68 ORF50 (forward primer, 5' GGCCGCAGACATTTAATGAC3', reverse primer 5' GCCTCAACTTCTCTGGATATGCC 3') and primers for murine GAPDH (forward primer, 5' CCTGCACCACCAACTGCTTAG 3', reverse primer 5' GTGGATGCAGGGATGATGTTC 3'). A standard curve was generated using known DNA

copies of ORF50 and GAPDH plasmids and the absolute ORF50 DNA copy number within each infection was extrapolated from the standard curve.

Antibodies and immunoblotting. Total protein lysate was harvested in lysis buffer (150 mM sodium chloride, 1.0% IGEPAL CA-630, 0.5% sodium deoxycholate, 0.1% sodium dodecyl sulfate, 50 mM Tris pH 8.0) supplemented with a protease inhibitor cocktail (Sigma, St. Louis MO) and PMSF. Twenty micrograms of each lysate were separated on a gradient 4-15% SDS PAGE gel (Bio rad, Hercules CA) and transferred to polyvinylidene fluoride membrane. ORF59 and ORF75C were detected using affinity-purified chicken anti-peptide antibodies against MHV68 ORF59 (173) and ORF75C (generated from peptides PRSRSFSRHKPMKFDQS and YDAENLQCTPWQI, Gallus Immunotech, Ontario, Canada). For ORF65 detection, a rabbit polyclonal antibody was used (kind gift from Ren Sun, UCLA) (174)**.** A rabbit polyclonal antibody to glyceraldehyde 3-phosphate dehydrogenase (GAPDH) (SIGMA, St. Louis MO) was used as a loading control. HRP-conjugated secondary antibodies were detected using an enhanced chemiluminescence reagent (ECL, Thermo Scientific, Waltham MA).

Uracil DNA glycosylase activity. HEK 293T, NIH 3T12 and primary MEF cells or single cell suspensions of splenocytes and collagenase-digested lung tissues were harvested in HEPES EDTA buffer (10 mM HEPES [pH 7.4], 1 mM EDTA, 1 mM dithothreitol) and disrupted by sonication. For lung lysates, mice lungs were perfused with phosphate buffered saline (PBS), minced with scissors, and then digested with collagenase (Type IV, Sigma, St. Louis MO). Protein concentration was quantified by the Bio-Rad DC^{TM} protein assay (Bio-Rad, Hercules, CA). Twenty ul cleavage reactions consisting of 2ug (Figure 3C) or 20 μg of protein lysate (Figure 8) and 0.1 pmol of an Alexa 488 modified, 19-mer single-stranded DNA oligonucleotide containing a single uracil (Alexa 488- CATAAAGTGUAAAGCCTGG) were carried out at 37°C for 15 min in reaction buffer (10 mM Tris pH 7.4, 1 mM EDTA, 50 mM NaCl). Reactions were stopped with 20 μl of UDG stop buffer (80% Formamide, 10mM EDTA, 0.4M NaOH, 1mg/ml

orange G) and heated at 95°C for 15 mins prior to resolution in a 7.4 M urea, 15% polyacrylamide gel in 0.5 X Tris borate EDTA at 120 V for 1 hr. Quantitaion of uracil cleavage was measured using ImageQuant software (GE Healthcare, Piscataway NJ)**.**

Infections and organ harvests. 8 to 10 week old WT mice were either infected by intranasal inoculation with 100 PFU or 100,000 PFU of MHV68 in a 20 µl bolus or by intraperitoneal injection of 0.5 ml with 100 PFU of MHV68 under isoflurane anesthesia. The inoculum was back-titered to confirm the infectious dose. Mice were sacrified by terminal isoflurane anesthesia. For acute titers, mouse lungs or spleens were harvested in 1 ml of DMEM supplemented with 10% FBS and stored at -80^{0}C prior to disruption in a Mini-BeadBeater (BioSpec, Bartlesville, OK). The homogenates were titered by plaque assay. For latency and reactivation experiments, mouse spleens were homogenized, treated to remove red blood cells, and then filtered through a 100 µm nylon filter. For peritoneal cells, 10 ml of media was injected into the peritoneal cavity and an 18-gauge needle was used to withdraw approximately 7 ml of media from each mouse. The peritoneal exudate cells were pelleted by centrifugation and then resuspended in 1 ml of DMEM supplemented with 10% FBS.

Limiting dilution PCR detection of MHV68 genome positive cells. To determine the frequency of cells harboring the viral genome, single cell suspensions were prepared and used in a single-copy nested PCR. Six three-fold serial dilutions of cells were plated in a 96-well PCR plate in a background of NIH 3T12 cells and lysed overnight at 56^{0}C with proteinase K. The plate was subjected to an 80-cycle nested PCR with primers specific for MHV68 ORF50 (57, 229). Twelve replicates were analyzed at each serial dilution and plasmid DNA at 0.1,1 and 10 copies was included to verify the sensitivity of the assay.

Limiting dilution *ex vivo* reactivation assay. To determine the frequency of cells harboring latent virus capable of reactivation upon explant, single cell suspensions were prepared from mice 16 or 18 dpi, resuspended in DMEM supplemented with 10% FBS and plated in twelve serial two-fold dilutions onto a monolayer of mouse embryonic fibroblast (MEF) cells prepared from C57BL/6 mice in 96-well tissue culture plates. Twenty-four replicates were plated per

serial dilution. The wells were scored for cytopathic effect (CPE) two to three weeks after plating. To differentiate between pre-formed infectious virus and virus spontaneously reactivating upon cell explant, parallel samples were mechanically disrupted using a mini-bead beater prior to plating on the monolayer of MEFs to release preformed virus that is scored as CPE (57, 229).

Flow Cytometry. For the analysis of B cells, $2x10^6$ splenocytes were resuspended in 200 µl of FACS buffer (PBS with 2% Fetal Bovine Serum) and then blocked with TruStain fcX (Clone 93, Biolegend, San Diego, CA). The cells were subsequently washed, and stained with CD19 (clone 6D5), CD95 (15A7), CD4 (GK1.5), and CD8 (53-6.7) (all from Biolegend, San Diego, CA). The data were collected using a Dxp8-FACScan (Cytek Development; BD Biosciences) and analyzed using FlowJo v10.0.6 (Treestar Inc, Ashland, OR).

Statistical analyses. Data were analyzed using GraphPad Prism Software (Prism 5, La Jolla CA). Statistical significance was determined using either an ANOVA test followed by a Bonferroni correction or a non-paired two-tailed t-test. Under Poisson distribution analysis, the frequencies of latency establishment and reactivation from latency were determined by the intersection of nonlinear regression curves with the line at 63.2.

RESULTS

The viral UNG of murine gammaherpesvirus 68 rescues class switch recombination in B cells lacking UNG. UNG recognizes and cleaves the N-glycosidic bond of uracils to generate an abasic site that is subsequently incised by host endonucleases prior to repair by the base-excision repair pathway (286). In addition, host UNG2 excises uracils from activation induced deaminase (AID) induced U:G lesions within the immunoglobulin locus to facilitate somatic hypermutation and class switch recombination, two functions essential for generating antibody diversity (271, 287). To determine if the vUNG exhibits uracil excision activity and if disruption of this gene impairs this activity, we tested the ability of the vUNG to rescue immunoglobulin class switch recombination in UNG-null B cells. Naïve resting B cells were purified from the spleen of WT and $UNG^{-/-}$ mice and stimulated with IL-4 and LPS to induce class switch recombination (CSR). CSR was monitored by flow cytometry with antibodies to IgG_1. $UNG^{-/-}$ cells were unable to switch to IgG_1 while WT cells exhibited about a 20% shift to IgG_1 upon stimulation (**Fig. 1A**). To test complementation, we transduced $UNG^{-/-}$ cells with a retrovirus expressing host UNG or the WT MHV68 vUNG together with GFP to mark UNG-expressing B cells (**Fig. 1B**). Transduction of WT MHV68 vUNG or host UNG2 resulted in restoration of CSR to the $UNG^{-/-}$ cells, an equivalent proportion of cells became GFP+/IgG_1+ (9.0% and 8.4% respectively) (**Fig. 1C)**. In contrast, transduction with a retrovirus encoding a vUNG that harbors a premature stop codon (vUNG.stop) did not rescue CSR in $UNG^{-/-}$ cells (**Fig. 1C**). These results demonstrate that the vUNG encoded by MHV68 exhibits uracil glycosylase activity and that a premature stop codon in the MHV68 vUNG abrogates this catalytic function.

Uracil DNA glycosylase promotes gammaherpesvirus replication in primary fibroblasts. To examine the function of the vUNG in MHV68 pathogenesis, we generated a recombinant MHV68 encoding the premature ORF46-stop codon utilized in the CSR assay. The ORF46-stop virus, hereafter termed ΔUNG, was generated from the MHV68-H2bYFP marking virus using allelic exchange (45, 288). The cytosine at nucleotide (nt) position 114 was replaced

with two adenines. This insertion introduced a TAA stop codon and a unique *Dra*I site (underlined) (**Fig. 2A**). ΔUNG1 was repaired back to the WT sequence and is termed ΔUNG1.MR (marker rescue). The presence of the UNG mutation was confirmed by *Dra*I digestion of the ORF46 gene (**Fig. 2B)** and restriction fragment length polymorphism analysis **(Fig. 2C).** The lack of additional mutations in the MR and mutant viruses was confirmed by whole genome sequencing **(Fig. 2D)**. ΔUNG1 and ΔUNG2 refer to mutant viruses derived from two independent BAC clones.

In multi-step growth curves, we observed a lag in virus replication with loss of the vUNG. ΔUNG1 and ΔUNG2 replication lagged behind WT and ΔUNG1.MR between 24 and 120 hpi before reaching similar peak titers at 148 hpi. (**Fig. 2E**). We next compared replication in immortalized fibroblasts (NIH 3T3) or primary MEFs following infection at an MOI of 5. In these single-step growth curves, loss of the vUNG resulted in a 2.5-fold replication defect in immortalized NIH 3T3 cells (**Fig. 3A**) and a significant eight-fold defect in primary MEFs (**Fig. 3B**). Viral DNA synthesis between 24 and 6 hpi (**Fig 3C**) and viral transcripts from different kinetic classes were not impacted by the loss of the vUNG (data not shown). An immunoblot analysis of viral proteins representative of early and late gene classes did not reveal significant defects in gene expression during infection of the MEFs (**Fig. 3D**). Interestingly, we observed an increase in the levels of ORF75C tegument protein delivered to cells newly infected with viruses lacking vUNG compared to UNG.MR (**Fig 3E**). We examined the particle to PFU ratio by quantitating the encapsidated viral genomes and plaque forming units from a concentrated stock prepared in parallel for ΔUNG1 and ΔUNG1.MR. The ΔUNG1 virus had a six-fold increase in the particle to PFU ratio as compared to the repaired ΔUNG1.MR (data not shown). Taken together, we propose that the vUNG promotes an aspect of virus replication distinct from DNA synthesis or selected early and late gene product expression, likely impacting assembly or infectivity of the virions.

The vUNG of MHV68 retains enzymatic UNG activity in infected primary fibroblasts. We next examined UNG activity in MEFs infected with MHV68. Protein lysates

harvested from primary MEFs 24 hpi were incubated with a 19-mer single-stranded oligonucleotide containing a single uracil. Uracil excision followed by alkaline treatment of the abasic site generates a 9-mer product that is resolved by denaturing PAGE electrophoresis (**Fig. 4A**). Lysates from WT- or MR-infected MEFs cleaved approximately 50% of the uracil-containing oligonucleotide at 24 hpi (**Fig. 4B**). In contrast, there was no significant difference in oligonucleotide cleavage between ΔUNG1-infected and uninfected MEFs over an extended timecourse (**Fig. 4C**). This data indicates that the vUNG drives the enzymatic UNG activity that is detected in the infected MEFs.

Loss of the MHV68 UNG reduces acute viral replication in the lungs and the establishment of latency in mice. To assess the role of the vUNG in replication within an infected animal, we examined acute replication in the lung after an intranasal infection of C57BL/6 mice. ΔUNG1 and ΔUNG2 exhibited reduced replication in the lung as compared to ΔUNG1.MR, with undetectable virus titers in 9 out of 10 mice at 4 dpi. ΔUNG1.MR titers increased by 20-fold at 7 dpi, and were comparable to WT-infected mice. At 9 dpi, we observed a further 2.5-fold increase in ΔUNG1.MR titers, with complete clearance from the lungs by 12 dpi. In contrast, virus replication in the lungs of mice infected with ΔUNG viruses failed to reach the levels of WT and UNG.MR replication, with an approximately two-log defect in viral titers at 9 dpi. Virus was not detected in the lungs of ΔUNG infected mice at 12 dpi, indicating that there was no delay in clearance with loss of the vUNG (**Fig. 5**). Thus, the vUNG promotes acute replication of MHV68 in the lung.

Within two weeks of intranasal infection, virus replication in the lung is resolved and the virus transits to the spleen where it targets B-lymphocytes. The peak in splenic latency occurs between 14 and 18 dpi and coincides with splenomegaly. Mice infected with ΔUNG1.MR exhibited splenomegaly with a two-fold increase in splenic weight at 16 dpi while mice infected with ΔUNG viruses did not exhibit significant splenomegaly (**Fig. 6A**). This defect in splenomegaly correlated with a two-log reduction in the frequency of splenocytes that harbor the viral genome in mice infected with the ΔUNG viruses as compared to ΔUNG1.MR (**Fig. 6B,**

summarized in Table 1). This impairment in latency establishment was accompanied by a similar reduction in the frequency of reactivation from latency upon explant (**Fig. 6C, summarized in Table 2**). The severity of the defect in the establishment of latency precluded a determination of whether vUNG plays a role in splenic reactivation. In spite of a severe latency defect at 16 dpi, the frequency of genome-positive splenocytes six weeks after infection with ΔUNG1 was nearly equivalent to ΔUNG1.MR (**Fig. 6D**). Thus, loss of vUNG delays latency establishment in the spleen after intranasal inoculation of mice.

An increase in dose partially rescues the latency defect of the virus lacking UNG. Since the intranasal inoculation of mice with 100 PFU of virus identified defects in both acute replication in the lung as well as the establishment of splenic latency in ΔUNG-infected animals, we reasoned that the delay in splenic latency might solely be attributed to a failure of the UNG null viruses to expand in the lung. To test this hypothesis, we increased the virus inoculum by three orders of magnitude to 100,000 PFU. Mean lung titers from mice infected with 100,000 PFU (**Fig. 7A)** were increased overall as compared to lung titers from mice infected with 100 PFU (**Fig. 5**). Acute replication in the lungs of mice infected with ΔUNG1 was partially restored, but still reduced by six- and ten-fold as compared to ΔUNG1.MR-infected mice at 4 and 9 dpi, respectively (**Fig. 7A**). Coupled with this partial rescue of replication in the lung, splenomegaly was restored in ΔUNG1-infected animals at 16 dpi (**Fig. 7B**). Moreover, spleens from mice infected with ΔUNG1 exhibited a slight, but statistically insignificant, four-fold reduction in the frequency of genome positive cells (**Fig. 7C, summarized in Table 1**). Reactivation from latency was only slightly reduced in mice infected with ΔUNG1 relative to ΔUNG1.MR (**Fig. 7D, summarized in Table 2**). In summary, an increase in virus dose was able to partially overcome a deficit in replication in the lung and led to near complete restoration of latency in the spleen. Thus, a large portion of the splenic defect in latency and reactivation observed with a low dose of ΔUNG viruses stems from a requirement for the vUNG to drive MHV68 replication in the lung and subsequent dissemination from the lung to the spleen.

Bypassing the lung via intraperitoneal inoculation rescues the splenic latency defect of murine gammaherpesvirus lacking UNG. The intranasal route of infection identified a critical role for the vUNG in seeding the spleen that was partially overcome with an increase in virus dose. We next bypassed lung replication using direct administration of virus by intraperitoneal inoculation (IP). In general, acute splenic titers were lower than the lungs, with mean peak titers at 9 dpi of ~50 PFU/ml and ~150 PFU/ml for ΔUNG1 and ΔUNG1.MR respectively (**Fig. 8A**). No significant difference in splenomegaly was observed between ΔUNG1 and ΔUNG1.MR infected animals (Fig. 8**B**). Loss of the vUNG resulted in a slight three-fold decrease in the frequency of genome positive splenocytes at 18 dpi (**Fig. 8C, summarized in Table 1**). The frequency of reactivation from latency at this early time point was not impacted by the loss of the vUNG (**Fig. 8D, summarized in Table 2**). We tracked the splenic cells harboring MHV68 using the YFP reporter (19), and found that ΔUNG1 and ΔUNG1.MR colonized $CD95^{hi}$ CD19+ B cells with equivalent frequencies (**Fig. 8E and 8F**). At six weeks post-infection, there was no difference in either spleen weights (**Fig. 8G**) or the frequency of genome positive splenocytes (**Fig. 8H**). These experiments using direct IP infection demonstrate that the loss of the vUNG does not have a significant impact on latency in the splenic reservoir between 18 and 42 dpi.

The viral UNG is dispensable for latency in peritoneal exudate cells. In addition to the major latent reservoir, B-lymphocytes, MHV68 latency is also established in macrophages and dendritic cells (58, 60). We examined whether the vUNG plays a role in latency establishment in peritoneal exudate cells (PEC), which are comprised largely of macrophages. Loss of the vUNG did not influence the frequency of genome positive cells at either 18 or 42 dpi after IP inoculation. Additionally, we did not observe a reduction in explant reactivation from PECs following infection with ΔUNG1 as compared to ΔUNG1.MR **(Fig. 9, summarized in Table 1 and Table 2)**. We conclude that MHV68 latency establishment, reactivation from latency, and long-term maintenance in the peritoneal compartment is independent of the vUNG.

The viral UNG plays a critical role in replication in mouse cells with reduced host UNG activity. A striking observation from our studies was the differential impact of the loss of the vUNG in various murine cells and tissues. We observed significant replication defects in primary MEFs and in the lung, but not in immortalized fibroblasts or in primary splenocytes. Although all murine tissues express UNG2, reduced UNG2 mRNA levels have previously been noted for lung tissue (267). We examined host UNGase levels between the different cell types infected by MHV68. We examined host UNG activity by incubating a uracil-containing single-stranded oligonucleotide with protein lysates from cells in culture and tissues from mice. Incubation with lysates from HEK 293T cells, immortalized fibroblasts, or primary MEFs resulted in 98%, 75%, and 73% cleavage of the oligonucleotide, respectively (**Fig 10A**). The block in cleavage in the presence of the UNG-specific inhibitor UGI confirmed that UNG is the major UDG responsible for uracil excision within these cell lysates. We observed robust UNGase activity in the naïve spleen and PEC, (**Fig. 10B**) tissues where the vUNG is dispensable. In sharp contrast, UNG activity in the lung was undetectable, indicating that the lung tissue is nearly devoid of host UNG expression. We observed a slight increase in UNGase activity in the lungs and PECs upon infection with MHV68, but the level of UNG activity in the lungs was comparable upon infection with ΔUNG1 and ΔUNG1.MR (**Fig. 10C**). This may be attributed to the immune infiltrate in the infected lung. Overall, the reduction in acute replication in the lungs upon loss of the vUNG correlated with impaired host UNG activity in this tissue. These data are consistent with a requirement for the vUNG to compensate for the absence of the host enzyme in tissues that are critical for viral replication.

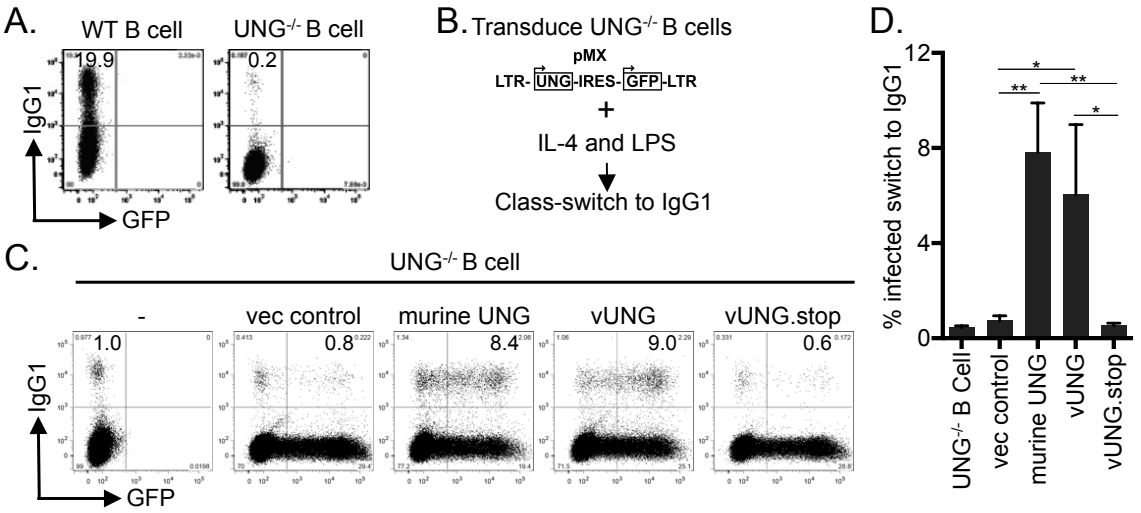

FIG 1. MHV68 UNG complements UNG$^{-/-}$ B lymphocytes for class switch recombination (CSR). (**A**) Representative flow cytometry plot demonstrating that WT, but not UNG$^{-/-}$ B cells undergo CSR to IgG_1. (**B**) Schematic of CSR assay. Primary B cells from the indicated naïve mice are treated with LPS and IL-4 for 4 days. (**C**) Representative flow cytometry plot of CSR to IgG_1 in UNG$^{-/-}$ splenocytes transduced with empty vector or pMX expressing murine UNG2, MHV68 vUNG, or MHV68 vUNG.stop. The percentage of infected (GFP+) cells expressing IgG_1 is indicated on the plot. (**D**) Summary graph of percentage of GFP+ cells that underwent CSR to IgG_1 4 days after retroviral infection. Bars represent the mean +/- standard deviation, * $p \leq 0.05$. and ** $p \leq 0.005$. UNG complementation data is representative of three independent experiments.

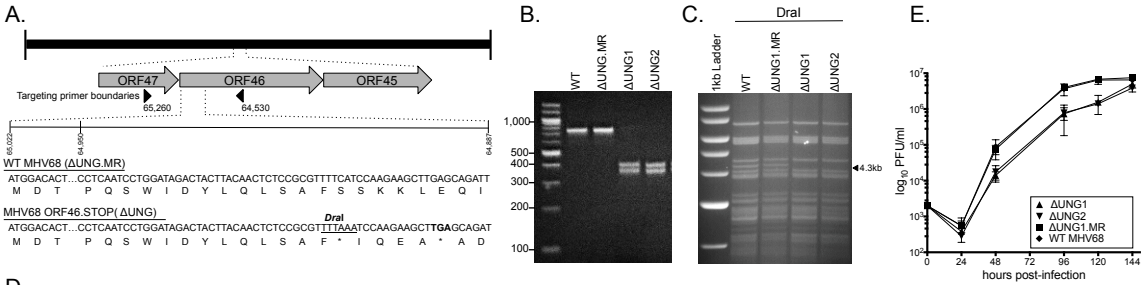

MHV68ΔUNG1 changes relative to MHV68ΔUNG1.MR Sequence

Genomic position	BAC+ position	Type	Length	Reference	Sequenced	Count	Coverage	Frequency	Average quality	Gene	Coding region change	Amino acid change
64910	77459	SNV	1	G	T	16870	16923	99.69	38.51	ORF46	C to A	Ser38*
64909	77458	Ins	1	-	T	16824	18052	93.20	38.4	ORF46	Ins A	Ser38fs

FIG 2. Construction and characterization of a recombinant MHV68ΔUNG virus. (**A**) Schematic of the ΔUNG virus. Comparison of WT and mutant ORF46 nucleotide sequences highlighting the presence of the unique *Dra*I site and insertion of the TAA stop codon in ΔUNG (underlined). Underneath the nucleotide sequence is the translated amino acid sequence. (*) indicates the presence of the stop codon. Arrows indicate the boundaries of primers to generate a 725 bp amplimer to verify the mutation. (**B**) *Dra*I digestion of a 725 bp amplimer to confirm the unique *Dra*I site in the two independent ORF46.STOP viruses (ΔUNG1 and ΔUNG2), but not the marker rescue ofΔUNG1 (ΔUNG1.MR) or wild-type (WT) MHV68. (**C**) Confirmation of mutant and repaired MHV68 viruses by restriction fragment length polymorphism analysis. 10 ug of WT BAC DNA, ΔUNG1.MR, ΔUNG1 and ΔUNG2 digested with *Dra*I and resolved on a 0.8% agarose gel. Arrowhead indicates the loss of a 4.3 kb fragment with the insertion of the unique *Dra*I site into ORF46. (**D**) Analysis of MHV68 BAC by whole genome sequencing. (**Top**) Illumina reads were aligned to the MHV68.H2bYFP BAC genome. Shown in the histogram are levels of coverage across the genome, scale is 0-30,000X, 56M total mapped reads for ΔUNG1, and 39M reads for ΔUNG1.MR. Variants indicated by inverted triangle. The two regions of low coverage are due to the paucity of uniquely-mapped reads in the small repeat

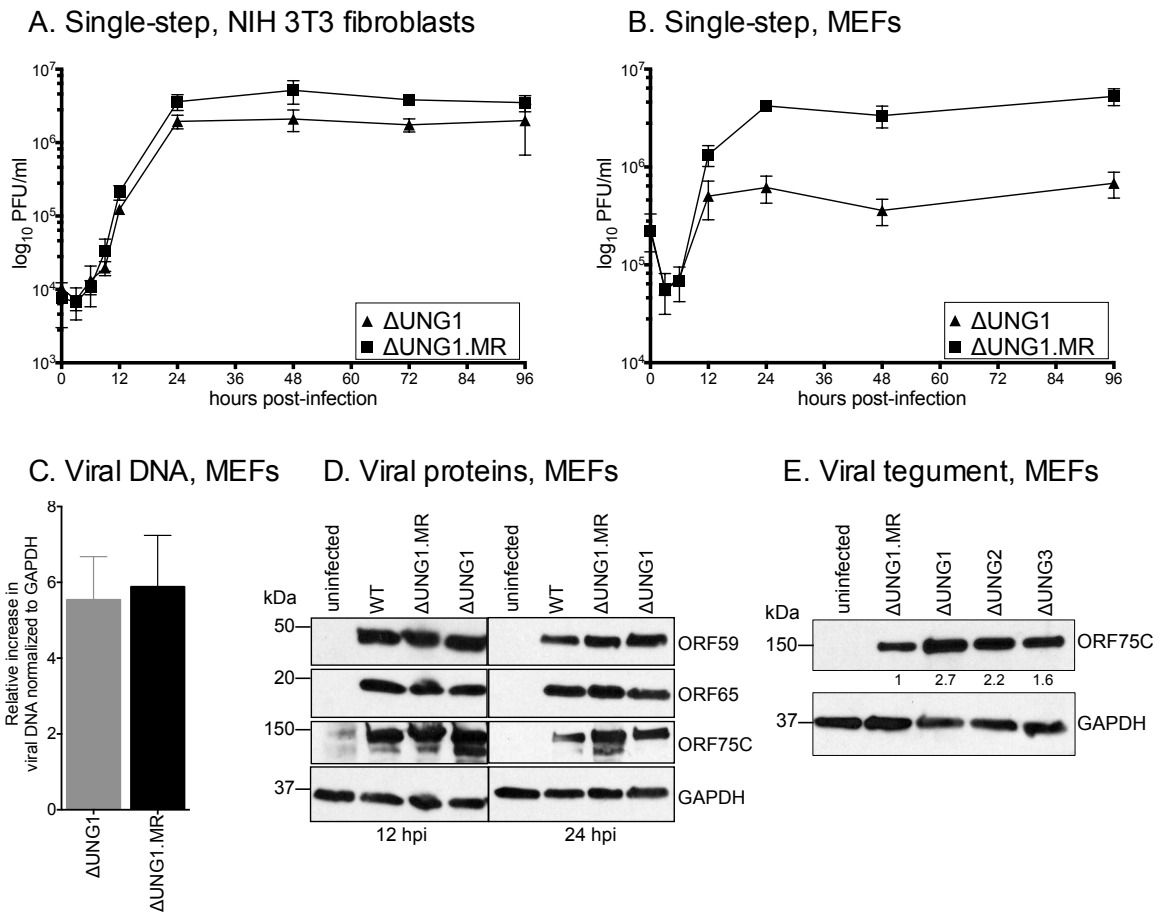

FIG 3. The vUNG of MHV68 promotes replication in primary fibroblasts. (**A**) Single-step growth curve in immortalized NIH 3T3 fibroblasts at an MOI of 5.0 with ΔUNG1 and ΔUNG1.MR. (**B**) Single-step growth curve in primary murine embryonic fibroblasts (MEFs) at an MOI of 5.0 with ΔUNG1 and ΔUNG1.MR. (**C**) Relative increase in viral DNA levels from ΔUNG1 or ΔUNG1.MR – infected MEFs 24 hpi at an MOI of 5. Data is normalized to 6 hpi input DNA. (**D**) Timecourse analysis of early (ORF59) and late (ORF65 and ORF75C) gene products upon a high MOI infection of MEFs. (**E**) Immunoblot analysis of ORF75C tegument protein levels delivered with incoming virus 1 hpi. The increase in GAPDH-normalized ORF75C levels relative to the MR virus is indicated below the gel.

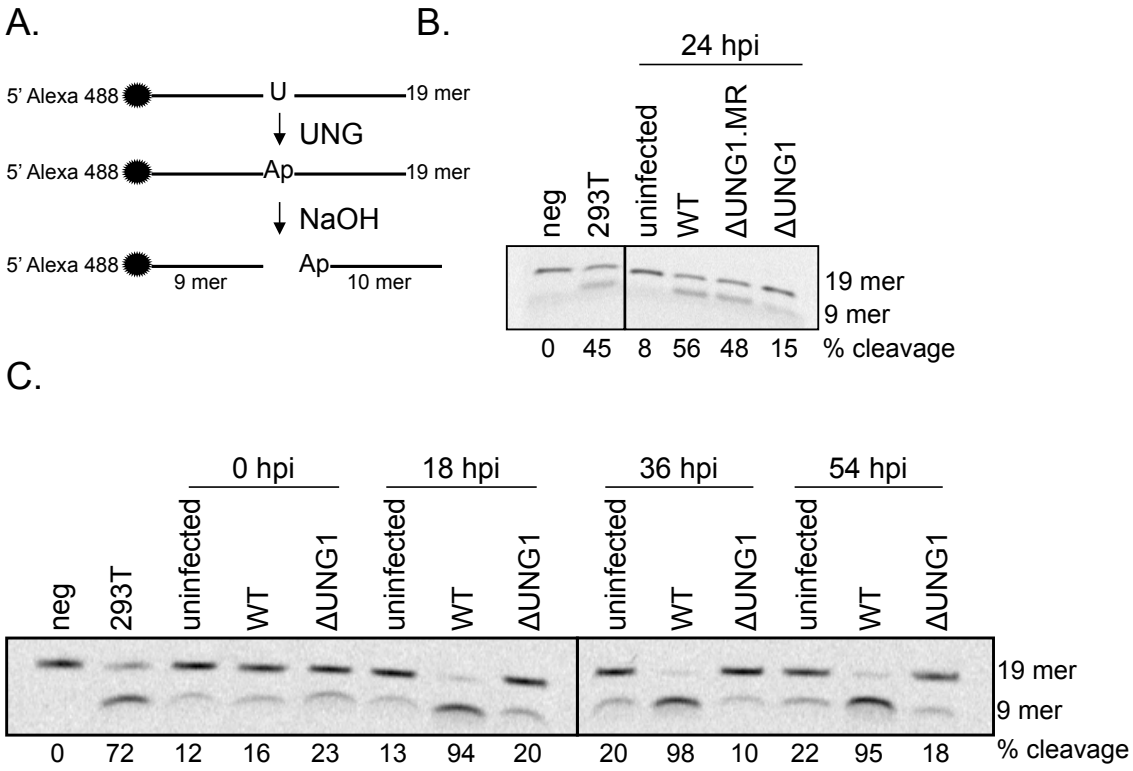

FIG 4. The vUNG of MHV68 retains enzymatic UNG activity in infected primary fibroblasts. (A) Schematic of UNGase assay using an Alexa 488-labeled oligonucleotide containing a single uracil. Uracil excision leads to oligonucleotide cleavage. (**B**) Denaturing polyacrylamide gel analysis of oligonucleotide cleavage upon incubation with lysates prepared from MEFs uninfected or infected with WT, ΔUNG1.MR, ΔUNG1 at 24 hpi. (**C**) Timecourse analysis UNG activity within primary MEFs infected with WT or ΔUNG1 viruses. The percentage of cleavage relative to the negative control is indicated below each gel.

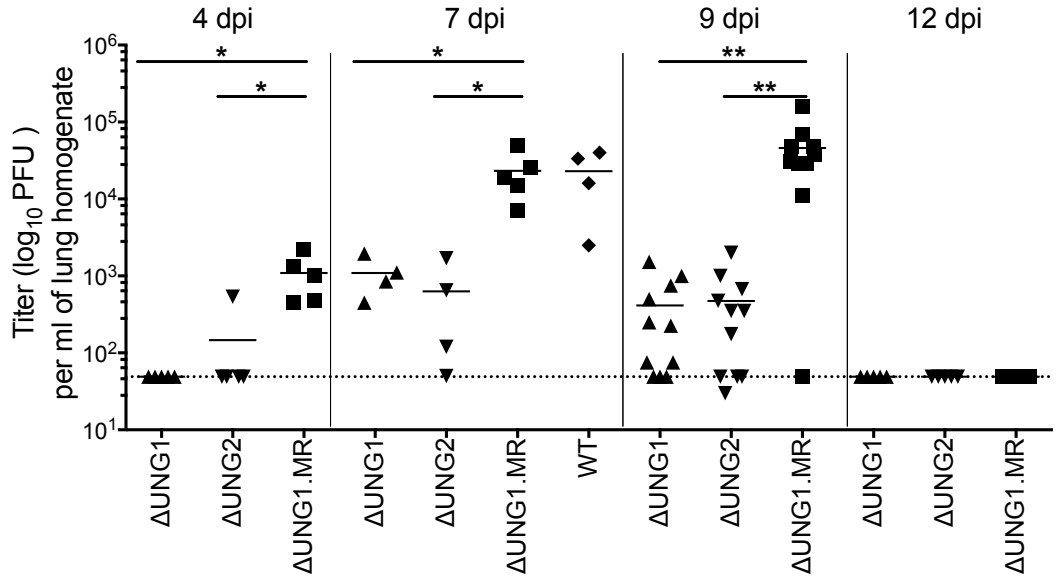

FIG 5. The vUNG of MHV68 is critical for replication in the lungs of infected mice. C57BL/6 mice were infected at 100 PFU by the intranasal route with two independent viruses encoding stop codon disruptions in ORF46 (ΔUNG1 and ΔUNG2) and the marker rescue virus of ΔUNG1 (ΔUNG1.MR). Lung homogenates from mice were titered by plaque assay, line indicates geometric mean titer. Each symbol represents an individual mouse. The dashed line depicts the limit of detection at 50 PFU/ml of lung homogenate (log_{10} of 1.7). * $p \leq 0.05$. and ** $p \leq 0.005$

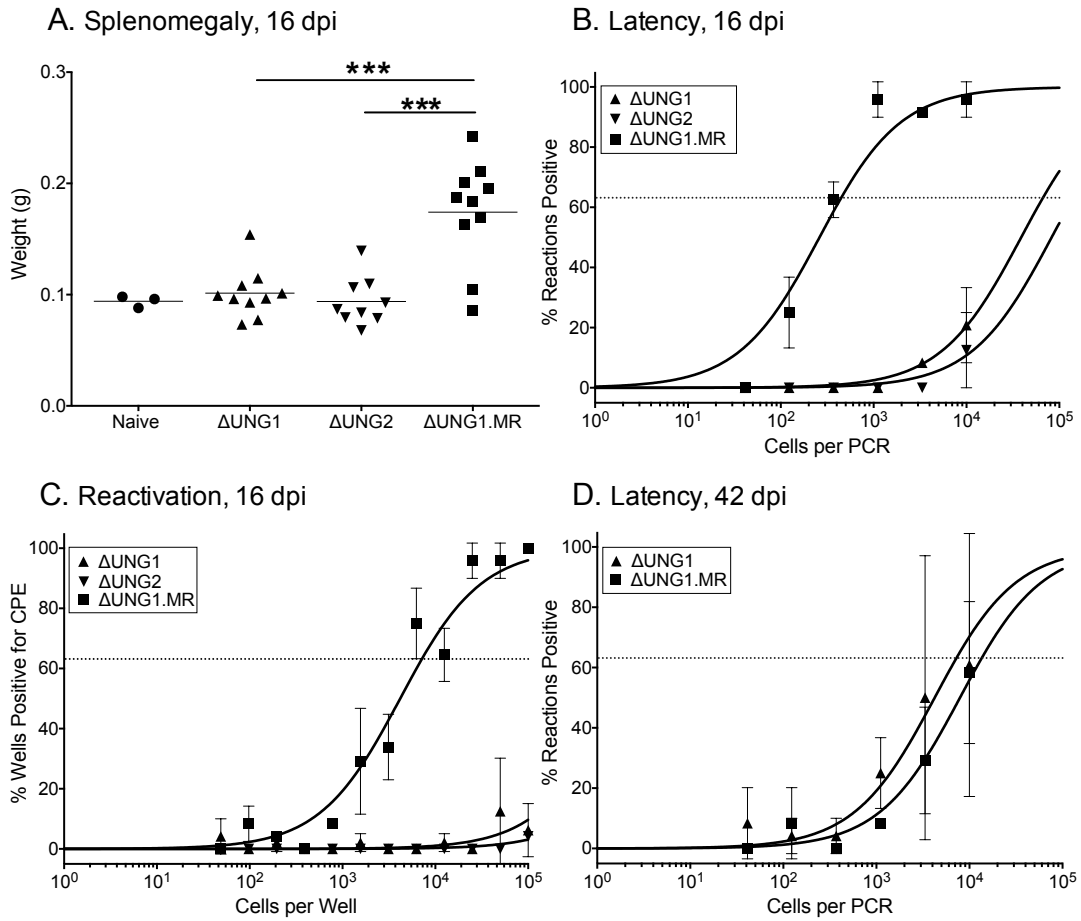

FIG 6. MHV68 vUNG is essential for the establishment of latency in the spleen at early, but not late times during chronic infection after low dose intranasal inoculation. C57BL/6 mice were infected at 100 PFU by the intranasal route with the indicated viruses. (**A**) Weights of spleens harvested 16 dpi, *** $p \leq 0.001$. (**B**) Frequency of splenocytes harboring latent genomes at 16 dpi. (**C**) Frequency of splenocytes undergoing reactivation from latency upon explant. (**D**) Frequency of splenocytes harboring latent genomes at six weeks post-infection. For the limiting dilution analyses, curve fit lines were determined by nonlinear regression analysis. Using Poisson distribution analysis, the intersection of the nonlinear regression curves with the dashed line at 63.2% was used to determine the frequency of cells that were either positive for the viral genome or reactivating virus. Data is generated from at least three independent experiments for 16 dpi and two independent experiments for 42 dpi.

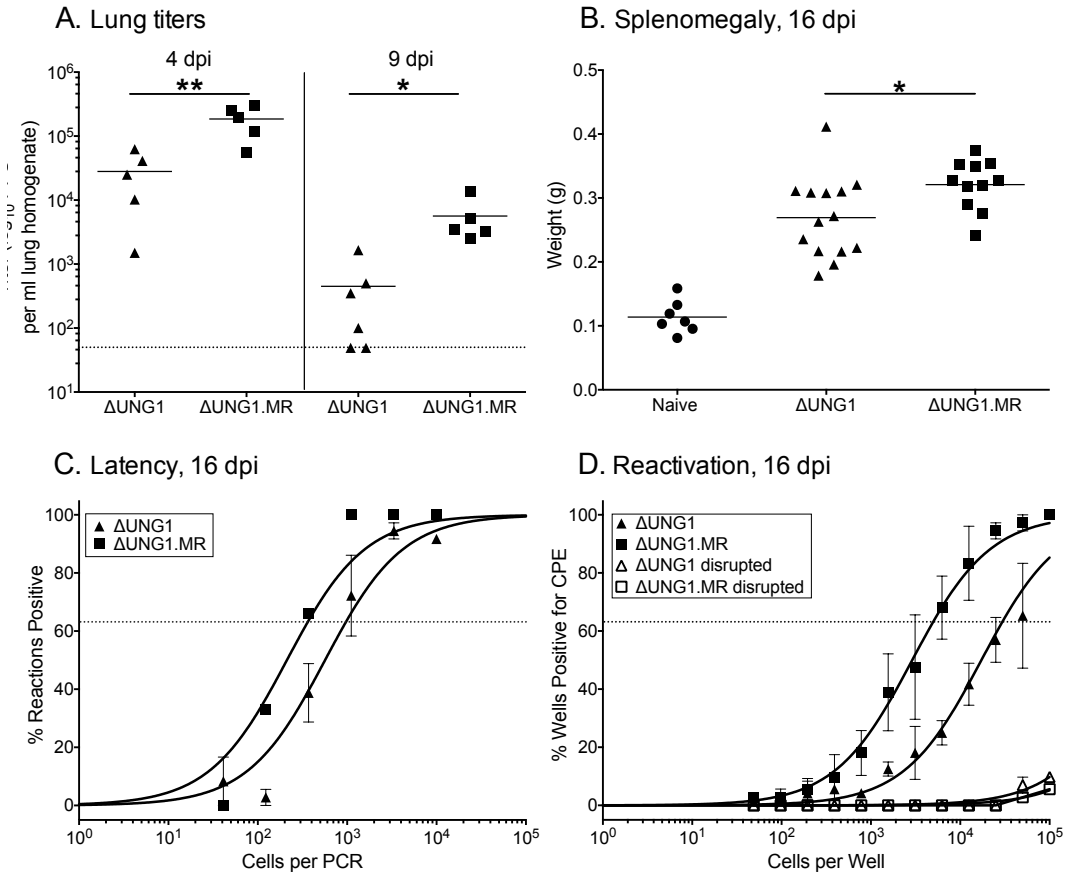

FIG 7. Infection with a higher dose partially overcomes the loss of vUNG. C57BL/6 mice were infected at 100,000 PFU by the intranasal route with the indicated viruses. (**A**) Lung homogenates from mice were titered by plaque assay, line indicates geometric mean titer. Each symbol represents an individual mouse. The dashed line depicts the limit of detection at 50 PFU/ml of lung homogenate or a $\log_{10}$ of 1.7. * $p \leq 0.05$. and ** $p \leq 0.005$. (**B**) Weights of spleens harvested from the indicated infections 16 dpi. Each symbol represents an individual mouse. * $p \leq 0.05$. and ** $p \leq 0.005$. (**C**) Frequency of splenocytes harboring latent genomes. (**D**) Frequency of splenocytes undergoing reactivation from latency upon explant. For the limiting dilution analyses, curve fit lines were determined by nonlinear regression analysis. Using Poisson distribution analysis, the intersection of the nonlinear regression curves with the dashed line at 63.2% was used to determine the frequency of cells that were either positive for the viral genome or reactivating virus. Data is generated from at least three independent experiments.

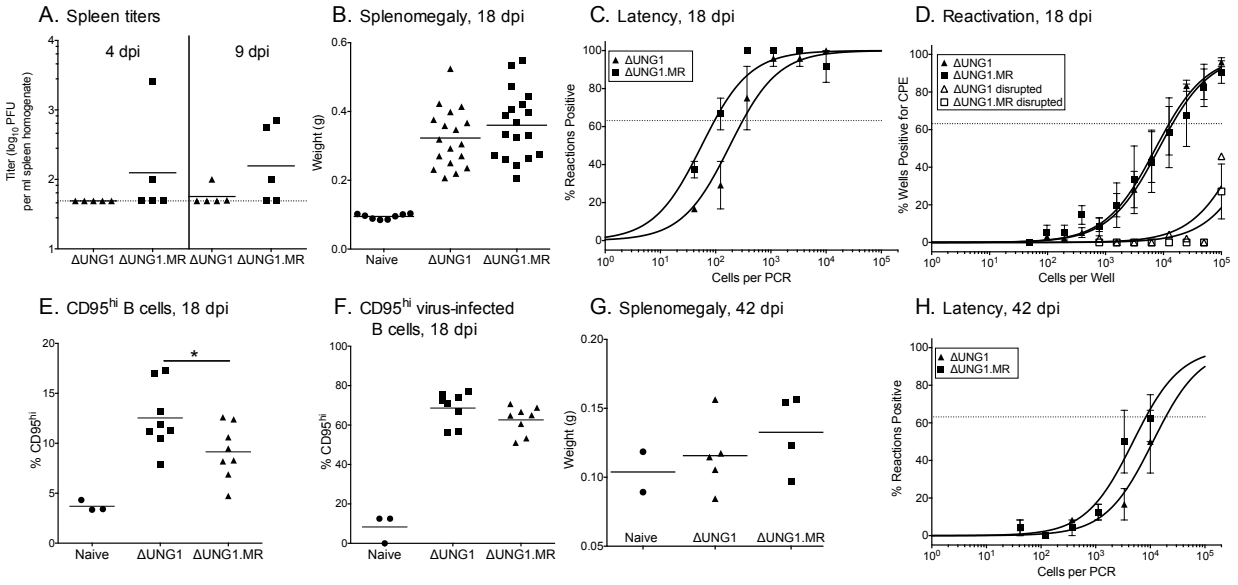

FIG 8. ORF46 is not essential for establishment of latency upon direct intraperitoneal inoculation. C57BL/6 mice were infected at 100 PFU by the intraperitoneal route with the indicated viruses. (**A**) Lung homogenates from mice were titered by plaque assay, line indicates geometric mean titer. Each symbol represents an individual mouse. The dashed line depicts the limit of detection at 50 PFU/ml of lung homogenate (log_{10} of 1.7). * $p \leq 0.05$. and ** $p \leq 0.005$. (**B**) Weights of spleens harvested from the indicated infections 18 dpi. Each symbol represents an individual mouse. (**C**) Frequency of splenocytes harboring latent genomes 18 dpi. (**D**) Frequency of splenocytes spontaneously reactivating from latency 18 dpi. (**E**) Proportion of $CD95^{hi}$ of CD19+ B cells in response to the indicated infection. (**F**) Proportion of $CD95^{hi}$ cells in the virus-infected YFP+ CD19+ B cell subset. * $p \leq 0.05$. (**G**) Weights of spleens harvested 42 dpi. (**H**) Frequency of splenocytes harboring latent genomes 42 dpi. For the limiting dilution analyses, curve fit lines were determined by nonlinear regression analysis. The dashed lines represent 63.2%. Using Poisson distribution analysis, the intersection of the nonlinear regression curves with the dashed line was used to determine the frequency of cells that were either positive for the viral genome or reactivating virus. Data is generated from at least three independent experiments for 18 dpi and two independent experiments for 42 dpi.

Table 1. Frequencies of cell populations harboring viral genomes in C57BL/6 mice.

Virus[a]	Dose, PFU	Route of infection[b]	Organ[c]	dpi	Frequency of viral genome-positive cells (one in) [d]	Total # of genome-positive cells [e]	Total # of cells harvested
ΔUNG.MR	100	i.n	Spleen	16	469	2.3×10^6	11.2×10^8
			Spleen	42	14,933	3.1×10^4	4.7×10^8
ΔUNG.1	100	i.n	Spleen	16	67,652	1.2×10^4	7.8×10^8
			Spleen	42	7,544	5.2×10^4	$3.9x\ 10^8$
ΔUNG.2	100	i.n	Spleen	16	<100,000	$<5.7 \times 10^3$	5.7×10^8
ΔUNG.MR	100,000	i.n	Spleen	16	267	3.7×10^6	$10.2x\ 10^8$
ΔUNG.1	100,000	i.n	Spleen	16	977	1.1×10^6	11.2×10^8
ΔUNG.MR	100	i.p	Spleen	18	99	1.7×10^7	16.7×10^8
			Spleen	42	8,397	4.0×10^4	3.4×10^8
			PEC	18	196	6.6×10^5	1.3×10^8
			PEC	42	963	2.1×10^4	0.2×10^8
ΔUNG.1	100	i.p	Spleen	18	327	5.6×10^6	18.2×10^8
			Spleen	42	20,167	1.9×10^4	3.8×10^8
			PEC	18	467	1.7×10^5	0.8×10^8
			PEC	42	647	3.1×10^4	0.2×10^8

[a] Infection with either MHV68.ΔUNG(MHV68 lacking the viral UNG) or MHV68. ΔUNG.MR (repaired UNG mutant virus)
[b] i.n., intranasal; i.p., intraperitoneal
[c] Organ harvested for limiting dilution analysis
[d] The frequency data were determined from the mean of at least three independent experiments with cells from the indicated organs. Organs were pooled from three to five mice per experiment.
[e] The total number of genome positive cells harvested from the mice was extrapolated using the frequency value generated from the limiting dilution analysis together with the total number of splenocytes or PEC cells harvested.
[F] Statistical difference in the frequency of viral genome-positive cells from ΔUNG infected mice as compared to ΔUNG.MR infections

Table 2. Frequencies of cell populations reactivating viral genomes in C57BL/6 mice.

Virus[a]	Dose, PFU	Route of infection[b]	Organ[c]	dpi	Frequency of reactivating cells (one in) [e]	Total # of cells reactivating latent virus [e]	Total # of cells harvested
ΔUNG.MR	100	i.n	Spleen	16	7490	1.5×10^5	11.2×10^8
			Spleen	42	n.d	n.d	4.7×10^8
ΔUNG.1	100	i.n	Spleen	16	<100,000[f]	$<4.7 \times 10^3$	7.8×10^8
			Spleen	42	n.d	n.d	3.9×10^8
ΔUNG.2	100	i.n	Spleen	16	<100,000[f]	$<5.7 \times 10^3$	5.7×10^8
ΔUNG.MR	100,000	i.n	Spleen	16	5,250	1.9×10^5	10.2×10^8
ΔUNG.1	100,000	i.n	Spleen	16	31,335[f]	3.6×10^4	11.2×10^8
ΔUNG.MR	100	i.p	Spleen	18	15,561	1.1×10^5	16.7×10^8
			Spleen	42	n.d	n.d	3.4×10^8
			PEC	18	1,677	7.8×10^4	1.3×10^8
			PEC	42	n.d	n.d	0.2×10^8
ΔUNG.1	100	i.p	Spleen	18	12,885	1.4×10^5	18.2×10^8
			Spleen	42	n.d	n.d	3.8×10^8
			PEC	18	5,086	1.6×10^4	0.8×10^8
			PEC	42	n.d	n.d	0.2×10^8

[a] Infection with either MHV68.ΔUNG(MHV68 lacking the viral UNG) or MHV68. ΔUNG.MR (repaired UNG mutant virus)
[b] i.n., intranasal; i.p., intraperitoneal
[c] Organ harvested for limiting dilution analysis
[d] The frequency data were determined from the mean of at least three independent experiments with cells from the indicated organs. Organs were pooled from three to five mice per experiment.
[e] The total number of genome positive cells harvested from the mice was extrapolated using the frequency value generated from the limiting dilution analysis together with the total number of splenocytes or PEC cells harvested.
[f] Statistical difference in the frequency of reactivating cells from ΔUNG infected mice as compared to ΔUNG.MR infections.

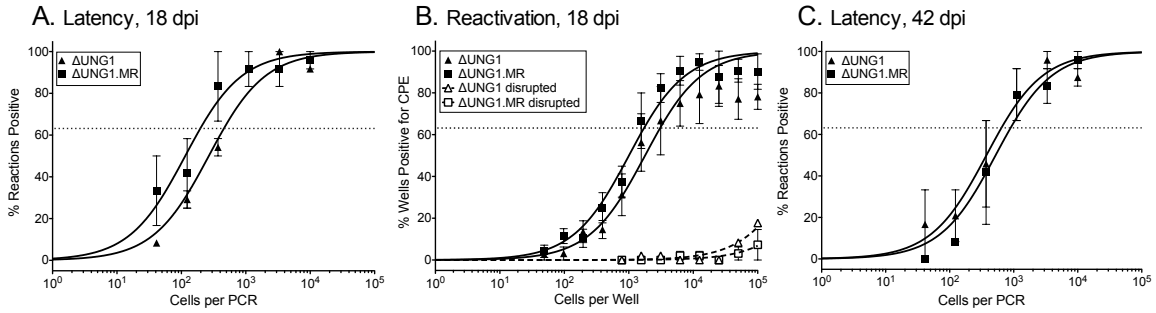

FIG 9. MHV68 vUNG is not required for the establishment or reactivation of latency in the peritoneal exudate compartment after intraperitoneal inoculation. C57BL/6 mice were infected at 100 PFU by the intraperitoneal route with ΔUNG1.MR, ΔUNG1 MHV68 viruses. (**A**) Frequency of peritoneal exudate cells harboring latent genomes 18 dpi. (**B**) Frequency of splenocytes spontaneously reactivating from latency 18 dpi. (**C**) Frequency of peritoneal exudate cells harboring latent genomes 42 dpi. For the limiting dilution analyses, curve fit lines were determined by nonlinear regression analysis. The dashed lines represent 63.2%. Using Poisson distribution analysis, the intersection of the nonlinear regression curves with the dashed line was used to determine the frequency of cells that were either positive for the viral genome or reactivating virus. Data is generated from at least 3 independent experiments.

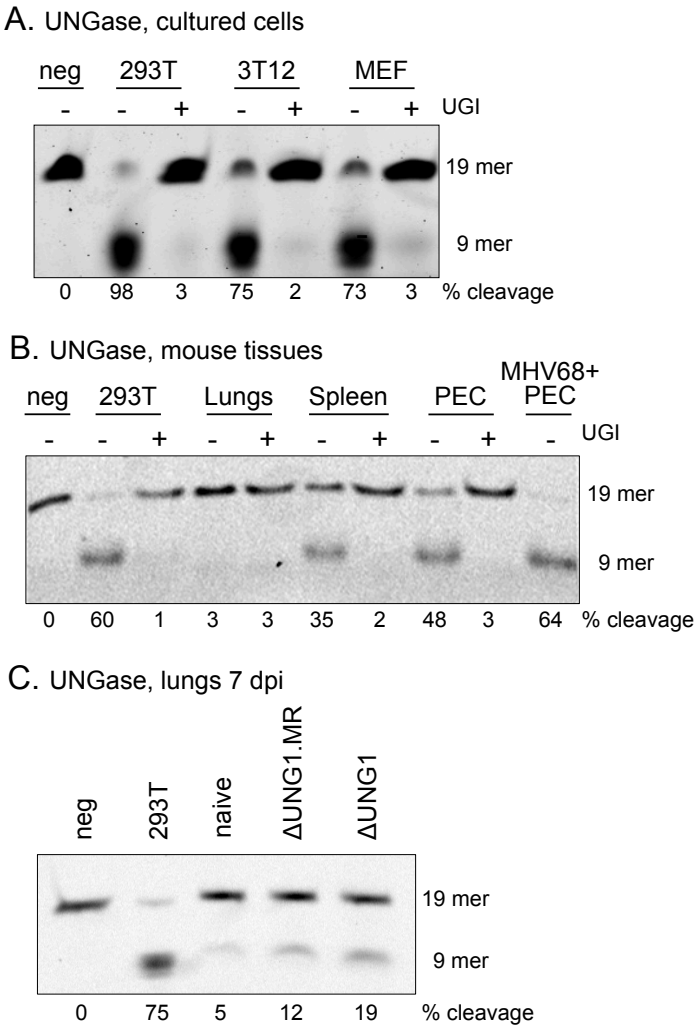

FIG 10. Analysis of uracil DNA glycosylase activity in cells and tissues that MHV68 infects. Denaturing polyacrylamide gel analysis of oligonucleotide cleavage upon incubation with lysates prepared from the indicated cells or tissue. The percentage of cleavage relative to the negative control is indicated below. (**A**) UNGase assay from cultured cell lysates. (**B**) Lysates from mouse tissues. (**C**) Lung lysates from naïve mice or mice infected with either ΔUNG1.MR or ΔUNG1 at 7 dpi.

DISCUSSION

MHV68 encodes a functional UNG that promotes viral replication in primary fibroblasts and in the lungs of infected mice. This defect in replication within the lung delays latency establishment and reactivation in the spleen. Increasing the virus dose or bypassing the lungs altogether by intraperitoneal inoculation eliminates the requirement for the vUNG, and identifies a route-dependent role for the vUNG. Finally, we observed varying levels of host UNG activity in cells and tissues targeted by MHV68, with mouse lungs exhibiting the lowest levels of UNG activity. To our knowledge this is the first report to directly correlate a tissue-specific absence of detectable host UNG activity with a requirement for vUNG.

Intranasal infection with MHV68 ΔUNG resulted in a dramatic reduction in replication in lung tissues that impaired latency establishment in the spleen. However, the ΔUNG latency defect was overcome with an increased dose of virus that largely restored lung titers. Bypassing the lung altogether by changing the route of virus administration to intraperitoneal inoculation fully restored latency. This supports a role for the vUNG in virus dissemination from initial sites of virus entry or replication to latent reservoirs, a finding consistent with studies in a mouse model of HSV-1 lacking the vUNG (UL2) (283). Primary HSV-1 infection occurs in the epithelium, after which the virus traverses the peripheral nervous system to invade the central nervous system. In contrast to WT infected mice, mice infected with HSV-1ΔUNG (ΔUL2) virus did not exhibit either hind limb paralysis or encephalitis. Moreover, loss of the HSV-1 vUNG (UL2) led to reduced virus titers in the footpads and tissues of the peripheral and central nervous system (283).

The route-dependent phenotype of MHV68 ΔUNG is similar to pathogenesis studies of other replication accessory proteins. MHV68 mutants lacking the ribonucleotide reductase small subunit (RNR-S/ORF60) (165), the ribonucleotide reductase large subunit (RNR-L/ORF61) (166) or thymidine kinase (TK/ORF21) (167, 168) are unable to establish latency after an upper respiratory infection, yet exhibit normal latency establishment upon intraperitoneal inoculation (165-168). Moreover, similar to the data reported herein, infections with an increased dose of the

RNR-S null virus helped overcome the latency defect upon upper respiratory infection. Thus our data for the vUNG are consistent with a model whereby the virus requires these 'accessory' proteins *in vivo* to promote productive replication in primary cells lacking potent expression of host metabolic or repair enzymes (280, 283).

The absence of vUNG did not impact MHV68 reactivation from latent splenocytes or peritoneal exudate cells. Moreover maintenance of latency six weeks post-infection was not impaired. At first glance, this observation contrasts with reactivation defects that were observed in mice infected with a mutant HSV-1 lacking UNG. However, HSV-1 reactivation was measured post-explant from trigeminal ganglia: a tissue composed of terminally differentiated adult neurons with low levels of host UNG (283, 289). Reactivation is also reduced in human gammaherpesvirus latency cell systems lacking the EBV viral UNG (BKRF3) alone or in the absence of both the vUNG and the host UNG (278, 283, 290-292). Interestingly, Su et al. (278) recently reported that host UNG2 levels decrease as EBV reactivation proceeds, indicating that the viral UNG is needed to promote replication in conditions of low host UNG levels (278). We attribute the lack of a reactivation defect for MHV68 ΔUNG to the latency reservoir under analysis at 16-18 dpi: actively proliferating peritoneal exudate cells or germinal center $CD95^{hi}$ B cells with high levels of host UNG2 (293).

Our data clearly demonstrate an important role for the vUNG in virus replication in the lung that is largely devoid of host UNG, yet the mechanisms by which the host and viral UNGs contribute to gammaherpesvirus replication are not well characterized. The EBV and HSV-1 vUNG (UL2) promote viral DNA replication (278, 280, 294). Interaction of the HSV-1 origin binding protein with the Ori_S is impaired by the presence of uracils in the target sequence (295). The requirement of EBV UNG (BKRF3) for DNA replication during reactivation from latency appears to be largely independent of glycosylase function, suggesting that vUNG protein interactions with other viral or host replication factors might play a role (278). However, the specific role the vUNG plays in viral replication complex formation, fork progression and DNA repair is not known.

B-lymphocytes utilize UNG activity in class switch recombination and somatic hypermutation, two processes critical for the development of a diverse antibody repertoire required for host immunity. To mediate class switch recombination, AID deaminates cytosines in immunoglobulin switch regions to generate deoxyuridine which is then excised by two host DNA glycosylases: UNG2 and, to a lesser extent, SMUG1. MHV68 UNG can substitute for host UNG2 in class switch recombination. This novel finding suggests that the MHV68 UNG retains the ability to recognize and cleave the N-glycosidic bond of uracil and may interact with other proteins critical for the mutagenic process of CSR. This implicates a possible role for the vUNG in impacting B cell processes critical for gammaherpesvirus pathogenesis. Alternatively, given that gammaherpesviruses target B cells that undergo isotype-class switching and, in some reports, upregulate the B cell specific host cytidine deaminase, AID (292, 296), it is possible that mutagenic effects of AID may exert a selective pressure that must be countered by the vUNG. Indeed, overexpression of AID impairs reactivation in KSHV-positive latent BCBL cell lines and this defect is exacerbated with depletion of host UNG2 (292). A role for the vUNG in countering AID restriction of gammaherpesvirus pathogenesis has not been studied. We recently reported that MHV68 replication is restricted by several host antiviral APOBEC3 cytidine deaminases (297). However, we did not observe an enhaced restriction by the most restrictive APOBEC3, APOBEC3A, in the absence of the viral UNG (data not shown).

Overall, our data support a model wherein the herpesvirus vUNG is required to promote viral replication in conditions of low host UNG levels. Importantly, we extend this finding to an *in vivo* gammaherpesvirus system and demonstrate that vUNG-dependent replication at the site of initial infection in the host has a substantial influence on the kinetics of dissemination and establishment of latency in distal reservoirs. Structure-function studies will be required to address differences between host and viral UNGs and dissect the possible roles played by the vUNG during replication. Given the critical role for the herpesvirus vUNG across all subfamilies, the vUNGs merit further investigation as targets of intervention to block herpesvirus replication and infection-associated diseases.

ACKNOWLEDGMENTS

We would like to thank Steven Reddy for technical support and the laboratories of Drs. Erich Mackow and Nancy Reich for sharing critical equipment. We would also like to thank Upasana Roy and Dr. Orlando Scharer for assisting with the UNGase assays as well as helpful discussions regarding UNG function. L.T.K. was supported by an American Cancer Society Research Scholar Grant RSG-11-160-01-MPC. L.T.K. and K.M. were supported by NIH AI111129-01. D.O. and D.W. are supported by the Gundersen Medical Foundation. N.M., D.O., D.W., M.M, K.M., and L.T.K. designed the experiments. N.M., D.O., M.M, and K.M. executed the experiments. N.M., D.O., D.W., M.M, K.M., C.P., and L.T.K analyzed the data. N.M., D.O., D.W., K.M., and L.T.K. prepared the manuscript.

REFERENCES

1. **Davison AJ.** 2002. Evolution of the herpesviruses. Veterinary microbiology **86:**69-88.
2. **Hedrick RP, McDowelll TS, Gilad O, Adkison M, Bovo G.** 2003. Systemic herpes-like virus in catfish Ictalurus melas (Italy) differs from Ictalurid herpesvirus 1 (North America). Diseases of aquatic organisms **55:**85-92.
3. **Burge CA, Griffin FJ, Friedman CS.** 2006. Mortality and herpesvirus infections of the Pacific oyster Crassostrea gigas in Tomales Bay, California, USA. Diseases of aquatic organisms **72:**31-43.
4. **Garcia C, Thebault A, Degremont L, Arzul I, Miossec L, Robert M, Chollet B, Francois C, Joly JP, Ferrand S, Kerdudou N, Renault T.** 2011. Ostreid herpesvirus 1 detection and relationship with Crassostrea gigas spat mortality in France between 1998 and 2006. Veterinary research **42:**73.
5. **Thiry J, Keuser V, Muylkens B, Meurens F, Gogev S, Vanderplasschen A, Thiry E.** 2006. Ruminant alphaherpesviruses related to bovine herpesvirus 1. Veterinary research **37:**169-190.
6. **Kramer T, Enquist LW.** 2013. Directional spread of alphaherpesviruses in the nervous system. Viruses **5:**678-707.
7. **Steiner I, Kennedy PG, Pachner AR.** 2007. The neurotropic herpes viruses: herpes simplex and varicella-zoster. The Lancet. Neurology **6:**1015-1028.
8. **Looker KJ, Garnett GP.** 2005. A systematic review of the epidemiology and interaction of herpes simplex virus types 1 and 2. Sexually transmitted infections **81:**103-107.
9. **Xu F, Sternberg MR, Kottiri BJ, McQuillan GM, Lee FK, Nahmias AJ, Berman SM, Markowitz LE.** 2006. Trends in herpes simplex virus type 1 and type 2 seroprevalence in the United States. Jama **296:**964-973.
10. **Wald A, Selke S, Warren T, Aoki FY, Sacks S, Diaz-Mitoma F, Corey L.** 2006. Comparative efficacy of famciclovir and valacyclovir for suppression of recurrent genital herpes and viral shedding. Sexually transmitted diseases **33:**529-533.
11. **Sawtell NM, Bernstein DI, Stanberry LR.** 1999. A temporal analysis of acyclovir inhibition of induced herpes simplex virus type 1 In vivo reactivation in the mouse trigeminal ganglia. The Journal of infectious diseases **180:**821-823.
12. **Gershon AA, Gershon MD.** 2010. Perspectives on vaccines against varicella-zoster virus infections. Current topics in microbiology and immunology **342:**359-372.
13. **Mendelson M, Monard S, Sissons P, Sinclair J.** 1996. Detection of endogenous human cytomegalovirus in CD34+ bone marrow progenitors. The Journal of general virology **77 (Pt 12):**3099-3102.
14. **Sinzger C, Grefte A, Plachter B, Gouw AS, The TH, Jahn G.** 1995. Fibroblasts, epithelial cells, endothelial cells and smooth muscle cells are major targets of human cytomegalovirus infection in lung and gastrointestinal tissues. The Journal of general virology **76 (Pt 4):**741-750.
15. **Sinzger C, Kahl M, Laib K, Klingel K, Rieger P, Plachter B, Jahn G.** 2000. Tropism of human cytomegalovirus for endothelial cells is determined by a post-entry step

dependent on efficient translocation to the nucleus. The Journal of general virology **81:**3021-3035.
16. **Streblow DN, Orloff SL, Nelson JA.** 2007. Acceleration of allograft failure by cytomegalovirus. Current opinion in immunology **19:**577-582.
17. **Grosse SD, Ross DS, Dollard SC.** 2008. Congenital cytomegalovirus (CMV) infection as a cause of permanent bilateral hearing loss: a quantitative assessment. Journal of clinical virology : the official publication of the Pan American Society for Clinical Virology **41:**57-62.
18. **Biron KK.** 2006. Antiviral drugs for cytomegalovirus diseases. Antiviral research **71:**154-163.
19. **Krug LT.** 2014. Editorial overview: Roseoloviruses: stopping to smell the roses--the Roseoloviruses have come of age as human pathogens. Current opinion in virology **9:**vi-vii.
20. **Caserta MT, Krug LT, Pellett PE.** 2014. Roseoloviruses: unmet needs and research priorities: perspective. Current opinion in virology **9:**167-169.
21. **Thompson MP, Kurzrock R.** 2004. Epstein-Barr virus and cancer. Clinical cancer research : an official journal of the American Association for Cancer Research **10:**803-821.
22. **Malnati MS, Dagna L, Ponzoni M, Lusso P.** 2003. Human herpesvirus 8 (HHV-8/KSHV) and hematologic malignancies. Reviews in clinical and experimental hematology **7:**375-405.
23. **Carbone A, Cesarman E, Spina M, Gloghini A, Schulz TF.** 2009. HIV-associated lymphomas and gamma-herpesviruses. Blood **113:**1213-1224.
24. **Carbone A, Gloghini A, Cabras A, Elia G.** 2009. Differentiating germinal center-derived lymphomas through their cellular microenvironment. American journal of hematology **84:**435-438.
25. **Epstein MA, Barr YM.** 1964. Cultivation in Vitro of Human Lymphoblasts from Burkitt's Malignant Lymphoma. Lancet **1:**252-253.
26. **Henle G, Henle W, Diehl V.** 1968. Relation of Burkitt's tumor-associated herpes-ytpe virus to infectious mononucleosis. Proceedings of the National Academy of Sciences of the United States of America **59:**94-101.
27. **Cohen JI.** 2000. Epstein-Barr virus infection. The New England journal of medicine **343:**481-492.
28. **Young LS, Rickinson AB.** 2004. Epstein-Barr virus: 40 years on. Nature reviews. Cancer **4:**757-768.
29. **Gulley ML, Tang W.** 2010. Using Epstein-Barr viral load assays to diagnose, monitor, and prevent posttransplant lymphoproliferative disorder. Clinical microbiology reviews **23:**350-366.
30. **Loren AW, Porter DL, Stadtmauer EA, Tsai DE.** 2003. Post-transplant lymphoproliferative disorder: a review. Bone marrow transplantation **31:**145-155.

31. **Styczynski J, Einsele H, Gil L, Ljungman P.** 2009. Outcome of treatment of Epstein-Barr virus-related post-transplant lymphoproliferative disorder in hematopoietic stem cell recipients: a comprehensive review of reported cases. Transplant infectious disease : an official journal of the Transplantation Society **11:**383-392.
32. **Heslop HE, Savoldo B, Rooney CM.** 2004. Cellular therapy of Epstein-Barr-virus-associated post-transplant lymphoproliferative disease. Best practice & research. Clinical haematology **17:**401-413.
33. **Soulier J, Grollet L, Oksenhendler E, Cacoub P, Cazals-Hatem D, Babinet P, d'Agay MF, Clauvel JP, Raphael M, Degos L, et al.** 1995. Kaposi's sarcoma-associated herpesvirus-like DNA sequences in multicentric Castleman's disease. Blood **86:**1276-1280.
34. **Dupin N, Grandadam M, Calvez V, Gorin I, Aubin JT, Havard S, Lamy F, Leibowitch M, Huraux JM, Escande JP, et al.** 1995. Herpesvirus-like DNA sequences in patients with Mediterranean Kaposi's sarcoma. Lancet **345:**761-762.
35. **Chang Y, Cesarman E, Pessin MS, Lee F, Culpepper J, Knowles DM, Moore PS.** 1994. Identification of herpesvirus-like DNA sequences in AIDS-associated Kaposi's sarcoma. Science **266:**1865-1869.
36. **Morfeldt L, Torssander J.** 1994. Long-term remission of Kaposi's sarcoma following foscarnet treatment in HIV-infected patients. Scandinavian journal of infectious diseases **26:**749-752.
37. **Temple RM, Zhu J, Budgeon L, Christensen ND, Meyers C, Sample CE.** 2014. Efficient replication of Epstein-Barr virus in stratified epithelium in vitro. Proceedings of the National Academy of Sciences of the United States of America **111:**16544-16549.
38. **Myoung J, Ganem D.** 2011. Generation of a doxycycline-inducible KSHV producer cell line of endothelial origin: maintenance of tight latency with efficient reactivation upon induction. Journal of virological methods **174:**12-21.
39. **Blaskovic D, Stancekova M, Svobodova J, Mistrikova J.** 1980. Isolation of five strains of herpesviruses from two species of free living small rodents. Acta virologica **24:**468.
40. **Blasdell K, McCracken C, Morris A, Nash AA, Begon M, Bennett M, Stewart JP.** 2003. The wood mouse is a natural host for Murid herpesvirus 4. The Journal of general virology **84:**111-113.
41. **Telfer S, Bennett M, Carslake D, Helyar S, Begon M.** 2007. The dynamics of murid gammaherpesvirus 4 within wild, sympatric populations of bank voles and wood mice. Journal of wildlife diseases **43:**32-39.
42. **Mistrikova J, Hricova M, Supolikova M.** 2006. Contribution to the problem of infection of humans with a murine gammaherpesvirus. Acta virologica **50:**71-72.
43. **Virgin HWt, Latreille P, Wamsley P, Hallsworth K, Weck KE, Dal Canto AJ, Speck SH.** 1997. Complete sequence and genomic analysis of murine gammaherpesvirus 68. Journal of virology **71:**5894-5904.
44. **Speck SH, Ganem D.** 2010. Viral latency and its regulation: lessons from the gamma-herpesviruses. Cell host & microbe **8:**100-115.

45. **Tischer BK, Smith GA, Osterrieder N.** 2010. En passant mutagenesis: a two step markerless red recombination system. Methods in molecular biology **634:**421-430.
46. **Gillet L, Gill MB, Colaco S, Smith CM, Stevenson PG.** 2006. Murine gammaherpesvirus-68 glycoprotein B presents a difficult neutralization target to monoclonal antibodies derived from infected mice. The Journal of general virology **87:**3515-3527.
47. **Sieczkarski SB, Whittaker GR.** 2005. Viral entry. Current topics in microbiology and immunology **285:**1-23.
48. **Shen S, Jia X, Guo H, Deng H.** 2015. Gammaherpesvirus Tegument Protein ORF33 Is Associated With Intranuclear Capsids at an Early Stage of the Tegumentation Process. Journal of virology **89:**5288-5297.
49. **Mettenleiter TC, Klupp BG, Granzow H.** 2006. Herpesvirus assembly: a tale of two membranes. Current opinion in microbiology **9:**423-429.
50. **Bortz E, Wang L, Jia Q, Wu TT, Whitelegge JP, Deng H, Zhou ZH, Sun R.** 2007. Murine gammaherpesvirus 68 ORF52 encodes a tegument protein required for virion morphogenesis in the cytoplasm. Journal of virology **81:**10137-10150.
51. **Forrest JC, Speck SH.** 2008. Establishment of B-cell lines latently infected with reactivation-competent murine gammaherpesvirus 68 provides evidence for viral alteration of a DNA damage-signaling cascade. Journal of virology **82:**7688-7699.
52. **Liang X, Paden CR, Morales FM, Powers RP, Jacob J, Speck SH.** 2011. Murine gamma-herpesvirus immortalization of fetal liver-derived B cells requires both the viral cyclin D homolog and latency-associated nuclear antigen. PLoS pathogens **7:**e1002220.
53. **Suarez AL, van Dyk LF.** 2008. Endothelial cells support persistent gammaherpesvirus 68 infection. PLoS pathogens **4:**e1000152.
54. **Glauser DL, Milho R, Frederico B, May JS, Kratz AS, Gillet L, Stevenson PG.** 2013. Glycoprotein B cleavage is important for murid herpesvirus 4 to infect myeloid cells. Journal of virology **87:**10828-10842.
55. **Frederico B, Chao B, May JS, Belz GT, Stevenson PG.** 2014. A murid gamma-herpesviruses exploits normal splenic immune communication routes for systemic spread. Cell host & microbe **15:**457-470.
56. **Gaspar M, May JS, Sukla S, Frederico B, Gill MB, Smith CM, Belz GT, Stevenson PG.** 2011. Murid herpesvirus-4 exploits dendritic cells to infect B cells. PLoS pathogens **7:**e1002346.
57. **Weck KE, Kim SS, Virgin HI, Speck SH.** 1999. B cells regulate murine gammaherpesvirus 68 latency. Journal of virology **73:**4651-4661.
58. **Weck KE, Kim SS, Virgin HI, Speck SH.** 1999. Macrophages are the major reservoir of latent murine gammaherpesvirus 68 in peritoneal cells. Journal of virology **73:**3273-3283.
59. **Doherty PC, Christensen JP, Belz GT, Stevenson PG, Sangster MY.** 2001. Dissecting the host response to a gamma-herpesvirus. Philosophical transactions of the Royal Society of London. Series B, Biological sciences **356:**581-593.

60. **Barton E, Mandal P, Speck SH.** 2011. Pathogenesis and host control of gammaherpesviruses: lessons from the mouse. Annual review of immunology **29:**351-397.
61. **Flano E, Woodland DL, Blackman MA.** 1999. Requirement for CD4+ T cells in V beta 4+CD8+ T cell activation associated with latent murine gammaherpesvirus infection. Journal of immunology **163:**3403-3408.
62. **Evans AG, Moser JM, Krug LT, Pozharskaya V, Mora AL, Speck SH.** 2008. A gammaherpesvirus-secreted activator of Vbeta4+ CD8+ T cells regulates chronic infection and immunopathology. The Journal of experimental medicine **205:**669-684.
63. **Flano E, Husain SM, Sample JT, Woodland DL, Blackman MA.** 2000. Latent murine gamma-herpesvirus infection is established in activated B cells, dendritic cells, and macrophages. Journal of immunology **165:**1074-1081.
64. **Sunil-Chandra NP, Arno J, Fazakerley J, Nash AA.** 1994. Lymphoproliferative disease in mice infected with murine gammaherpesvirus 68. The American journal of pathology **145:**818-826.
65. **Tarakanova VL, Suarez F, Tibbetts SA, Jacoby MA, Weck KE, Hess JL, Speck SH, Virgin HWt.** 2005. Murine gammaherpesvirus 68 infection is associated with lymphoproliferative disease and lymphoma in BALB beta2 microglobulin-deficient mice. Journal of virology **79:**14668-14679.
66. **Zhou ZH, Chen DH, Jakana J, Rixon FJ, Chiu W.** 1999. Visualization of tegument-capsid interactions and DNA in intact herpes simplex virus type 1 virions. Journal of virology **73:**3210-3218.
67. **Vittone V, Diefenbach E, Triffett D, Douglas MW, Cunningham AL, Diefenbach RJ.** 2005. Determination of interactions between tegument proteins of herpes simplex virus type 1. Journal of virology **79:**9566-9571.
68. **Chen DH, Jiang H, Lee M, Liu F, Zhou ZH.** 1999. Three-dimensional visualization of tegument/capsid interactions in the intact human cytomegalovirus. Virology **260:**10-16.
69. **Dai W, Jia Q, Bortz E, Shah S, Liu J, Atanasov I, Li X, Taylor KA, Sun R, Zhou ZH.** 2008. Unique structures in a tumor herpesvirus revealed by cryo-electron tomography and microscopy. Journal of structural biology **161:**428-438.
70. **Sciortino MT, Taddeo B, Poon AP, Mastino A, Roizman B.** 2002. Of the three tegument proteins that package mRNA in herpes simplex virions, one (VP22) transports the mRNA to uninfected cells for expression prior to viral infection. Proceedings of the National Academy of Sciences of the United States of America **99:**8318-8323.
71. **Sciortino MT, Suzuki M, Taddeo B, Roizman B.** 2001. RNAs extracted from herpes simplex virus 1 virions: apparent selectivity of viral but not cellular RNAs packaged in virions. Journal of virology **75:**8105-8116.
72. **Terhune SS, Schroer J, Shenk T.** 2004. RNAs are packaged into human cytomegalovirus virions in proportion to their intracellular concentration. Journal of virology **78:**10390-10398.

73. **Bresnahan WA, Shenk T.** 2000. A subset of viral transcripts packaged within human cytomegalovirus particles. Science **288:**2373-2376.
74. **Greijer AE, Dekkers CA, Middeldorp JM.** 2000. Human cytomegalovirus virions differentially incorporate viral and host cell RNA during the assembly process. Journal of virology **74:**9078-9082.
75. **Bechtel J, Grundhoff A, Ganem D.** 2005. RNAs in the virion of Kaposi's sarcoma-associated herpesvirus. Journal of virology **79:**10138-10146.
76. **Cliffe AR, Nash AA, Dutia BM.** 2009. Selective uptake of small RNA molecules in the virion of murine gammaherpesvirus 68. Journal of virology **83:**2321-2326.
77. **Amen MA, Griffiths A.** 2011. Identification and expression analysis of herpes B virus-encoded small RNAs. Journal of virology **85:**7296-7311.
78. **Kalejta RF.** 2008. Tegument proteins of human cytomegalovirus. Microbiology and molecular biology reviews : MMBR **72:**249-265, table of contents.
79. **Kelly BJ, Fraefel C, Cunningham AL, Diefenbach RJ.** 2009. Functional roles of the tegument proteins of herpes simplex virus type 1. Virus research **145:**173-186.
80. **Sathish N, Wang X, Yuan Y.** 2012. Tegument Proteins of Kaposi's Sarcoma-Associated Herpesvirus and Related Gamma-Herpesviruses. Frontiers in microbiology **3:**98.
81. **Dai X, Gong D, Wu TT, Sun R, Zhou ZH.** 2014. Organization of capsid-associated tegument components in Kaposi's sarcoma-associated herpesvirus. Journal of virology **88:**12694-12702.
82. **Bortz E, Whitelegge JP, Jia Q, Zhou ZH, Stewart JP, Wu TT, Sun R.** 2003. Identification of proteins associated with murine gammaherpesvirus 68 virions. Journal of virology **77:**13425-13432.
83. **Vidick S, Leroy B, Palmeira L, Machiels B, Mast J, Francois S, Wattiez R, Vanderplasschen A, Gillet L.** 2013. Proteomic characterization of murid herpesvirus 4 extracellular virions. PloS one **8:**e83842.
84. **Noh CW, Cho HJ, Kang HR, Jin HY, Lee S, Deng H, Wu TT, Arumugaswami V, Sun R, Song MJ.** 2012. The virion-associated open reading frame 49 of murine gammaherpesvirus 68 promotes viral replication both in vitro and in vivo as a derepressor of RTA. Journal of virology **86:**1109-1118.
85. **Gaspar M, Gill MB, Losing JB, May JS, Stevenson PG.** 2008. Multiple functions for ORF75c in murid herpesvirus-4 infection. PloS one **3:**e2781.
86. **Kang HR, Cheong WC, Park JE, Ryu S, Cho HJ, Youn H, Ahn JH, Song MJ.** 2014. Murine gammaherpesvirus 68 encoding open reading frame 11 targets TANK binding kinase 1 to negatively regulate the host type I interferon response. Journal of virology **88:**6832-6846.
87. **Zhu FX, Sathish N, Yuan Y.** 2010. Antagonism of host antiviral responses by Kaposi's sarcoma-associated herpesvirus tegument protein ORF45. PloS one **5:**e10573.
88. **Sathish N, Zhu FX, Yuan Y.** 2009. Kaposi's sarcoma-associated herpesvirus ORF45 interacts with kinesin-2 transporting viral capsid-tegument complexes along microtubules. PLoS pathogens **5:**e1000332.

89. **Jia Q, Chernishof V, Bortz E, McHardy I, Wu TT, Liao HI, Sun R.** 2005. Murine gammaherpesvirus 68 open reading frame 45 plays an essential role during the immediate-early phase of viral replication. Journal of virology **79:**5129-5141.
90. **Guo H, Wang L, Peng L, Zhou ZH, Deng H.** 2009. Open reading frame 33 of a gammaherpesvirus encodes a tegument protein essential for virion morphogenesis and egress. Journal of virology **83:**10582-10595.
91. **Rozen R, Sathish N, Li Y, Yuan Y.** 2008. Virion-wide protein interactions of Kaposi's sarcoma-associated herpesvirus. Journal of virology **82:**4742-4750.
92. **Stutz A, Golenbock DT, Latz E.** 2009. Inflammasomes: too big to miss. The Journal of clinical investigation **119:**3502-3511.
93. **Gregory SM, Davis BK, West JA, Taxman DJ, Matsuzawa S, Reed JC, Ting JP, Damania B.** 2011. Discovery of a viral NLR homolog that inhibits the inflammasome. Science **331:**330-334.
94. **Song MJ, Hwang S, Wong WH, Wu TT, Lee S, Liao HI, Sun R.** 2005. Identification of viral genes essential for replication of murine gamma-herpesvirus 68 using signature-tagged mutagenesis. Proceedings of the National Academy of Sciences of the United States of America **102:**3805-3810.
95. **Gonzalez CM, Wang L, Damania B.** 2009. Kaposi's sarcoma-associated herpesvirus encodes a viral deubiquitinase. Journal of virology **83:**10224-10233.
96. **Sompallae R, Gastaldello S, Hildebrand S, Zinin N, Hassink G, Lindsten K, Haas J, Persson B, Masucci MG.** 2008. Epstein-barr virus encodes three bona fide ubiquitin-specific proteases. Journal of virology **82:**10477-10486.
97. **Gredmark S, Schlieker C, Quesada V, Spooner E, Ploegh HL.** 2007. A functional ubiquitin-specific protease embedded in the large tegument protein (ORF64) of murine gammaherpesvirus 68 is active during the course of infection. Journal of virology **81:**10300-10309.
98. **Inn KS, Lee SH, Rathbun JY, Wong LY, Toth Z, Machida K, Ou JH, Jung JU.** 2011. Inhibition of RIG-I-mediated signaling by Kaposi's sarcoma-associated herpesvirus-encoded deubiquitinase ORF64. Journal of virology **85:**10899-10904.
99. **Sun C, Schattgen SA, Pisitkun P, Jorgensen JP, Hilterbrand AT, Wang LJ, West JA, Hansen K, Horan KA, Jakobsen MR, O'Hare P, Adler H, Sun R, Ploegh HL, Damania B, Upton JW, Fitzgerald KA, Paludan SR.** 2015. Evasion of innate cytosolic DNA sensing by a gammaherpesvirus facilitates establishment of latent infection. Journal of immunology **194:**1819-1831.
100. **An S, Kumar R, Sheets ED, Benkovic SJ.** 2008. Reversible compartmentalization of de novo purine biosynthetic complexes in living cells. Science **320:**103-106.
101. **An S, Deng Y, Tomsho JW, Kyoung M, Benkovic SJ.** 2010. Microtubule-assisted mechanism for functional metabolic macromolecular complex formation. Proceedings of the National Academy of Sciences of the United States of America **107:**12872-12876.

102. **Anand R, Hoskins AA, Stubbe J, Ealick SE.** 2004. Domain organization of Salmonella typhimurium formylglycinamide ribonucleotide amidotransferase revealed by X-ray crystallography. Biochemistry **43:**10328-10342.
103. **Davison AJ.** 2002. Evolution of the herpesviruses. Vet Microbiol **86:**69-88.
104. **Keil G, Fleckenstein B, Bodemer W.** 1983. Structural proteins of Herpesvirus saimiri. Journal of virology **47:**463-470.
105. **Hughes DJ, Kipar A, Milligan SG, Cunningham C, Sanders M, Quail MA, Rajandream MA, Efstathiou S, Bowden RJ, Chastel C, Bennett M, Sample JT, Barrell B, Davison AJ, Stewart JP.** 2010. Characterization of a novel wood mouse virus related to murid herpesvirus 4. The Journal of general virology **91:**867-879.
106. **Ling PD, Tan J, Sewatanon J, Peng R.** 2008. Murine gammaherpesvirus 68 open reading frame 75c tegument protein induces the degradation of PML and is essential for production of infectious virus. Journal of virology **82:**8000-8012.
107. **Everett RD, Chelbi-Alix MK.** 2007. PML and PML nuclear bodies: implications in antiviral defence. Biochimie **89:**819-830.
108. **Lallemand-Breitenbach V, de The H.** 2010. PML nuclear bodies. Cold Spring Harbor perspectives in biology **2:**a000661.
109. **Isaac A, Wilcox KW, Taylor JL.** 2006. SP100B, a repressor of gene expression preferentially binds to DNA with unmethylated CpGs. Journal of cellular biochemistry **98:**1106-1122.
110. **Michaelson JS, Leder P.** 2003. RNAi reveals anti-apoptotic and transcriptionally repressive activities of DAXX. Journal of cell science **116:**345-352.
111. **Bernardi R, Pandolfi PP.** 2007. Structure, dynamics and functions of promyelocytic leukaemia nuclear bodies. Nature reviews. Molecular cell biology **8:**1006-1016.
112. **Van Damme E, Laukens K, Dang TH, Van Ostade X.** 2010. A manually curated network of the PML nuclear body interactome reveals an important role for PML-NBs in SUMOylation dynamics. International journal of biological sciences **6:**51-67.
113. **Tavalai N, Adler M, Scherer M, Riedl Y, Stamminger T.** 2011. Evidence for a dual antiviral role of the major nuclear domain 10 component Sp100 during the immediate-early and late phases of the human cytomegalovirus replication cycle. Journal of virology **85:**9447-9458.
114. **Saffert RT, Kalejta RF.** 2007. Human cytomegalovirus gene expression is silenced by Daxx-mediated intrinsic immune defense in model latent infections established in vitro. Journal of virology **81:**9109-9120.
115. **Sivachandran N, Cao JY, Frappier L.** 2010. Epstein-Barr virus nuclear antigen 1 Hijacks the host kinase CK2 to disrupt PML nuclear bodies. Journal of virology **84:**11113-11123.
116. **Adamson AL, Kenney S.** 2001. Epstein-barr virus immediate-early protein BZLF1 is SUMO-1 modified and disrupts promyelocytic leukemia bodies. Journal of virology **75:**2388-2399.

117. **Rivas C, Thlick AE, Parravicini C, Moore PS, Chang Y.** 2001. Kaposi's sarcoma-associated herpesvirus LANA2 is a B-cell-specific latent viral protein that inhibits p53. Journal of virology **75:**429-438.
118. **Izumiya Y, Kobayashi K, Kim KY, Pochampalli M, Izumiya C, Shevchenko B, Wang DH, Huerta SB, Martinez A, Campbell M, Kung HJ.** 2013. Kaposi's sarcoma-associated herpesvirus K-Rta exhibits SUMO-targeting ubiquitin ligase (STUbL) like activity and is essential for viral reactivation. PLoS pathogens **9:**e1003506.
119. **Tsai K, Thikmyanova N, Wojcechowskyj JA, Delecluse HJ, Lieberman PM.** 2011. EBV tegument protein BNRF1 disrupts DAXX-ATRX to activate viral early gene transcription. PLoS pathogens **7:**e1002376.
120. **Tsai K, Chan L, Gibeault R, Conn K, Dheekollu J, Domsic J, Marmorstein R, Schang LM, Lieberman PM.** 2014. Viral reprogramming of the Daxx histone H3.3 chaperone during early Epstein-Barr virus infection. Journal of virology **88:**14350-14363.
121. **Full F, Jungnickl D, Reuter N, Bogner E, Brulois K, Scholz B, Sturzl M, Myoung J, Jung JU, Stamminger T, Ensser A.** 2014. Kaposi's sarcoma associated herpesvirus tegument protein ORF75 is essential for viral lytic replication and plays a critical role in the antagonization of ND10-instituted intrinsic immunity. PLoS pathogens **10:**e1003863.
122. **Full F, Reuter N, Zielke K, Stamminger T, Ensser A.** 2012. Herpesvirus saimiri antagonizes nuclear domain 10-instituted intrinsic immunity via an ORF3-mediated selective degradation of cellular protein Sp100. Journal of virology **86:**3541-3553.
123. **Sewatanon J, Ling PD.** 2013. Murine gammaherpesvirus 68 ORF75c contains ubiquitin E3 ligase activity and requires PML SUMOylation but not other known cellular PML regulators, CK2 and E6AP, to mediate PML degradation. Virology **440:**140-149.
124. **Konrad A, Wies E, Thurau M, Marquardt G, Naschberger E, Hentschel S, Jochmann R, Schulz TF, Erfle H, Brors B, Lausen B, Neipel F, Sturzl M.** 2009. A systems biology approach to identify the combination effects of human herpesvirus 8 genes on NF-kappaB activation. Journal of virology **83:**2563-2574.
125. **He S, Zhao J, Song S, He X, Minassian A, Zhou Y, Zhang J, Brulois K, Wang Y, Cabo J, Zandi E, Liang C, Jung JU, Zhang X, Feng P.** 2015. Viral pseudo-enzymes activate RIG-I via deamidation to evade cytokine production. Molecular cell **58:**134-146.
126. **Dong X, Feng P.** 2011. Murine gamma herpesvirus 68 hijacks MAVS and IKKbeta to abrogate NFkappaB activation and antiviral cytokine production. PLoS pathogens **7:**e1002336.
127. **Dong X, Feng H, Sun Q, Li H, Wu TT, Sun R, Tibbetts SA, Chen ZJ, Feng P.** 2010. Murine gamma-herpesvirus 68 hijacks MAVS and IKKbeta to initiate lytic replication. PLoS pathogens **6:**e1001001.
128. **Fitzgerald KA, McWhirter SM, Faia KL, Rowe DC, Latz E, Golenbock DT, Coyle AJ, Liao SM, Maniatis T.** 2003. IKKepsilon and TBK1 are essential components of the IRF3 signaling pathway. Nature immunology **4:**491-496.

129. **Sharma S, tenOever BR, Grandvaux N, Zhou GP, Lin R, Hiscott J.** 2003. Triggering the interferon antiviral response through an IKK-related pathway. Science **300:**1148-1151.
130. **Antinone SE, Smith GA.** 2010. Retrograde axon transport of herpes simplex virus and pseudorabies virus: a live-cell comparative analysis. Journal of virology **84:**1504-1512.
131. **Feederle R, Neuhierl B, Baldwin G, Bannert H, Hub B, Mautner J, Behrends U, Delecluse HJ.** 2006. Epstein-Barr virus BNRF1 protein allows efficient transfer from the endosomal compartment to the nucleus of primary B lymphocytes. Journal of virology **80:**9435-9443.
132. **Krug LT, Torres-Gonzalez E, Qin Q, Sorescu D, Rojas M, Stecenko A, Speck SH, Mora AL.** 2010. Inhibition of NF-kappaB signaling reduces virus load and gammaherpesvirus-induced pulmonary fibrosis. The American journal of pathology **177:**608-621.
133. **Cheng BY, Zhi J, Santana A, Khan S, Salinas E, Forrest JC, Zheng Y, Jaggi S, Leatherwood J, Krug LT.** 2012. Tiled microarray identification of novel viral transcript structures and distinct transcriptional profiles during two modes of productive murine gammaherpesvirus 68 infection. Journal of virology **86:**4340-4357.
134. **Damania B.** 2004. Modulation of cell signaling pathways by Kaposi's sarcoma-associated herpesvirus (KSHVHHV-8). Cell biochemistry and biophysics **40:**305-322.
135. **Hiscott J, Kwon H, Genin P.** 2001. Hostile takeovers: viral appropriation of the NF-kappaB pathway. The Journal of clinical investigation **107:**143-151.
136. **Santoro MG, Rossi A, Amici C.** 2003. NF-kappaB and virus infection: who controls whom. The EMBO journal **22:**2552-2560.
137. **Krug LT, Collins CM, Gargano LM, Speck SH.** 2009. NF-kappaB p50 plays distinct roles in the establishment and control of murine gammaherpesvirus 68 latency. Journal of virology **83:**4732-4748.
138. **Krug LT, Moser JM, Dickerson SM, Speck SH.** 2007. Inhibition of NF-kappaB activation in vivo impairs establishment of gammaherpesvirus latency. PLoS pathogens **3:**e11.
139. **Mercurio F, Zhu H, Murray BW, Shevchenko A, Bennett BL, Li J, Young DB, Barbosa M, Mann M, Manning A, Rao A.** 1997. IKK-1 and IKK-2: cytokine-activated IkappaB kinases essential for NF-kappaB activation. Science **278:**860-866.
140. **Grossmann C, Podgrabinska S, Skobe M, Ganem D.** 2006. Activation of NF-kappaB by the latent vFLIP gene of Kaposi's sarcoma-associated herpesvirus is required for the spindle shape of virus-infected endothelial cells and contributes to their proinflammatory phenotype. Journal of virology **80:**7179-7185.
141. **Martin D, Galisteo R, Ji Y, Montaner S, Gutkind JS.** 2008. An NF-kappaB gene expression signature contributes to Kaposi's sarcoma virus vGPCR-induced direct and paracrine neoplasia. Oncogene **27:**1844-1852.

142. **Bakker RA, Casarosa P, Timmerman H, Smit MJ, Leurs R.** 2004. Constitutively active Gq/11-coupled receptors enable signaling by co-expressed G(i/o)-coupled receptors. The Journal of biological chemistry **279:**5152-5161.
143. **Forrest JC, Paden CR, Allen RD, 3rd, Collins J, Speck SH.** 2007. ORF73-null murine gammaherpesvirus 68 reveals roles for mLANA and p53 in virus replication. Journal of virology **81:**11957-11971.
144. **Gargano LM, Moser JM, Speck SH.** 2008. Role for MyD88 signaling in murine gammaherpesvirus 68 latency. Journal of virology **82:**3853-3863.
145. **Kim IJ, Flano E, Woodland DL, Lund FE, Randall TD, Blackman MA.** 2003. Maintenance of long term gamma-herpesvirus B cell latency is dependent on CD40-mediated development of memory B cells. Journal of immunology **171:**886-892.
146. **Willer DO, Speck SH.** 2005. Establishment and maintenance of long-term murine gammaherpesvirus 68 latency in B cells in the absence of CD40. Journal of virology **79:**2891-2899.
147. **Moorman NJ, Willer DO, Speck SH.** 2003. The gammaherpesvirus 68 latency-associated nuclear antigen homolog is critical for the establishment of splenic latency. Journal of virology **77:**10295-10303.
148. **Paden CR, Forrest JC, Moorman NJ, Speck SH.** 2010. Murine gammaherpesvirus 68 LANA is essential for virus reactivation from splenocytes but not long-term carriage of viral genome. Journal of virology **84:**7214-7224.
149. **Bai D, Ueno L, Vogt PK.** 2009. Akt-mediated regulation of NFkappaB and the essentialness of NFkappaB for the oncogenicity of PI3K and Akt. International journal of cancer. Journal international du cancer **125:**2863-2870.
150. **Upton JW, Speck SH.** 2006. Evidence for CDK-dependent and CDK-independent functions of the murine gammaherpesvirus 68 v-cyclin. Journal of virology **80:**11946-11959.
151. **Hoge AT, Hendrickson SB, Burns WH.** 2000. Murine gammaherpesvirus 68 cyclin D homologue is required for efficient reactivation from latency. Journal of virology **74:**7016-7023.
152. **Chandriani S, Xu Y, Ganem D.** 2010. The lytic transcriptome of Kaposi's sarcoma-associated herpesvirus reveals extensive transcription of noncoding regions, including regions antisense to important genes. Journal of virology **84:**7934-7942.
153. **Arias C, Weisburd B, Stern-Ginossar N, Mercier A, Madrid AS, Bellare P, Holdorf M, Weissman JS, Ganem D.** 2014. KSHV 2.0: a comprehensive annotation of the Kaposi's sarcoma-associated herpesvirus genome using next-generation sequencing reveals novel genomic and functional features. PLoS pathogens **10:**e1003847.
154. **Guo YE, Steitz JA.** 2014. Virus meets host microRNA: the destroyer, the booster, the hijacker. Molecular and cellular biology **34:**3780-3787.
155. **Lee N, Moss WN, Yario TA, Steitz JA.** 2015. EBV noncoding RNA binds nascent RNA to drive host PAX5 to viral DNA. Cell **160:**607-618.

156. **Lin YT, Kincaid RP, Arasappan D, Dowd SE, Hunicke-Smith SP, Sullivan CS.** 2010. Small RNA profiling reveals antisense transcription throughout the KSHV genome and novel small RNAs. Rna **16:**1540-1558.
157. **Kincaid RP, Sullivan CS.** 2012. Virus-encoded microRNAs: an overview and a look to the future. PLoS pathogens **8:**e1003018.
158. **Stern-Ginossar N, Weisburd B, Michalski A, Le VT, Hein MY, Huang SX, Ma M, Shen B, Qian SB, Hengel H, Mann M, Ingolia NT, Weissman JS.** 2012. Decoding human cytomegalovirus. Science **338:**1088-1093.
159. **Jaber T, Yuan Y.** 2013. A virally encoded small peptide regulates RTA stability and facilitates Kaposi's sarcoma-associated herpesvirus lytic replication. Journal of virology **87:**3461-3470.
160. **Johnson LS, Willert EK, Virgin HW.** 2010. Redefining the genetics of murine gammaherpesvirus 68 via transcriptome-based annotation. Cell host & microbe **7:**516-526.
161. **Collins CM, Speck SH.** 2012. Tracking murine gammaherpesvirus 68 infection of germinal center B cells in vivo. PloS one **7:**e33230.
162. **Sunil-Chandra NP, Efstathiou S, Nash AA.** 1992. Murine gammaherpesvirus 68 establishes a latent infection in mouse B lymphocytes in vivo. The Journal of general virology **73 (Pt 12):**3275-3279.
163. **Moser JM, Farrell ML, Krug LT, Upton JW, Speck SH.** 2006. A gammaherpesvirus 68 gene 50 null mutant establishes long-term latency in the lung but fails to vaccinate against a wild-type virus challenge. Journal of virology **80:**1592-1598.
164. **Flano E, Jia Q, Moore J, Woodland DL, Sun R, Blackman MA.** 2005. Early establishment of gamma-herpesvirus latency: implications for immune control. Journal of immunology **174:**4972-4978.
165. **Milho R, Gill MB, May JS, Colaco S, Stevenson PG.** 2011. In vivo function of the murid herpesvirus-4 ribonucleotide reductase small subunit. The Journal of general virology **92:**1550-1560.
166. **Gill MB, May JS, Colaco S, Stevenson PG.** 2010. Important role for the murid herpesvirus 4 ribonucleotide reductase large subunit in host colonization via the respiratory tract. Journal of virology **84:**10937-10942.
167. **Coleman HM, de Lima B, Morton V, Stevenson PG.** 2003. Murine gammaherpesvirus 68 lacking thymidine kinase shows severe attenuation of lytic cycle replication in vivo but still establishes latency. Journal of virology **77:**2410-2417.
168. **Gill MB, Wright DE, Smith CM, May JS, Stevenson PG.** 2009. Murid herpesvirus-4 lacking thymidine kinase reveals route-dependent requirements for host colonization. The Journal of general virology **90:**1461-1470.
169. **Minkah N, Macaluso M, Oldenburg DG, Paden CR, White DW, McBride KM, Krug LT.** 2015. Absence of the uracil DNA glycosylase of murine gammaherpesvirus 68 impairs replication and delays the establishment of latency in vivo. Journal of virology **89:**3366-3379.

170. **Tibbetts SA, Suarez F, Steed AL, Simmons JA, Virgin HWt.** 2006. A gamma-herpesvirus deficient in replication establishes chronic infection in vivo and is impervious to restriction by adaptive immune cells. Virology **353:**210-219.
171. **May JS, Walker J, Colaco S, Stevenson PG.** 2005. The murine gammaherpesvirus 68 ORF27 gene product contributes to intercellular viral spread. Journal of virology **79:**5059-5068.
172. **Frederico B, Milho R, May JS, Gillet L, Stevenson PG.** 2012. Myeloid infection links epithelial and B cell tropisms of Murid Herpesvirus-4. PLoS pathogens **8:**e1002935.
173. **Upton JW, van Dyk LF, Speck SH.** 2005. Characterization of murine gammaherpesvirus 68 v-cyclin interactions with cellular cdks. Virology **341:**271-283.
174. **Jia Q, Sun R.** 2003. Inhibition of gammaherpesvirus replication by RNA interference. Journal of virology **77:**3301-3306.
175. **Cantrell SR, Bresnahan WA.** 2006. Human cytomegalovirus (HCMV) UL82 gene product (pp71) relieves hDaxx-mediated repression of HCMV replication. Journal of virology **80:**6188-6191.
176. **Geoffroy MC, Chadeuf G, Orr A, Salvetti A, Everett RD.** 2006. Impact of the interaction between herpes simplex virus type 1 regulatory protein ICP0 and ubiquitin-specific protease USP7 on activation of adeno-associated virus type 2 rep gene expression. Journal of virology **80:**3650-3654.
177. **Everett RD, Rechter S, Papior P, Tavalai N, Stamminger T, Orr A.** 2006. PML contributes to a cellular mechanism of repression of herpes simplex virus type 1 infection that is inactivated by ICP0. Journal of virology **80:**7995-8005.
178. **Lukashchuk V, McFarlane S, Everett RD, Preston CM.** 2008. Human cytomegalovirus protein pp71 displaces the chromatin-associated factor ATRX from nuclear domain 10 at early stages of infection. Journal of virology **82:**12543-12554.
179. **Lukashchuk V, Everett RD.** 2010. Regulation of ICP0-null mutant herpes simplex virus type 1 infection by ND10 components ATRX and hDaxx. Journal of virology **84:**4026-4040.
180. **Negorev DG, Vladimirova OV, Ivanov A, Rauscher F, 3rd, Maul GG.** 2006. Differential role of Sp100 isoforms in interferon-mediated repression of herpes simplex virus type 1 immediate-early protein expression. Journal of virology **80:**8019-8029.
181. **Everett RD, Parada C, Gripon P, Sirma H, Orr A.** 2008. Replication of ICP0-null mutant herpes simplex virus type 1 is restricted by both PML and Sp100. Journal of virology **82:**2661-2672.
182. **Tavalai N, Papior P, Rechter S, Leis M, Stamminger T.** 2006. Evidence for a role of the cellular ND10 protein PML in mediating intrinsic immunity against human cytomegalovirus infections. Journal of virology **80:**8006-8018.
183. **Cieniewicz B, Dong Q, Li G, Forrest JC, Mounce BC, Tarakanova VL, van der Velden A, Krug LT.** 2015. Murine Gammaherpesvirus 68 Pathogenesis Is Independent of Caspase-1 and Caspase-11 in Mice and Impairs Interleukin-1beta Production upon Extrinsic Stimulation in Culture. Journal of virology **89:**6562-6574.

184. **Mounce BC, Mboko WP, Kanack AJ, Tarakanova VL.** 2014. Primary macrophages rely on histone deacetylase 1 and 2 expression to induce type I interferon in response to gammaherpesvirus infection. Journal of virology **88:**2268-2278.
185. **Reese TA, Wakeman BS, Choi HS, Hufford MM, Huang SC, Zhang X, Buck MD, Jezewski A, Kambal A, Liu CY, Goel G, Murray PJ, Xavier RJ, Kaplan MH, Renne R, Speck SH, Artyomov MN, Pearce EJ, Virgin HW.** 2014. Coinfection. Helminth infection reactivates latent gamma-herpesvirus via cytokine competition at a viral promoter. Science **345:**573-577.
186. **Leang RS, Wu TT, Hwang S, Liang LT, Tong L, Truong JT, Sun R.** 2011. The anti-interferon activity of conserved viral dUTPase ORF54 is essential for an effective MHV-68 infection. PLoS pathogens **7:**e1002292.
187. **Benach J, Wang L, Chen Y, Ho CK, Lee S, Seetharaman J, Xiao R, Acton TB, Montelione GT, Deng H, Sun R, Tong L.** 2007. Structural and functional studies of the abundant tegument protein ORF52 from murine gammaherpesvirus 68. The Journal of biological chemistry **282:**31534-31541.
188. **Covarrubias S, Richner JM, Clyde K, Lee YJ, Glaunsinger BA.** 2009. Host shutoff is a conserved phenotype of gammaherpesvirus infection and is orchestrated exclusively from the cytoplasm. Journal of virology **83:**9554-9566.
189. **Abernathy E, Clyde K, Yeasmin R, Krug LT, Burlingame A, Coscoy L, Glaunsinger B.** 2014. Gammaherpesviral gene expression and virion composition are broadly controlled by accelerated mRNA degradation. PLoS pathogens **10:**e1003882.
190. **Raab-Traub N.** 2012. Novel mechanisms of EBV-induced oncogenesis. Current opinion in virology **2:**453-458.
191. **Soni V, Cahir-McFarland E, Kieff E.** 2007. LMP1 TRAFficking activates growth and survival pathways. Advances in experimental medicine and biology **597:**173-187.
192. **Dong X, He Z, Durakoglugil D, Arneson L, Shen Y, Feng P.** 2012. Murine gammaherpesvirus 68 evades host cytokine production via replication transactivator-induced RelA degradation. Journal of virology **86:**1930-1941.
193. **Banerjee AS, Pal AD, Banerjee S.** 2013. Epstein-Barr virus-encoded small non-coding RNAs induce cancer cell chemoresistance and migration. Virology **443:**294-305.
194. **Cao S, Moss W, O'Grady T, Concha M, Strong MJ, Wang X, Yu Y, Baddoo M, Zhang K, Fewell C, Lin Z, Dong Y, Flemington EK.** 2015. New non-coding lytic transcripts derived from the Epstein Barr virus latency origin of replication oriP are hyper-edited, bind the paraspeckle protein, NONO/p54nrb, and support lytic viral transcription. Journal of virology.
195. **Ahn JW, Powell KL, Kellam P, Alber DG.** 2002. Gammaherpesvirus lytic gene expression as characterized by DNA array. Journal of virology **76:**6244-6256.
196. **Glass M, Everett RD.** 2013. Components of promyelocytic leukemia nuclear bodies (ND10) act cooperatively to repress herpesvirus infection. Journal of virology **87:**2174-2185.

197. **Sewatanon J, Ling PD.** 2014. Murine gammaherpesvirus 68 encodes a second PML-modifying protein. Journal of virology **88:**3591-3597.
198. **Vink EI, Zheng Y, Yeasmin R, Stamminger T, Krug LT, Hearing P.** 2015. Impact of Adenovirus E4-ORF3 Oligomerization and Protein Localization on Cellular Gene Expression. Viruses **7:**2428-2449.
199. **Tavalai N, Stamminger T.** 2009. Interplay between Herpesvirus Infection and Host Defense by PML Nuclear Bodies. Viruses **1:**1240-1264.
200. **Paludan SR, Bowie AG, Horan KA, Fitzgerald KA.** 2011. Recognition of herpesviruses by the innate immune system. Nature reviews. Immunology **11:**143-154.
201. **Smith HC, Bennett RP, Kizilyer A, McDougall WM, Prohaska KM.** 2012. Functions and regulation of the APOBEC family of proteins. Seminars in cell & developmental biology **23:**258-268.
202. **Bransteitter R, Prochnow C, Chen XS.** 2009. The current structural and functional understanding of APOBEC deaminases. Cellular and molecular life sciences : CMLS **66:**3137-3147.
203. **Driscoll DM, Zhang Q.** 1994. Expression and characterization of p27, the catalytic subunit of the apolipoprotein B mRNA editing enzyme. The Journal of biological chemistry **269:**19843-19847.
204. **Mehta A, Driscoll DM.** 1998. A sequence-specific RNA-binding protein complements apobec-1 To edit apolipoprotein B mRNA. Molecular and cellular biology **18:**4426-4432.
205. **Mikl MC, Watt IN, Lu M, Reik W, Davies SL, Neuberger MS, Rada C.** 2005. Mice deficient in APOBEC2 and APOBEC3. Molecular and cellular biology **25:**7270-7277.
206. **Okuyama S, Marusawa H, Matsumoto T, Ueda Y, Matsumoto Y, Endo Y, Takai A, Chiba T.** 2012. Excessive activity of apolipoprotein B mRNA editing enzyme catalytic polypeptide 2 (APOBEC2) contributes to liver and lung tumorigenesis. International journal of cancer. Journal international du cancer **130:**1294-1301.
207. **Cullen BR.** 2006. Role and mechanism of action of the APOBEC3 family of antiretroviral resistance factors. Journal of virology **80:**1067-1076.
208. **Refsland EW, Harris RS.** 2013. The APOBEC3 family of retroelement restriction factors. Current topics in microbiology and immunology **371:**1-27.
209. **Munk C, Beck T, Zielonka J, Hotz-Wagenblatt A, Chareza S, Battenberg M, Thielebein J, Cichutek K, Bravo IG, O'Brien SJ, Lochelt M, Yuhki N.** 2008. Functions, structure, and read-through alternative splicing of feline APOBEC3 genes. Genome biology **9:**R48.
210. **Bogerd HP, Tallmadge RL, Oaks JL, Carpenter S, Cullen BR.** 2008. Equine infectious anemia virus resists the antiretroviral activity of equine APOBEC3 proteins through a packaging-independent mechanism. Journal of virology **82:**11889-11901.
211. **Sheehy AM, Gaddis NC, Choi JD, Malim MH.** 2002. Isolation of a human gene that inhibits HIV-1 infection and is suppressed by the viral Vif protein. Nature **418:**646-650.

212. **Zhang H, Yang B, Pomerantz RJ, Zhang C, Arunachalam SC, Gao L.** 2003. The cytidine deaminase CEM15 induces hypermutation in newly synthesized HIV-1 DNA. Nature **424:**94-98.
213. **Goila-Gaur R, Strebel K.** 2008. HIV-1 Vif, APOBEC, and intrinsic immunity. Retrovirology **5:**51.
214. **Bishop KN, Holmes RK, Sheehy AM, Malim MH.** 2004. APOBEC-mediated editing of viral RNA. Science **305:**645.
215. **Mahieux R, Suspene R, Delebecque F, Henry M, Schwartz O, Wain-Hobson S, Vartanian JP.** 2005. Extensive editing of a small fraction of human T-cell leukemia virus type 1 genomes by four APOBEC3 cytidine deaminases. The Journal of general virology **86:**2489-2494.
216. **Suspene R, Guetard D, Henry M, Sommer P, Wain-Hobson S, Vartanian JP.** 2005. Extensive editing of both hepatitis B virus DNA strands by APOBEC3 cytidine deaminases in vitro and in vivo. Proceedings of the National Academy of Sciences of the United States of America **102:**8321-8326.
217. **Suspene R, Henry M, Guillot S, Wain-Hobson S, Vartanian JP.** 2005. Recovery of APOBEC3-edited human immunodeficiency virus G->A hypermutants by differential DNA denaturation PCR. The Journal of general virology **86:**125-129.
218. **Suspene R, Sommer P, Henry M, Ferris S, Guetard D, Pochet S, Chester A, Navaratnam N, Wain-Hobson S, Vartanian JP.** 2004. APOBEC3G is a single-stranded DNA cytidine deaminase and functions independently of HIV reverse transcriptase. Nucleic acids research **32:**2421-2429.
219. **Mangeat B, Turelli P, Caron G, Friedli M, Perrin L, Trono D.** 2003. Broad antiretroviral defence by human APOBEC3G through lethal editing of nascent reverse transcripts. Nature **424:**99-103.
220. **Delebecque F, Suspene R, Calattini S, Casartelli N, Saib A, Froment A, Wain-Hobson S, Gessain A, Vartanian JP, Schwartz O.** 2006. Restriction of foamy viruses by APOBEC cytidine deaminases. Journal of virology **80:**605-614.
221. **Stenglein MD, Burns MB, Li M, Lengyel J, Harris RS.** 2010. APOBEC3 proteins mediate the clearance of foreign DNA from human cells. Nature structural & molecular biology **17:**222-229.
222. **Vartanian JP, Guetard D, Henry M, Wain-Hobson S.** 2008. Evidence for editing of human papillomavirus DNA by APOBEC3 in benign and precancerous lesions. Science **320:**230-233.
223. **Narvaiza I, Linfesty DC, Greener BN, Hakata Y, Pintel DJ, Logue E, Landau NR, Weitzman MD.** 2009. Deaminase-independent inhibition of parvoviruses by the APOBEC3A cytidine deaminase. PLoS pathogens **5:**e1000439.
224. **Suspene R, Aynaud MM, Koch S, Pasdeloup D, Labetoulle M, Gaertner B, Vartanian JP, Meyerhans A, Wain-Hobson S.** 2011. Genetic editing of herpes simplex virus 1 and Epstein-Barr herpesvirus genomes by human APOBEC3 cytidine deaminases in culture and in vivo. Journal of virology **85:**7594-7602.

225. **Langlois MA, Kemmerich K, Rada C, Neuberger MS.** 2009. The AKV murine leukemia virus is restricted and hypermutated by mouse APOBEC3. Journal of virology **83:**11550-11559.
226. **Okeoma CM, Lovsin N, Peterlin BM, Ross SR.** 2007. APOBEC3 inhibits mouse mammary tumour virus replication in vivo. Nature **445:**927-930.
227. **Low A, Okeoma CM, Lovsin N, de las Heras M, Taylor TH, Peterlin BM, Ross SR, Fan H.** 2009. Enhanced replication and pathogenesis of Moloney murine leukemia virus in mice defective in the murine APOBEC3 gene. Virology **385:**455-463.
228. **Takeda E, Tsuji-Kawahara S, Sakamoto M, Langlois MA, Neuberger MS, Rada C, Miyazawa M.** 2008. Mouse APOBEC3 restricts friend leukemia virus infection and pathogenesis in vivo. Journal of virology **82:**10998-11008.
229. **Weck KE, Barkon ML, Yoo LI, Speck SH, Virgin HI.** 1996. Mature B cells are required for acute splenic infection, but not for establishment of latency, by murine gammaherpesvirus 68. Journal of virology **70:**6775-6780.
230. **Hakata Y, Landau NR.** 2006. Reversed functional organization of mouse and human APOBEC3 cytidine deaminase domains. The Journal of biological chemistry **281:**36624-36631.
231. **Yu Q, Chen D, Konig R, Mariani R, Unutmaz D, Landau NR.** 2004. APOBEC3B and APOBEC3C are potent inhibitors of simian immunodeficiency virus replication. The Journal of biological chemistry **279:**53379-53386.
232. **Senavirathne G, Jaszczur M, Auerbach PA, Upton TG, Chelico L, Goodman MF, Rueda D.** 2012. Single-stranded DNA scanning and deamination by APOBEC3G cytidine deaminase at single molecule resolution. The Journal of biological chemistry **287:**15826-15835.
233. **Liddament MT, Brown WL, Schumacher AJ, Harris RS.** 2004. APOBEC3F properties and hypermutation preferences indicate activity against HIV-1 in vivo. Current biology : CB **14:**1385-1391.
234. **Zheng YH, Irwin D, Kurosu T, Tokunaga K, Sata T, Peterlin BM.** 2004. Human APOBEC3F is another host factor that blocks human immunodeficiency virus type 1 replication. Journal of virology **78:**6073-6076.
235. **Hultquist JF, Lengyel JA, Refsland EW, LaRue RS, Lackey L, Brown WL, Harris RS.** 2011. Human and rhesus APOBEC3D, APOBEC3F, APOBEC3G, and APOBEC3H demonstrate a conserved capacity to restrict Vif-deficient HIV-1. Journal of virology **85:**11220-11234.
236. **Taylor BJ, Nik-Zainal S, Wu YL, Stebbings LA, Raine K, Campbell PJ, Rada C, Stratton MR, Neuberger MS.** 2013. DNA deaminases induce break-associated mutation showers with implication of APOBEC3B and 3A in breast cancer kataegis. eLife **2:**e00534.
237. **Jern P, Russell RA, Pathak VK, Coffin JM.** 2009. Likely role of APOBEC3G-mediated G-to-A mutations in HIV-1 evolution and drug resistance. PLoS pathogens **5:**e1000367.

238. **MacMillan AL, Kohli RM, Ross SR.** 2013. APOBEC3 inhibition of mouse mammary tumor virus infection: the role of cytidine deamination versus inhibition of reverse transcription. Journal of virology **87:**4808-4817.
239. **Madsen P, Anant S, Rasmussen HH, Gromov P, Vorum H, Dumanski JP, Tommerup N, Collins JE, Wright CL, Dunham I, MacGinnitie AJ, Davidson NO, Celis JE.** 1999. Psoriasis upregulated phorbolin-1 shares structural but not functional similarity to the mRNA-editing protein apobec-1. The Journal of investigative dermatology **113:**162-169.
240. **Trivedi NR, Gilliland KL, Zhao W, Liu W, Thiboutot DM.** 2006. Gene array expression profiling in acne lesions reveals marked upregulation of genes involved in inflammation and matrix remodeling. The Journal of investigative dermatology **126:**1071-1079.
241. **Quinlan MP, Chen LB, Knipe DM.** 1984. The intranuclear location of a herpes simplex virus DNA-binding protein is determined by the status of viral DNA replication. Cell **36:**857-868.
242. **OhAinle M, Kerns JA, Malik HS, Emerman M.** 2006. Adaptive evolution and antiviral activity of the conserved mammalian cytidine deaminase APOBEC3H. Journal of virology **80:**3853-3862.
243. **Lackey L, Demorest ZL, Land AM, Hultquist JF, Brown WL, Harris RS.** 2012. APOBEC3B and AID have similar nuclear import mechanisms. Journal of molecular biology **419:**301-314.
244. **Kinomoto M, Kanno T, Shimura M, Ishizaka Y, Kojima A, Kurata T, Sata T, Tokunaga K.** 2007. All APOBEC3 family proteins differentially inhibit LINE-1 retrotransposition. Nucleic acids research **35:**2955-2964.
245. **Bogerd HP, Wiegand HL, Hulme AE, Garcia-Perez JL, O'Shea KS, Moran JV, Cullen BR.** 2006. Cellular inhibitors of long interspersed element 1 and Alu retrotransposition. Proceedings of the National Academy of Sciences of the United States of America **103:**8780-8785.
246. **Li MM, Emerman M.** 2011. Polymorphism in human APOBEC3H affects a phenotype dominant for subcellular localization and antiviral activity. Journal of virology **85:**8197-8207.
247. **Chen H, Lilley CE, Yu Q, Lee DV, Chou J, Narvaiza I, Landau NR, Weitzman MD.** 2006. APOBEC3A is a potent inhibitor of adeno-associated virus and retrotransposons. Current biology : CB **16:**480-485.
248. **Boutell C, Everett RD.** 2013. Regulation of alphaherpesvirus infections by the ICP0 family of proteins. The Journal of general virology **94:**465-481.
249. **Penkert RR, Kalejta RF.** 2012. Tale of a tegument transactivator: the past, present and future of human CMV pp71. Future virology **7:**855-869.
250. **de Bruyn Kops A, Knipe DM.** 1994. Preexisting nuclear architecture defines the intranuclear location of herpesvirus DNA replication structures. Journal of virology **68:**3512-3526.

251. **Weller SK.** 2010. Herpes simplex virus reorganizes the cellular DNA repair and protein quality control machinery. PLoS pathogens **6:**e1001105.
252. **Saffert RT, Kalejta RF.** 2008. Promyelocytic leukemia-nuclear body proteins: herpesvirus enemies, accomplices, or both? Future virology **3:**265-277.
253. **Sanchez-Martinez S, Aloia AL, Harvin D, Mirro J, Gorelick RJ, Jern P, Coffin JM, Rein A.** 2012. Studies on the restriction of murine leukemia viruses by mouse APOBEC3. PloS one **7:**e38190.
254. **Doehle BP, Schafer A, Wiegand HL, Bogerd HP, Cullen BR.** 2005. Differential sensitivity of murine leukemia virus to APOBEC3-mediated inhibition is governed by virion exclusion. Journal of virology **79:**8201-8207.
255. **Mariani R, Chen D, Schrofelbauer B, Navarro F, Konig R, Bollman B, Munk C, Nymark-McMahon H, Landau NR.** 2003. Species-specific exclusion of APOBEC3G from HIV-1 virions by Vif. Cell **114:**21-31.
256. **Malim MH.** 2009. APOBEC proteins and intrinsic resistance to HIV-1 infection. Philosophical transactions of the Royal Society of London. Series B, Biological sciences **364:**675-687.
257. **Malim MH, Emerman M.** 2008. HIV-1 accessory proteins--ensuring viral survival in a hostile environment. Cell host & microbe **3:**388-398.
258. **Stavrou S, Nitta T, Kotla S, Ha D, Nagashima K, Rein AR, Fan H, Ross SR.** 2013. Murine leukemia virus glycosylated Gag blocks apolipoprotein B editing complex 3 and cytosolic sensor access to the reverse transcription complex. Proceedings of the National Academy of Sciences of the United States of America **110:**9078-9083.
259. **Kitamura K, Wang Z, Chowdhury S, Simadu M, Koura M, Muramatsu M.** 2013. Uracil DNA glycosylase counteracts APOBEC3G-induced hypermutation of hepatitis B viral genomes: excision repair of covalently closed circular DNA. PLoS pathogens **9:**e1003361.
260. **Sewatanon J, Liu H, Ling PD.** 2013. PML protein modulates establishment and maintenance of latent gamma-herpesvirus infection in peritoneal cells. Journal of virology.
261. **Clambey ET, Virgin HWt, Speck SH.** 2000. Disruption of the murine gammaherpesvirus 68 M1 open reading frame leads to enhanced reactivation from latency. Journal of virology **74:**1973-1984.
262. **Jacoby MA, Virgin HWt, Speck SH.** 2002. Disruption of the M2 gene of murine gammaherpesvirus 68 alters splenic latency following intranasal, but not intraperitoneal, inoculation. Journal of virology **76:**1790-1801.
263. **Petit V, Guetard D, Renard M, Keriel A, Sitbon M, Wain-Hobson S, Vartanian JP.** 2009. Murine APOBEC1 is a powerful mutator of retroviral and cellular RNA in vitro and in vivo. Journal of molecular biology **385:**65-78.
264. **Renard M, Henry M, Guetard D, Vartanian JP, Wain-Hobson S.** 2010. APOBEC1 and APOBEC3 cytidine deaminases as restriction factors for hepadnaviral genomes in non-humans in vivo. Journal of molecular biology **400:**323-334.

265. **Gee P, Ando Y, Kitayama H, Yamamoto SP, Kanemura Y, Ebina H, Kawaguchi Y, Koyanagi Y.** 2011. APOBEC1-mediated editing and attenuation of herpes simplex virus 1 DNA indicate that neurons have an antiviral role during herpes simplex encephalitis. Journal of virology **85:**9726-9736.
266. **Krokan HE, Drablos F, Slupphaug G.** 2002. Uracil in DNA--occurrence, consequences and repair. Oncogene **21:**8935-8948.
267. **Nilsen H, Steinsbekk KS, Otterlei M, Slupphaug G, Aas PA, Krokan HE.** 2000. Analysis of uracil-DNA glycosylases from the murine Ung gene reveals differential expression in tissues and in embryonic development and a subcellular sorting pattern that differs from the human homologues. Nucleic acids research **28:**2277-2285.
268. **Nilsen H, Krokan HE.** 2001. Base excision repair in a network of defence and tolerance. Carcinogenesis **22:**987-998.
269. **Kavli B, Sundheim O, Akbari M, Otterlei M, Nilsen H, Skorpen F, Aas PA, Hagen L, Krokan HE, Slupphaug G.** 2002. hUNG2 is the major repair enzyme for removal of uracil from U:A matches, U:G mismatches, and U in single-stranded DNA, with hSMUG1 as a broad specificity backup. The Journal of biological chemistry **277:**39926-39936.
270. **Akbari M, Otterlei M, Pena-Diaz J, Aas PA, Kavli B, Liabakk NB, Hagen L, Imai K, Durandy A, Slupphaug G, Krokan HE.** 2004. Repair of U/G and U/A in DNA by UNG2-associated repair complexes takes place predominantly by short-patch repair both in proliferating and growth-arrested cells. Nucleic acids research **32:**5486-5498.
271. **Imai K, Slupphaug G, Lee WI, Revy P, Nonoyama S, Catalan N, Yel L, Forveille M, Kavli B, Krokan HE, Ochs HD, Fischer A, Durandy A.** 2003. Human uracil-DNA glycosylase deficiency associated with profoundly impaired immunoglobulin class-switch recombination. Nature immunology **4:**1023-1028.
272. **Chen R, Wang H, Mansky LM.** 2002. Roles of uracil-DNA glycosylase and dUTPase in virus replication. The Journal of general virology **83:**2339-2345.
273. **Reddy SM, Williams M, Cohen JI.** 1998. Expression of a uracil DNA glycosylase (UNG) inhibitor in mammalian cells: varicella-zoster virus can replicate in vitro in the absence of detectable UNG activity. Virology **251:**393-401.
274. **Pyles RB, Thompson RL.** 1994. Mutations in accessory DNA replicating functions alter the relative mutation frequency of herpes simplex virus type 1 strains in cultured murine cells. Journal of virology **68:**4514-4524.
275. **Prichard MN, Duke GM, Mocarski ES.** 1996. Human cytomegalovirus uracil DNA glycosylase is required for the normal temporal regulation of both DNA synthesis and viral replication. Journal of virology **70:**3018-3025.
276. **Bogani F, Chua CN, Boehmer PE.** 2009. Reconstitution of uracil DNA glycosylase-initiated base excision repair in herpes simplex virus-1. The Journal of biological chemistry **284:**16784-16790.

277. **Strang BL, Coen DM.** 2010. Interaction of the human cytomegalovirus uracil DNA glycosylase UL114 with the viral DNA polymerase catalytic subunit UL54. The Journal of general virology **91:**2029-2033.
278. **Su MT, Liu IH, Wu CW, Chang SM, Tsai CH, Yang PW, Chuang YC, Lee CP, Chen MR.** 2014. Uracil DNA Glycosylase BKRF3 Contributes to Epstein-Barr Virus DNA Replication through Physical Interactions with Proteins in Viral DNA Replication Complex. Journal of virology **88:**8883-8899.
279. **Prichard MN, Lawlor H, Duke GM, Mo C, Wang Z, Dixon M, Kemble G, Kern ER.** 2005. Human cytomegalovirus uracil DNA glycosylase associates with ppUL44 and accelerates the accumulation of viral DNA. Virology journal **2:**55.
280. **Courcelle CT, Courcelle J, Prichard MN, Mocarski ES.** 2001. Requirement for uracil-DNA glycosylase during the transition to late-phase cytomegalovirus DNA replication. Journal of virology **75:**7592-7601.
281. **Bogani F, Corredeira I, Fernandez V, Sattler U, Rutvisuttinunt W, Defais M, Boehmer PE.** 2010. Association between the herpes simplex virus-1 DNA polymerase and uracil DNA glycosylase. The Journal of biological chemistry **285:**27664-27672.
282. **Weller SK, Coen DM.** 2012. Herpes simplex viruses: mechanisms of DNA replication. Cold Spring Harbor perspectives in biology **4:**a013011.
283. **Pyles RB, Thompson RL.** 1994. Evidence that the herpes simplex virus type 1 uracil DNA glycosylase is required for efficient viral replication and latency in the murine nervous system. Journal of virology **68:**4963-4972.
284. **McBride KM, Gazumyan A, Woo EM, Barreto VM, Robbiani DF, Chait BT, Nussenzweig MC.** 2006. Regulation of hypermutation by activation-induced cytidine deaminase phosphorylation. Proceedings of the National Academy of Sciences of the United States of America **103:**8798-8803.
285. **Gazumyan A, Timachova K, Yuen G, Siden E, Di Virgilio M, Woo EM, Chait BT, Reina San-Martin B, Nussenzweig MC, McBride KM.** 2011. Amino-terminal phosphorylation of activation-induced cytidine deaminase suppresses c-myc/IgH translocation. Molecular and cellular biology **31:**442-449.
286. **Kim YJ, Wilson DM, 3rd.** 2012. Overview of base excision repair biochemistry. Current molecular pharmacology **5:**3-13.
287. **Rada C, Williams GT, Nilsen H, Barnes DE, Lindahl T, Neuberger MS.** 2002. Immunoglobulin isotype switching is inhibited and somatic hypermutation perturbed in UNG-deficient mice. Current biology : CB **12:**1748-1755.
288. **Tischer BK, von Einem J, Kaufer B, Osterrieder N.** 2006. Two-step red-mediated recombination for versatile high-efficiency markerless DNA manipulation in Escherichia coli. BioTechniques **40:**191-197.
289. **Focher F, Mazzarello P, Verri A, Hubscher U, Spadari S.** 1990. Activity profiles of enzymes that control the uracil incorporation into DNA during neuronal development. Mutation research **237:**65-73.

290. **Lu CC, Huang HT, Wang JT, Slupphaug G, Li TK, Wu MC, Chen YC, Lee CP, Chen MR.** 2007. Characterization of the uracil-DNA glycosylase activity of Epstein-Barr virus BKRF3 and its role in lytic viral DNA replication. Journal of virology **81:**1195-1208.
291. **Verma SC, Bajaj BG, Cai Q, Si H, Seelhammer T, Robertson ES.** 2006. Latency-associated nuclear antigen of Kaposi's sarcoma-associated herpesvirus recruits uracil DNA glycosylase 2 at the terminal repeats and is important for latent persistence of the virus. Journal of virology **80:**11178-11190.
292. **Bekerman E, Jeon D, Ardolino M, Coscoy L.** 2013. A role for host activation-induced cytidine deaminase in innate immune defense against KSHV. PLoS pathogens **9:**e1003748.
293. **Gramlich HS, Reisbig T, Schatz DG.** 2012. AID-targeting and hypermutation of non-immunoglobulin genes does not correlate with proximity to immunoglobulin genes in germinal center B cells. PloS one **7:**e39601.
294. **Fixman ED, Hayward GS, Hayward SD.** 1995. Replication of Epstein-Barr virus oriLyt: lack of a dedicated virally encoded origin-binding protein and dependence on Zta in cotransfection assays. Journal of virology **69:**2998-3006.
295. **Focher F, Verri A, Verzeletti S, Mazzarello P, Spadari S.** 1992. Uracil in OriS of herpes simplex 1 alters its specific recognition by origin binding protein (OBP): does virus induced uracil-DNA glycosylase play a key role in viral reactivation and replication? Chromosoma **102:**S67-71.
296. **Kim JH, Kim WS, Park C.** 2013. Epstein-Barr virus latent membrane protein 1 increases genomic instability through Egr-1-mediated up-regulation of activation-induced cytidine deaminase in B-cell lymphoma. Leukemia & lymphoma **54:**2035-2040.
297. **Minkah N, Chavez K, Shah P, Maccarthy T, Chen H, Landau N, Krug LT.** 2014. Host restriction of murine gammaherpesvirus 68 replication by human APOBEC3 cytidine deaminases but not murine APOBEC3. Virology **454-455:**215-226.